Design and Synthesis of Planar Antenna Array in RF Domain using GA Modified Discretizing Technique of Taylor distribution and Analysis of Nanoparticle Arrays for Optical Antenna and Filter Design

Ph. D. Thesis

Submitted by

Vinay Kanungo
(College ID:- 2012REC9056)

Under Supervision of

Dr. MOHAMMAD SALIM
Associate Professor, Department of ECE, MNIT Jaipur

DEPARTMENT OF ELECTRONICS AND COMMUNICATION ENGINEERING

MALAVIYA NATIONAL INSTITUTE OF TECHNOLOGY JAIPUR

(October, 2017)

Design and Synthesis of Planar Antenna Array in RF Domain using GA Modified Discretizing Technique of Taylor distribution and Analysis of Nanoparticle Arrays for Optical Antenna and Filter Design

Ph. D. Thesis

Submitted by

Vinay Kanungo
(College ID:- 2012REC9056)

Under Supervision of

Dr. MOHAMMAD SALIM
Associate Professor, Department of ECE, MNIT Jaipur

Submitted as a partial fulfillment of the degree of Doctor of Philosophy
in

DEPARTMENT OF ELECTRONICS AND COMMUNICATION ENGINEERING

MALAVIYA NATIONAL INSTITUTE OF TECHNOLOGY JAIPUR

(October, 2017)

Certificate

It is certified that:

- The thesis has not been submitted in part or full to any other University or Institute for award of any degree.
- I have fulfilled all the requirements for submission of the thesis.

Mr. Vinay Kanungo

ID: 2012REC9056

This is to certify that the thesis entitled "Design and Synthesis of Planar Antenna Array in RF Domain using GA Modified Discretizing Technique of Taylor distribution and Analysis of Nanoparticle Arrays for Optical Antenna and Filter Design", being submitted by Vinay Kanungo to the Department of Electronics and Communication Engineering, Malaviya National Institute of Technology, Jaipur, for the award of the degree of Doctor of Philosophy, is a bonafide research work carried out by her under my supervision and guidance. The results obtained in this thesis have not been submitted to any other university or institute for the award of any other degree.

(Dr. Mohammad Salim)

Associate Professor, Department of ECE

Malaviya National Institute of Technology, Jaipur

Jaipur-302017, Rajasthan (India).

Thesis was examined and approved for award of degree of Doctor of Philosophy.

_____

_____

_____

External Examiner

Declaration of Authorship

I, Vinay Kanungo, declare that this thesis titled, 'Design and Synthesis of Planar Antenna Array in RF Domain using GA Modified Discretizing Technique of Taylor distribution and Analysis of Nanoparticle Arrays for Optical Antenna and Filter Design' and the work presented in it are my own. I confirm that:

- This work was done wholly or mainly while in candidature for a Ph.D. degree at MNIT.
- Where any part of this thesis has previously been submitted for a degree or any other qualification at MNIT Jaipur or any other institution, this has been clearly stated.
- Where I have consulted the published work of others, this is always clearly attributed.
- Where I have quoted from the work of others, the source is always given. With the exception of such quotations, this thesis is entirely my own work.
- I have acknowledged all main sources of help.
- Where the thesis is based on work done by myself jointly with others, I have made clear exactly what was done by others and what I have contributed myself.

Signed:_____

Date:_____

Acknowledgements

This beautiful journey of my research has been accompanied by many important people of my life and I would like to convey my sincere gratitude to these people by dedicating them “the joy of this triumph”.

First of all, I would like to express my thanks to my supervisor Dr. Mohammad Salim for his invaluable guidance throughout my research work. He has been a great inspiration for me always and I have learned a lot from his calm and patient personality. His innovative, simple yet completely different research oriented thinking has helped me to pursue my research smoothly and to make it a great success.

I am very much grateful to Prof. K.K. Sharma, Head of the ECE department, who have always been a great teacher and a well-wisher for me. He provided all the facilities and support required for this research work at the departmental end. In addition, I would like to express my great regards and thanks to all my DREC committee members Dr. Vijay Janyani, Dr. Ghanshyam Singh, Dr. Ritu Sharma, and Dr. Ravi Kumar Maddila, who always guided me whenever I encountered problems in my research and provided me significant feedbacks. I extend my sincere thank to all the faculty members of the ECE department who always supported me and helped me tangibly and intangibly in my research work.

My strength is my beautiful family and whatever I have achieved is because of their unconditional love and support. I am extremely thankful to my parents Mr. Anil Kanungo and Mrs. Raj Dulari Kanungo, my little sister Bharti and my loving wife Ranu.

Finally, I would like to convey my heartiest thank to my dear friends and fellow research scholars for giving me all their help and support throughout my research work.

(Vinay Kanungo)

Abstract

Concept of optimization has been utilized in various fields, be in computer science engineering or any other field of engineering. The basic idea behind the optimization is to have the parameter values of a function calculating the cost such that the function either take its minimum possible value or maximum possible value for a given search space. In this work, the prevailing idea of optimization for antenna array pattern has been utilized in order to have optimum well behaved side lobe pattern with high directivity and high sensitivity. There are various optimization algorithms present in the literature and some of them have been used for antenna pattern optimization for a long time, such as Particle swarm algorithm (PSO), Ant Colony Optimization (ACO), Genetic algorithm (GA), hybrid Particle Swarm Optimization (HSPSO), etc. Due to the versatility and capability of optimizing in complex multimodal search spaces, Genetic algorithm has found its application in most of the heuristic search based optimization problems. Here, in the proposed work the GA has been used to obtain the optimized thinned configuration and in the latter improvement of the design it has been combined with the Taylor synthesis for planar array. The planar antenna proposed here has been investigated in the context of the SKA application for the design of aperture arrays in the frequency range from 100 MHz to 1 GHz, covering the design of dense aperture array with the inter-element spacing of $\lambda/2$. In the quest of a properly shaped main beam and competitive values of other performance parameters of antenna array, a solution comprising selection of the design and optimized excitation of the array elements has been proposed. Tailoring the main beam to focus the radiation to the desired area without the need of complex and costly attenuators and amplifiers network is one of the main advantages of this approach. In this work, Emphasis on the array geometry to achieve the goal for the above mentioned applications has been given. Unlike previously reported work, hexagonal array geometry with 484 elements has been chosen to have a well controlled main beam with elliptical shape which also has its impact on beam width. The selection of the beam shape has been made on the ground that a particular shape of the main beam can be achieved with the proper selection of array element placement i.e., with the aperture size and shape. After geometry selection the optimized array thinning configuration has been obtained for minimum side lobe peaks and high directivity using the Binary GA. The design has the elements arranged hexagonally to avail the geometry associated advantages of high directivity, radiation pattern flexibility and less element density requirement for the same coverage area. In the proposed work the GA crossover operator has been modified according

to the design and a new **Double stage uniform crossover operation** has been proposed. Further, the performance on side lobe level, directivity, radiation pattern, power requirement, and 3 dB beam width has been improved by utilizing the concept of Taylor synthesis for discrete array. Taylor synthesis allows to have a well beahved radition pattern along with the desired shape of the main beam. With the design approach of Taylor sythesis it is possible to obtain excitation values for discrete arrays as in this approach the continuous aperture distribution can be sampled for the elements of discrete array. Moreover, Taylor synthesis approch for discrete array can be extended to the planar array design with circular or elliptical boundaries and this extension is not possible with Dolph's synthesis. For large number of elements, the sampling period is small and it leads to more accurate approximation of element excitation. Now, there are some drawbacks with conventional sampling of generalized Taylor continuous aperture distributions as it causes pattern degradation which is more serious when the number of elements in the circular grid array is small. In order to achieve the desired pattern, Taylor proposed, the current perturbation method in which linear equation in the unknown current perturbation are solved to obtain the current distribution for desired radiation pattern. This method is less feasible with the increment in array size as the number of equations increases with increment in the array elements. The proposed work consists the solution in terms of the proposed **GA Modified discretizing technique** for the planar array. In this GA has been used to find the optimum current perturbation combination for the desired radiation pattern. This method improves the performance of antenna array in comparison to the previously presented method of optimization of design and excitation of proposed planar array.

Second part of the thesis consists the application of metal nano particles for the design of optical antenna and optical filter. A detailed study of metal nano particle and their application for optical antenna design has been discussed in the thesis. The work proposed here focus on the nano particle array design for the antenna and filter application. The results have been carried out using the Finite Difference Time Domain method by calculating the power extinction and power radition by the nano particles. Concept of variation of metal nano particle characteristic with its size, shape, and surrounding enviornment have been utilized to obtain the desired combination of particle for desired application. Nano shells of dielectric have been considered for the placement of nano particles. Spherical particles with different size shells can work as narrow band radiator and elliptical particles with different size shells can work as wide band radiator. As far as filter design is concern, the Spherical particles with

different shell diameters results in very closely spaced dips in power spectrum. This can be utilized to form an array with shell size variation corresponding to the particle placed in it and the surrounding index of the particle and the contrast. Wide band filters can be designed by taking the elliptical particles in place of the spherical because these particles with shell diameter variation causes the power spectrum dips to occur at significantly larger distances. Application of the optimization using GA has been discussed for the antenna and filter design. Combination of different parameters for maximum radiation at a given wavelength has been achieved with optimization. It gives the parameter set of nano particle for the design of antenna and filter.

Contents

List of Figures

List of Tables

List of Symbols and Acronyms

Acronyms

AAs	:	Aperture Arrays
ACO	:	Ant Colony Optimization
ADF	:	Adaptive Desirability Function
AT	:	Atmospheric Transmission
ATM	:	Atmospheric Transmission at Microwave
DFT	:	Discrete Fourier Transform
DWDM	:	Dense Wavelength Division Multiplexing
EM	:	Electro Magnetic
FDTD	:	Finite Difference Time Domain
GA	:	Genetic Algorithm
HSPSO	:	Hybrid Particle Swarm Optimization
IFTDT	:	Iterative Fourier Transform with Suitable Density Taper Approach
ITU	:	International Telecommunication Union
LSPs	:	Localized Surface Plasmons
LSPR	:	Localized Surface Plasmon Resonance
MTLBO	:	Modified Teaching Learning Based Optimization
NPs	:	Nanoparticles
PAF	:	Phased Array Feed
PSO	:	Particle Swarm Algorithm
RDT	:	Random Density Taper
RF	:	Radio Frequency
RFI	:	Radio Frequency Interference
RSLLs	:	Relative Side Lobe Levels
SD	:	Standard Deviation
SKA	:	Square Kilometer Array
SPs	:	Surface Plasmons
SPF	:	Single Pixel Field
SPPs	:	Surface Plasmon Polaritons
URSI	:	International Union for Radio Science
WDM	:	Wavelength Division Multiplexing

Symbols

(λ_{eff})	:	Effective Wavelength
$\varepsilon(\omega)$	:	Complex Dielectric constant of the metals
ω_p	:	Plasma frequency
ω	:	Frequency
m	:	Effective optical mass of an electron
ε_0	:	Electric permittivity
σ_{sca}	:	Scattering cross-section
σ_{abs}	:	Absorption cross-section
σ_{ext}	:	Extinction cross-section
α	:	Polarizability of nano particle
ε_p	:	Dielectric constant of nano particle
ε_m	:	Dielectric constant of metal
ϕ	:	Azimuth angle
θ	:	Elevation angle
d	:	Antenna element separation
λ	:	Wavelength
AF_{11}	:	Array factor of non-central element array first of section-1 of the proposed array geometry
AF_{12}	:	Array factor of non-central element array second of section-1 of the proposed array geometry
AF_{21}	:	Array factor of central element array on x axis of section-2 of the proposed array geometry
AF_{22}	:	Array factor of central element array on y axis of section-2 of the proposed array geometry
$AF_{Hexagonal}$	:	Array factor of the proposed hexagonal planar antenna array
$(AF_{Hexagonal})_{max}$	:	Maximum value of the array factor for the proposed hexagonal planar array
$cost_{Hexagonal}$	:	Cost function of GA for the optimization of the proposed hexagonal planar array
I_{mn}	:	Current excitation Amplitude of m^{th} element in n^{th} string

$I_{m_0}^{c_1}$	:	Central element excitation along x axis of the proposed array geometry
$I_{n_0}^{c_1}$	:	Central element excitation along y axis of the proposed array geometry
δ_{mn}	:	Excitation phase shift of m^{th} element in n^{th} string of the proposed array geometry
θ_{FN}	:	First null angle
σ_{ϕ_n}	:	Standard deviation of SLL in n^{th} plane
P_S	:	Probability of selection
D_a	:	Antenna directivity
$F(\theta, \phi)$	:	Antenna array radiation pattern (Field pattern)
$\delta(\theta)$	:	Desired raditaion pattern in Taylor synthesis
$g(z)$	:	Aperture distribution in Taylor synthesis $(z = element\ position)$
$f(u)$	:	Radiation pattern in Taylor synthesis
$\delta(u)$	:	Radiation pattern with shifted nulls in Taylor synthesis
$K(\rho, \beta)$	:	Planar apertutre distribution in Taylor synthesis $(\rho = radial\ coordinate, \beta = azimuth\ coordinate)$
σ	:	Dialation factor in Taylor synthesis
δI_{mn}	:	Current perturbation Amplitude of m^{th} element in n^{th} string in Taylor synthesis (current perturbation method)
$\delta I'_{mn}$	:	Current perturbation amplitude of m^{th} element in n^{th} string in proposed GA modified discretizing technique
L_{lower}	:	Lower limit of current perturbation amplitude in proposed GA modified discretizing technique
L_{upper}	:	Upper limit of current perturbation amplitude in proposed GA modified discretizing technique
$(L'_{lower})_m$	:	Minimum value of the current distribution corresponding to the m^{th} string as lower limit of current perturbation amplitude
$SLL_{P_{\phi_n}}$	:	Side lobe level peak in n^{th} ϕ plane
$(SLL_{P_{\phi_n}})_{max}$	:	Maximum value of side lobe peak in n^{th} ϕ plane
$(SLL_{P_{\phi_n}})_{random}$	:	Randomly selected side lobe peaks in n^{th} ϕ plane
$((SLL_{P_{\phi_n}})_{max})_{all}$	:	Maximum side lobe peaks for all the ϕ planes

$((SLL_{P_{\phi_n}})_{random})_{all}$	:	Randomly selected side lobe peaks for all the ϕ planes
$(SLL_{P_{max}})_{complete}$	:	Maximum side lobe level for complete radiation pattern
$SLL_{P_{combined}}$	:	Combined side lobe peaks from maximum side lobe level for complete radiation and randomly selected side lobe peaks for all ϕ planes
f_{cost}	:	Cost function of GA
$SD_{P_{combined}}$	:	Standard deviation for combined side lobe peaks
η_{ap}	:	Antenna aperture efficiency
A_{ap}	:	Antenna aperture area
ν	:	Frequency of atmospheric absorption calculation
k_{o_2}	:	Absorption coefficient for oxygen molecule
P	:	Atmospheric pressure
T	:	Atmospheric temperature
F_{o_2}	:	Line shape function of oxygen
ϕ_j	:	Fractional population of initial state of the jth line
γ_j	:	Resonant line width parameter
γ_b	:	Non-resonant line width parameter
$\upsilon_{j\pm}$	:	Resonant frequencies
$d_{j\pm}$	:	Amplitude of lines $\upsilon_{j\pm}$
$Y_{j\pm}$	:	Interference coefficients
k_{H_2O}	:	Absorption coefficients for water vapor molecule
ρ_v	:	Water vapor density
F_{H_2O}	:	Line shape function of water vapor molecule
k_a	:	Atmospheric absorption coefficient
a_n	:	Path traveled by the ray in nth layer of atmosphere
δ_n	:	Thickness of nth layer of atmosphere
δ_n	:	Ray entrance angle in the nth layer of atmosphere
β_n	:	Ray departure angle from the nth layer of atmosphere
r_n	:	Radial distance of the nth layer from earth centre
n_n	:	Refractive index profile of the nth layer of atmosphere
k_{at}	:	Total atmospheric attenuation

I_v	:	Specific intensity
τ_v	:	Opacity of the medium
T_b, T_{sky}	:	Sky brightness temperature
T_{bo}	:	Temperature due to background cosmic emission
T_{eff}	:	Effective temperature
T_a	:	Antenna noise temperature
η_T	:	Total antenna efficiency
η_{rad}	:	Antenna radiation efficiency
T_{Sys}	:	Antenna system noise temperature
T_{sur}	:	Antenna surrounding temperature
T_{LNA}	:	Temperature of low noise amplifier
A_{eff}	:	Antenna effective area
S	:	Antenna sensitivity
D	:	Dielectric displacement (Maxwell's equation)
B	:	Magnetic flux density (Maxwell's equation)
E	:	electric filed (Maxwell's equation)
H	:	magnetic field (Maxwell's equation)
ρ_{ext}	:	External charge density
J_{ext}	:	External current density
P	:	Polarization (electric dipole moment)
M	:	Magnetization
ρ_{tot}	:	Total charge density
χ	:	Dielectric susceptibility
J	:	Current density
σ	:	Conductivity
K	:	Wave vector
c	:	Velocity of light

Chapter 1

Introduction

Antennas are one of the main building blocks of wireless communication systems. For long haul communication systems it is required to have an antenna with high directivity or gain and with minimum side lobes. Radiations in unwanted direction in terms of side lobe can cause false target detection in most radar systems and thus need to be suppressed. An antenna with high directivity and minimum side lobe levels can only be achieved by increasing the electrical size of the antenna. Electrical dimensions of an antenna can be increased either by enlarging the size of single antenna element or by assembling the individual elements in a certain configuration. The former approach is practically less feasible and hence has not been adopted, whereas the latter one is most popular and known as antenna array. Ubiquitous applications of digital beam forming in adaptive and smart antennas forced the development of antenna arrays. Generally these array elements are considered identical to reduce complexity and they can have any shape such as wires, apertures, etc [Balanis, "Antenna Theory: Analysis and Design", 1997]. In the proposed work these elements have been considered as simple identical radiating points. These elements can be arranged linearly in one dimension or in two dimensions as planar geometries leading to the designs of linear and planar antenna arrays, respectively. Antenna arrays are now being looked as a great mean to study the radio frequency spectrum of the universe to unveil some unknown phenomena and objects of the universe. These arrays forms the ultrasensitive radio telescope operating over a frequency range of 30 GHz to 70 MHz (1 cm to 4.3 meters) and these high sensitive radio telescopes have been deployed under Square Kilometer Array (SKA) project [Peter E. Dewdney, 2009]. Some of the challenges associated with these antenna arrays are the requirement of high spatial resolution with highly directive main beam and high sensitivity in terms of minimum noise temperature [Peter E. Dewdney, 2009],**[**Ahmed El-makadema, 2014**]**. Planar antenna array with its associated degree of freedom can perform well on these parameters. Geometry plays an important role in the realisation of these antenna arrays as the performance parameters such as sensitivity, directivity and side lobe peaks have a great dependency on geometry of the array **[**Ahmed El-makadema, 2014**]**. Emphasis on the array geometry to achieve the goal for the above mentioned applications has been given. The geometry has been optimized to have a controlled main beam with specific shape in order to have the coverage by the array over an elliptically shaped region. Selection of the beam shape has been made on the ground that a particular shape of the main beam can be achieved with

the proper selection of array element placement i.e., with the aperture size and shape. To obtain minimum side lobes and higher directivity antenna characteristics can be controlled by arrangement of elements, inter-element spacing, excitation amplitude and phase of elements and element pattern [Balanis, "Antenna Theory: Analysis and Design", 1997]. A wide literature is there in which, array geometries have been optimized for peak side lobe reduction and high directivity using heuristic approaches either by searching for element density with non periodic arrangement (space tapered arrays **[**R. Harrington, 1961],[R. E. Willey, 1962]) or using the more feasible counterpart which is called array thinning [R.L. Haupt][R. L. Haupt, 1994]. Array thinning provides same performance as with fully filled array and hence it is cost and energy efficient [W. P. M. N. Keizer, 2014]. Placing the elements periodically makes the task less complex and it becomes finding the proper combination of on and off elements. Although with exhaustive search, this becomes time and memory consuming with increment in array size (2^nsolutions for n elements) and hence finds the application of heuristic approaches [R. L. Haupt, 1994; K.-K. Yan and Y. Lu, 1997; F. Ares-Pena et al., 1999; D. Marcano and F. Duran, 2000; Y.-B. Tian and J. Qian, 2005; M. Fernández-Delgado et al., 2010; L. Zhang et al.,2010; C. Ding and L. Jianxin, 2009; E. Hassan and H. Ragheb, 2012]**, [**Kalyanmoy Deb, KanGAL Report number 2003002**]**. Adaptive programming has provided a numerical optimization method to obtain lowest side lobe level of a thinned antenna array [R.L. Haupt and D. H. Werner,1995]. Planar array design with optimization of the element position and excitation coefficients with the constraint of minimum main beam ripple and side lobe level in a prescribed limit have been investigated in [Rajeev C. Nongpiur, 2014]. The method in [Rajeev C. Nongpiur, 2014] was proposed to have minimum element selection in the array in order to have less power consumption. This iterative search with large number of degree of freedom in design had offered quite improved side lobe pattern but the beam width could not compete with the high resolution applications. In [Rajeev C. Nongpiur, 2014], the offered fill factor (ratio of turned on elements to the total elements) was 64%. Quite low fill factors have been reported in [Will P. M. N. Keizer, 2014] with the two new synthesis techniques, Iterative Fourier Transform with suitable density taper approach (IFTDT), and Random Density Taper (RDT) which identify the turned on elements for different size and shape planar arrays by dividing the whole array into ring sectors [Will P. M. N. Keizer, 2014] . In [Will P. M. N. Keizer, 2014], these two techniques have been applied for the optimized array thinning configuration to have minimum side lobe level, high directivity and a minimum 3 dB beam width. A performance comparison with array thinning approaches proposed in [Will P. M. N. Keizer,

2014] along with other heuristic search approaches such as Ant Colony Optimization (ACO) [S. Mosen and M. Ciattaglia,2006], Genetic algorithm (GA) [C. Ding and L. Jianxin, 2009],[M. Fernández-Delgado et al., 2010], hybrid Particle Swarm Optimization (HSPSO) [M. Donelli et al., 2009] have been considered for comparison in [Will P. M. N. Keizer, 2014]. In the presented work, this comparison has been extended with our proposed array design and synthesis over the performance parameters: side lobe level, directivity and 3 dB beam width. Cancellation of the side lobes in a planar array have been achieved in [J. R. Mohammed and K. H. Sayidmarie, 2014] at the cost of increment in side lobe peak and beam width. In [J. R. Mohammed and K. H. Sayidmarie, 2014], the feeding network complexity has been addressed with change in amplitude and phase of boundary elements only. Simplified feeding network may be applicable where cost is more important than performance, but for applications such as SKA high spatial resolution and high directivity with reduced side lobe peaks require a different approach altogether. A modified teaching learning based optimization (MTLBO) approach has been proposed in [Xuedong Chen et al.,2014] and performs well for small size planar array thinning as far as side lobe levels, fill factor and beam width are concern. As it is a multi objective thinning approach, suffers with the limitations of non dominated solutions.

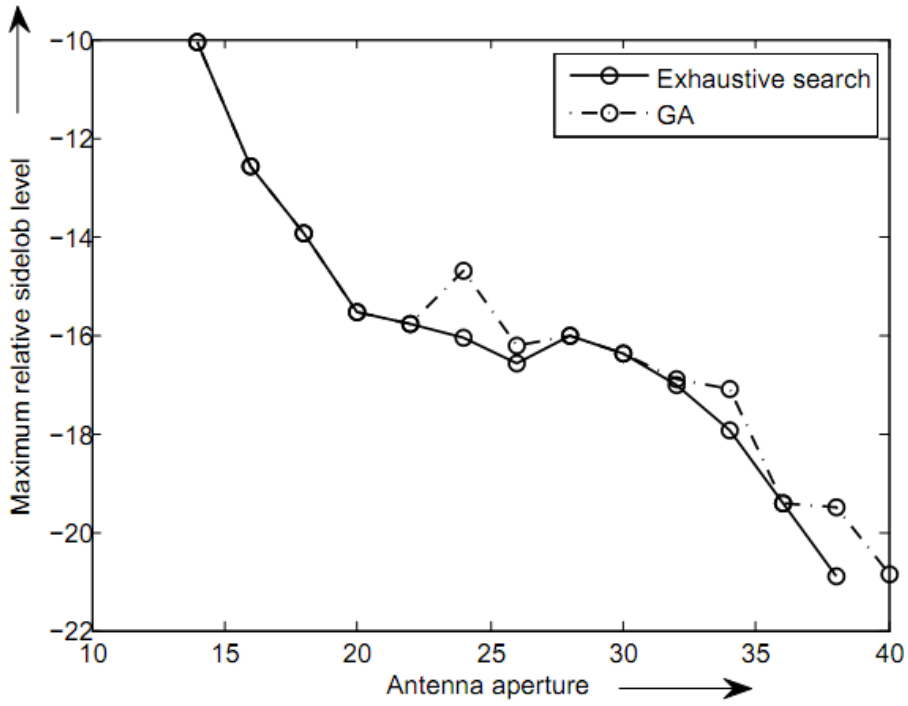

Figure 1. 1 A comparison between exhaustive search and GA

Due to the versatility and capability of optimizing in complex multimodal search spaces, Binary Genetic algorithm has found its application in most of the heuristic search based optimization problems [D. H. W. R.L. Haupt, 2007; R. L. Haupt, 1994; M. Fernández-Delgado et al. 2010],[S.G. Tanyer, 2012]. A GA has several advantages over the traditional numerical optimization approaches such as it optimizes with continuous or discrete parameters, doesn't require derivative information, simultaneously searches from a wide sampling of the cost surface, works with a large number of variables, it is well suited for parallel computers, optimizes variables with extremely complex cost surfaces, Provides a list of optimum parameters, not just a single solution, May encode the parameters, and the optimization is done with the encoded parameters, Works with numerically generated data, experimental data, or analytical functions [R. L. Haupt, 1994]. Figure 1.1 is showing a comparison between GA and exhaustive search approach showing the accuracy of the GA in comparison to the time and memory consuming exhaustive search. Optimization for single parameter does not fulfil the practical requirements and hence non dominated solution sets, called pareto front, are obtained using multi objective evolutionary search algorithms [J. Petko and D. Werner, 2011; D. S. Weile and E. Michielssen, 1996]. Multi objective GA with side lobe reduction and a desired beam width is not sufficient to ensure a pattern with well behaved main beam [D. S. Weile and E. Michielssen, 1996]. Controlling the main beam variation from the desired one at the cost of other performance parameters has been a problem with array thinning [D. H. Werner and A. J. Ferraro, 1989]. Moreover, obtaining a pareto front for both the main beam shape and side lobe levels could not provide the results as better as a dominated solution can provide [W. P. M. N. Keizer, 2014]. Although, an adaptive cost function multi objective optimization have been investigated in [S.G. Tanyer A.E. Yılmaz and F. Yaman, 2012] using GA and the performance was tested for small linear arrays. Here, GA proves to be a better choice for optimization with proposed adaptive desirability function (ADF) [S.G. Tanyer A.E. Yılmaz and F. Yaman, 2012]. In the proposed work, GA has been applied in Taylor synthesis and GA modified sampled Taylor distribution has been obtained for the proposed planar array. In Taylor synthesis, shifting of null method is used to control the side lobe level and to have a predefined pattern. Still the pattern degradation is there and to overcome that current perturbation method is used. Set of linear equation in current perturbation is used to obtain the current excitation for the desired radiation pattern [Robert S. Elliot, "Antenna theory and design", 2003]. These equation increases with the size of antenna array so this problem needs to be addressed if the method is

to be utilized for the design of large planar array. GA modified discretizing technique for Taylor distribution has been used to achieve the desired radiation pattern.

Second part of the thesis consisting the design and analysis of nano particle antenna and filters for optical domain, contains the full characteristic study of gold nano particle and its application as antenna and filter. It utilizes the concept of generation of surface plasmons at the metal dielectric interface. Small particles supports the generation of localized surface Plasmon resonances which follows the Frohlich condition at resonance. Metals behave like dielectric material (no perfect reflection) at optical frequencies and EM field penetrates into the metal up to a certain distance called skin depth. At optical frequency incident radiation couples to the electron plasma and it causes the rapid oscillation of electron density. Electrons do not respond to the incident wavelength, but to an effective wavelength (λ_{eff}) expressed in terms of plasma wavelength and incident wavelength. Some of the challenges are: impedance matching between antenna and source, electro-optical transduction, phase control of coupled optical antennas, antenna feeding, radiation pattern dependence of transmitting and receiving antennas, angular response pattern, type of antenna, modelling of complex antenna geometries, surrounding medium of antenna.

In [T. Dattoma, et al., 2011], the effect of nano antenna geometry on its resonant mode formation has been investigated. The geometry comprises of a gold nano rod placed on a Gallium Nitride (GaN) substrate. The electric field distribution has been evaluated using Discrete Fourier Transform (DFT) and numerical analysis has been proposed using finite difference time domain method. The complex refractive index of the gold nano particle is given by the Drude-Lorentz model. According to the Drude dispersion model, the complex dielectric constant of the metals is given by

$$\varepsilon(\omega) = 1 - \frac{\omega_p^2}{\omega^2 + i\gamma\omega} \tag{1.1}$$

Where ω_p is the plasma frequency of the free electron gas of number density n and it is expressed as

$\omega_p = \frac{ne^2}{m\varepsilon_0}$, Here m is the effective optical mass of an electron.

Now generation of surface plasmons can be understood with the phenomenon occurring at the metal dielectric interface. Plasmons are collective oscillations of the free electron density

with respect to the fixed positive ion in metal. Plasmon is a quantum of plasma oscillation and can be considered as a quasi particle just like phonon. Plasma oscillation take place under the influence of external electromagnetic field applied on the metal, when electrons shifts from their equilibrium position and a restoring force of the nucleus pulls electrons back to their original position, resultantly causing the electrons to oscillate at plasma frequency. Surface plasmons (SPs) as their name indicates are the electron density oscillations at the interface between the two materials of dielectric functions with opposite sign, for example metal dielectric interfaces [Stefan Alexander Maier, "Plasmonics: Fundamentals and Application," 2007]. Surface plasmons have attracted the attention of physicists, chemists, biologists and material scientists for widespread use in areas such as electronics, optical sensing, biomedicine, data storage and light generation. Recent developments in nanotechnology have generated new insights about control of various properties of nanomaterials that can support surface plasmons for specific applications. Localized surface plasmon resonance (LSPR) is an optical phenomena generated by a light wave trapped within conductive nanoparticles (NPs) smaller than the wavelength of light.

The phenomenon is a result of the interactions between the incident light and surface electrons in a conduction band. This interaction produces coherent localized plasmon oscillations with a resonant frequency that strongly depends on the composition, size, geometry, dielectric environment and particle–particle separation distance of NPs. Common materials used for NP production are noble metals such as Ag and Au, which due to the energy levels of d–d transitions exhibit LSPR in the visible range of the spectrum. Although, Ag exhibits the sharpest and strongest bands among all metals, Au is preferred for biological applications due to its inert nature and biocompatibility, and thiol-gold association for immobilization of bio-molecules [Eleonora Petryayeva and Ulrich J. Krull, 2011]. When the light interacts with nano particle, at resonance, maximum amount of light got extinct by the particle due to the occurrence of two phenomenons. One is absorption of light and the second one is scattering of light by the particle. Absorption and scattering phenomenon are many magnitudes higher than that is possible without LSPR. The resonant condition is defined by the poles of the following two Eq.

$$\sigma_{abs} = k \times Im(\alpha) = 4\pi k R^3 Im(\frac{\varepsilon_p - \varepsilon_m}{\varepsilon_p + 2\varepsilon_m}) \tag{1.2}$$

$$\sigma_{sca} = \frac{k^4}{6\pi} \times |\alpha|^2 = 8\pi k^4 R^6 \left| \frac{\varepsilon_p - \varepsilon_m}{\varepsilon_p + 2\varepsilon_m} \right|^2 \quad (1.3)$$

When the denominator of the above two equations are zero, it correspond to the resonant condition and it is known as Frohlich condition. In the proposed work these two phenomenons have been utilized to design an optical antenna array radiating in multiple band and optical filter attenuating power over a range of frequencies.

The work described in this thesis addresses the following problems

- Design of antenna array for satellite and space communication require highly directive and well shaped main beam pattern. Applications such as Square Kilometer array (SKA), in which antennas are used as radio telescopes must possess high directivity, minimum 3 dB beam width, and high sensitivity over a wide range of geographical conditions.
- Optimization techniques with multiple optimizations could perform well but cannot provide the results at par the dominated solutions. For above mentioned applications, shape of the main beam along with the side lobe pattern should be as better as possible over a wide wavelength range.
- In optical domain an antenna array is required that can efficiently transfer the near field to the detector or can efficiently convert the propagating surface plasmons into Radiative field required in applications such as OLEDs.
- Wavelength selective design of nano particle array is required to have the efficient radiation in that particular band or on a single wavelength. Optimum combination of parameters must be known to the designer so that an antenna can be designed with efficient radiation. Similarly, the absorption characteristic of nano particle can be utilized as filtering in optical domain provided that designer must know the parameters that are required for optimum performance at a given wavelength.

1.1. Motivation

The proposed work has been carried out in context of the SKA application which serves as the state of the art radio telescopes. These are highly sensitive and have high spatial and spectral resolution. These are under development phase and require antenna system over a wide wavelength range from 100 MHz to 300 GHz [Peter E. Dewdney et al., 2009]. Right

now in initial phase antennas are being developed for a frequency range 70 MHz to 30 GHz. The proposed work is focused on the development of antenna array for dense aperture array covering a frequency range from 100 MHz to 500 MHz. The requirement of high sensitivity leads to the requirement of minimum power radiation in unwanted directions. As the sensitivity is inversely proportional to the system temperature and antenna temperature, which is the convolution of brightness temperature and antenna pattern, derives the system temperature. Minimizing the peak side lobe level with well behaved main beam is the design requirement of the proposed work. High spatial resolution has been achieved with minimum 3 dB beam width and geometry selection plays an important role as far as main beam and side lobe pattern is concern. Further, as the Taylor synthesis provides a well behaved pattern with desired side lobe level, application of Taylor synthesis for SKA antenna design has been investigated so that improvement in main beam shape, power consumption and sensitivity can be achieved. The optimization approach for RF antenna array design has been extended to the optical antenna array design in terms of improved radiation and absorption by the particle at the desired wavelength. As the nano particle shows the property of localized surface Plasmon resonance after interaction with light at certain condition, this property could be utilized to efficiently transfer the near field information to the detector by the efficient use of antenna array. Similarly the extinction of power due to scattering and absorption has been utilized for optical filter operation. Variation in the particle size, shape, and surrounding causes the operation wavelength to change and thus an array of particles with different controlling parameters can be utilized to form a multiple band radiator and/or a multiple band attenuator. Optimization can be an efficient tool to have the optimum set of parameter values for the desired operation at a given wavelength or set of wavelengths.

1.2. Organization of the Thesis

In this thesis the work proposed is devided into two parts: one contain the design amd analysis of planar antenna array for state of the art SKA application and second part is devoted to the recent work being carried out for desining antennas in optical domain. Both the sections of the thesis deals with different applications all together though both are being studied to bridge the gap in between these two antenna technologies. Objective of the thesis is to relate the current application challenges with the recent technological approaches and to explore and utilize these technologies for further performance enhancement.

Chapter 2 descrbes the recent work being carried out along with the work done in the area of planar antenna array design. The challenges associated with planar array performance has been addresed in context of the SKA application. A planar array geometry has been proposed and optimized with the genetic algorithm. The proposed geometry has been optimized in order to have a particular shape of the main beam and than optimized array thinning configuration has been achieved. Geometry induced modification in GA has been done with the proposed Double stage uniform cross-over.

Chapter 3 discusses the challenges encountered with the proposed work in chapter 2 and Taylor sythesis approach with proposed modification has been presented. A GA modified discretizing technique for sampled Taylor distribution has been proposed. Results obtained with the proposed synthesis approach has been discussed in context of SKA application.

Chapter 4 has been introduced particularly for SKA application and antenna design with addresing the technical challenges being encountered by the researchers. Some of the paramount performance paramters: antenna temerature, sensitivity, aperture efficiency have been investigted for the design with proposed synthesis approach. Results have been compared with some recent work carried out in the area.

Chapter 5 contains the second part of the thesis which describes the properties of nano particles in order to design optical antenna and filter. Characteristics of the nano particle in optical domain have been studied in detail and a optical antenna array design containg a combination of nano dielectric shell and metal nano particle has been propoposed. Simulations for antenna and filter design have been done using the finite difference time domain (FDTD) method.

In the end the thesis has been concluded with the work proposed and the associated challenges still need to addressed in both RF and optical domain. References have been provided in the end of each chaoter of the thesis for easy viewing to the reader.

References

- C. A. Balanis, Antenna Theory. Boca Raton, FL: CRC Press, 2002.
- P. E. Dewdney, P. J. Hall, R. T. Schilizzi and T. J. L. W. Lazio, "The Square Kilometre Array," in Proceedings of the IEEE, vol. 97, no. 8, pp. 1482-1496, Aug. 2009.

- A. El-makadema, L. Rashid and A. K. Brown, "Geometry Design Optimization of Large-Scale Broadband Antenna Array Systems," in IEEE Transactions on Antennas and Propagation, vol. 62, no. 4, pp. 1673-1680, April 2014.
- R. Willey, "Space tapaering of linear and planar arrays," IRE Transactions on Antennas and Propagation, vol. 10, no. 4, pp. 369-377, July 1962.
- D. H. W. R.L. Haupt, Genetic algorithm in electromagnetic. Hoboken, New Jersey: John Wiley and Sons, 2007.
- R. L. Haupt, "Thinned arrays using genetic algorithms," IEEE Transactions on Antennas and Propagation, vol. 42, no. 7, pp. 993-999, July 1994.
- M. Fernández-Delgado, J. A. Rodríquez-González, R. Iglesias, S.Barro, and F. Ares-Pena, "Fast Array Thinning using Global Optimization Methods," J. of Electromagn. Waves and Appl., Vol. 24, 2259–2271, 2010.
- D. Marcano and F. Duran, "Synthesis of antenna arrays using genetic algorithms," IEEE Antennas and Propagation Magazine, vol. 42, no. 3, pp. 12-20, June 2000.
- H. Wang, D.-G. Fang, and Y. Chow, "Grating lobe reduction in a phased array of limited scanning," IEEE Transactions on Antennas and Propagation, vol. 56, no. 6, pp. 1581-1586, June 2008.
- R. C. Nongpiur and D. J. Shpak, "Synthesis of Linear and Planar Arrays With Minimum Element Selection," in IEEE Transactions on Signal Processing, vol. 62, no. 20, pp. 5398-5410, Oct.15, 2014.
- W. P. M. N. Keizer, "Synthesis of Thinned Planar Circular and Square Arrays Using Density Tapering," IEEE Transactions on Antennas and Propagation, vol. 62, no. 4, pp. 1555-1563, April 2014.
- S. Mosen and M. Ciattaglia, "Ant colony optimization to design thinned arrays," in Proc. IEEE Antennas Propag. Soc. Int. Symp., July 2006, pp. 4675-4678.
- M. Donelli, A. Martini, and A. Massa, "A hybrid approach based on PSO and Hadamard difference sets for the synthesis of square thinned arrays," IEEE Trans. On Antennas Propag., vol. 57, no. 8, pp. 2491-2495,Aug. 2009.
- J. R. Mohammed and K. H. Sayidmarie, "Sidelobe Cancellation for Uniformly Excited Planar Array Antennas by Controlling the Side Elements," IEEE Antennas and Wireless Propagation Letters, vol. 13, pp. 987-990, May 2014.
- Xuedong Chen, Zailei Luo, Xueming He and Lianli Zhu, "Thinning and weighting of planar arrays by modified teaching–learning-based optimization algorithm," Journal of Electromagnetic Waves and Applications, vol. 28, No. 15, pp. 1924-1934, 2014.

- J. Petko and D. Werner, “Pareto optimization of thinned planar arrays with elliptical mainbeams and low sidelobe levels,” IEEE Transactions on Antennas and Propagation, vol. 59, no. 5, pp. 1748-1751, May 2011.
- D. S. Weile and E. Michielssen, “Integer coded Pareto genetic algorithm design of constrained antenna arrays,” Electron. Lett., vol. 32, pp. 1744-1745, Sep. 1996.
- D. H. Werner and A. J. Ferraro, “Cosine pattern synthesis for single and multiple main beam uniformly spaced linear arrays,” IEEE Trans. Antennas Propag., vol. 37, no. 11, pp. 1480-1484, Nov. 1989.
- S.G. Tanyer A.E. Yılmaz and F. Yaman, "adaptive desirability function for multiobjective design of thinned array antennas," Journal of Electromagnetic Waves and Applications, Vol. 26, Nos. 17–18, pp. 2410-2417, December 2012.
- K. R. Mahmoud, M. El-Adawy, S. M. M. Ibrahem, R. Bansal, and S. H. Zainud-Deen, "A comparison between circular and hexagonal array geometries for smart antenna systems using particle swarm optimization algorithm," Progress In Electromagnetics Research, Vol. 72, pp.75-90, 2007.
- W. Spears and V. Anand, “A study of crossover operators in genetic programming,” in Methodologies for Intelligent Systems, ser. Lecture Notes in Computer Science, Z. Ras and M. Zemankova, Eds. Springer Berlin Heidelberg, vol. 542, pp. 409-418, 1991.
- P. Lopez, J. A. Rodriguez, F. Ares, and E. Moreno, “Low-sidelobe patterns from linear and planar arrays with uniform excitations except for phases of a small number of elements,” Electron. Lett., vol. 37, no. 25, pp. 1495-1497, Dec. 2001.
- R. S. Elliot, Antenna theory and Design, John Wiley & Sons. Inc.. Hoboken. New Jersey, 2003.
- T. Dattoma, M. Grande*, R.Marani, G.Morea, V.Marrocco and A. D'Orazio, "Resonance Wavelength Dependence Andmode Formation in Gold Nanorod Optical Antennas with Finite Thickness" Progress In Electromagnetics Research B, Vol. 30, 337-353, 2011.
- Stefan Alexander Maier, “Plasmonics: Fundamentals and Application,” Springer (2007).
- Peter E. Dewdney, Peter J. Hall, Richard T. Schilizzi, and T. Joseph L. W. Lazio, "The Square Kilometre Array" Proceedings of the IEEE, Vol.97,No.8,August 2009.

- A. El-makadema, L. Rashid and A. K. Brown, "Geometry Design Optimization of Large-Scale Broadband Antenna Array Systems," in IEEE Transactions on Antennas and Propagation, vol. 62, no. 4, pp. 1673-1680, April 2014.
- Eleonora Petryayeva, Ulrich J. Krull, "Localized surface plasmon resonance: Nanostructures, bioassays and biosensing—A review" Analytica Chimica Acta 706, 8– 24 (2011).
- Leandro dos Santos Coelho, Cezar Augusto Sierakowski, "A software tool for teaching of particle swarm optimization fundamentals" Advances in Engineering Software 39 (2008) 877–887.
- Kalyanmoy Deb, "Multi-Objective Optimization Using Evolutionary Algorithms: An Introduction" KanGAL Report Number 2011003, February 10, 2011.

Chapter 2

Main Beam Controlling Planar Antenna Array Design and Synthesis

In context of the sensitive observation of the universe through the coming radio spectrum, ultra-sensitive radio telescopes are required. Antenna arrays with aperture size varying from few meters to millions of meters (covering a frequency range from 30 GHz to 70 MHz) are being used for the application in the project called Square Kilometer Array (SKA) along with the state of the art signal processing circuitry. In this chapter, the proposed planar array has been investigated to match the high spatial resolution and high sensitivity requirements of the SKA, and satellite applications where power conservation and minimum adjacent channel interference are the prime requirements. The proposed planar array has 484 elements arranged hexagonally with elements eliminated from the four corners resulting in a planar array of variable string length. The proposed design with the introduction of non uniformity in element arrangement along the orthogonal axis offers a well controlled and elliptically shaped main beam. In addition, Optimized thinned configuration of the array has been obtained to have minimum side lobe peaks and high directivity by applying modified Binary Genetic algorithm. Design induced modification in the heuristic search has been made and a double stage uniform crossover operation has been proposed to make the whole process an effective uniform crossover. Array factor (AF), forming the cost function with the constraint of uniform side lobe pattern, has been derived for the proposed design. At first, the design has been examined for side lobe peaks along with their pattern, and directivity in the orthogonal planes ($\phi = 0$ and $\phi = \pi/2$). This gives an idea about the performance of the synthesis technique in particular directions.

For direction specific optimization, design offers directivity on the order of 32 dB and a peak side lobe level on the order of -25 dB. A comprehensive investigation involving optimization in all the planes with full scan range of ϕ from 0 to π has been carried out for the design giving side lobe peaks on the order of -20 dB and directivity on the order of 30 dB. The achievable 3 dB beam width with the proposed design is 0.088, which evidently fulfils the high resolution requirement of SKA applications. A performance comparison with several state of the art synthesis methods show that the proposed design in combination with the

modified heuristic approach can provide high directivity and low beam width, well controlled main beam and a radiation pattern with quite competitive side lobe peaks.

2.1. Introduction

In the quest of a properly shaped main beam and competitive values of other performance parameters of antenna array, a solution comprising selection of the design and optimized excitation of the array elements has been proposed. Tailoring the main beam to focus the radiation to the desired area without the need of complex and costly attenuators and amplifiers network is one of the main advantages of this approach.

In the proposed work, emphasis on the array geometry to achieve the goal for the above mentioned applications has been given. Unlike previously reported work, hexagonal array geometry with 484 elements has been chosen to have a well controlled main beam with elliptical shape which also has its impact on beam width. Two arrays with variable string length have been interlaced to form the resultant geometry of the array. Variable string length geometry has the minimum non contributing elements in resultant radiation pattern. Moreover, the most contributing and main beam controlling centre elements remain intact with variable string length. The design with elements arranged hexagonally avail geometry associated advantages of high directivity, radiation pattern flexibility and less element density requirement for the same coverage area [L. C. Kretly et al., 2002; K. R. Mahmoud et al., 2007]. After geometry selection the optimized array thinning configuration (Figure.2.8) has been obtained for minimum side lobe peaks and high directivity using the Binary GA. Geometry induced modification has been done in GA and a Double stage uniform crossover operation has been proposed. More on the proposed array geometry and optimized thinned array configuration has been discussed in the next sections.

Initially the design has been optimized in the orthogonal planes, giving the optimum side lobe radiation pattern with quasi constant height of the side lobe levels. Orthogonal radiation patterns with variation in their beam width confirm the elliptical shape of main beam, obtained with the design. After this, a comprehensive optimization of the design, covering the whole region with full scan range of θ and φ ($-\pi/2$ to $\pi/2$ and 0 to π, respectively) has been presented. Cases of isotropic elements, elements with $\cos\theta$ pattern, and steering of the main beam has been discussed. In the end, the proposed work has been compared with some state of the art antenna synthesis approaches on the performance

parameters required for satellite applications and for the SKA project to make highly sensitive radio telescopes.

2.2. The design

A thinned planar antenna array with square geometry and 200 elements was first optimized in [R. L. Haupt, 1994] for its minimum side lobe peaks in two azimuth planes. This was the simplest planar array design to optimize and the optimum solution had an approximate value of minimum side lobe peak of -20 dB in both the planes. Since then a wide research on linear array optimization has been done [R. L. Haupt,1994], [K.-K. Yan and Y. Lu, 1997; F. Ares-Pena et al., 1999; D. Marcano and F. Duran, 2000; Y.-B. Tian and J. Qian, 2005; L. Zhang et al.,2010; E. Hassan and H. Ragheb, 2012] but as far as planar arrays are concern there is a requirement of exploration of new planar array geometries and their optimization.

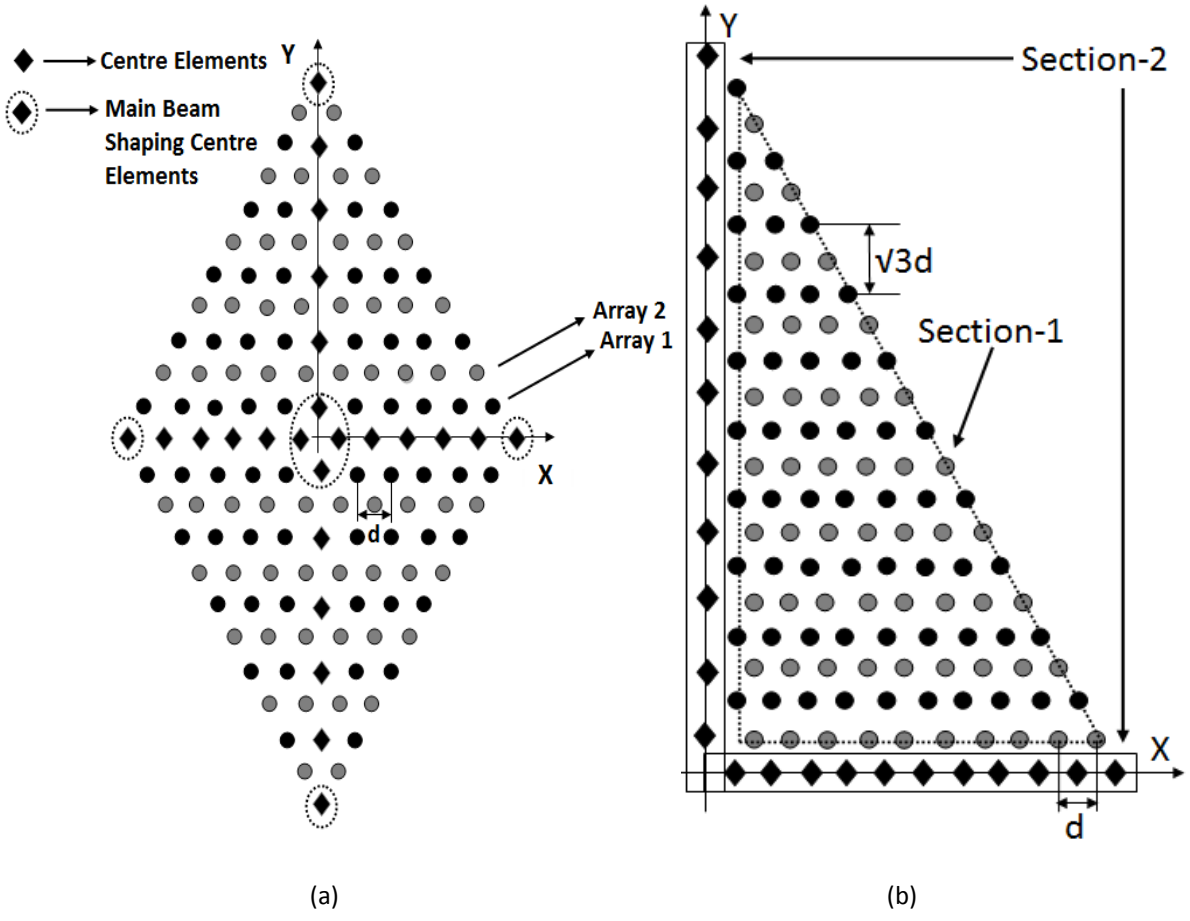

Figure 2.1 The proposed hexagonal planar array antenna geometry. (a) Hexagonal planar array antenna with 484 elements arranged hexagonally. Circles with different colours are denoting the elements of two distinct arrays collectively forming the whole array. (b) The elementary block of the array which gets repeated in the array containing two sections of the block. Each section (section-1 and section-2) has its different repetition rate.

Selection of the array geometry to have a particular shaped main beam in addition with thinning of the array to have improved side lobe pattern and high directivity performance can provide a better solution in comparison to the multi objective search approaches in which either main beam shaping or other performance parameters have to be compromised [D. H. Werner and A. J. Ferraro, 1989; D. S. Weile and E. Michielssen, 1996; Joshua S. Petko and Douglas H. Werner, 2011]. In the presented work, hexagonal planar array antenna geometry has been proposed with all the 484 elements arranged periodically in hexagonal manner. The number of elements of the proposed array have been selected on the basis of a comprehensive antenna array synthesis with different number of elements carried out in [Will P. M. N. Keizer, 2014]. A square geometry of dimension 12/12 corresponding to a total number of 144 elements could not provide improved side lobe levels as with the synthesis approaches proposed in [Will P. M. N. Keizer, 2014] the achievable side lobe peak with 144 elements was -17.6 dB. Further improvement in the side lobe peaks requires increment in the number of elements. From [Will P. M. N. Keizer, 2014], a geometry of dimension 24/24 corresponding to a total number of 576 elements offers maximum side lobe peak on the order of -22 dB, whereas a geometry of dimension 30/30 corresponding to a total number of 900 elements offers maximum side lobe peak on the order of -24 dB. Here it can be observed that with 1.5 times of increment in number of elements causes only 2 dB of side lobe level improvement. Side lobe improvement is significant for a 24/24 geometry in comparison to a 12/12 geometry. So, it is desirable to achieve improved side lobe with less number of elements and a 24/24 geometry better suits for this objective .In our proposed design, we have taken a planar array with varying string length. The string which has maximum length posses 22 elements and this string lies on the centre of the array. The string length reduces as we move away from the origin. Section-1 and section-2 of the elementary block (shown in Fig. 2.1(b)) contain non central elements and central elements, respectively. There are total 440 non central elements and 44 central elements which collectively forms an array with 484 elements which corresponds to a square geometry of 22/22. The maximum side lobe peaks with HSPSO, IFTDT and RDT with square geometry of 24/24 were -19.0 dB, -22.8 dB, and -20.7 dB, respectively [Will P. M. N. Keizer, 2014]. Proposed design can prove its edge over these synthesis approaches even if it can perform similar to these techniques with relatively less number of elements

Hexagonally arranged elements provide high steerability and directivity of the main beam and require approximately 30% less elements in comparison to the square geometries

for same coverage area [L. C. Kretly et al., 2002; K. R. Mahmoud et al., 2007]. As we can see in Figure.2.1 (a) Each element has a distance d with its nearest neighbour and this distance is called pitch of the geometry and in the present case it has been taken half of the wavelength (λ/2). Tailoring of the whole array Geometry is inspired by the fact that the elements at the corners of the planar array has least involvement in resulting radiation pattern and hence can be omitted in order to have cost efficiency [R. L. Haupt,1994]. The elimination of corner elements leads to a design which has varying string lengths within the chromosome as we move along y axis. As we can see that the array forms its mirror image on both side of the axis. The whole array is repetition of the triangular elementary block (shown in Figure. 2.1 (b)) about the axis. This elementary block has two sections denoted as section-1 (represented by dotted triangle in Figure.2.1 (b)) and section-2 (represented by solid rectangles in Figure.2.1 (b)) and these two sections have their own repetition rate in the whole array. As we can see in figure2.1 (b) that section-1 is formed by the non-central elements which are divided by the centre lines and have their mirror image around both x and y axis. Elements of section-1 are represented by circles and this section can be assumed to be a combination of two similar dimension arrays. These two arrays are differentiated by two different colour circles that are black and gray. Displacing one array with respect to another along x axis by a certain amount creates the hexagonal geometry. This assumption of two distinct planar arrays with relative displacement simplifies the analysis of the design. Section-2 of elementary block is formed by the central elements which lie on the centre lines or on the axis, and these elements are represented by squares in Figure.2.1. The four edge elements and the centre four elements are used to control the shape of the main beam and the radiation pattern, respectively (see Figure.2.1). Centre elements on x axis have their mirror image around origin in x axis only and centre elements on y axis have their mirror image around origin in y axis only. In this manner the elements of section-2 get repeated one time only whereas, elements of section-1 get repeated three times in the design of whole array.

The spacing d between the two antenna elements has been taken λ/2. In case of a planar array with elements arranged in square form, the spacing between the adjacent elements varies with direction, whereas in the proposed hexagonal design the adjacent element spacing remains constant with direction. The geometry associated non uniformity in periodicity of central elements along the x axis and y axis forms the shape of the main beam and this shape remain preserved with array thinning through the shape controlling elements (Figure.2.1).

2.3. Optimization of the Design

In the optimization of the design to have minimum side lobe peaks maintaining the optimal distribution, high directivity and properly shaped main beam, it is required to have a particular configuration of elements which are off and on i.e. connected to matched load and feed network respectively. For such a large antenna array, one of the potential ways to obtain the optimum thinned configuration is to use binary genetic algorithm. The binary GA has been one of the initial uses of GA [R.L. Haupt and D. H. Werner,1995] for antenna design and it is a natural selection for the design being discussed here. In binary GA, an on state is represented by '1' and an off state is represented by '0' [R.L. Haupt and D. H. Werner,1995].

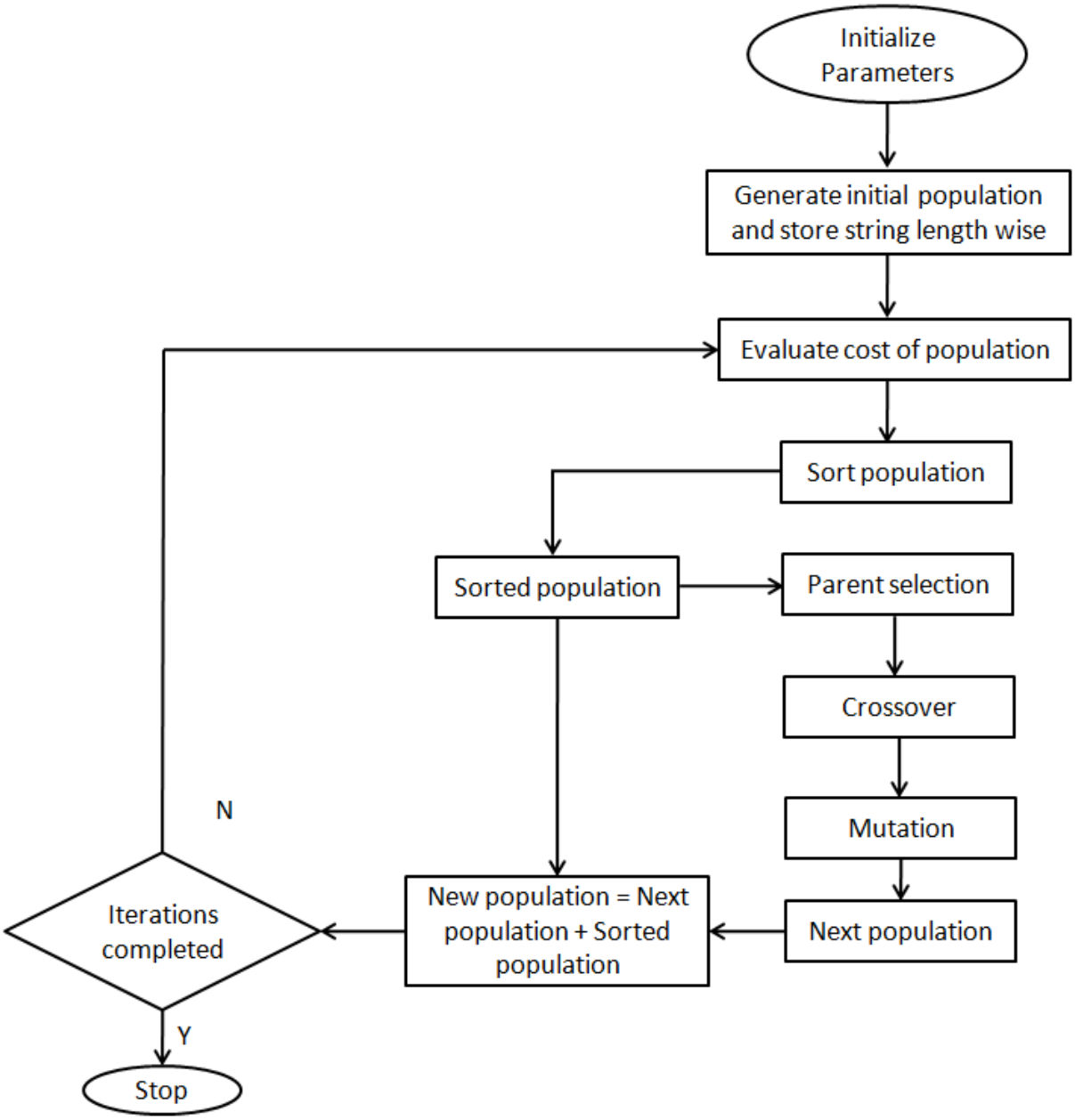

Figure 2.1 Flow chart of the evolution

The optimization algorithm is shown in Figure. 2.2, which is similar to the conventional GA [R.L. Haupt and D. H. Werner,1995], [D. Marcano and F. Duran,2000] but some changes to the genetic algorithm operations for conventional planar array optimization have been made according to the varying string length hexagonal structure of the antenna. The cost calculation of the proposed design has been carried out on the basis of array factor [D. Marcano and F. Duran,2000]. Formulation of the array factor for cost calculation of proposed design has also been proposed.

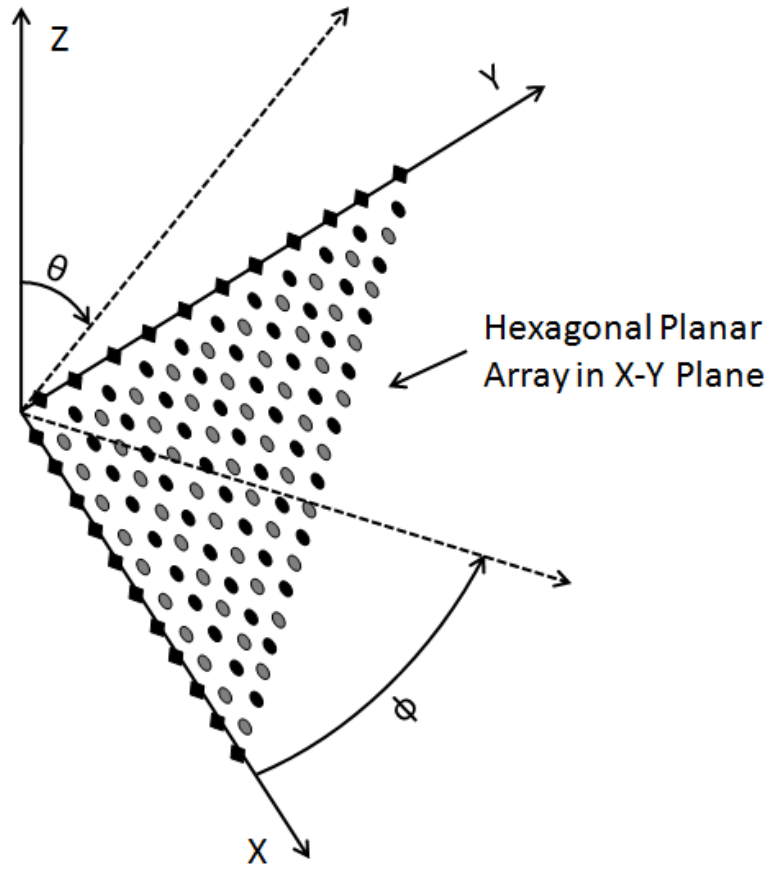

Figure 2.2 Coordinate system for the analysis of the design showing antenna in xy plane with variation of azimuth and elevation angles from 0 to π/2.

Initial population of 484 elements with varying string length planar geometry and adjacent separation of d=λ/2 is generated. The centre four elements (figure.2.1) are always turned on because low side lobe amplitude tapers always have a maximum at the centre. A controlled and effective elliptical main beam is obtained by keeping the four edge elements on x and y axis (shown in Figure. 2.1(a)) always one [D. Marcano and F. Duran,2000]. The periodicity of the array elements along the x and y axis varies in order to have the whole arrangement of

array elements hexagonal. This design requirement helps to obtain the desired elliptical shape of the main beam as the main beam width has a dependency on the array element spacing [Balanis, "Antenna Theory: Analysis and Design", 1997]. Since the proposed Hexagonal antenna array design varies from the conventional rectangular planar array antenna design in its elemental arrangement and dimensions, the cost for optimization of the proposed design cannot be estimated directly as in the case of a simple rectangular planar array antenna. In conventional rectangular planar array antenna the array factor or far field of the antenna is calculated and normalized to its maximum value giving the cost function of the planar antenna array [R. L. Haupt,1994]. The array factor calculation of the proposed design has been carried out in different steps giving the final expression of the array factor.

As shown in Figure 2.1, the calculation of the array factor for the proposed planar array geometry could be understood on the basis of its elementary block (Figure 2.1(b)). As discussed in the design section, this elementary block is further divided into two sections, section 1 and section 2, depending upon the position of the array elements in these sections. Now, in order to calculate the array factor for the whole array, individual array factors for the central and non central elements have been calculated and these array factors collectively forms the expression of array factor for the design. The expressions of array factor for non-central element arrays of section-1 are given by [R.L. Haupt and D. H. Werner,1995**]**

$$AF_{11}(\theta,\phi) = \sum_{n=0}^{N_1-1}\sum_{m=0}^{N_1-n-1} I_{mn}^{nc1} e^{i[k(m+1)d\sin\theta\cos\phi + k(n+0.5)\sqrt{3}d\sin\theta\sin\phi + \delta_{mn}]} \tag{2.1}$$

$$AF_{12}(\theta,\phi) = \sum_{n=0}^{N_1-1}\sum_{m=0}^{N_1-n-1} I_{mn}^{nc2} e^{i[k(m+0.5)d\sin\theta\cos\phi + k(n+1)\sqrt{3}d\sin\theta\sin\phi + \delta_{mn}]} \tag{2.2}$$

The expressions of array factor for central element arrays of section-2 are given by

$$AF_{21}(\theta,\phi) = \sum_{m_0=0}^{N_2-1} I_{m_0}^{c_1} e^{i[k(m_0+0.5)d\sin\theta\cos\phi + \delta_{m_0}]} \tag{2.3}$$

$$AF_{22}(\theta,\phi) = \sum_{n_0=0}^{N_2-1} I_{n_0}^{c_2} e^{i[k(n_0+0.5)\sqrt{3}d\sin\theta\sin\phi + \delta_{n_0}]} \tag{2.4}$$

Now, the expression of the array factor for whole hexagonal planar antenna array is given by

$$AF_{Hexagonal} = AF_{11} + AF_{12} + AF_{21} + AF_{22} \tag{2.5}$$

The proposed design has been optimized to achieve minimum value of maximum relative side lobe level keeping the constraint of uniform side lobe levels in order to have the optimum solution. The cost function for optimization is given by

$$cost_{Hexagonal} = max\left|\frac{AF_{Hexagonal}}{(AF_{Hexagonal})_{max}}\right| \; for\; \theta \geq \theta_{FN} \tag{2.6}$$

Uniformity constraint is applied with standard deviation (SD) as

$$min\left[\sum \sigma_{\phi_n}\right], \qquad n = 1,2,..N \tag{2.7}$$

$$\sigma_{\phi_n} = \sqrt{\frac{1}{r-1}\sum_{i=1}^{r}[sll_i - sll_{avg}]^2} \tag{2.8}$$

Where

$AF_{11} = Array\ factor\ of\ non-central\ element\ array\ first\ of\ section-1$

$AF_{12} = Array\ factor\ of\ non-central\ element\ array\ second\ of\ section-1$

$AF_{21} = Array\ factor\ of\ central\ element\ array\ on\ x\ axis\ of\ section-2$

$AF_{22} = Array\ factor\ of\ central\ element\ array\ on\ y\ axis\ of\ section-2$

$N_1 = Number\ of\ elements\ in\ the\ longest\ string\ of\ non-central\ \ array\ one\ or\ array\ two\ \ of\ section-1$

$N_2 = Number\ of\ elements\ in\ the\ central\ array\ on\ x\ axis\ or\ y\ axis\ of\ section-2$

$I_{mn} = Amplitude\ of\ m^{th}\ element\ in\ n^{th}\ string$

$\mathrm{I}_{m_0}^{c_1} = Central\ element\ excitation\ along\ x\ axis$

$\mathrm{I}_{n_0}^{c_1} = Central\ element\ excitation\ along\ y\ axis$

$\delta_{mn} = Excitation\ phase\ shift\ of\ m^{th}\ element\ in\ n^{th}\ string\ of\ array$;

$for\ in\ phase\ excitation, \delta_{mn} = 0$

$u = \sin\theta\cos\phi; v = \sin\theta\sin\phi; \theta_{FN} = first\ null\ angle$

σ_{ϕ_n} = Standard deviation of SLL in n^{th} plane corresponding to ϕ_n; r is the number of randomly selected samples of SLL to calculate SD in n^{th} plane.

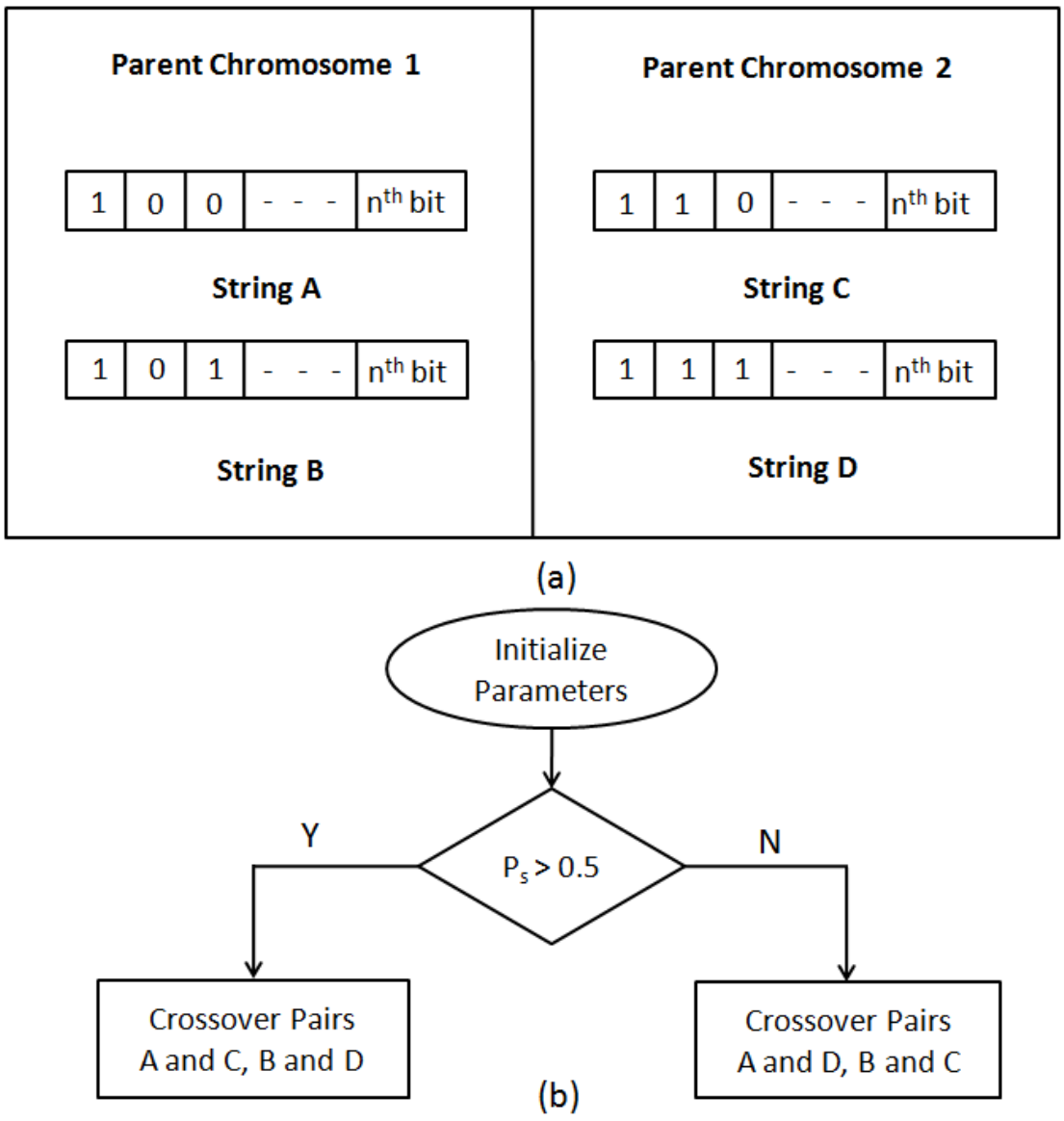

Figure 2.3 A two stage uniform crossover. (a) Strings of same length for crossover between the two parent chromosomes. (b) Flowchart of the crossover.

Cost function defined in Eq. 2.6 gives the normalized values of side lobe peaks and the search objective is to find the configuration of antenna elements which has minimum cost along with the uniform distribution of the side lobe levels to maintain the directivity of the design within a prescribed limit and to have minimum antenna noise [R.L. Haupt and D. H. Werner,1995]

[Ahmed El-makadema, 2014]. This equation assumes that the array lies in x-y plane (Figure 2.3) and it is symmetrical about x axis and y axis. After evaluating the costs of different configurations the generation is sorted by putting them in order from minimum cost configuration at the top to maximum cost configuration at the bottom. Selection of the parents is carried out using Roulette wheel selection method [R.L. Haupt and D. H. Werner, 1995] in which fittest parent gets highest probability of selection. Unlike conventional planar array the crossover can only be performed between the corresponding similar length strings.

Current search for the best results adopt uniform crossover and the choice has been made on the basis of the comparative study carried out in [W. Spears and V. Anand, 1991] showing best results for uniform crossover in case of large search space. The crossover operation for two sections of elementary block is performed separately. Figure 2.4 shows a double stage uniform crossover operation algorithm for section one. In this section the crossover is performed between the strings of same length of the two parent chromosomes. There are two strings of same length corresponding to the two different arrays within the same parent chromosome hence each string of first parent chromosome has two choices for crossover in the second parent chromosome. Probability of selection P_s of both the string has been kept equal and after selection of the strings the uniform crossover operation has been performed consequently making the whole crossover process a uniform crossover in order to have best results. In case of section two of elementary block uniform crossover is performed between the central elements of corresponding axis of the two parent chromosomes. The newly generated chromosomes are now applied to random variation through the process of mutation. Mutation diversifies the search and avoids the search to be stuck in local minima. A new pool of chromosomes is now checked for their cost and improvement from the previous generation is carried to the next iteration of GA. The proposed design has been investigated to obtain optimum results up to a maximum of 1000 GA iterations.

2.4. Results and Discussion

The proposed design has been analyzed for optimum side lobes, directivity and the shape of the main beam and GA in combination with the proposed array geometry has been applied to obtain optimum results. In the first section, the performance of the design has been checked over two planes in order to check the method for directional optimization. One is x-z plane at $\phi = 0$ and second one is y-z plane at $\phi = \pi/2$ (see Figure 2.3).

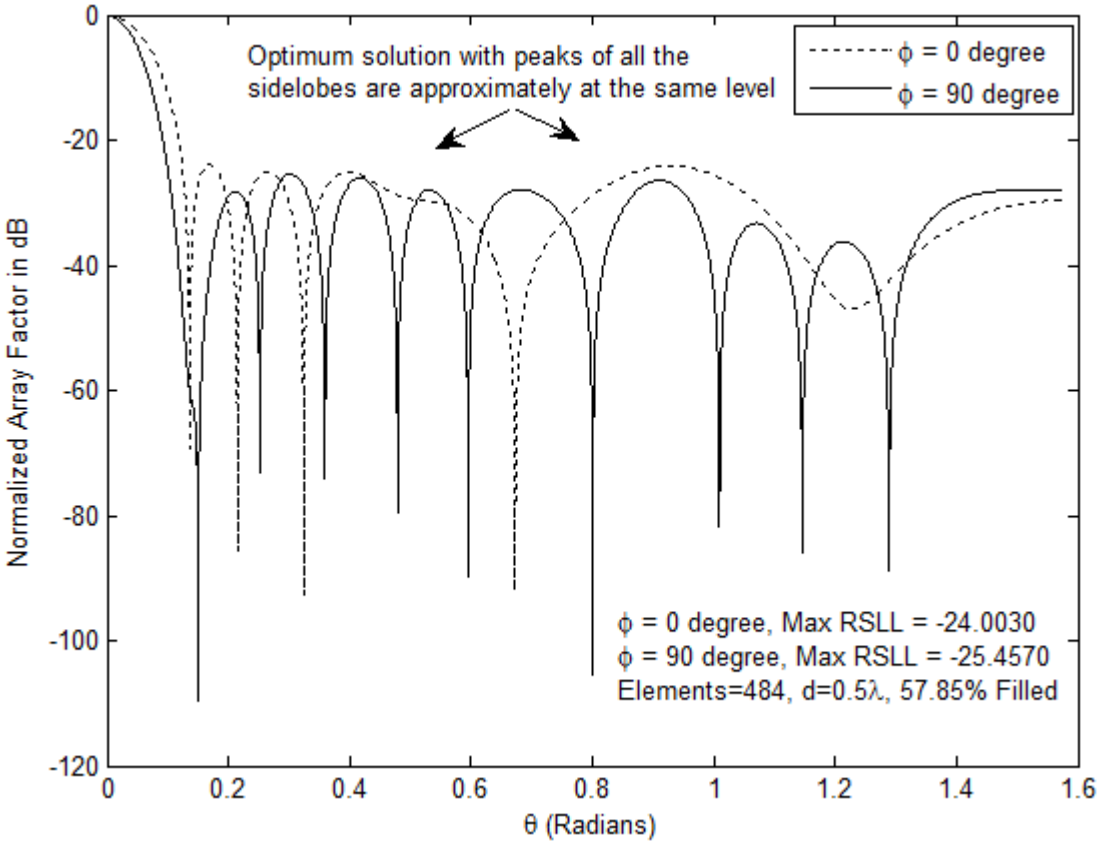

Figure 2. 4 (a)

This analysis gives an idea about beam shape and directivity along with its side lobe level reduction in the two extreme planes of the antenna. The design has been investigated for both isotropic elements and elements with certain element pattern. Second section of the analysis contains a comprehensive investigation of the design with both the angles (azimuth and elevation) scanning through the full range, $\phi = 0$ to π and $\theta = -\pi/2$ to $\pi/2$. This multidimensional Optimization of the design with variation of both azimuth and elevation angles gives a comprehensively optimum design performing well at all the parameters mentioned above.

2.4.1. Two Plane Optimization of the Design

Space tapering reduces the maximum side lobe level but at the same time increases the lowest side lobe level. In an optimum solution the peaks of all the side lobes are at about the same level [R.L. Haupt and D. H. Werner, 1995]. As discussed earlier in this section, results for side lobes and directivity of 484 hexagonally arranged elements with element spacing of 0.5λ have been analyzed. In two plane optimization the cost of selection is based on the total cost of the two planes i.e. the solution will have a balance between the maximum relative side lobe levels (RSLLs) in the two orthogonal planes. Figure 2.5(a) shows the side lobes of

hexagonal array of 484 isotropic elements in orthogonal planes ($\phi = 0$ and $\phi = \pi/2$) after 10^{th} generation of GA with end fire ($\theta = 0$ degree) main beam forming. Quite low values, on the order of -24 dB to -25 dB, of side lobe peaks have been obtained with all the side lobe peaks approaching approximately same level.

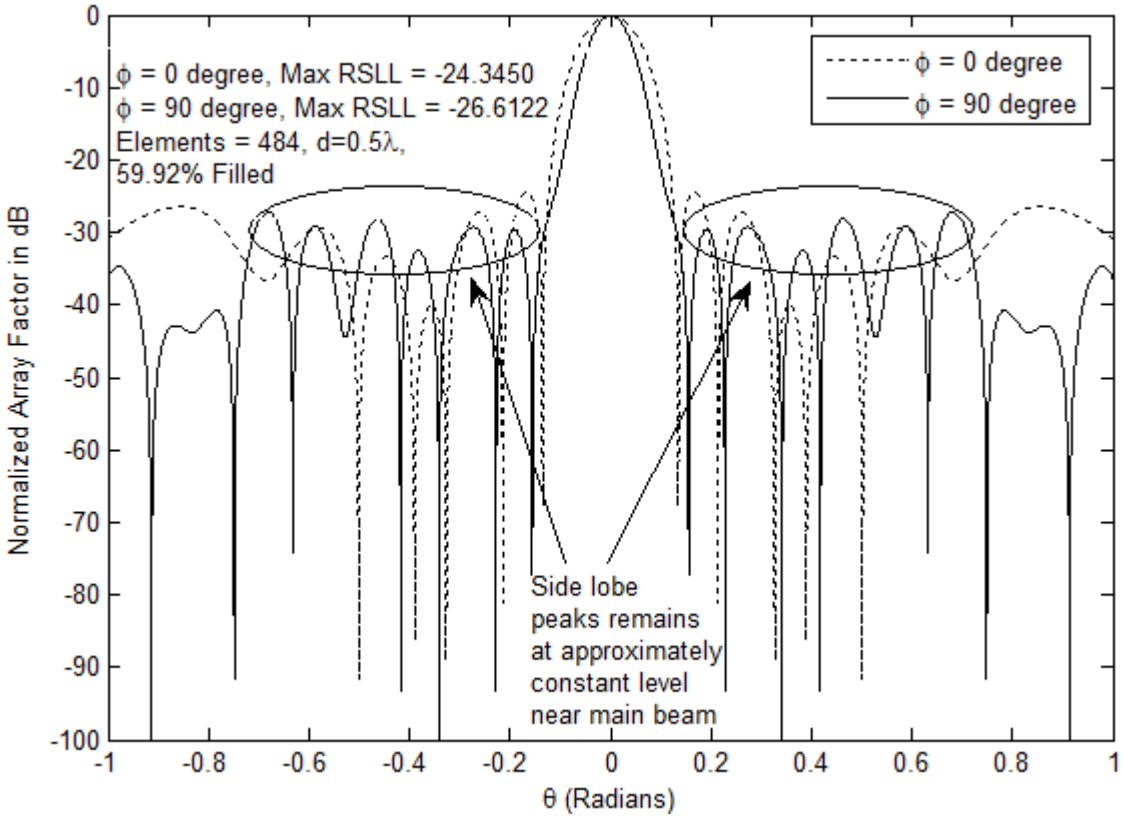

Figure 2. 5 (b)

Table 2. 1 Results of directivity and max RSLL after two plane optimization.

Element pattern	Iterations	Directivity in dB	Max RSLL at $\phi = 0^{\circ}$ in dB	Max RSLL at $\phi = 90^{\circ}$ in dB
Isotropic	10	31.7930	-24.0030	-25.4570
	100	32.0813	-24.3450	-26.6122
	1000	32.2969	-25.2405	-27.7471
$\cos\theta$ element pattern	10	32.4448	-24.0154	-24.5115
	100	31.9462	-24.0339	-29.0032
	1000	31.7453	-24.3825	-31.0687

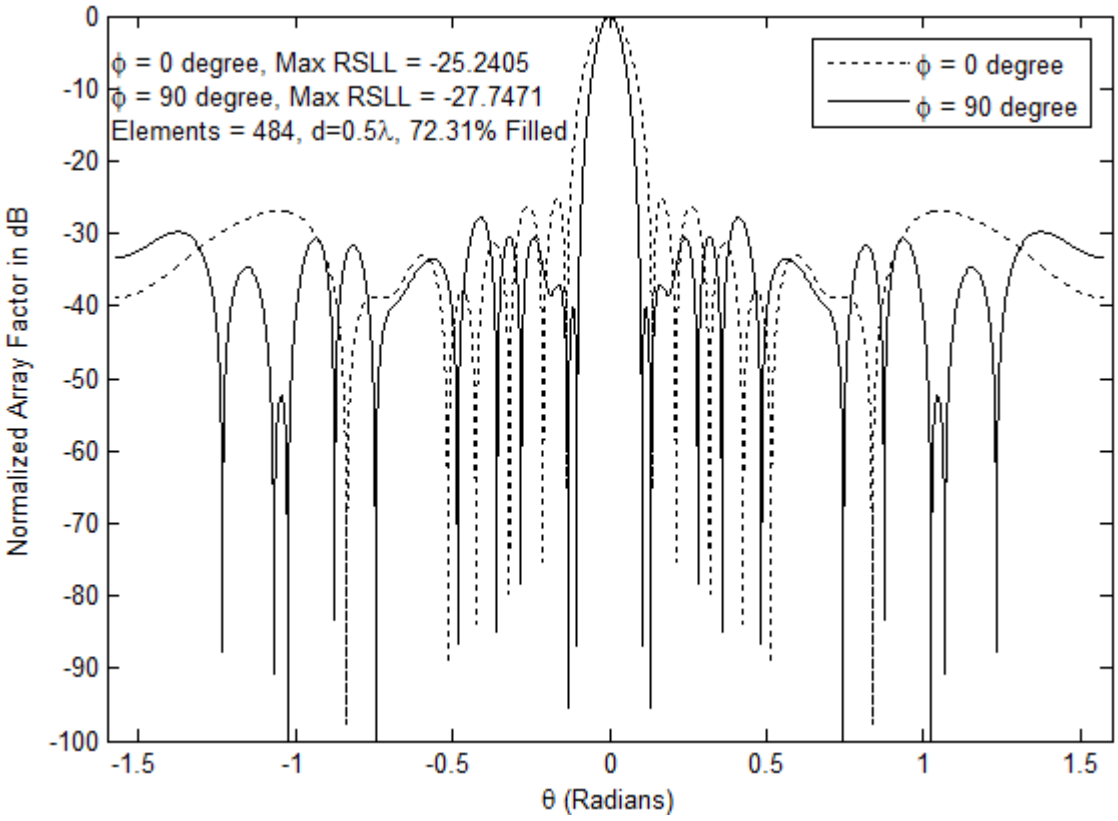

Figure 2. 6 (c)

Figure 2. 7 Radiation pattern of a Hexagonal planar array antenna of 484 isotropic elements in ϕ = 0 degree and ϕ = 90 degree planes. The results have been optimized with multiple GA runs and plotted for 10^{th} (a), 100^{th} (b) and 1000^{th} (c) generation of Genetic algorithm.

Further, figure 2.5(b) and 2.5(c) are showing the optimum results for maximum relative side lobe level (RSLL) of 484 isotropic element array after 100^{th} and 1000^{th} generation of GA in two orthogonal (x-z and y-z) planes. Max RSLL after 1000^{th} generation of GA approaches to a level less than -25 dB and -27 dB for ϕ = 0 and ϕ= π/2, respectively, with a 72.31% filled array. The three generation results for side lobe level improvement have been discussed in order to have an idea about the relation between side lobe improvements and fill factor of the thinned configuration, and to observe the pattern in regular intervals showing a proper trace of main beam shape and side lobe peak constraint. It is clear from the results that with a generation increment of 100 times (after 10^{th} generation), the reduction in side lobe is only of the order of -1 dB to -2 dB. It is to be noted here that the fill factor of the array increases quite significantly over the generations of GA. This trade off between power requirement and performance should be look after in accordance with the application of the design. More discussion on this has been done latter in this section.

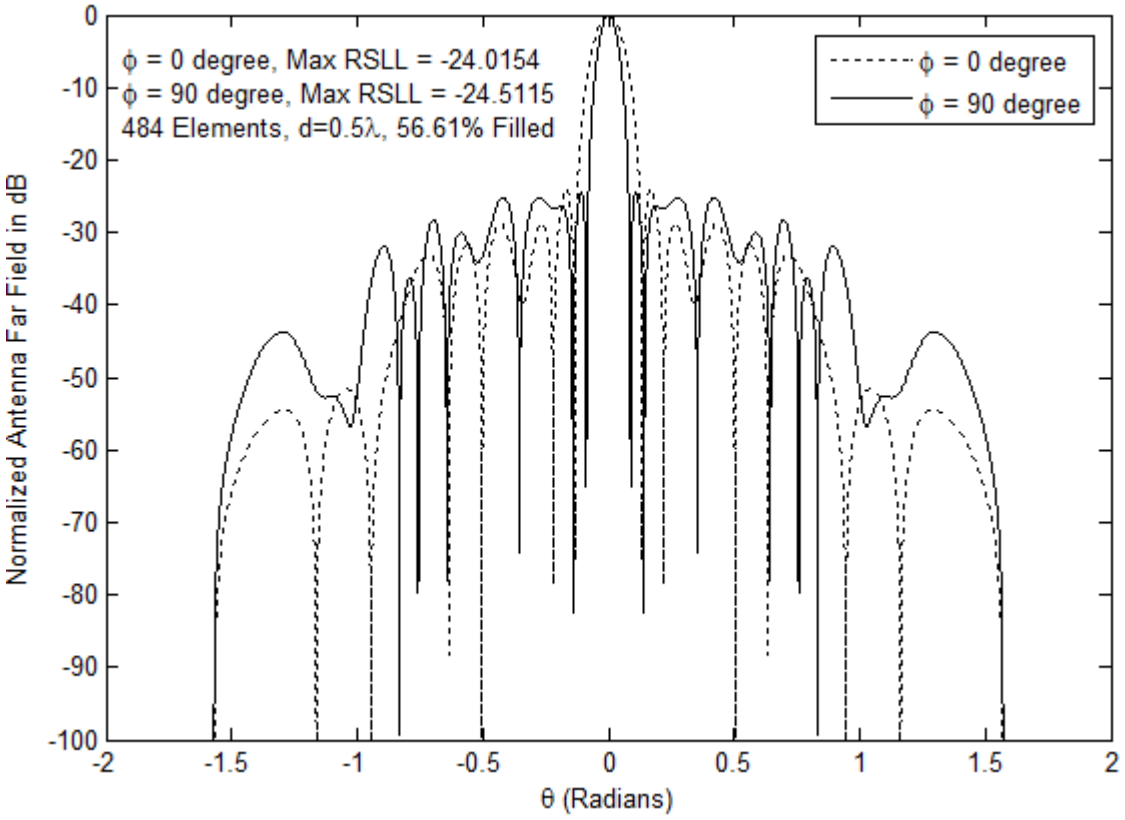

Figure 2. 8 (a)

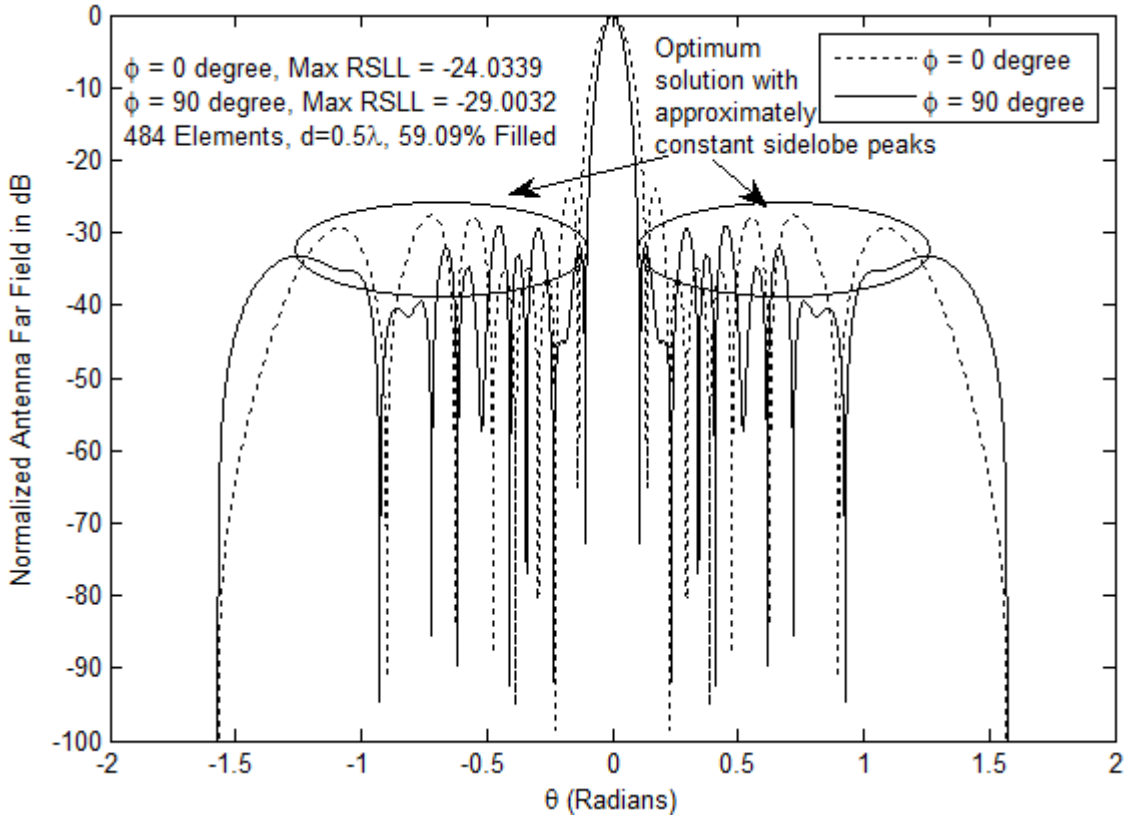

Figure 2. 9 (b)

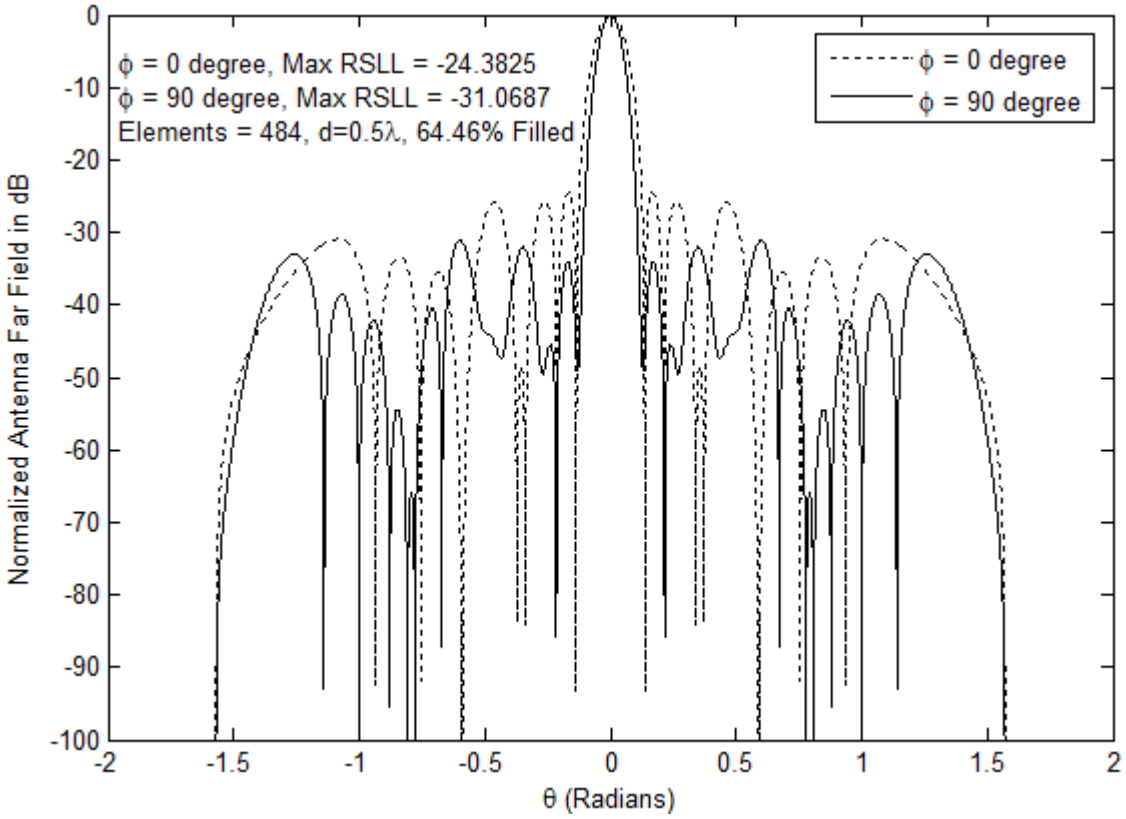

Figure 2. 10 (c)

Figure 2. 11 Radiation pattern of a Hexagonal planar array antenna of 484 elements in ϕ = 0 degree and ϕ = 90 degree planes with $|\cos\theta|$ element pattern. The figure provides detailed information of main beam and near main beam patterns of the optimized 10th (a), 100th (b) and 1000th (c) generation of Genetic algorithm.

Optimized side lobe peaks for the 484 element antenna array with $|\cos\theta|$element pattern, at 10th, 100th, and 1000th generation of GA, are shown in Figure 2.6. Improvement in the side lobes can be observed in case of elements with certain pattern in comparison to the isotropic elements. Max side lobe peak at ϕ = 90˚ drop down to a level more than -29 dB after 100th generation and it settles at a level more than -31 dB after 1000th generation of GA. The side lobe peaks at ϕ = 0˚ remains approximately constant throughout the evolution and in comparison to the observations for isotropic elements as well. From Figure 2.6 we should note that as the search evolves, the configuration comes with reduced side lobe peaks approximately maintaining the same level. From Figure 2.6(a), we can observe that side lobes after 10th generation has a slope in the side lobe peaks going down towards the edge whereas this slope disappears after 100th and 1000th generation (Figure 2.6(b)and 2.6(c)) with reduction in side lobe peaks. Table 2.1 summarizes the maximum RSLL values of hexagonal planar antenna array of 484 elements with isotropic and $|\cos\theta|$element pattern along with the corresponding values of directivity. Antenna directivity has been evaluated by calculating the ratio of maximum power radiated by the array in the direction $(\theta_{max}, \phi_{max})$ to the power

radiated by an isotropic radiator. It is given by the following expression as [Ahmed El-makadema, 2014]

$$D_a = \frac{4\pi F^2(\theta_{max}, \phi_{max})}{\int_0^{2\pi}\int_0^{\pi} F^2(\theta,\phi)\sin\theta\, d\theta d\phi} \tag{2.9}$$

As we can see high directive main beams with directivity on the order of 32 dB along with significantly reduced values of side lobe peaks have been obtained with the proposed design. The directivity is consistent with increment in iterations i.e. with reduction in the side lobe levels. Here the reciprocal relation between the beam width and side lobe peak have been controlled in an optimum way. Previously reported results, in [R. L. Haupt,1994] and [H. Wang et al., 2008] of side lobe peaks for planar antenna were on the order of -20 dB whereas, in this work comparatively quite reduced values of side lobe peaks have been obtained simultaneously with high directivity in the two, x-z and y-z, orthogonal planes.

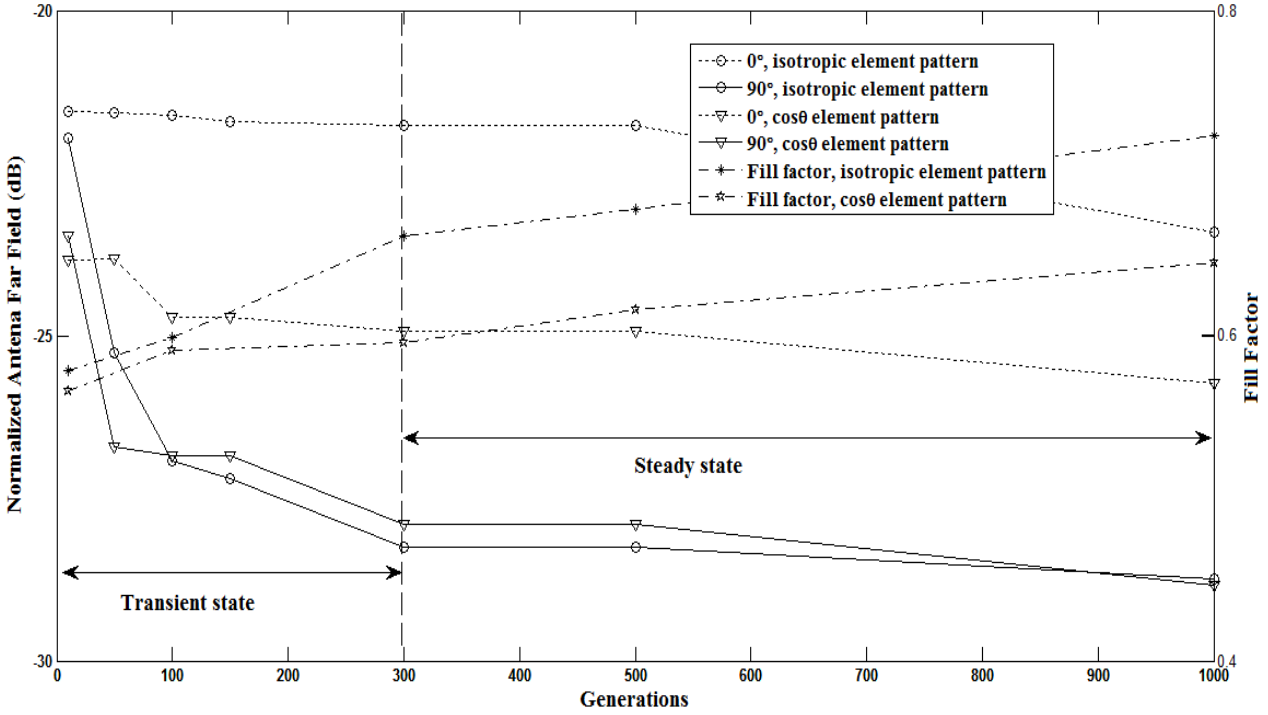

Figure 2.12 A comparison between array performance and power requirement for Hexagonal planar antenna array of isotropic elements and elements with $|\cos\theta|$ element pattern with varying generation of Genetic algorithm. The comparison has been carried out in ϕ = 0 degree and ϕ = 90 degree planes with θ varying from 0 to π/2 and generation varying from 10 to 1000.

Figure 2.7 shows a comparison and a trade off between performance and power requirement for the two cases of element excitations. The average side lobe peaks of hexagonal planar antenna with isotropic element pattern and with $|\cos\theta|$element pattern have been plotted with the fill factor of the corresponding array over the increment of GA generations. From

Figure 2.7, the transient and study states of the curves are showing the transformation of the side lobe reduction rate from high to low, especially in case of $\phi = 90^{\circ}$ plane. In $\phi = 0^{\circ}$ plane this transformation is comparatively stable. Power requirement by the array has been shown in terms of fill factor calculated by evaluating the ratio of turn on elements to the total number of elements in the array. In transient state the fill factor for isotropic element acquire a sharper slope in comparison to the elements with certain pattern. This leads to the higher power requirement of the array with isotropic elements. A selection of the performance in terms of side lobe level is required according to the bearable power requirement of the application. Here, array with $|\cos\theta|$ element pattern has outperformed the array with isotropic array elements in both the planes.

2.4.2. Comprehensive Optimization of the Design

Planar antenna arrays are now being investigated in the context of new generation radio telescopes (SKA) for the study of important phenomenon of the universe using wide band RF signals. Here, we have discussed the performance of the proposed planar array on the parameters such as directivity, side lobe radiation, main beam shaping and beam width, which plays an important role in the above mentioned application. Moreover, one of the important figures of merit in planar antenna applications for SKA is sensitivity. It is very important to design antennas which can be placed under different atmospheric conditions with very small variation in their sensitivity. As the atmospheric conditions play a very important role in deciding the antenna noise temperature and consequently the sensitivity of the antenna, a detailed analysis has been presented in chapter 5. This section includes the optimization of the proposed design in all the planes by varying the azimuth angle along with elevation angle i.e. for scan range of ϕ and θ from 0 to π and $-\pi/2$ to $\pi/2$, respectively. Here, we investigated the 484 element hexagonal planar antenna array for better side lobe peaks maintaining the constraint of side lobe uniformity, directivity and the shape of the main beam with isotropic elements and elements with certain element pattern. Effect of radiation pattern on performance by scanning the main beam at an angle of $\pi/4$ in both azimuth and elevation planes have also been investigated.

Distribution of the turned on elements across the aperture has been depicted in Figure 2.8. The centre elements of section 2, indicated with squares, are all turned on providing the controlled and desired beam shape with reduced side lobe levels. Element density distribution can be seen organised with four hexagons. The outer hexagon consist all active elements and

the inner (the densest) hexagon showing the elements which have highest effect on radiation pattern. Two small hexagons along the central line with six elements contribute to the main beam shaping. Note that a low side lobe amplitude taper always have maximum turned on elements near the origin and the turned on edge elements contribute to the main beam shaping.

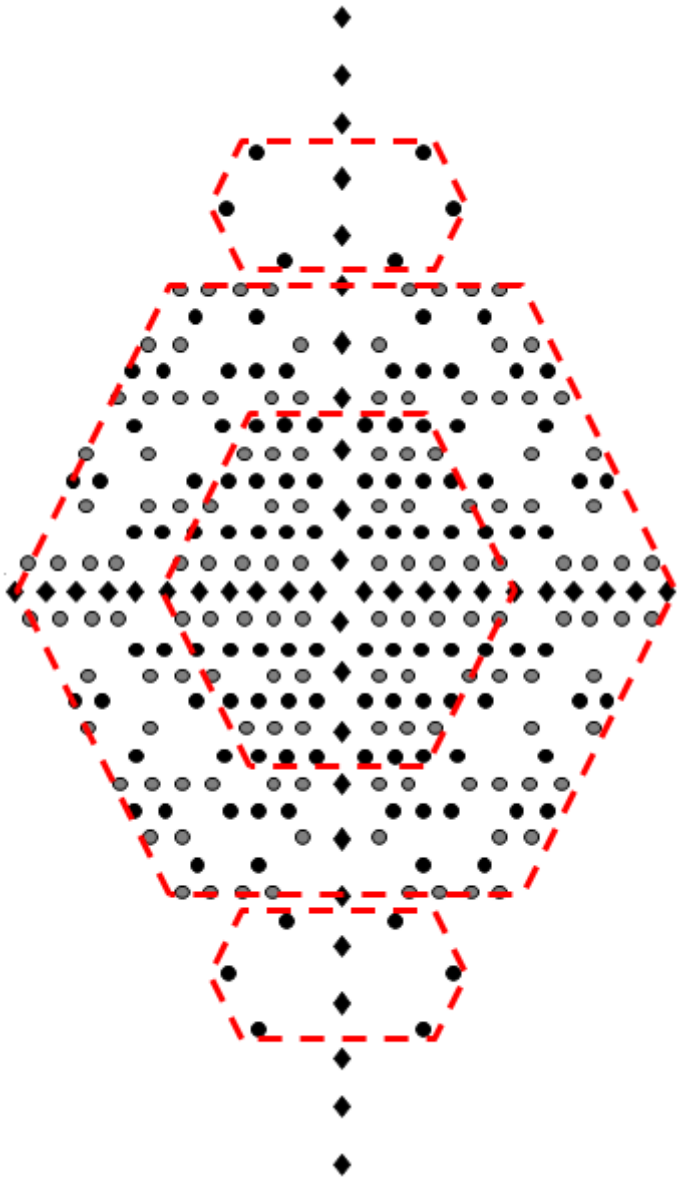

Figure 2.13 Optimized thinned configuration of the proposed array showing the active elements. Square elements are central, whereas circular are non central (inter displaced array elements indicated with gray and black color). Four hexagons, showing the organised element density distribution. Inner hexagon with highest density forms the pattern and small hexagons lying along the axis along central elements forms the main beam shape.

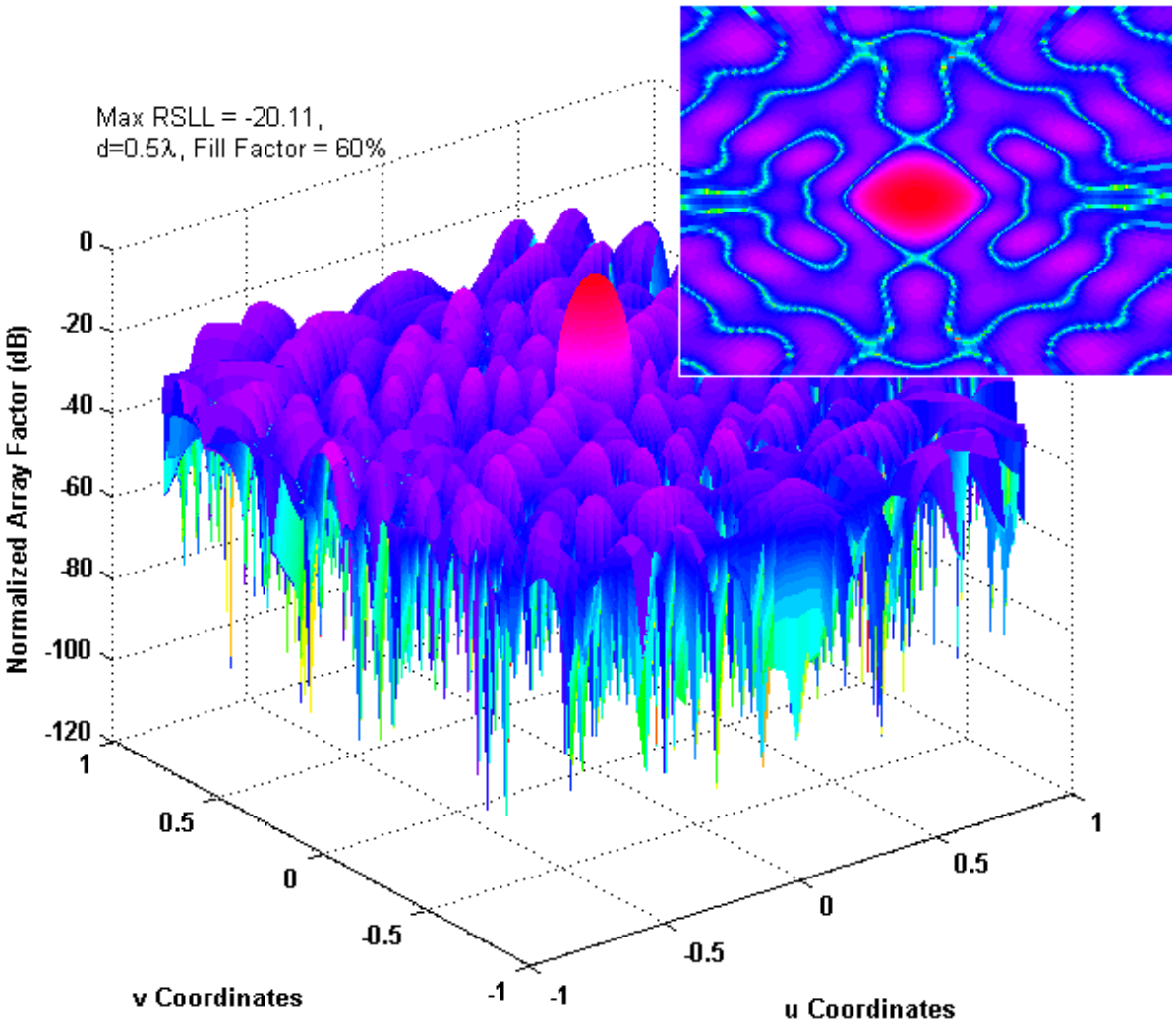

Figure 2.14 Radiation pattern of a Hexagonal planar array antenna of 484 isotropic elements. The result has been plotted for 1000th generation of Genetic algorithm. Inset is showing the main beam of the pattern.

Radiation pattern of the proposed hexagonal planar array antenna, obtained by varying the azimuth and elevation angles from 0 to π and - π/2 to π/2, respectively, has been shown in Figure 2.9. In this observation, the elements have been considered isotropic and the main beam is forming at θ= 0 degree (End fire). The maximum relative side lobe peak for the planar array is -20.11 dB, which is quite competitive with the results obtained with some recent synthesis approaches of array thinning [Will P. M. N. Keizer, 2014]. The proposed design with optimization also offers a directivity of 29.96 dB. The trade off between directivity and the side lobe pattern has been handled in an optimal way in order to have better performance on both the parameters. As shown in the inset of Figure 2.9, the desired shape of the main beam is well maintained. The requirement of the main beam shaping is essential for the satellite applications where coverage of the beam has to be precise.

Applications such as SKA, the design fulfils the most prime design requirements such as high directivity and lower side lobe peaks consequently reduced antenna noise [Ahmed El-makadema, 2014].

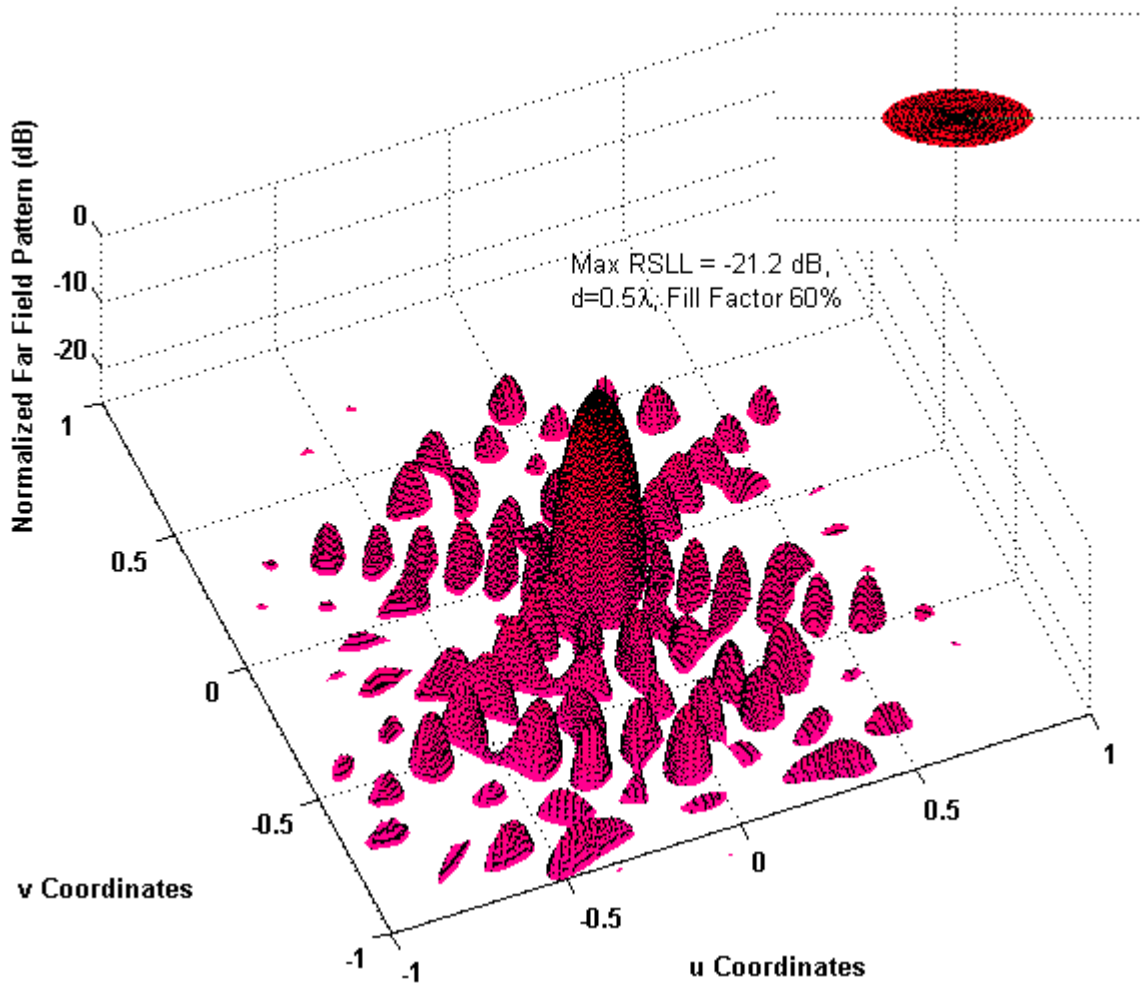

Figure 2.15 Radiation pattern of a Hexagonal planar array antenna of 484 elements with cos θ element pattern. Inset is showing the elliptical main beam, the shape remain intact with change in element pattern.

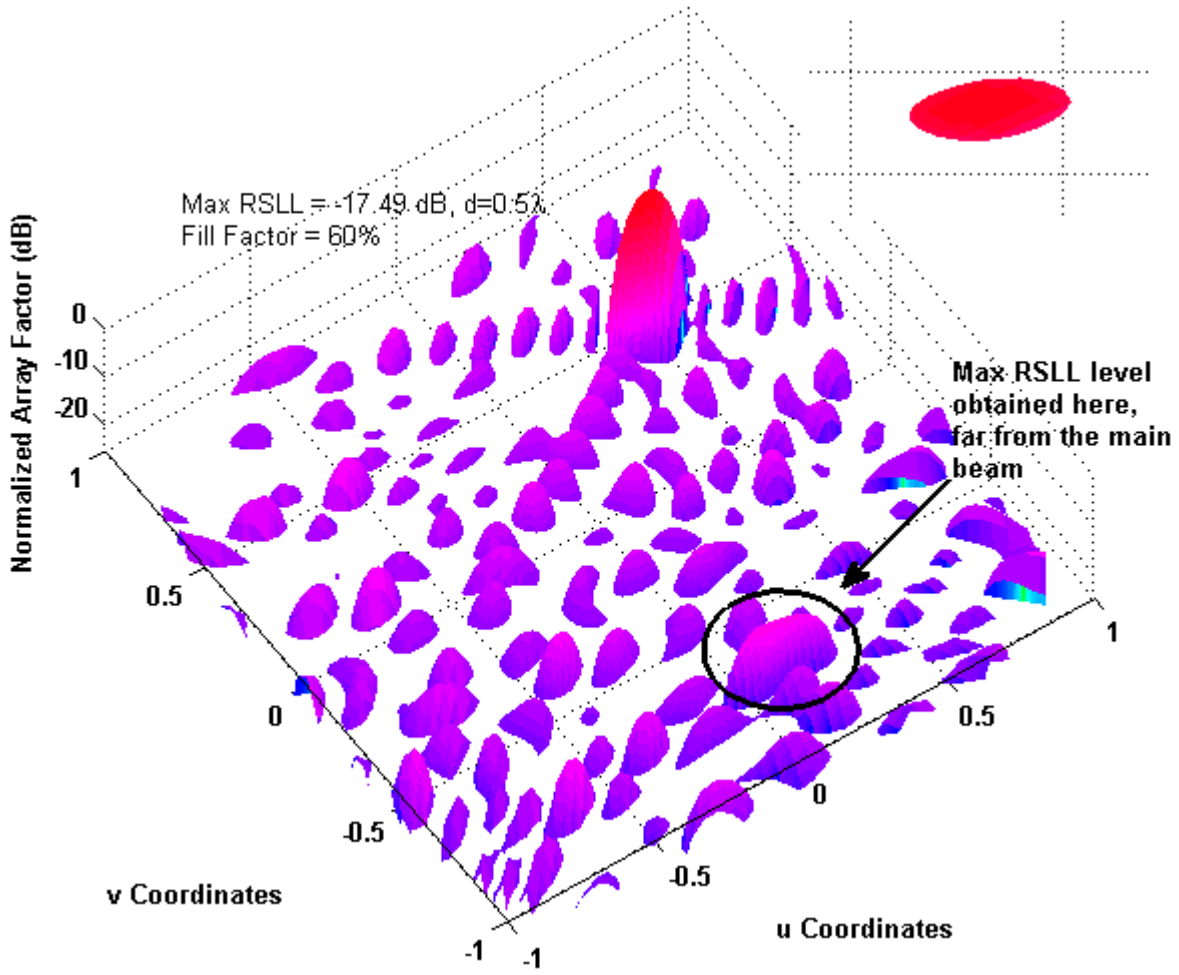

Figure 2.16 Radiation pattern of a Hexagonal planar array antenna of 484 elements with isotropic elements. The main beam has been steered at an angle of π/4 in both azimuth and elevation planes. The result has been plotted for 1000th generation of Genetic algorithm. Inset is showing the elliptical shape of the main beam after steering and the encircled region (far from the main beam) is showing the location of the max RSLL.

From Figure 2.10, an improvement in the side lobe level can be seen from the pattern obtained with isotropic elements and here the main beam shape remains intact with change in the array element pattern. This proves the significance of the design in order to achieve the desired shape of the main beam as in the proposed design the elliptical shape of the main beam is achieved due to the non uniformity in the periodicity of the elements along the orthogonal axis. The shape preserving edge elements of the array also have their key role in maintaining the shape of the main beam. This highly directive main beam offers a directivity of 30.39 dB, the inverse relation between the directivity [Balanis, "Antenna Theory: Analysis and Design", 1997] and side lobe levels has been controlled with the cascaded combination of proposed geometry and thinned array optimisation technique. Steering of the main beam ($\theta_0 = \frac{\pi}{4}, \phi_0 = \frac{\pi}{4}$; where θ_0 and ϕ_0 are the beam steering angles in elevation plan and

azimuth plan respectively) causes the pattern to degrade and it results in increment in the side lobe level hence degradation of the radiation pattern. As can be seen from Figure 2.11, the degradation is quite evident with increased side lobe level of -17.49 dB, although the proposed design has its influence on the main beam shape and it still remains intact with the change in direction of radiation. Note that, Pattern has its maximum RSLL quite far from the main beam (encircled region in Figure 2.11) and the side lobes near main beam are below the level of -20 dB, hence highly directive and less power losses in the desired direction of radiation. The directivity of 27.72 dB in case of the proposed design with steering of the main beam has been achieved.

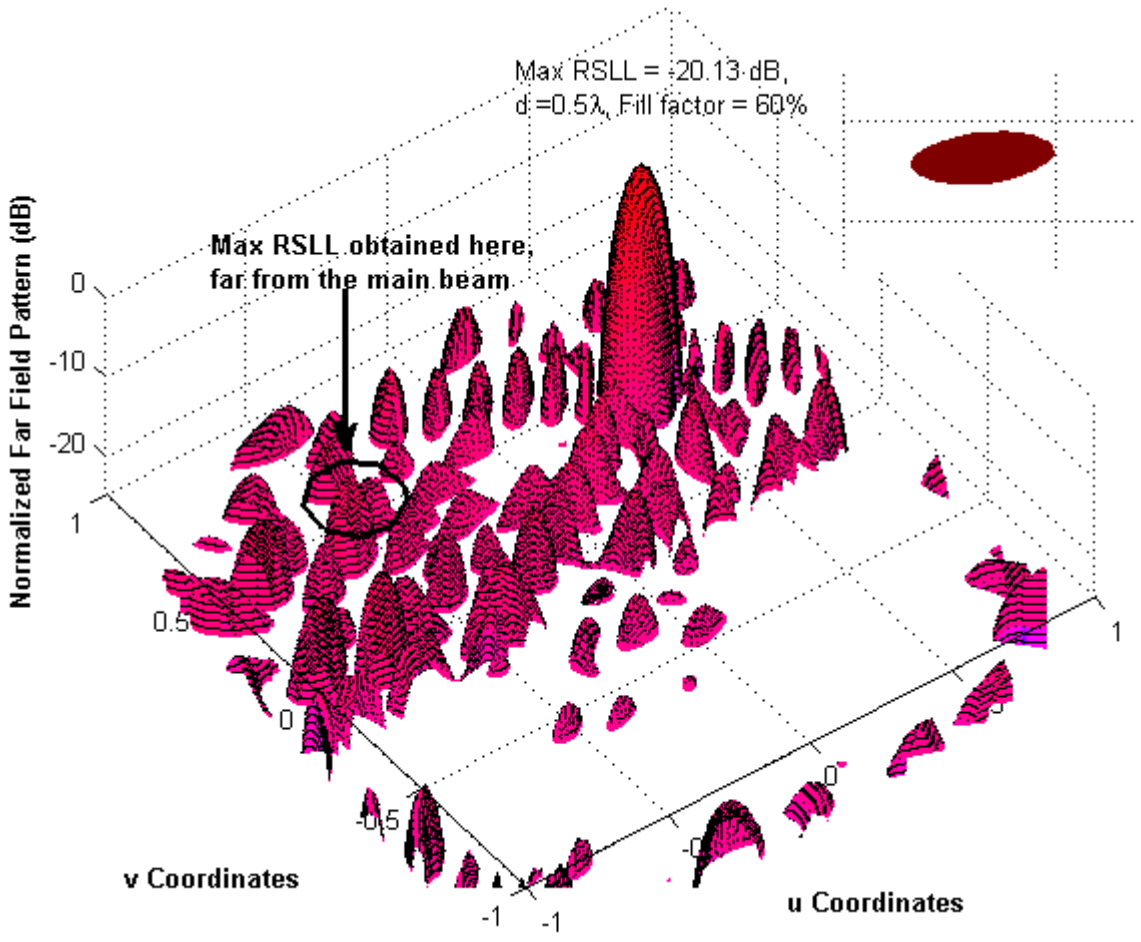

Figure 2.17 Radiation pattern of a Hexagonal planar array antenna of 484 elements with cos θ element pattern. The main beam has been steered at an angle of $\pi/4$ in both azimuth and elevation planes. The result has been plotted for 1000th generation of Genetic algorithm. Inset is showing the elliptical shape of the main beam after steering and the encircled region (far from the main beam) is showing the location of the max RSLL.

Table 2.2 Results of directivity and side lobe peaks after comprehensive optimization for planar array with isotropic and $\cos\theta$ element pattern and steering of the main beam.

Element pattern	Main beam(θ, φ)	Directivity in dB	Max RSLL in dB
Isotropic	Endfire (θ=0 °)	29.96	-20.11
	Steered at $\theta_0 = \pi/4, \phi_0 = \pi/4$	27.72	-17.49
$\cos\theta$ element pattern	Endfire (θ=0 °)	30.39	-21.2
	Steered at $\theta_0 = \pi/4, \phi_0 = \pi/4$	27.74	-20.13

Elements with certain pattern ($\cos\theta$ in our case) have an improved radiation pattern with steering of the main beam in comparison to their isotropic counterpart (Figure 2.12). It manages to have a side lobe peak below -20 dB with properly shaped main beam (shown in inset of Figure 2.12). Element with specific radiation pattern, after steering of the main beam in both the planes, offer a directivity of 27.74 dB.

Table 2.2 summarizes the performance of the proposed planar array design with its optimized thinned configuration of array excitation. Results for directivity and maximum side lobe peaks for the cases considered have been included in the table. The performance of the proposed design on different parameters have been discussed in detail and compared with some recent array synthesis technique in the next section. In context of the applications mentioned earlier such as for SKA application [Peter E. Dewdney, 2009; Ahmed El-makadema, 2014] where high sensitivity (to be discussed in chapter 5) and high directivity are among the essential attributes of the array, proposed array with quite reduced side lobe peaks and high directivity explains its potential for this application. In addition, for satellite application, where a desired main beam shape is required with high directivity and sensitivity, proposed design in combination with GA can be a better solution in comparison to the multi objective GA optimization discussed in [Joshua S. Petko and Douglas H. Werner, 2011], where main beam shape and side lobe peak both form the cost function of optimization.

2.5. Performance Comparison of the Proposed Synthesis

The maximum peak of the side lobe level, directivity, fill factor and the achievable 3 dB beam width have been compared. These parameters are associated with challenges of SKA application to achieve high spatial resolution, minimum noise and high sensitivity, and high directivity. A detailed performance analysis of the design for noise and sensitivity has been

presented in chapter 5. Table 2.3 summarizes the results for the proposed design and synthesis method along with the results of some recent antenna array synthesis techniques discussed in literature. The IFTDT performs well on RSLL with -22.8 dB and with smallest fill factor [Will P. M. N. Keizer, 2014]. The proposed method provides an array with -20.11 dB RSLL, slightly increased with elements having $\cos\theta$ pattern to -21.2 dB, which is competitive to the IFTDT results. Directivity offered by the proposed synthesis is highest among all and the achievable 3 dB beam width is quite competitive as well. These two parameters are accountable for minimum interference in satellite communication [Joshua S. Petko and Douglas H. Werner, 2011] and high spatial resolution required by the SKA application [Peter E. Dewdney, 2009]. Quite decent values of the side lobe peaks have been obtained in order to have less power losses in unwanted direction and minimum antenna system noise. The reduced power in side lobe levels ensures the less convolved power between sky brightness temperature and radiation pattern, hence reduced antenna temperature [Ahmed El-makadema, 2014]. Side lobe removal proposed in [J. R. Mohammed and K. H. Sayidmarie, 2014] is required for improved sensitivity of the array but it costs much as far as offered side lobe peaks and 3 dB beam width are concern. Proposed synthesis offers optimum side lobe level radiation pattern with a constraint of uniform side lobe peaks. On directivity and 3 dB beamwidth, the proposed synthesis out performs the synthesis methods discussed in [Will P. M. N. Keizer, 2014]. Although, the synthesis proposed in this work needs improvement in power requirement indicated by fill factor of the array. Comparatively large number of active element requires more power in comparison to the IFTDT, HSPSO, and RDT techniques.

Table 2.3 Performance comparison of the proposed synthesis method with recent array synthesis approaches in literature.

Synthesis	Max RSLL (dB)	Directivity (dB)	Turned on elements	Fill Factor	Achievable 3 dB beam width (Δu)	Side lobe removal
IFTDT [Will P. M. N. Keizer, 2014]	-22.8	28.2	254	44%	0.1028	No
HSPSO [M. Donelli et al., 2009]	-19.0	-	254	44%	-	No
RDT [Will P. M. N. Keizer, 2014]	-20.7	28.2	254	44%	0.0938	No
Proposed synthesis (isotropic elements)	-20.11	29.96	290	60%	0.088	No
Proposed synthesis (cosθ element patern)	-21.2	30.39	290	60%	0.088	No

Side lobe cancellation approach in [J. R. Mohammed and K. H. Sayidmarie, 2014]	-14.5	-	400	100%	0.0875	Yes
Uniformly excited planar array [J. R. Mohammed and K. H. Sayidmarie, 2014]	-13.22	-	400	100%	0.084	No
Optimized Planar array in [P. Lopez et al., 2001], referred and compared in[J. R. Mohammed and K. H. Sayidmarie, 2014]	-20.2	-	400	100%	0.097	No

2.6. Conclusion

The work presented here emphasizes on the performance parameters required in SKA and satellite applications. Deployment of antenna arrays for the state of the art spectroscopy requires array to have high spatial resolution with highly directive main beam and high sensitivity in terms of minimum noise temperature. In satellite communication where power conservation and minimum adjacent channel interference are prime requirements, properly shaped main beam and highly directive pattern with minimum side lobes solve the purpose. In this proposed work, an elliptical main beam shape controlling design with hexagonal arrangement of elements has been proposed. The hexagonal geometry has associated advantages of high directivity, steerability and maximum coverage with low element density. Design offer controlled and well behaved elliptical main beam with 3 dB beam width as low as 0.088. In addition, the drawbacks of multi objective search have been overcome by combining the proposed design with Binary GA for array thinning to have improved side lobe peaks and high directivity. Optimized thinned configuration consists of four hexagons which take part in shaping the beam and the radiation pattern. Modification in the GA has been introduced with the proposed Double stage uniform cross over operation in accordance with the geometry of the planar array. Directional optimization in orthogonal plane ($\varphi = 0^{o}$ and $\varphi = 90^{o}$) has been discussed with the proposed synthesis approach in context of radiation pattern, directivity and corresponding fill factors. Comprehensive optimization of the design provides the radiation pattern of the array for a full scan range of azimuth and elevation angles.

Isotropic elements and elements with $\cos\theta$ pattern have been considered for the synthesized array analysis. Pattern with steering of the main beam have also been obtained for the proposed synthesis. All patterns show a well behaved and elliptically shaped main beam. SLL peak as low as -21 dB and directivity as high as 30 dB have been achieved. In the end, performance comparison of the proposed synthesis with some other recent synthesis approaches has been carried out. Proposed synthesis outperforms the planar array optimized for side lobe cancellation and uniformly excited planar array. It is quite competitive with the IFTDT, RDT and HSPSO in peak SLL, whereas performs well for directivity and 3 dB beam width. The synthesis approach needs improvement in power requirement and side lobe level while maintaining the proper main beam shape. These challenges have been discussed in the next chapter and Taylor synthesis approach along with proposed GA modified discretzing technique for Taylor circular aperture distribution has been presented.

References

- C. A. Balanis, Antenna Theory. Boca Raton, FL: CRC Press, 2002.
- P. E. Dewdney, P. J. Hall, R. T. Schilizzi and T. J. L. W. Lazio, "The Square Kilometre Array," in Proceedings of the IEEE, vol. 97, no. 8, pp. 1482-1496, Aug. 2009.
- El-makadema, L. Rashid and A. K. Brown, "Geometry Design Optimization of Large-Scale Broadband Antenna Array Systems," in IEEE Transactions on Antennas and Propagation, vol. 62, no. 4, pp. 1673-1680, April 2014.
- R. Willey, "Space tapaering of linear and planar arrays," IRE Transactions on Antennas and Propagation, vol. 10, no. 4, pp. 369-377, July 1962.
- D. H. W. R.L. Haupt, Genetic algorithm in electromagnetic. Hoboken, New Jersey: John Wiley and Sons, 2007.
- R. L. Haupt, "Thinned arrays using genetic algorithms," IEEE Transactions on Antennas and Propagation, vol. 42, no. 7, pp. 993-999, July 1994.
- M. Fernández-Delgado, J. A. Rodríquez-González, R. Iglesias, S.Barro, and F. Ares-Pena, "Fast Array Thinning using Global Optimization Methods," J. of Electromagn. Waves and Appl., Vol. 24, 2259–2271, 2010.
- D. Marcano and F. Duran, "Synthesis of antenna arrays using genetic algorithms," IEEE Antennas and Propagation Magazine, vol. 42, no. 3, pp. 12-20, June 2000.

- H. Wang, D.-G. Fang, and Y. Chow, “Grating lobe reduction in a phased array of limited scanning,” IEEE Transactions on Antennas and Propagation, vol. 56, no. 6, pp. 1581-1586, June 2008.
- R. C. Nongpiur and D. J. Shpak, "Synthesis of Linear and Planar Arrays With Minimum Element Selection," in IEEE Transactions on Signal Processing, vol. 62, no. 20, pp. 5398-5410, Oct.15, 2014.
- W. P. M. N. Keizer, "Synthesis of Thinned Planar Circular and Square Arrays Using Density Tapering," IEEE Transactions on Antennas and Propagation, vol. 62, no. 4, pp. 1555-1563, April 2014.
- S. Mosen and M. Ciattaglia, “Ant colony optimization to design thinned arrays,” in Proc. IEEE Antennas Propag. Soc. Int. Symp., July 2006, pp. 4675-4678.
- M. Donelli, A. Martini, and A. Massa, “A hybrid approach based on PSO and Hadamard difference sets for the synthesis of square thinned arrays,” IEEE Trans. On Antennas Propag., vol. 57, no. 8, pp. 2491-2495,Aug. 2009.
- J. R. Mohammed and K. H. Sayidmarie, "Sidelobe Cancellation for Uniformly Excited Planar Array Antennas by Controlling the Side Elements," IEEE Antennas and Wireless Propagation Letters, vol. 13, pp. 987-990, May 2014.
- Xuedong Chen, Zailei Luo, Xueming He and Lianli Zhu, "Thinning and weighting of planar arrays by modified teaching–learning-based optimization algorithm," Journal of Electromagnetic Waves and Applications, vol. 28, No. 15, pp. 1924-1934, 2014.
- J. Petko and D. Werner, “Pareto optimization of thinned planar arrays with elliptical mainbeams and low sidelobe levels,” IEEE Transactions on Antennas and Propagation, vol. 59, no. 5, pp. 1748-1751, May 2011.
- D. S. Weile and E. Michielssen, “Integer coded Pareto genetic algorithm design of constrained antenna arrays,” Electron. Lett., vol. 32, pp. 1744-1745, Sep. 1996.
- D. H. Werner and A. J. Ferraro, “Cosine pattern synthesis for single and multiple main beam uniformly spaced linear arrays,” IEEE Trans. Antennas Propag., vol. 37, no. 11, pp. 1480-1484, Nov. 1989.
- S.G. Tanyer A.E. Yılmaz and F. Yaman, "adaptive desirability function for multiobjective design of thinned array antennas," Journal of Electromagnetic Waves and Applications, Vol. 26, Nos. 17–18, pp. 2410-2417, December 2012.
- K. R. Mahmoud, M. El-Adawy, S. M. M. Ibrahem, R. Bansal, and S. H. Zainud-Deen, "A comparison between circular and hexagonal array geometries for smart antenna

systems using particle swarm optimization algorithm," Progress In Electromagnetics Research, Vol. 72, pp.75-90, 2007.

- W. Spears and V. Anand, "A study of crossover operators in genetic programming," in Methodologies for Intelligent Systems, ser. Lecture Notes in Computer Science, Z. Ras and M. Zemankova, Eds. Springer Berlin Heidelberg, vol. 542, pp. 409-418, 1991.
- P. Lopez, J. A. Rodriguez, F. Ares, and E. Moreno, "Low-sidelobe patterns from linear and planar arrays with uniform excitations except for phases of a small number of elements," Electron. Lett., vol. 37, no. 25, pp. 1495-1497, Dec. 2001.
- R. Harrington, Sidelobe reduction by nonuniform element spacing, IEEE AP-S Trans. 9:187–192 (March 1961).
- C. Ding and L. Jianxin, "GA design of large thinned arrays," in Proc. EuCAP 2009, 3rd Eur. Conf. Antennas Propag., Berlin, Germany,Mar.23–27, 2009, pp. 451–455.
- F. J. Ares-Pena, J. A. Rodriguez-Gonzalez, E. Villanueva-Lopez and S. R. Rengarajan, "Genetic algorithms in the design and optimization of antenna array patterns," in IEEE Transactions on Antennas and Propagation, vol. 47, no. 3, pp. 506-510, Mar 1999.
- Yu-Bo Tian and Jian Qian, "Improve the performance of a linear array by changing the spaces among array elements in terms of genetic algorithm," in IEEE Transactions on Antennas and Propagation, vol. 53, no. 7, pp. 2226-2230, July 2005.
- Keen-Keong Yan and Yilong Lu, "Sidelobe reduction in array-pattern synthesis using genetic algorithm," in IEEE Transactions on Antennas and Propagation, vol. 45, no. 7, pp. 1117-1122, Jul 1997.
- L. Zhang, Y. C. Jiao, F. S. Zhang and H. Li, "Linear array thinning based on orthogonal genetic algorithm," 2010 International Conference on Microwave and Millimeter Wave Technology, Chengdu, 2010, pp. 1057-1059.
- D. Marcano and F. Duran, "Synthesis of antenna arrays using genetic algorithms," IEEE Antennas and Propagation Magazine, vol. 42, no. 3, pp. 12-20, June 2000.
- E. E. Hassan and H. A. Ragheb, "Sidelobes Level Reduction Using Spatial Optimization of the Array Factor," in IEEE Antennas and Wireless Propagation Letters, vol. 11, no. , pp. 756-759, 2012.

Chapter 3

Synthesis of Planar Antenna Array Using Genetic Algorithm Modified Discretizing Technique for Taylor Distribution

The strength of Taylor synthesis approach has been utilized to improve the performnace of the proposed planar array discussed in previous chapter. Taylor synthesis can provide a ϕ independent radition pattern, i.e., annular ring of side lobes with pencil beam and all the side lobes under a pre-defined level. Limitation of discretizing technique of Taylor synthesis for large arrays has been overcome by applying the heuristic approach Genetic algorithm with unconventional representation of chromosomes. Quite improved values of side lobe peaks, directivity, antenna aperture efficiency have been obtained. Antenna design offers a good main beam shape control and keeps the main beam elliptical. A sharp main beam with desired side lobe pattern fulfills the SKA and other satellite application requirements.

3.1. Introduction

In context of the SKA application the proposed planar antenna array with emphasis on its geometry has been analyzed and compared with some recent array synthesis approaches. In view of the fact that the performance parameters such as directivity, sensititvity, and sidelobe peaks have a great depdency on geometry of the array, the design performs well as far as the peak side lobe level, directivity, and 3 dB beam width is concern. Design offers aperture efficiency as high as 84% with the GA optimized thinning configuration. Further, it is required to have improved side lobe levels and less power requirement.

Now in order to obtain a specified radition pattern such as the pattern with single main beam of specified beam width and scan position along with the sidelobe level at specified height, the synthesis approach that can be applied is Taylor synthesis. Taylor synthesis allows to have a well beahved radition pattern along with the desired shape of the main beam. With the design approach of Taylor sythesis it is possible to obtain excitation values for discrete arrays as in this approach the continuous aperture distribution can be sampled for the elements of discrete array. Moreover, Taylor synthesis approch for discrete array can be extended to the planar array design with circular or elliptical boundaries and this extension is not possible with Dolph's synthesis. The general array factor Eq. for an antenna

array of length $2a$ considered by the Taylor is given by [Robert S. Elliot, "Antenna theory and design", 2002]

$$\delta(\theta) = \int_{-a}^{a} g(z) e^{ikz\cos\theta} dz \tag{3.1}$$

Now, the antenna with desired raditaion pattern $\delta(\theta)$ can be sythesiszed by finding the aperture distribution $g(z)$ for the antenna array. If $g(z) = \alpha e^{-j\beta z}$ then for a uniform excitation and uniform progressive phase shift with α and β constant, the radiation pattern in Eq.3.1 is given by[Robert S. Elliot, "Antenna theory and design", 2002]

$$\delta(\theta) = 2\alpha a \frac{\sin[ka\,(\cos\theta - \frac{\beta}{k})]}{ka\,(\cos\theta - \frac{\beta}{k})} \tag{3.2}$$

With the substititution

$$u = \frac{2a}{\lambda}(\cos\theta - \frac{\beta}{k}) \tag{3.3}$$

The power pattern can be obtained by using Eq. 3.4 as [Robert S. Elliot, "Antenna theory and design", 2002]

$$f(u) = 20\log_{10}\frac{\delta(\theta)}{\delta(\theta_0)} = 20\ \log_{10}\frac{\sin\pi u}{\pi u} \tag{3.4}$$

Where $\theta_0 = \cos^{-1}\left(\frac{\beta}{k}\right)$ is the main beam pointing angle. The radiation pattern $f(u)$ can be seen in figure 3.1 . The sidelobes are uniform and their height decreases as the inverse of u. From Eq. 3.3, it should be noted that the value of u moves to the left from $\frac{2a}{\lambda}\left(1 - \frac{\beta}{k}\right)$ to 0 to $-\frac{2a}{\lambda}(1 + \frac{\beta}{k})$ as the θ moves from 0 to θ_0 to π. This indicates that in the visible range the number of sidelobes has a dependeny on the array length. Now, if a method can be deviced to suppress the sidelobes near the main beam below a certain specified height, leaving the outer sidelobes, could be a way to achieve the desired radiatio pattern. Taylor provided the method to achieve the radition pattern with the side lobes near to the main beam under a prespecified level. This method to achieve the radiation pattern with side lobe level controlling is called

shifting of nulls method. The method can be explained with the following steps [Robert S. Elliot, "Antenna theory and design", 2002]

- Select an intiger value $\bar{n}$ such that all the nulls occuring above this value have the same position as in the original pattern, i.e., for $|u| \geq \bar{n}$ the nulls of the new pattern are to occur at integral values of u.
- Next pair of null for the new pattern, when moving towards the main beam, occurs at new position $u = \pm u_{\bar{n}-1}$ where $|u_{\bar{n}-1}| > \bar{n} - 1$, similarly position of next pair of nulls is $u = \pm u_{\bar{n}-2}$ where $|u_{\bar{n}-2}| > \bar{n} - 2$ and so on.
- After shifting the nulls to the new positions, the expression for the new radition pattern is given by the following expression

$$\delta(u) = \frac{\sin \pi u}{\pi u} \frac{\prod_{n=1}^{\bar{n}-1}\left(1 - \frac{u^2}{u_n^2}\right)}{\prod_{n=1}^{\bar{n}-1}\left(1 - \frac{u^2}{n^2}\right)} \tag{3.5}$$

- Taylor formulated the following expression to determine the new null positions

$$u_n = \bar{n}\left[\frac{A^2 + \left(n - \frac{1}{2}\right)^2}{A^2 + \left(\bar{n} - \frac{1}{2}\right)^2}\right]^{1/2} \tag{3.6}$$

Where A is a paremeter to measure side lobe level and it is related to the SLL by $\cosh \pi A = b$ with $20\log 10b = SLL$.

Analysis of planar array starts with the selection of the arrangemet type of the array elements. Basicaly, these elements can be arranged either in rectangular grid or in form of concentric rings. The arrays considered in the upcoming analysis has been considred with constant element spacing in the two orthogonal direction. Although, the spacing constant or pitch of the array may vary in orthogonal directions. In case of uniform excitation with constatnt progressive phase shift, the whole array is assumed to be divided into four symmetrical quradrants and resultant sum and difference patterns can be computed. Rectangular grid arrays can be synthesized with different boundary approximations such as square, rectangular, circular, or elliptical, whereas for circular grid array circular boundary approximation is considered [Robert S. Elliot, "Antenna theory and design", 2002]. A seperable current distribution for the planar array of dimension m rows by n columns is $I_{mn} = I_m I_n$. With the seperable current distribution in Planar array with elements arrangd in

rectangular grid and rectangular or square boundary, the radition pattern of the array is the resulatnt product of the individual patterns of linear arrays along the two orthogonal axis. Consequently making the analysis of the design easy, although designs with seperable current distribution suffers with the gain limitation problem. This limitation of seperable distribution can be omitted with the ϕ symmetric patterns. Taylor proided the extension of the linear array design to the planar array with circular boundary and ϕ symmetric distribution. In addition, extension of Taylor synthesis is possible for discerete arrays with either rectangular grid or circular grid by sampling the continuous aperture distribution.

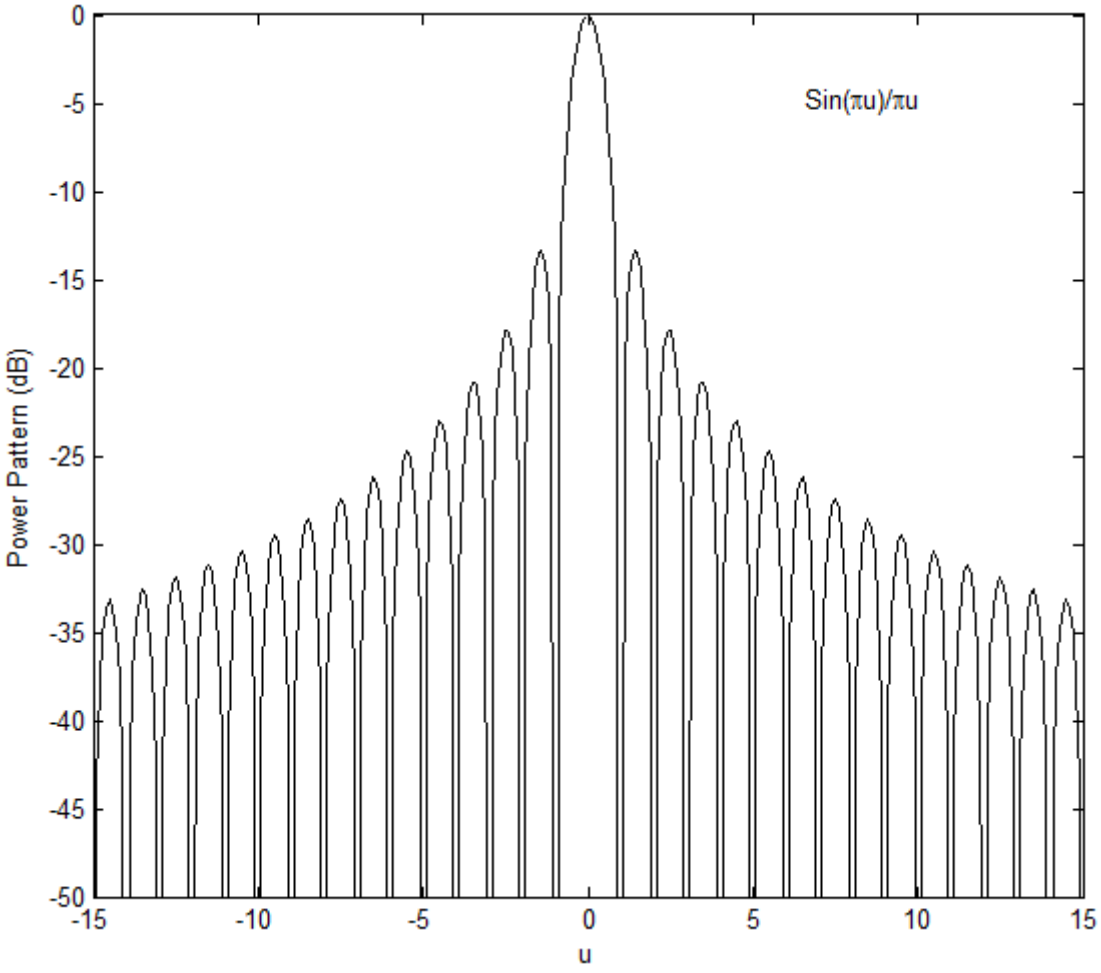

Figure 3. 1 Power pattern of a continuous line source with uniform excitation [Robert S. Elliot, "Antenna theory and design", 2002].

3.2. Taylor Sythesis of the Planar Arrays

The taylor synthesis of planar array discussed in [Robert S. Elliot, "Antenna theory and design", 2002] deals with two basic types of array geometry. One that has the arrangement of elements in rectangular manner and the other one in which all the elements lie on concentric circles. This literature assumes the pitch of the planar array to be constant, though it can be different in two orthogonal directions of the design. In case of symmetrical geometry, the whole array can be divided into four symmetrical quardrants to have element excitations provoding the sum and difference patterns. In [Robert S. Elliot, "Antenna theory and design", 2002], synthesis of the rectangular grid array with rectangular, square, circular, and elliptical boundary assumptions have been discussed whereas circular grid arrays always have the circular boundary assumption.

Now, for the planar array with rectangular or square boundary conditions and elements excited with seperable current distribution [Robert S. Elliot, "Antenna theory and design", 2002], the resultant pattern of the planar array is the pattern multiplication of two orthogonal linear arrays. So these planar arrays could be synthesized with the approches developed for linear arrays. However, with seperable current distributions antennas encounter the problem of gain limitation and this problem can be solved by using ϕ symmetric patterns. Taylor provided the extension of linear array to the planar array with the circular boundary approximation and a continuous ϕ symmetric distribution. Taylor circular distribution can be sampled to achieve the discrete array elements current excitation values for either rectangular grid or circular grid arrays.

Extension of the linear array synthesis technique to the planar array with different boundary assumptions and with different element arrangement makes the Taylor synthesis key choice for planar array design over other synthesis approches. Dolph's technique of array design can not be utilized in this way, moreover, Tseng and Cheng provided this extension for rectangular grid array with rectanular boundary and with the constraint of same number of elements in both the directions.

In case of seperable distribution, array factor for planar array can easily be calculated using the array factors of orthogonal linear arrays that constitute that planar array. In this case, antenna performs well for side lobe reduction as it overachieves the sidelobe level requirement in most of the part of side lobe region but at the same time suffers with the directivity and resolution due to broading of the main beam. This leads to the use of

nonseperable aperture distributions. Moreover, antenna radiation pattern with all the side lobes under controlled height can be achieved with a phi-symmetric radiation pattern. Periodic repition of Dolph-Chebyshev pattern in each phi cut leads to a phi-symmetric pattern. Radition pattern obtained in this way form a pencil beam and concentric rings of side lobes with uniform height. In order to achieve such radiaton pattern, it is required to have a phi-symmetric element excitation for the palanar array grid. Tseng and Cheng planar array synthesis technique, where elements are arrangened in rectangular grid with rectangular boundary and has the seperable aperture distribution, is not suitable for the phi-symmetric pattern. A ϕ symmetric pattern is more feasible with array elements arranged in circular grid and bounded by a circular boundry.

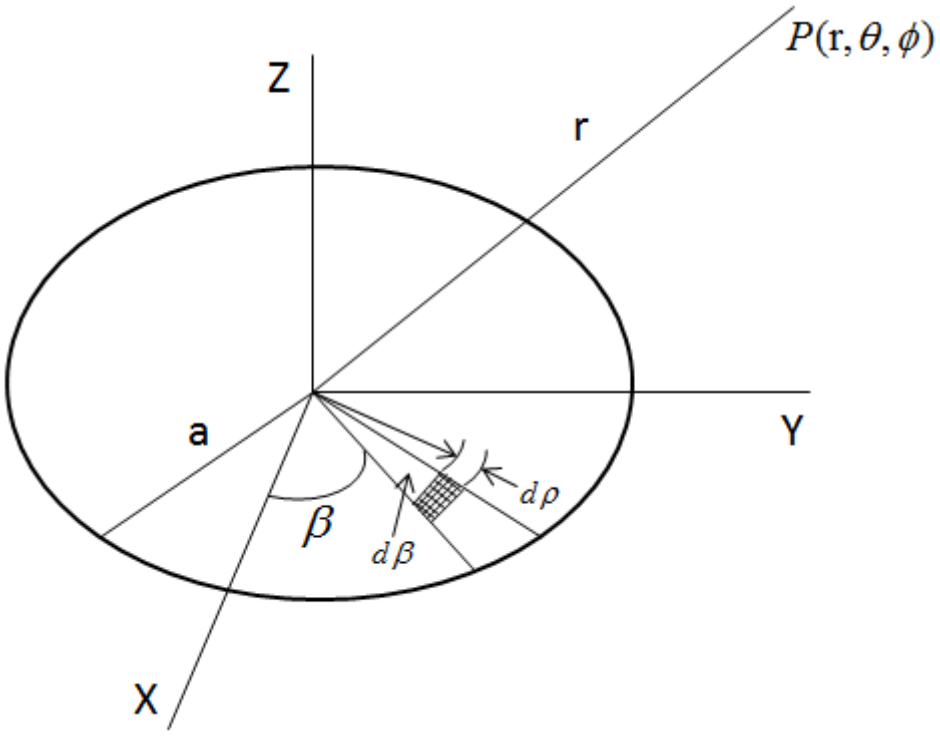

Figure 3. 2 Planar aperture in Cartesian/cylindrical/spherical system.

In Taylor synthesis, it is possible to obtain a phi independent aperture distribution. Now from Figure 3.2 , for a planar array with cirular boundary of radius a, the radiation pattern is given by [Robert S. Elliot, "Antenna theory and design", 2002]

$$F(\theta,\phi) = \int_0^a \int_0^{2\pi} K(\rho,\beta) e^{jk\rho \sin\theta \cos(\phi-\beta)} \rho \, d\rho d\beta \tag{3.7}$$

$K(\rho,\beta)$ is the aperture distribution and it can be represented by the Fourier series as [Robert S. Elliot, "Antenna theory and design", 2002]

$$K(\rho,\beta) = \sum_{n=-\infty}^{\infty} K_n(\rho) e^{jn\beta} \tag{3.8}$$

Now, from the bessel expension

$$e^{jk\rho \sin\theta \cos(\phi-\beta)} = \sum_{m=-\infty}^{\infty} (j)^m J_m(k\rho \sin\theta) e^{jm(\phi-\beta)} \tag{3.9}$$

From Eq. 3.7, 3.8 and 3.9 , the radiation pattern can be written as

$$F(\theta,\phi) = \sum_{m=-\infty}^{\infty} \sum_{n=-\infty}^{\infty} \int_0^{2\pi} \int_0^a K_n(\rho)(j)^m J_m(k\rho \sin\theta) e^{jm\phi}\, e^{j(n-m)\beta} \rho\, d\rho d\beta \tag{3.10}$$

The β integration in Eq. 3.10 only has a non zero value at m=n. So, rewriting the Eq. 3.10

$$F(\theta,\phi) = 2\pi \sum_{n=-\infty}^{\infty} (j)^n e^{jn\phi} \int_0^a K_n(\rho) J_n(k\rho \sin\theta)\, e^{j(n-m)\beta} \rho\, d\rho \tag{3.11}$$

Form Eq. 3.11, it is quite clear that a phi independent pattern can be obtained with n=0 resulting in a β independent aperture distribution $K_0(\rho)$ from Eq. 3.8. For this particular case the radiation pattern is given by

$$F(\theta) = 2\pi \int_0^a K_0(\rho) J_0(k\rho \sin\theta)\, \rho\, d\rho \tag{3.12}$$

Rewriting Eq. 3.12 with the following variable sbstitutons

$$p = \frac{\pi}{a}\rho \tag{3.13}$$

$$u = \frac{2a \sin\theta}{\lambda} \tag{3.14}$$

$$g_0(p) = \frac{2a^2}{\pi} K_0(\rho) \tag{3.15}$$

Gives

$$F(u) = \int_0^{\pi} p g_0(p) J_0(pu) dp \tag{3.16}$$

Where variable p is the tranformation of radial aperture coordinate, variable u is the transformation of pointing direction in real space and $g_0(p)$ is the transformation of aperture distribution.

Considering the special case of a uniformly excited circular array with assumption $g_0(p) = 1$, the radiation pattern from Eq. 3.16 is given by

$$\delta(u) = \frac{J_1(\pi u)}{\pi u} \tag{3.17}$$

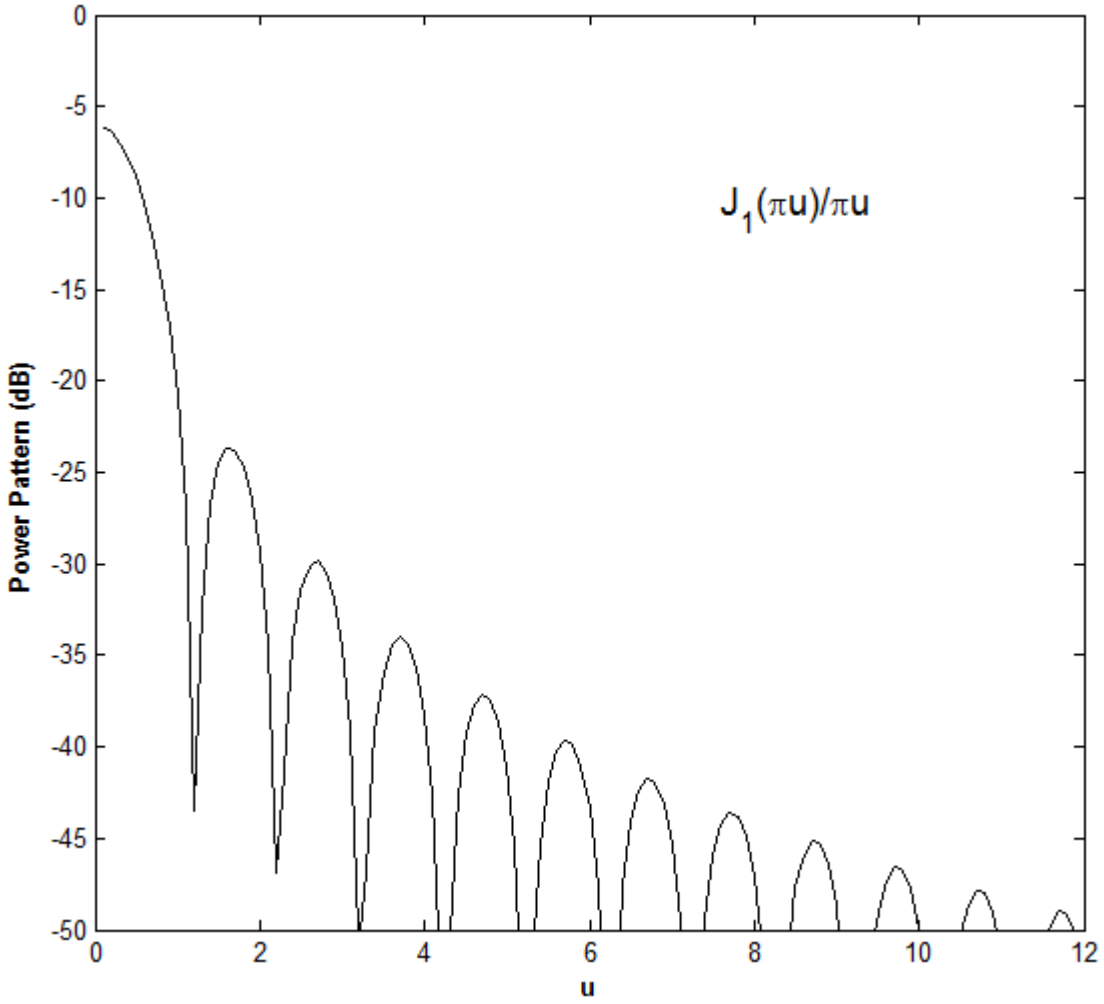

Figure 3. 3 Power pattern of a uniformly excited circular aperture.

The radiation pattern is symmetric in azimuth plane and side lobes decrease gradully away from the main beam (see figure 3.3). Phi-symmetric pattern forms the annular ring of side lobes with main beam as a pencil beam. Side lobes present in the visible space depend upon the aperture size and the visible range in terms of u is defined as $0 \leq u \leq \frac{2a}{\lambda}$. The quantity $\frac{\lambda}{2a}$ is known as standard beamwidth [Taylor, 1960], and for a uniformy excited circular array the beamwidth (in radians) between half power points is 1.029 standard beamwidth [Taylor, 1960]. Similar to the linear array synthesis, Taylor extended the shifting of nulls method for planar array to obtain the desired radition pattern and applied the inverse transform approach to obtain the corresponding aperture distribution [Taylor, 1960]. From Eq. 3.17, the null points of the pattern are given by the roots of $J_1(u)$ defined as [Robert S. Elliot, "Antenna theory and design", 2002]

$$J_1(\pi\gamma_{1n}) = 0, \qquad n = 0,1,2,\ldots \tag{3.18}$$

Table 3. 1 Solutions of $J_1(\pi\gamma_{1n}) = 0$

n	γ_{1n}
0	0
1	1.2196699
2	2.2331306
3	3.2383154
4	4.2410628
5	5.2427643
6	6.2439216
7	7.2447598
8	8.2453948
9	9.2458927
10	10.2462933

Table 3.1 shows the roots of $J_1(\pi\gamma_{1n})$ for $n = 0,1,2,..10$. Now in order to obtain the desired radiation pattern with near in sidelobes at quasi constant height under a pre-specified maximum level, Taylor modified the Eq. 3.17 and it is given by [Robert S. Elliot, "Antenna theory and design", 2002]

$$\delta(u) = \frac{J_1(\pi u)}{\pi u} \frac{\prod_{n=1}^{\bar{n}-1}\left(1 - \frac{u^2}{u_n^2}\right)}{\prod_{n=1}^{\bar{n}-1}\left(1 - \frac{u^2}{\gamma_{1n}^2}\right)} \tag{3.19}$$

From Eq. 3.19, it can be seen that the modification has been done by replacing the positions of $\bar{n}-1$ roots with new root positions given by the following expresssion

$$u_n = \pm\sigma\sqrt{A^2 + (n-1/2)^2} \tag{3.20}$$

σ is known as dialation factor and it should be chosen in such a way that the zeros of the desired pattern should fall on the new root positions given by the Eq. 3.20. σ is defined as [Taylor, 1960]

$$\sigma = \frac{\gamma_{1n}}{\sqrt{A^2 + \left(\bar{n} - \frac{1}{2}\right)^2}} \tag{3.21}$$

A is related to the desired side lobe level and has been defined for linear array case. Now Positions of the null points of radiation pattern can be defined at different intervals depending upon the value of $\bar{n}$ as [Taylor, 1960]

$$u_n = \begin{cases} \pm\sigma\sqrt{A^2 + \left(n - \frac{1}{2}\right)^2}, & 1 \le n < \bar{n} \\ \pm\gamma_{1n}, & \bar{n} \le n < \infty \end{cases} \tag{3.22}$$

Selection of the value of $\bar{n}$ is of great significnace as far as radiation pattern of the antenna is concern. The root $\gamma_{1\bar{n}}$ corresponding to the value $\bar{n}$ devides the sidelobes of radiation pattern into two regions. For all values of $u < \gamma_{1\bar{n}}$, the side lobes are at quasi constant height and the side lobes are uniform whereas, for $u > \gamma_{1\bar{n}}$, side lobes are decaying in nature. Hence higher values of $\bar{n}$ leads to a wider range of uniform side lobes. Though side lobes are uniform but still a very slight decrement in side lobe level with increment in the value of u can be observed. Side lobes near to the main beam has the heighest level and it is slightly less than the desired side lobe level. One more parameter that has been defined earlier in this section is dialation factor σ. Beam width of the actual pattern varies from that of desired pattern. Actual radiation pattern enounters an increment in beam width by a factor almost exactly equal to σ. There is an interdependency between the values of $\bar{n}$ and σ, and this can be utilized to find out the appropriate values of $\bar{n}$. Shifting of the zeros to obtain the desired pattern should not cause any change in the spacing between the zeros and this condition can be achieved by selecting the value of $\bar{n}$ in such a way that a unit increment in $\bar{n}$ does not increase σ . In order to achieve this condition, too small values of $\bar{n}$ must be avoided. For uniform side lobe pattern, higher values of $\bar{n}$ are chosen and this also has an

impact on main beam as increment in $\bar{n}$ makes the σ nearly equal to unity consequently sharpening the main beam. It is possible to achieve the uniform side lobe pattern for the whole visible range ($0 \leq u \leq \frac{2a}{\lambda}$) by selecting the value of $\bar{n}$ such that the root $\gamma_{1\bar{n}}$ lies beyond this range. However, further increment in the value of $\bar{n}$ does not cause any significant effect on the visible side lobes but it increases the energy of the side lobes apart form the visible range and resulting in super gain aperture [Robert S. Elliot, "Antenna theory and design", 2002]. Super gain apertures [Taylor, 1955] have high concentration of zeros in visible range due to the shifting of zeros towards the main beam. This phenomenon reduces the main beam width consequently sharpning the main beam. Moreover, for a value of $\bar{n}$ less than $\frac{2a}{\lambda}$, there is no movement of zeros into the visible range and hence only the effect on side lobes in the visible range can be observed. Even for the values of $\bar{n}$ slightly greater than $\frac{2a}{\lambda}$, the effect on the area of invisible side lobes is insignificant. Further an indefinite increase in $\bar{n}$ leads to the increment in the side lobe level of invisible spectrum consequently causing the energy of invisible side lobes to increase [Taylor, 1955]. Proposed deisgn for the planar antenna array has the value of $\bar{n} = 9$, which is less than the aperture dimension to wavelength ratio $\frac{2a}{\lambda}$ of the design and results in a $\sigma = 1.066953$, close to the unity. As stated earlier, no migration of the zeros from invisible to visible range take place in the present case and rearrangement of zeros has been achieved through shifting of null methods [Robert S. Elliot, "Antenna theory and design", 2002].

Further, to achieve the desired radiation pattern, computation of aperture distribution for that pattern is required. Taylor in his work obtained the distribution function $g_0(p)$ for a given space factor function $\delta(u, A, \bar{n})$ by applying the inverse transform approach called method of Dossier [Taylor, 1960]. The distribution function $g_0(p)$ is given by [Taylor, 1960]

$$g_0(p) = \sum_{m=0}^{\bar{n}-1} \frac{2\delta(\gamma_{1m}, A, \bar{n})}{[J_0(\pi\gamma_{1m})]^2\pi^2} J_0(\gamma_{1m}p) \tag{3.23}$$

The corresponding space factor function is given by [Taylor, 1960]

$$\delta(\gamma_{1m}, A, \bar{n}) = \begin{cases} 1 & m = 0 \\ -J_0(\pi\gamma_{1m}) \dfrac{\prod_{n=1}^{\bar{n}-1} 1 - \dfrac{{\gamma_{1m}}^2}{\sigma^2\left[A^2 + \left(n - \frac{1}{2}\right)^2\right]}}{\prod_{\substack{n=1 \\ n\neq m}}^{\bar{n}-1} 1 - \dfrac{{\gamma_{1m}}^2}{{\gamma_{1n}}^2}} & 0 < m < \bar{n} \\ 0 & m \geq \bar{n} \end{cases} \tag{3.24}$$

3.3. Taylor Synthesis for Discrete Arrays

Continuous aperture distributions for linear and planar arrays find very less applications whereas, it is hugely required to have such distribution for discrete element arrays. In context of the SKA application discussed in the proposed work, Taylor synthesis can be applied to obtain the distribution for aperture with given side lobe and main beam constraints. Now, in order to achieve the disrtibution for discrete arrays, Taylor approached the conventional method of sampling. These arrays will follow the pattern with minimum error if the sampling period is small, implying that arrays with large number of elements are more suited for sampled Taylor distribution. Large number of antennas deployed in SKA fulfill the requirement of the application of above approach.

For planar array geometries, as discussed earlier, there are two design factors to discuss. One is the arrangement of elements and second one is the boundary. For rectangular grid arrays different boundaries are possible whereas, circular grid posses circular boundary [Robert S. Elliot, "Antenna theory and design", 2002]. For both the geomerical arrangement element excitation values are obtained corresponding to the position of that element. Inherently, pattern degradation is obseved in comparison to the pattern that could be achieved with seperable distribution. This pattern degradation can be overcome by applying some techniques which have been discussed in [Robert S. Elliot, "Antenna theory and design", 2002].

These techniques utilizes the method of perturbation where non-seperable Taylor sampled current distribution is used as a strating point of the computation process. This method will be discussed here in the coming section as it forms the background of the proposed discretizing technique. Proposed planar array design posses the rectangular grid of elements and the elliptical boundary approximation has been applied to the geometry of the array. In order to compute the current for each element, distance of that element from the centre of the geometry is computed. For a rectangular grid array with $\mathbf{0.5}\boldsymbol{\lambda}$ inter element spacing and cirular boundary of radius a, the radial distance of $\boldsymbol{mn^t}$ element is given by [Robert S. Elliot, "Antenna theory and design", 2002]

$$\rho_{mn} = \sqrt{\left[\frac{(2m-1)d_x}{2}\right]^2 + \left[\frac{(2n-1)d_y}{2}\right]^2} \tag{3.25}$$

Here d_x and d_y are interelement spacings along x and y axis respectively and both are equal to 0.5λ. The corresponding element position p_{mn} and current excitation I_{mn} values can be evaluated as [Robert S. Elliot, "Antenna theory and design", 2002]

$$p_{mn} = \frac{\pi \rho_{mn}}{a} \tag{3.26}$$

$$I_{mn} = g_0(p_{mn}) \tag{3.27}$$

Where $g_0(p_{mn})$ can be computed from Eq. 3.23.

Although, all the side lobes can not be controlled but still for large number of elements, the pattern obtained with sampled Taylor distribution is in good agreement with the pattern obtained using continous aperture distribution. In case of a planar array with large number of elements and with an elliptical boundary approximation, the sampled Taylor distribution can be applied successfuly. For elliptical boundary, element coordinate transformation is done by one way stretching the ellipse to make it a circle. If a and b are the semi-major and semi-minor axis respectively, then the transformation of coordinates is given by [Robert S. Elliot, "Antenna theory and design", 2002]

$$x' = x, \qquad y' = \frac{a}{b} y \tag{3.28}$$

Now due to transformation of the coordinates of the mn^{th} element, the element position p'_{mn} is given by [Robert S. Elliot, "Antenna theory and design", 2002]

$$p'_{mn} = \frac{\pi}{a}[(x'_{mn})^2 + (y'_{mn})^2]^{\frac{1}{2}} \tag{3.29}$$

Again from Eq. 3.27, current distribution for the tranformed position can be computed. Here the elliptical boundary condition has been discussed in order to explain the computation of current distribution for the proposed design in which the planar array geometry has been approximated with an elliptical boundary. Taylor synthesis for discrete arrays is most suitable synthesis technique for the proposed planar array as it is supported by the large number of elements (small sampling interval) and provides a well behaved radiation pattern along with properly shaped main beam.

In order to bridge the gap between the actual desired pattern and the obtained pattern, as mentioned earlier in this section method of perturbation is used. This involves the computation of current values for each and every element such that the obtained pattern and the desired pattern has the minimum amount of variation. Current values that have been

obtained through the sampling of the Continuous Taylor distribution serve as the starting values for the computation process. Next section discusses the process in detail.

3.4. Discretizing Technique for Rectangular Grid Array

Taylor continuous aperture distribution for desired pattern when sampled for discrete arrays cause some pattern degradation even for large number of elements and the situation becomes worse for small arrays. Tseng-cheng distribution offers quite improved pattern for both small and large arrays but can only be applied for rectangular bondaries and uniformly placed elements in both the directions. In case of circular and elliptical boundary approximation of the rectangular grid array, Tseng-Cheng approach is not applicable. In the proposed planar array geometry the corner elements have been removed resulting in an elliptical boundary with rectangular grid. The design is not suitable for the application of Tseng-Cheng distribution as it can cause significant pattern degradation. Hence, it is required to have sampled Taylor distribution with minimum pattern variation from that of desired one.

3.4.1 Current Perturbation Method

Pertubation method starts with the current distribution I_{mn}^{0} obtained through the sampling of Taylor distribution. There is no restriction on the shape of the boundary and placement of the elements as far as application of the technique is concern. Since the proposed design has elements arranged in rectangular grid and possess an elliptical boundary, the perturbation method has been discussed in context of the proposed design. Once again, the radiation pattern for a rectangular grid array with quadrantal symmetry can be expressed as

$$\delta_0(\theta,\phi) = \sum_m \sum_n I_{mn}^{0} f_{mn} \tag{3.30}$$

Where $f_{mn} = \cos(mkd_x \sin\theta \cos\phi)\cos(nkd_y \sin\theta \sin\phi)$ and if $\delta(\theta,\phi)$ is the desired radiation pattern then it can be expressed as

$$\delta(\theta,\phi) = \sum_m \sum_n I_{mn} f_{mn} \tag{3.31}$$

Here I_{mn} is the desired current excitation value given by

$$I_{mn} = \delta I_{mn} + I_{mn}^{0} \tag{3.32}$$

Now from Eq. 3.30 and 3.31, the difference between the obtained pattern and the desired pattern can simply be written as

$$\delta(\theta,\phi) - \delta_0(\theta,\phi) = \sum_m \sum_n \delta\, I_{mn} f_{mn} \tag{3.33}$$

Eq. 3.32 is solved for number of directions (θ,ϕ) equal to the number of elements in the array in order to obtain the current perturbation values for every array element. In case of quadrantal symmetry, equations equal to the number of elements in one quadrant of the array need to be solved. Among different different directions of array pattern if one is the direction of main beam then $\delta = \delta_0$, and for rest of the directions (showing the side lobes) the pattern difference in Eq. 3.33 ($\delta(\theta,\phi) - \delta_0(\theta,\phi)$) is simply the difference between the desired side lobe level and the side lobe level that has been obtained in that particular direction. Now, a simple matrix inversion can be used to evaluate the current perturbation values. Eq. 3.32 gives the new current values and new pattern is obtained by Eq. 3.31. An ideal Taylor pattern has annular rings of side lobes (ϕ independent) and all the side lobes in selected region at a quasi-constant height. To achieve the discrete array pattern as close as possible to the Taylor pattern, the aperture distribution should be as ϕ symmetric as possible, i.e., $I_{mn} = I_{nm}$. Hence, a ϕ symmetric pattern reduces the number of equations. that are need to be solved for current perturbation values.

Disadvantages of the Approach

- Perturbation method evaluates the change in current for each and every element by solving the corresponding pattern difference equations Although, ϕ symmetric aperture distribution minimizes the number of evaluations but still as the number of elements in the array increases the number of equations to solve increases. Hence this approach is not feasible for the arrays with large number of elements such as used in SKA applications.
- The success of the method strongly depends upon the selection of the ϕ plane and the angle θ in that ϕ plane at which side lobes are compared with the desired pattern. Selection of the ϕ cuts are such that each ϕ cut occurs after a equal coverage area. In this technique selection of ϕ planes depends upon the number of equations need to be solved. Hence accuracy degrades for small arrays whereas, for large arrays (large number of ϕ cuts) the technique becomes more time and memory consuming.

- There is always a possibility of not getting desired results in single attempt, so it might take long time to obtain the desired current distribution for a large array.

In order to overcome the drawbacks of the dicretizing technique for discrete array element excitaion, a new discretizing technique has been proposed. This techniqe utilizes the heuristic search approch Genetic algorithm to find out the best possible current perturbation values. Sampled Taylor distribution serves as the starting generation of GA and further generations are optimized iteratively to obtain the best possible combination of current perturbation values. Next section discuss the proposed GA modified discretizing technique.

3.5. Genetic Algorithm Modified Discretizing Technique

The proposed technique deals with the drawbacks of the discretizing technique used for application of current perturbation method in sampled Taylor distribution. Similar to the conventional one, this technique also utilizes the sampled Taylor distribution as the starting point of the technique. Objective of the Proposed technique is to make the current perturbation method array size independent and to improve the accuracy for smaller arrays. Though the technique has been extensively discussed for the proposed planar array (large arrays) in context of the SKA application but here in this section discussion involves the smaller arrays as well.

In earlier chapters GA has been discussed in detail. The operations of GA are similar to what have been discussed previously. Initilal GA generation is formed by sampled Taylor distribution, the initial population for proposed planar array design is obtained by sampling the continuous circular Taylor distribution for rectangular grid and elliptical boundary approximation.

The Detailed Description of the GA for Proposed Technique is as Follows

(a) Population Generation

As stated earlier, like conventional technique the initial population is the discrete excitation values obtained from circular Taylor distribution. Figure 3.4 Shows the radiation pattern obtained with sampled Taylor circular distribution for the proposed planar array (see figure 2.1). It can be seen here that the radiation pattern is symmetric in ϕ plane and a pencil main beam is obtained. Inset is showing the top view of the radiation pattern from where the elliptical shape of the main beam can be seen quite clearly and all the side lobes follow the Taylor pattern.

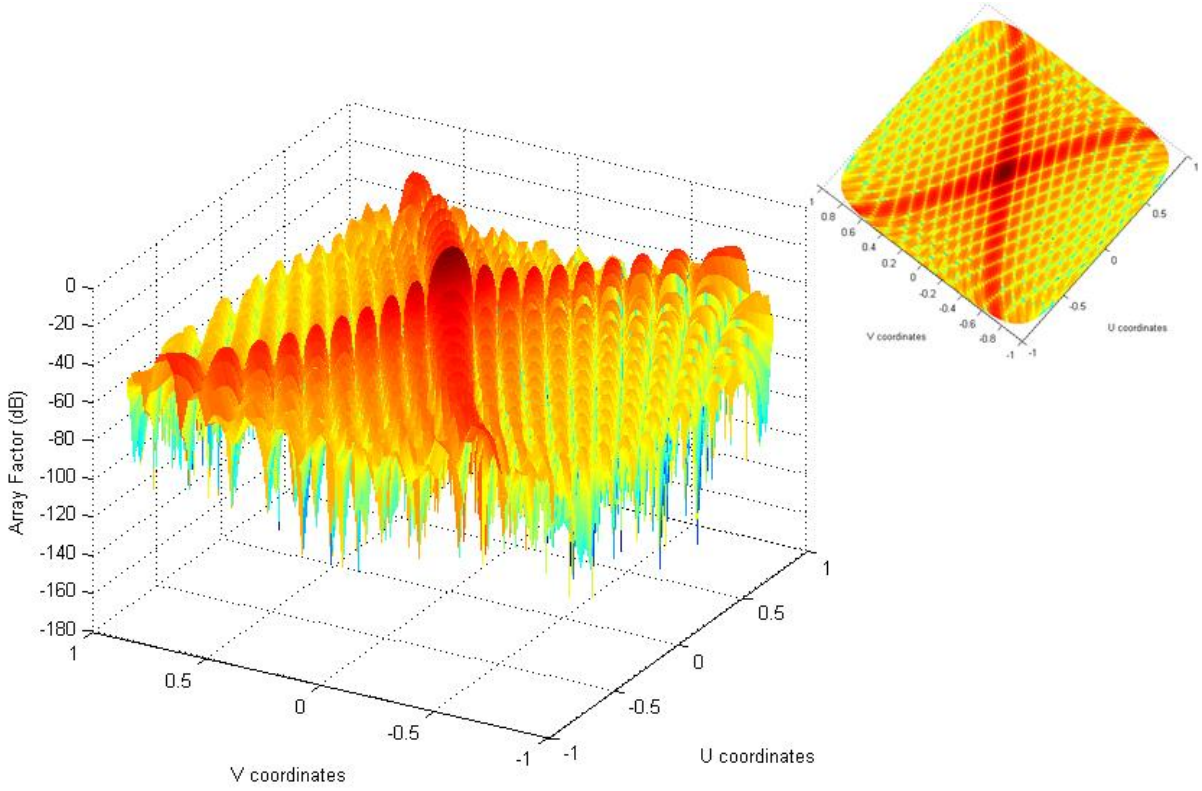

Figure 3. 4 Radiation pattern obtained with sampled conventional Taylor distribution for the proposed planar array

Though, a well behaved radiation pattern is obtained but still it deviates significantly from that of actual Taylor pattern. The side lobe peak obtained with the sampled Taylor distribution for the design is quite higher in comprison to the desired side lobe level and hence need to be improved.

The next step is to generate new chromosomes from the sampled Taylor distribution by using the perturbation method. Here, this approach is different from the conventional one in evaluation of current perturbation values as these values are now generated with random variation in initial current distribution. Once again from Eq. 3.30 to 3.33, the variation in current distribution values has been done in order to achieve the desired radiatioin pattern.

Now, if $\boldsymbol{\delta I'_{mn}}$ **is a randomly generated** current perturbation value for mn^{th}element of the array then the range of the random variation is given by

$$\boldsymbol{L_{lower} \leq \delta I'_{mn} \leq L_{upper}} \tag{3.34}$$

Where $L_{lower} = -0.1$ and $L_{upper} = 0.1$ are the lower and upper limit of variations respectively. Before applying the random variation to the generation it is required to check for the minimum current ditribution value in the population as a perturbation value greater

than the minimum currernt distribution value may lead to the deviation from the actual pattern. Hence the lower limit of perturbation in current distribution is now revised according to the minimum currernt value to incorporate the effect of perturbation of that value in the next population. In this case the range of perturbation is given by

$$(L'_{lower})_m \leq \delta I'_{mn} \leq L_{upper} \tag{3.35}$$

Where $(L'_{lower})_m$ is the minimum value of the current distribution corresponding to the m^{th} string of the array and it makes the lower bound of random variation. For different strings with different length, these lower bounds are evaluated for the corresponding range of random variation. A population on the basis of these random variations is generated and cost evalaution is done in the next step of the algorithm.

(b) Cost Estimation

Cost estimation for the optimization of the proposed design using the proposed discretizing technique is follows as

i. The radiation pattern for the population generated in step one is obtained in terms of RSLL initially.

ii. Cost estimation on the bases of RSLL is performed as follows

(a) First, all the SLL peaks of distribution in every ϕ plane are computed and are denoted as $SLL_{P_{\phi_n}}$, where P_{ϕ_n} corresponds to the side lobe peaks in n^{th} ϕ plane.

(b) Now maximum value of the peak for every ϕ plane is computed and it is denoted as $(SLL_{P_{\phi_n}})_{max}$. Moreover, it is important to include other SLL peaks from every ϕ plane in addition to the maximum one so that an optimized pattern with all the peaks at quasi constatnt hight can be obtained. Involvement of large number of SLL peaks strengthen the serach but it is important to control the computation time requirement as well. This tradoff between time and accuracy has been handelled in optimal way. A random selection of the SLL peaks from every ϕ plane has been done and for n^{th} ϕ plane it is denoted as $(SLL_{P_{\phi_n}})_{random}$. The number of randomly selected peaks may vary according to the design requirement as increased number increases the computation time. In the present case this number has been taken half of the $\bar{n}$ value, i.e. for $\bar{n}$=9, there are 5 randomly selected SLL peaks for each ϕ plane.

(c) Now maximum values of SLL peaks and randomly selected values of SLL peaks obtained from step 2 for all ϕ planes are stored as $((SLL_{P_{\phi_n}})_{max})_{all}$ and $((SLL_{P_{\phi_n}})_{random})_{all}$ respectively. Further peaks of maximum peaks are evaluated in order to have the maximum side lobe levels of the complete radiation pattern and it is given by

$$(SLL_{P_{max}})_{complete} = peaks\left\{(SLL_{P_{\phi_n}})_{max})_{all}\right\} \tag{3.36}$$

(d) Maximum side lobe level values for complete radiation pattern obtained from step 3 and the random peak values obtained from step 2 are combined to have a complete matrix of side lobe peaks for cost evaluation and it is given by

$$SLL_{P_{combined}} = ((SLL_{P_{\phi_n}})_{random})_{all} + (SLL_{P_{max}})_{complete} \tag{3.37}$$

(e) Now if the desired side lobe level is $SLL_{desired}$ than the cost estimation on the basis of standard deviation is given by the following expression as

$$f_{cost} = min\left\{\sum SD_{P_{combined}}\right\} \tag{3.38}$$

Where $SD_{P_{combined}}$ is the standard deviation of the combined peak values from the desired SLL and it is given by

$$SD_{P_{combined}} = \sqrt{\frac{1}{k-1}\sum_{i=1}^{k}[SLL_{P_{combined}}(i) - SLL_{desired}]^2} \tag{3.39}$$

For each chromosome the standard deviation is computed and the minimum value of standard deviation corresponds to the fittest chromosome in the population. This chromosome has a radiation pattern with maximum number of side lobe peaks near to the desired side lobe level in both ways, i.e., peaks are neither too high nor they are too much low from the desired side lobe level on dB scale.

(c) Reproduction

Afte calculating the cost, reproduction of the chromosomes is carried out. Parent selection, crossover and mutation are the three operations which completes the reproduction process. All the chromosomes are now sorted according to theri cost and the fittest chromosome with minmum value of cost functions gets the highest probability of becoming a parent chromosome. After parent selection with the selection probability, these parent chromosomes are now subjected to crossover operation. Unlike conventional GA, the chromosomes have

been represented directly in terms of current excitation values of antenna array elements. This improves the algorithm performance in terms of computation time as there is no need of encoding and decoding of the chromosomes. Moreover, this allows a simple representation of chromosomes and the decimal linear crossover can be carried out without any crossover site selection.

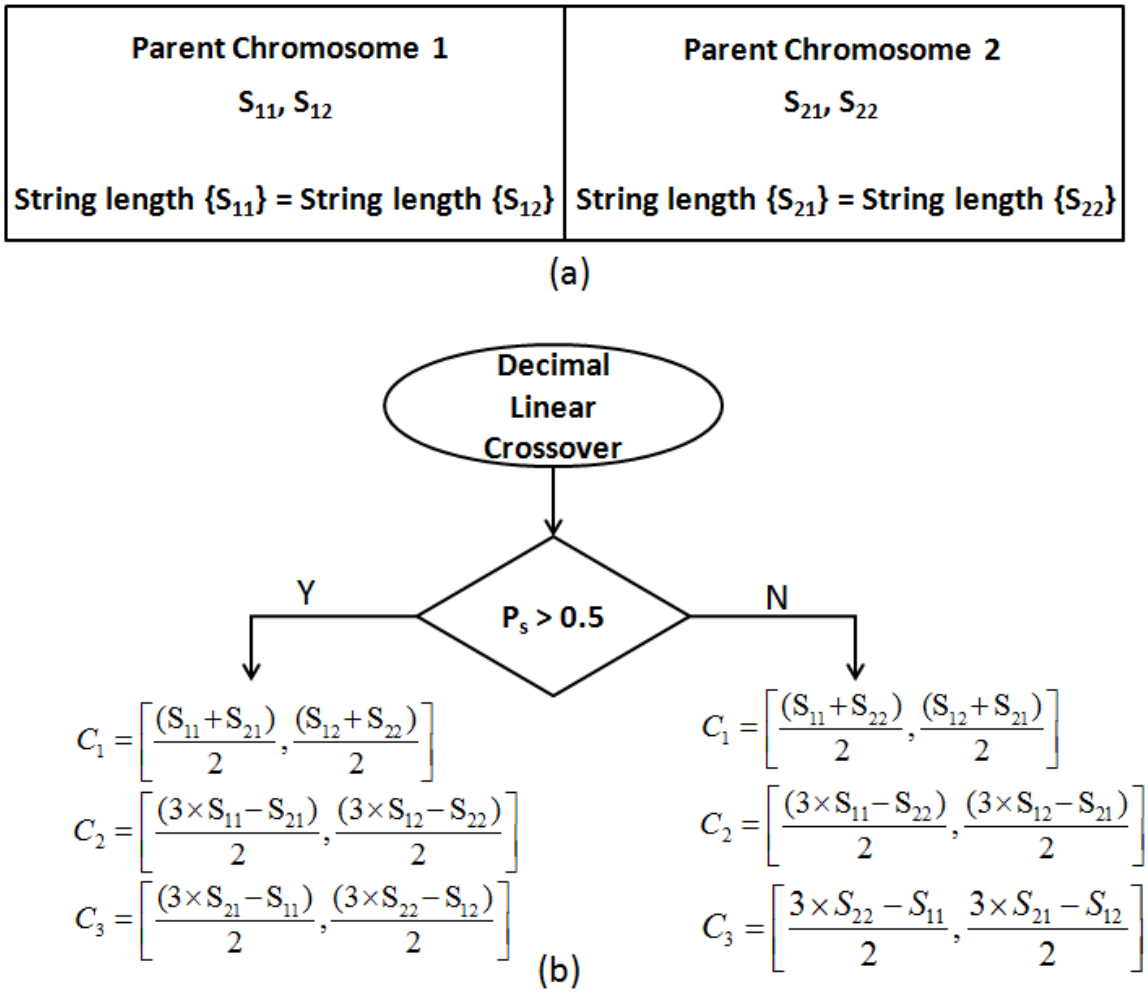

Figure 3. 5 Proposed hybrid decimal linear cross over operation of GA used for optimized current distribution values. (a) Parent strings of same length for crossover; (b) Children after cross over.

In the proposed synthesis a hybrid crossover operation has been performed. Linear crossover operation [Keen-Keong Yan, 1997] in combination with uniform crossover has been applied for new chromosome generation. As discussed earlier for double stage uniform crossover in chapter 2, the geometry induced modification in the crossover operation has been done. Unlike conventional crossover, decimal linear cross over operation in combination with uniform probility of selection of string out of two same length strings for linear crossover results in a hybrid uniform linear cross over operation. If S_{11} and S_{12} are two strings of parent cromosome 1 and S_{21} and S_{22} are of second parent chromosome than the crossover operation

can be understood with figure .Figure 3.5 (a) is showing the parent chromosemes with their corresponding strings and figure 3.5 (b) is showing the desing induced hybrid uniform decimal lineal crossover operation. The probability of generation of child chromosomes with either of the combination of parent choromsomes is uniform. From figure 3.5 it can be seen that there are three chid chromosomes $C_1, C_2,$ and C_3. C_1 corresponds to the mid point, and C_2, C_3 correspond to the extrapolation point of parent chromosomes. For large serach spaces uniform crossover outperforms the other corssover approches [William M. Spears,1991], and it involves each element of parent chromosome. Linear crossover also involves each element of parent chromosome. In linear crossover if the parents have same elements at same position than their children will also have the same element at that position and it is how it retains the quality of parent chromosomes in children by preserving the genetic material. Hybrid uniform linear crossover operation possess the qualities of both the crossover and performs well for the proposed synthesis.

Mutation allows the algorithm to diversify the search and prevents from getting stuck into local minimum. Mutation probability is checked for each element of the chromosome correspnding to a randomly generated number and if probility is higher then the element is changed with the new random element.

After reproduction the new population is generated and it further goes through the same process in the next iteration. The algorithm runs until it achieves the minimum value of standard deviation. After 500 generations of GA, the improvement in the cost becomes stable and algorithm converges.

3.6. Analysis of the Proposed Synthesis

The proposed GA modified discretizing technique for sampled circular Taylor distribution evaluates the current perturbation values for the array elements with Genetic Algorithm. As with conventional Taylor distribution the pattern obtained deviates sigficantly from the desired one and for the pattern improvement the conventional current perturbation method using current equations is limited by the array size. The proposed technique improves the pattern by minimizing the deviation from the desired pattern and the main beam shape remains intact by the proposed planar array geometry.

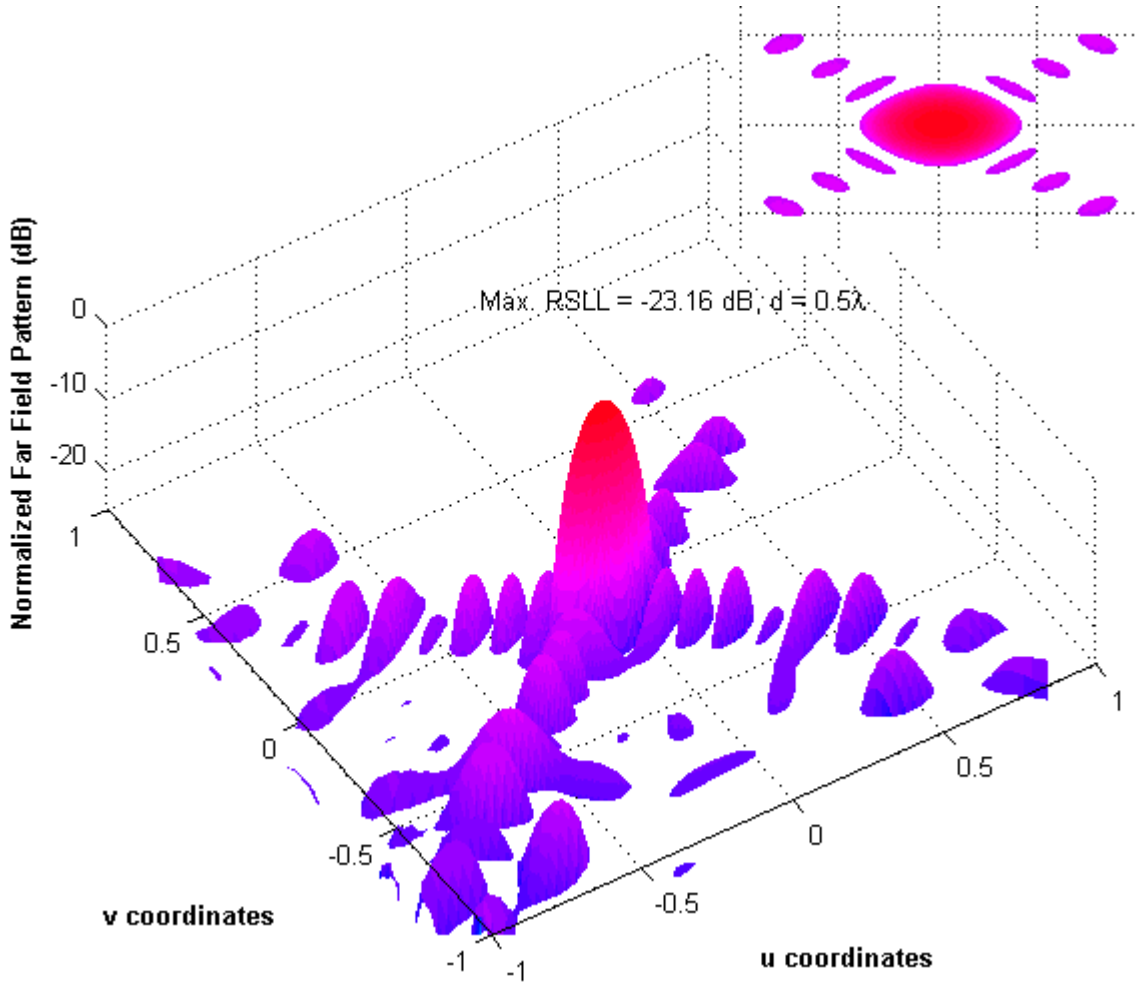

Figure 3. 6 Radiation pattern of the proposed planar antenna array for main beam radiating in end fire direction.

Figure 3.6 shows the radiation pattern for isotropic elements and main beam pointing at $\theta = 0°$ (end fire). The side lobes near to the main beam are at quasi constant hight and the peak side lobe level improves to a value of -23.16 dB. The improvement in side lobe level is quite significant from that of conventional Taylor pattern and from the pattern obtained with array thining approach discussed in chapter 2. Improvement in side lobe peak causes the increment in the 3 dB beamwidth and hence reduced directivity [Balanis, "Antenna Theory: Analysis and Design", 1997]. The proposed synthesis approach improves the side lobe peak value and simultaneously maintain the high directivity of 29.8 dB (given by Eq. 2.9), approximately equal to that of array thinning approach.

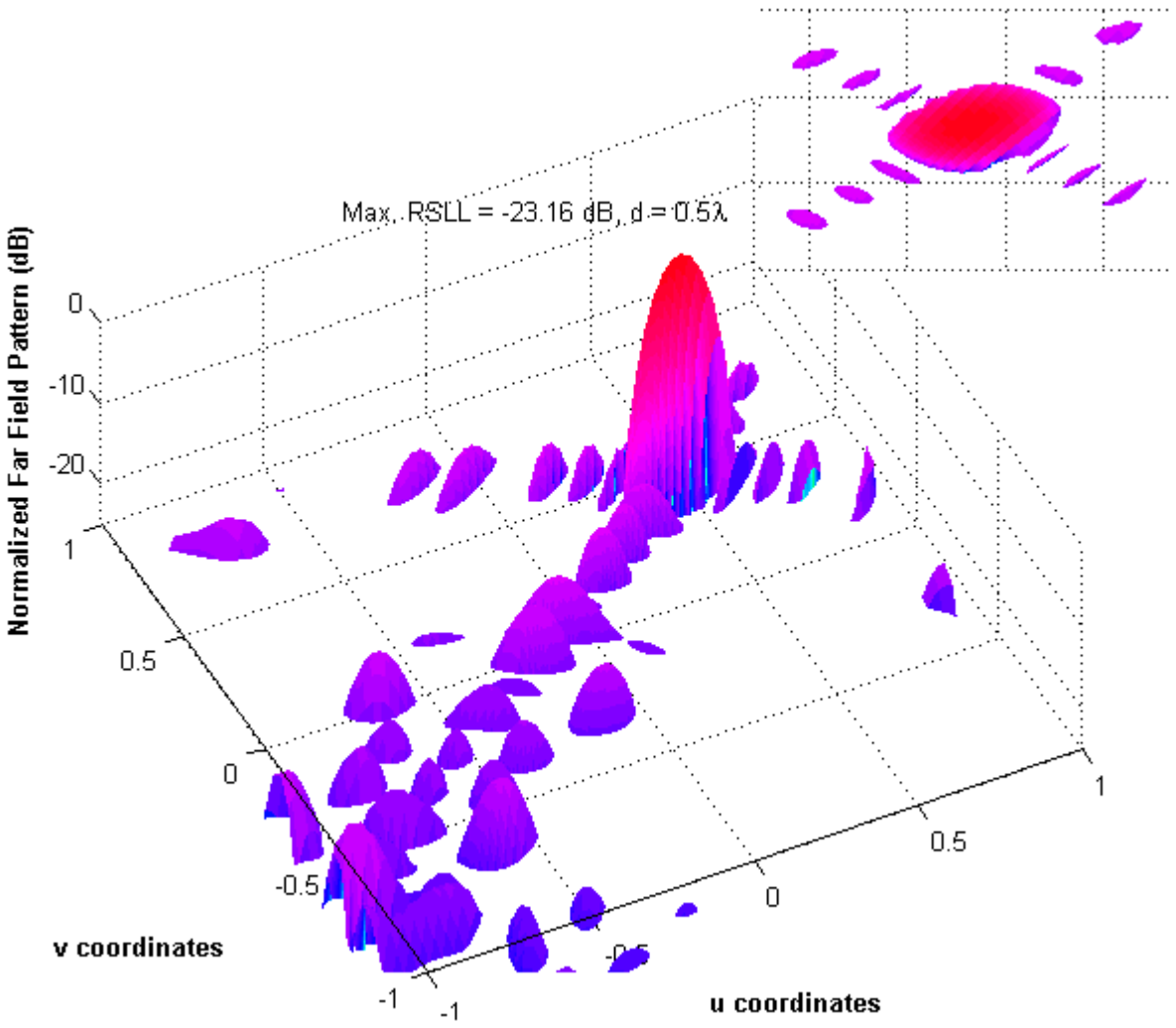

Figure 3. 7 Radiation pattern of the planar array with steered main beam.

Steering of the main beam with isotropic elements causes the radiation pattern to degrade as observed in the case of array thining approch discussed in chapter 2 (see figure 2.11). Although the main beam shape remains preserved with array steering but the side lobes degrades significantly. The proposed array synthesis approach with GA modified discretizing technique minimizes the deviation from the desired pattern and improves the side lobe level with uniformity in side lobes. For the proposed planar array, the sampled Taylor distribution after application of optimized current perturbation values offer the same side lobe level -23.16 dB as it offered for the main beam forming at $\theta = 0°$. Here, the main beam has been steered at an angle of $\frac{\pi}{4}$ in both azimuth and elevation planes. From figure 3.7 , uniform side lobes near the main beam can be observed and the inset is showing the shape of the main beam. It should be noted here that the shape of the main beam remains intact with even

variation in the main beam angle position which is a very important feature as far as satellite and SKA applications are concern. Preserved shape of the main beam is one of the geometry associated advantages of the design and the hexagonal arrangement of elements provides a good steerability of the main beam. Moreover, design offers high directivity of 28.17 dB while maintaining the reduced side lobe peak level.

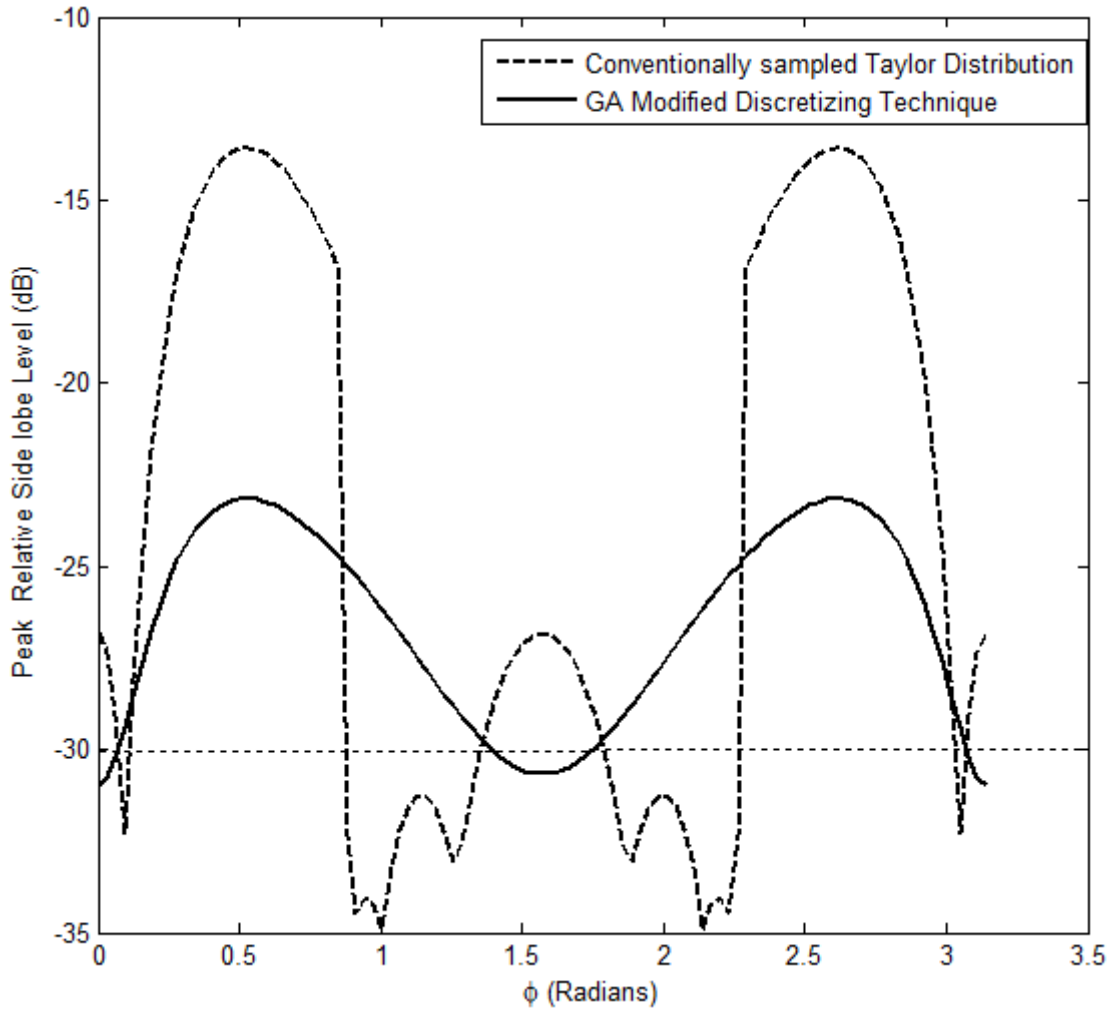

Figure 3. 8 Peak side lobe level comparison between propose GA modified technique and conventional Taylor synthesis

3.7. Performance Comparison

This section discusses the performance of the proposed synthesis technique for side lobe level, directivity, radiation pattern and main beam shape in context of the applications mentioned earlier. As all these are the essential attributes of a planar array offering high sensitivity, low antenna noise, precise coverage area and a well behaved radiation pattern. First a comparison with conventional Taylor pattern has been shown then a comprehensive performance analysis with previuosly proposed array thining approach has been presented.

3.7.1. Conventional Taylor Synthesis and Proposed Synthesis

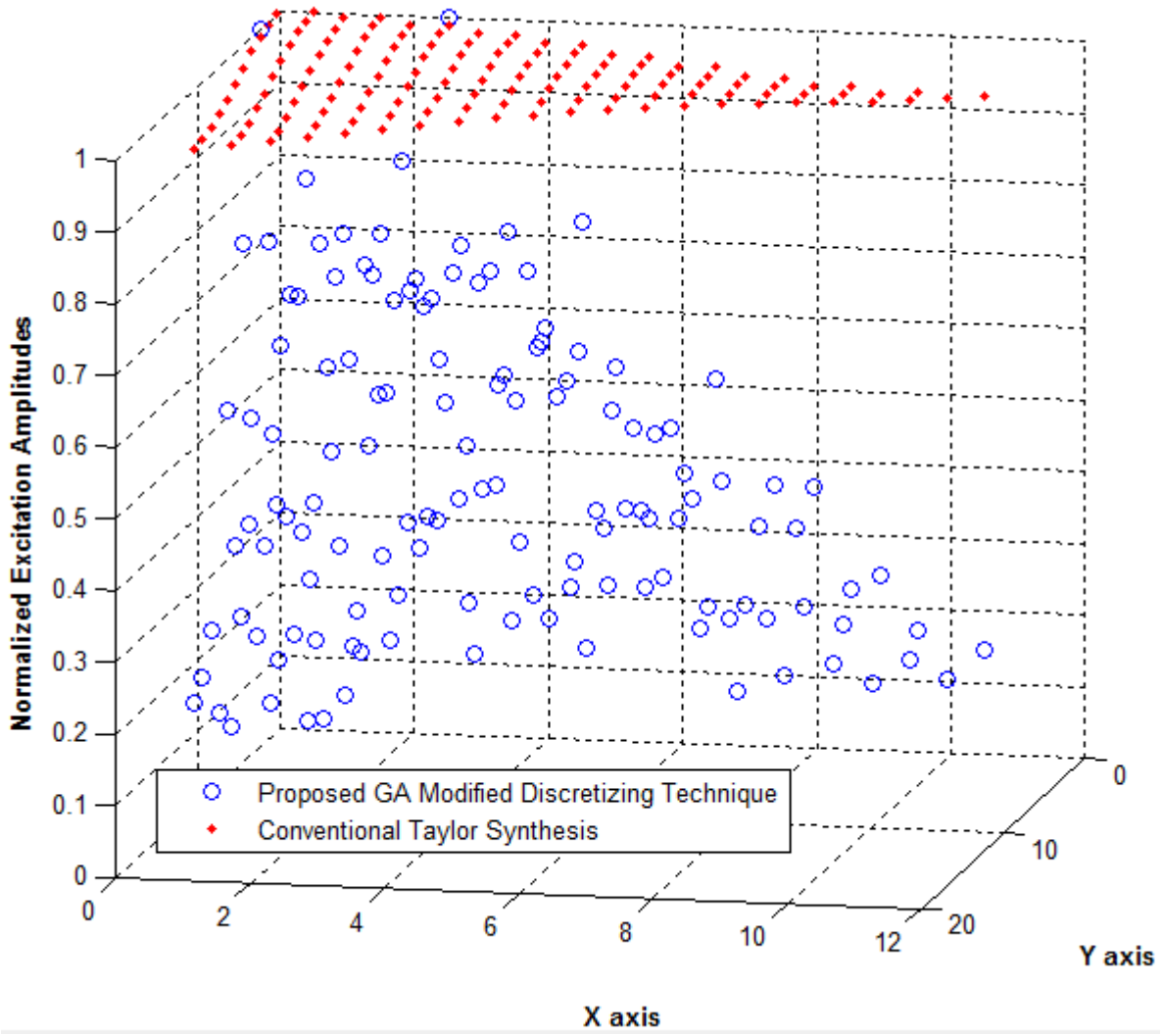

Figure 3. 9 Normalized power requirement comparison between propose GA modified technique and conventional Taylor synthesis

After observing the radiation pattern with the proposed GA modified discretizing technique, it is now compared with the conventional Taylor distribution. The comparison has been carried out on the basis of side lobe levels and the excitation amplitudes in order to investigate the the performance of the planar array for antenna noise reductuion and power requirement.

Figure 3.8 is showing a comparison in peak side lobe levels with variation in the ϕ plane between the proposed disctrezing technique and conventional Taylor distribution for end fire radiation and isotropic elements. It is quite clear from the observation that proposed synthesis approach offers quite improved levels of peak side lobes in all the ϕ planes, and

also the peak side lobes in case of the proposed technique have been obtained quite closer to the desired value of -30 dB represented by a dotted line (see figure 3.8). The dips in the peak side lobe curves are observed along the orthogonal axis and increases when moving away from the axis. Maximum RSLL is obtained in approximate in diagonal directions.

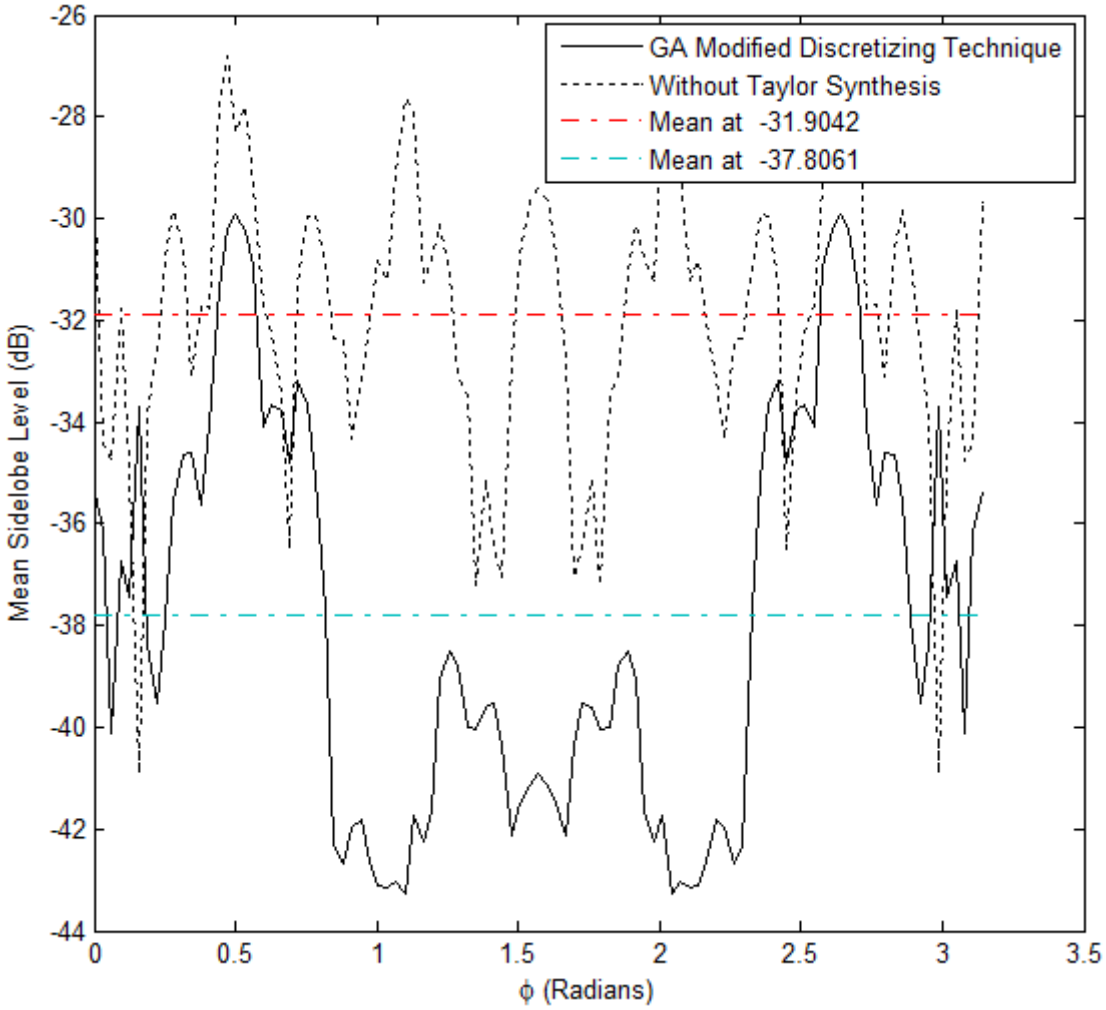

Figure 3. 10 Mean side lobe level comparison between proposed GA modified technique and the previously proposed thinning approach (isotropic elements)

Power requirement for the proposed synthesis in comparison to the conventional taylor distribution is shown in figure 3.9. Evidently, the proposed synthesis has a significant normalized amplitude variation in comparison to the conventional one. The normalized amplitude values for both the design techniques have been computed with respect to a maximum value among both the distributions. It is to be noted here that the excitation values in case of the proposed synthesis is quite less than that of conventional Taylor synthesis. figure 3.9 is showing the current excitation values of elements at their corresponding

positions on the x-y plane and approximately all the elemens in case of proposed synthesis have less current excitation values.

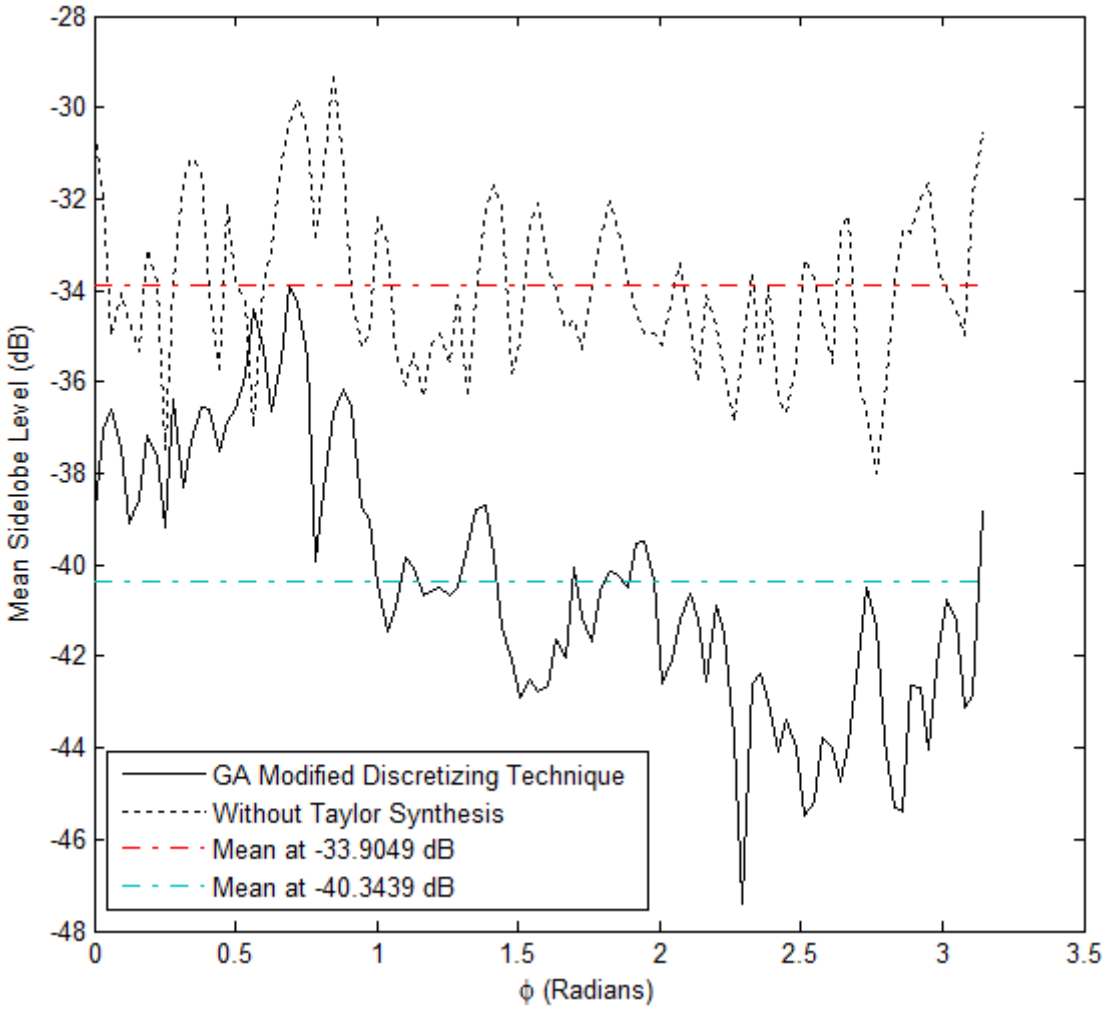

Figure 3. 11 Mean side lobe level comparison between proposed GA modified technique and the previously proposed thinning approach (main beam steered at $\theta = 45°$, isotropic elements)

Table 3. 2 Result of radiation pattern (SLL) for the proposed design with change in main beam position and element pattern.

Synthesis	Main beam position / element pattern	Mean Sidelobe level (dB)
Proposed planar array with array thinning	$\theta = 0$ / isotropic	-31.9042
Proposed planar array with array thinning	$\theta = 45$ / isotropic	-33.9049
Proposed planar array with array thinning	$\theta = 0$ / $cos\theta$	-38.5007
Proposed planar array with array thinning	$\theta = 45$ / $cos\theta$	-40.1805
Proposed planar array with GA Modified	$\theta = 0$ / isotropic	-37.8061

discretizing technique in Taylor distribution		
Proposed planar array with GA Modified discretizing technique in Taylor distribution	$\theta = 45$ ⁄ isotropic	-40.3439

3.7.2. Comprehensive Performance Analysis

Table 3.2 and table 3.3 collectively showing the performance analysis results of the proposed synthesis technique. Here, a comprehensive comparison of the proposed thining approach discussed previously (chapter 2) and GA modified discretizing approach has been done with some other state of the art synthesis approaches. For overall pattern side lobe investigation, mean side lobe levels of the pattern for both (discretizing technique and proposed array thining approach) have been compared. Isotropic elements with main beam pointing in $\theta = 0°$ (see figure 3.10) and $\theta = 45°$(see figure 3.11), the pattern mean side lobes are significantly improved than what had been achieved previuosly. Table 3.2 summarizes the data corresponding to the mean side lobes for both the techniques and approximately a level improvement of 6 dB in both the cases of main beam pointing ($\theta = 0°, \theta = 45°$) has been observed. This analysis shows that with the proposed GA modified discretizing technique for sampled Taylor distribution of circular aperture the limitations encountered by the array thining approach for the proposed design can be overcome.

Moreover, Table 3.3 is showing the performance comparison with some recent work carried out in the area. A peak side lobe level improvement from -20 dB to -23 dB for end fire radiation pattern, and from -17 dB to -23 dB for steered main beam pattern has been observed. Comments on other essential figure of merits can also be done from table . Proposed synthesis outperforms the other synthesis approaches as far as directivity is concern. Highly directive main beams have been obtained due to the proposed antenna geometry and optimized excitation. High spatial resolution of the design leads to high radio telescope resolution required in SKA application [A. R. Thompson, 1986][Peter E. Dewdney, 2009]. Highly directive design offers a high aperture efficiency (η_{ap}) given by the following expression [Karl F. Warnick and Brian D. Jeffs, 2008],[K. F. Warnick et al., 2010]

$$\eta_{ap} = \frac{\lambda^2}{4\pi}\frac{D_a}{A_{ap}} \tag{3.40}$$

Where A_{ap} is the antenna aperture area (physical area of antenna), λ is wavelength, and D_a is antenna directivity defined given by Eq. 2.9 apertuer efficiency is also a significant factor in

antenna noise calculation as it affects the total antenna efficiency. More on antenna noise and system tepmerature along with sensitivity of the antenna array has been discussed in the next chapter.

Table 3.3 A comparison of the proposed design with some recent synthesis approaches on different parameters required for SKA application.

Synthesis	Max RSLL (dB)	Fill Factor	Turned on Elements	Directivity (dB)	Aperture Efficiency (η_{ap})
IFTDT [Will P. M. N. Keizer, 2014]	-22.8	44 %	254	28.2	-
HSPSO [Will P. M. N. Keizer, 2014]	-19.0	44 %	254	-	-
RDT [Will P. M. N. Keizer, 2014]	-20.7	44 %	254	28.2	-
Proposed design thinned with GA	**-20.11**	**60 %**	**290**	**30.39**	**85.5 %**
Sampled Taylor distribution with GA modified discretizing technique	**-23.16**	**-**	**-**	**29.8**	**83.84 %**
Sidelobe cancellation by controlling side elements [J. R. Mohammed and K. H. Sayidmarie, 2014]	-14.5	-	-	31.1	93.7%

3.8. Conclusion

The proposed design (see figure 2.1) in combination with the proposed GA modified discretizing technique acheives the goals of SKA application requirement of high directivity consequently high aperture efficiency, high sensitivity in terms of reduced side lobe level (reduced antenna noise), and high spatial resolution with smaller 3 dB beam width. In this chapter, the proposed synthesis technique in sampling of Taylor circular aperture distribution plays a significant role. As the Taylor synthesis can be applied to discrete planar arrays

regardless of their shape and arrangement of array elements. But the pattern degradation still exist due to the sampling of the continuous aperture distribution and it has a dependency on sampling period. For large arrays with smaller sampling period the degradation due to variation from actual pattern is small. This variation limits the application of Taylor synthesis to large planar array required in SKA and satellite application. Hence in order to avail the advantages of Taylor synthesis it is required to improve the discretizing technique in Taylor synthesis which utilizes the linear equations of current perturbation. Solution of these current equation becomes time and memory consuming for large planar arrays. GA modified discretizing technique minimizes the deviation of obtained pattern from that of desired one by using the properties of Genetic algorithm. This hueristic approach searches for the optimum possible combination of current excitation values by applying the random perturbation to the current excitation value of each element. Unlike conventional GA, chromosomes are represented directly in terms of current exciation amplitudes, eliminating the need of encoding and decoding of chromosomes. This improves the algorithm efficiency in terms of time and memory. Modification in GA crossover operation has been presented in acordance with the geometry. A hybrid uniform decimal linear crossover operation has been proposed. This combines the properties of a decimal linear crossover with a uniform crossover operation. Standard deviation of the obtained pattern from the desired one forms the cost of algorithm. Algorithm searches for the minimum cost, i.e., for minimum standard deviation from the desired pattern. Proposed planar array also avails the geometry associated advantages and one of them is to have high steerability of the main beam while maintaining the desired beam shape. Proposed synthesis offers a side lobe peak on the order of -23.16 dB with main beam pointing at $\theta = 0°$ and planar antenna maintains this level with steering of the main beam. Comparison of peak side lobe level between the conventionally sampled Taylor distribution and proposed discretizing technique show that with the proposed technique the obtained distribution is closer to the desired one (minimum deviation from desired SLL). In addition, the power requirement in terms of array element excitation values show that with proposed synthesis a power efficient antenna array can be designed as antenna array is excited with far less current amplitudes than that of conventional Taylor distribution.

A performance comparison with other synthesis approches including the one proposed in this thesis has also been presented in the end. Obtained mean side lobe level with the synthesis is approximately 6 dB better than the mean level obtained with the priviously proposed thining

approach. This mean side lobe improvement is seen for both main beam pointing directions at $\theta = 0°$ and $\theta = 45°$. Planar array with the proposed synthesis offers a directivity of 29.8 dB, significantly larger than that of other approaches and approximately equal to the value obtained with proposed array thinning approach in chapter 2. It should be noted here that trade off between side lobe peaks and directvity has been handled in an optimum way and design with improvemet in side lobe peak offers high values of directivity. Further, high directivity leading to the higher aperture efficiency make the proposed planar array design and synthesis suitable for achieving low antenna noise. The proposed synthesis improves the results obtained for side lobe level, directivity, aperture efficiency, power requirement in case of the array thining approach with the proposed planar antenna array aperture design. Proposed synthesis outperforms the other antenna synthesis approaches, earlier discussed and mentioned in the thesis literature review, on all parameters of comparison. This comparison also includes the hueristic serach approaches such as HSPSO [Will P. M. N. Keizer, 2014], a combination of Hadamard type and Particle swarm optimization for array thining.

References

- Robert S. Elliot, “Antenna theory and design”, Wiley-IEEE Press, December 2002.
- Keen-Keong Yan and Yilong Lu, "Sidelobe reduction in array-pattern synthesis using genetic algorithm," in IEEE Transactions on Antennas and Propagation, vol. 45, no. 7, pp. 1117-1122, Jul 1997.
- W. Spears and V. Anand, “A study of crossover operators in genetic programming,” in Methodologies for Intelligent Systems, ser. Lecture Notes in Computer Science, Z. Ras and M. Zemankova, Eds. Springer Berlin Heidelberg, vol. 542, pp. 409-418, 1991.
- C. A. Balanis, Antenna Theory. Boca Raton, FL: CRC Press, 2002.
- K. F. Warnick and B. D. Jeffs, "Efficiencies and System Temperature for a Beamforming Array," in IEEE Antennas and Wireless Propagation Letters, vol. 7, no. , pp. 565-568, 2008.
- K. F. Warnick, M. V. Ivashina, R. Maaskant and B. Woestenburg, "Unified Definitions of Efficiencies and System Noise Temperature for Receiving Antenna Arrays," in IEEE Transactions on Antennas and Propagation, vol. 58, no. 6, pp. 2121-2125, June 2010.

- W. P. M. N. Keizer, "Synthesis of Thinned Planar Circular and Square Arrays Using Density Tapering," IEEE Transactions on Antennas and Propagation, vol. 62, no. 4, pp. 1555-1563, April 2014.
- J. R. Mohammed and K. H. Sayidmarie, "Sidelobe Cancellation for Uniformly Excited Planar Array Antennas by Controlling the Side Elements," IEEE Antennas and Wireless Propagation Letters, vol. 13, pp. 987-990, May 2014.
- A. R. Thompson, J. M. Moran, and G. W. Swenson, Interferometry and Aperture Synthesis in Radio Astronomy, 2nd ed. New York: Wiley, 1986.
- P. E. Dewdney, P. J. Hall, R. T. Schilizzi and T. J. L. W. Lazio, "The Square Kilometre Array," in Proceedings of the IEEE, vol. 97, no. 8, pp. 1482-1496, Aug. 2009.
- T. Taylor, "Design of circular apertures for narrow beamwidth and low sidelobes," in IRE Transactions on Antennas and Propagation, vol. 8, no. 1, pp. 17-22, January 1960.
- T. T. Taylor, "Design of line-source antennas for narrow beamwidth and low side lobes," in Transactions of the IRE Professional Group on Antennas and Propagation, vol. 3, no. 1, pp. 16-28, Jan. 1955.

Chapter 4

The Square Kilometer Array Application

Square kilometer array is amonsgt one of the extensively explored areas of research. This application has a huge amount of challenges associated with the wireless communication part. The application has been discussed in context of the proposed planar array synthesis approaches and the points where the proposed design proves its potential for the application have been highlighted.

4.1. Introduction

Antennas are now being used as a mean to study the most important phenomena of universe including the generation and distruction of universe intself. Right now the square kilometer array (SKA) project is in developing stage and antennas for the technical requirement of the applications are being studied. In this thesis the proposed design and the synthesis techniques have been investigated in context of the antenna requirements for this particular application. Earlier the design and the synthesis techniques were examined for radiation pattern including the beam shape, side lobe levels, directivity, spatial resolution in terms of beam width. All these parameters form the background for investigation of some other figure of merits, required for the applucation. In this chapter, the emphasis has been given on the practical challenges associated with the application and how the design can be a solution for those challenges. These challenges have been transformed into technical terms to find out how the proposed design along with proposed synthesis approaches can meet these challenges.

The SKA is an large array of coherently connected antennas spread over a large area (from few meters to hundreds of kilometers). The main application requirement is to collect information from a large space region with high sensitivity and to process the information as fast as possible. The processing part is itself a different field of reserach and state of the art circuitary enable the large data processing at a higher speed. The proposed work is related to the former part of the application, i.e., the collection of radio information with high sensitivity. The development in SKA will have its impact on astroparticle physics and cosmology, fundamental physics, galactic and extragalactic astronomy, solar system science, and astrobiology. SKA was initiated as an international project led by an astronomer. In 1993, The International Union for Radio Science (URSI) started the study for development of

a radio wavelength observatory. Since then, the project has become too large that there are 19 countries and 55 institutes which are working collectively to meet the challenges in realisation of the project. As far as technical concepts are concern, seven different concepts have been developed and two sites, one in Central South Africa and second in state of Western Australia have been identified for the deployment of the antenna arrays. These SKA project blue prints are expected to become operational, upto a frequency range of 10 GHz, by 2022. There are fifteen funding agencies which are continuously observing the development of the project [Peter E. Dewdney, 2009].

According to the U.S. Decadal Review Panel report [Astronomy and Astrophysics in the New Millennium, 2001] the objectives of the SKA project are summarized as

- To explain the generation of universe, the matter which forms the universe, charactetistics of that matter of universe, and how the universe is expanding with time.
- To explain the formation of galaxies and stars, and to understand the initial phase of development of universe.
- To understand the concept of black holes and history of their formation.
- To explain the formation of whole planetry system and their movement in the space.
- To understand how different phonomenas in the space affecting the enviornment of Earth.

These objectives are addresed by the novel application of antenna known as radio telescopes. In order to design telescopes for the application, they must possess qualities such as large field of view, high spectral and spatial resolution, and high sensitivity. It is required to design antenna arrays which can fulfil the application requirement of these telescopes. Although, the frequency range of operation is not fixed but SKA is expecting to receive signals in the frequency range starting from 70 MHz to 30 GHz [Peter E. Dewdney, 2009]. These telescopes have great significance in determinimg various unknown phenomnas of universe through the observation of spectral lines of hydrogen, pulses from the pulsars, magnetic field of universe, spectral line emission in microwave band due to astrophysical masers, synchrotron radiation from stars, galaxies and galaxy clusters due to interaction of high energy electron and magnetic field.

High sensitivity requirement of radio telescopes derives from the fact that the early stage of universe can be explained from the signals coming from far space. These signals with expansion of the universe become weak and their wavelength also get shifted to higher values (red shifting or Dopler shift). Hence it is required to detect these weak radio emission and to design antenna arrays with high sensitivity and high spatial resolution, in order to study the early universe and to detect the small objects in the space [C. Carilli, 2004].

In this chapter, the proposed planar antenna array with the synthesis approcahes proposed and discussed in chapter 2 and 3, has been investigated for the SKA application requirement. The sensitivity of the planar antenna array is a function of effective aperure area with direct proportionality and the system noise temperature with inverse proportionality [Ahmed El-makadema, 2014]. Hence, in order to enhance the sensitivity of the antenna array, one must reduce the antenna noise temperature (system noise temperature has a linear dependency on antenna noise temperature) for given effective area of an antenna. Consequently, the goal has become to reduce the antenna noise tepmerature which itself depend upon the antenna radiation pattern. Highly directive pattern and high antenna efficiency increases the effectve area of antenna and results in high sensitivity. directivity is also related to the antenna noise as with increased directivity, the radiation in unwanted direction decreases and it consequently reduces the system noise temperature (see Eq. 4.23). Radiation in side lobe region should be minimum and to achieve that the pattern must have reduced side lobe level. All these parameters are essential for SKA application. In chapter 2, antenna array thining for the proposed planar array was presented and the design and synthesis approach was investigated for side lobe peaks, directivity, 3 dB beam width, main beam shape and power requirement. In chapter 3, a new synthesis approach based on Taylor synthesis was presented and the lacunaes of previous work were addressed with the proposed work. Design with proposed discretizing technique for sampled Taylor distribution offered improved side lobe peaks, high directivity, high aperture efficiency, and a well behaved radiation pattern with properly shaped main beam. In order to examine the unwanted radiation, a comparison of mean side lobes was presented showing the improved level of side lobe peaks in all the ϕ planes.

Now it is important to investigate the design for system noise and for sensitivity. The required attribute of the antenna is to have highly sensitive design for SKA application. As in SKA the antenna arrays are deployed at different locations of the globe and here the factor which can affect the antenna performance is called Brightness temperature [G. C Medellin,

2004]. Brightness temperature depends upon the surrounding enviornment and changes according to the atmospheric conditions. In different atmospheric conditions the composition of gases changes leading to the variation in absorption of radio signals and consequently causing the variation in brightness temperature [G. C Medellin, 2004]. For SKA application it is a challenge to maintain the same performance level at different atmospheric conditions. The antenna sensitivity should not degrade below a certain level to be able to use as radio telescope. Hence the essential features of an antenna array for SKA application includes minimum system noise temperature, high antenna efficiency, large effective area, high directivity, small 3 dB beam width, minimum side lobe peak and high sensitivity with minimum atmospheric dependency.

Next section discuss about the technical requirements of SKA and then the solutions for these reqirements have been discussed. After that a detailed analysis of brightness temperature calculation, antenna noise temperature calculation has been presented. For the SKA frequency range of operation the specific gaseous absorption has been evaluated through the layer by layer calculation approach [ITU-R P.676-10]. Different standard atmospheric conditions have been refered from the recommendations of international telecommunication union (ITU) provided in [ITU-R P.835-5]. In the end, both the planar array synthesis approaches discussed in chapter 2 and 3 have been tested for antenna noise temperature and antenna sensitivity. Results sensitivity variation with atmospheric conditions have also been presented in order to justify the application of the array as SKA encountering different atmospheric conditions across the globe.

4.2. Technical Requirements

Among all radio telescope design techniques which have been developed over past four to five decades, the most complicated and refined technique is aperture synthesis. The analysis of radio signal through aperture syntheis follows the Van Cittert–Zernike theorem, where the signal is analyzed in three different domains: spectral, temporal, and spatial [A. R. Thompson, Wiley, 1986]. In addition, it is important to identify and nulify the effect of noise generated by man made sources causing radio frequency interference (RFI). A large array of antenna elements is required to meet the qualities of radio telescope, providing a great spatial resolution. Informatio from these antenna arrays is processed to obtain the spectral and spatial varitions with time, spectra at different points in the space, and to reconstruct the brightness distribution. Signals in pair from antennas are cross corelated and integrated to have

minimum effect of noise. The potential areas of reseatch related to SKA are design and synthesis of antenna arrays and large scale production of the centimeter wavelength antennas, optical fiber for high bandwidth of data transmission, signal processing, data computation and storage [Peter E. Dewdney, 2009]. In the proposed work, our focus is on the antenna design part of the application and in that particularly the dsign of dense aperture array that will be disussed later in the chapter. The technical requiremments and challenges in this chapter have been discussed in context of the aperture arrays.

4.2.1. Wavelength Coverage

SKA covers a wavelength range from 70 MHz to 30 GHz [R. T. Schilizzi, 2007], and this technical requirement on wavelength can not be solved through a single antenna technology as the antenna should perform well on all the parameters desired by the application. The proposed design has been investigated for the wavelength range of SKA low array (70 MHz to 350 MHz), starting range of SKA mid array (350 MHz to 1 GHz), and starting range of SKA survey array (350 MHz to 1 GHz). Project require additional sites for planar arrays operating at frequencies greater than 10 GHz [Peter E. Dewdney, 2009].

4.2.2. Sensitivity and Survey Speed

Radio telescopic applications such as SKA require high survey speed of the antenna arrays and consequently require high sensitivity. In context of SKA application, sensitivity describes the capability of an antenna to detect the weakest point source in the space. In a given observing time the strength of the detectable weakest point is inversely proportional to the sensitivity, i.e., higher the sensitivity of the antenna less will be the strength of the unresolved source that the antenna can detect. Time requirement for detection of the weakest objects also has an inverse dependency on sensitivity and this reduces with increment in sensitivity. One more figure of merit that is directly proportional to the sensitivity is the survey speed. Survey speed can be defined as the rate at which the much larger sky in comparison to the field of view can be surveyed for the unresolved point sources with strength above a specified limit. It can be expressed as the ratio of the field of view to the time required to detect the source of a specified strength and hence the survey speed has a direct proportionality to the sensitivity [Peter E. Dewdney, 2009]. Sensitivity also defines the telescopic field of view and it is given by the solid angle over which the sensitivity is greater than 0.5 of its maximum sensitivity. Expression for the sensitivity has been derived in the later part of the chapter.

4.2.3. Array Configuration

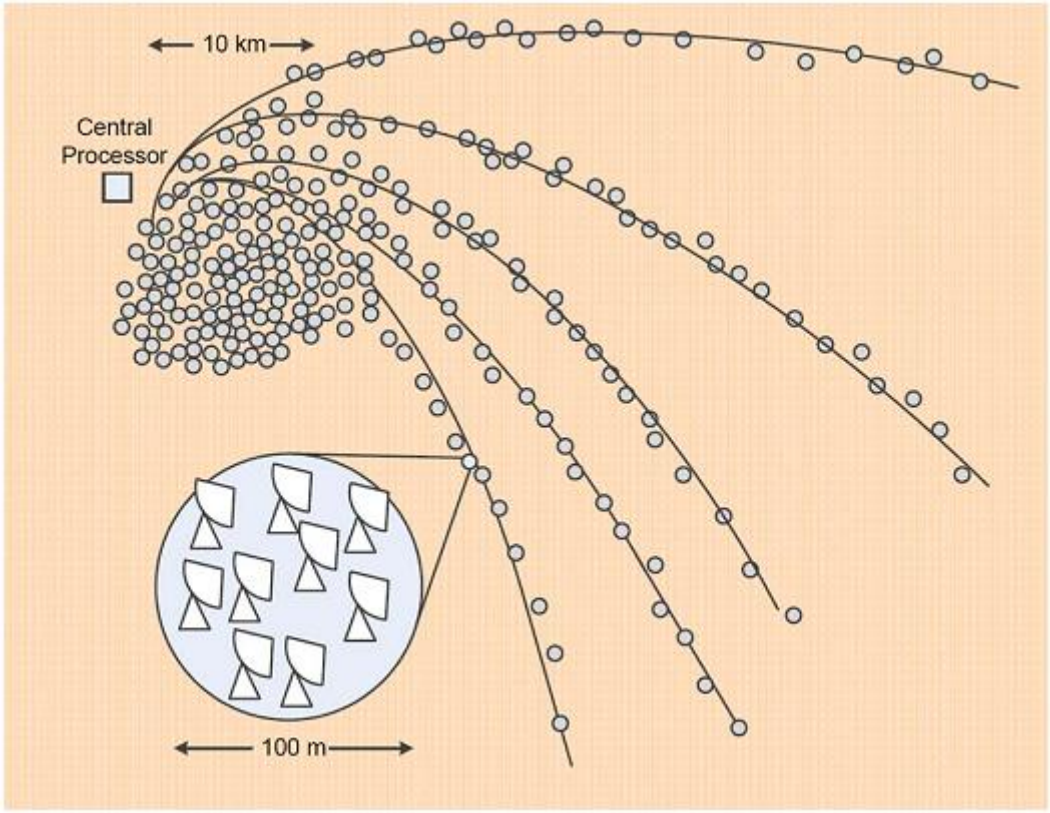

Figure 4. 1 A schematic representation of SKA configurations. Here each dot is representing a bunch of antennas and the dense part of the configuration provides very importantly needed high sensitivity [Peter E. Dewdney, 2009].

Placement of antennas plays a key role in radio frequency imaging of objects. As different antenna pairs identify different objects at different wavelength, they might add noise to other antenna pairs and hence must have minimum system noise. Arrangement of antennas in planar array determines the range of spatial frequencies that can be sampled by the array [Peter E. Dewdney, 2009]. Antenna in pairs are used in interferometer mode and close pairs sample low spatial frequencies are sampled by the close pairs determining the coarse objects whereas, high spatial frequencies are sampled by the distant pairs collecting the information for fine structures. High angular resolution requirement originates from the fact that the starting galaxies have very weak radio emission and needs a telescope resolution on the order of milliarcseconds. For galaxies containing atomic hydrogen, the resolution required to identify the objects is on the order of 10 arcseconds, i.e., antenna pairs at smaller distances are required. In case of close pairs, antennas at larger distances do not have any sensitivity to

these low resolution signals and they add noise to the signals detected by the close pairs. Hence, the overall antenna array system must have low noise in order to detect low resolution information coming from the space. This problem has been addressed by transportable antennas [P. J. Napier, 1983], but in case of SKA the number of antennas in an array is very large and the solution becomes impractical for these arrays. Although, some array geometries have been proposed [R. T. Schilizzi, 2007], in which the density of antenna elements reduces away from the centre of the distribution to minimize the effect of noise by the outermost antennas. Figure 4.1 is showing an example of such progressive reduction in density of antenna element when moving away from the core of the distribution [Peter E. Dewdney, 2009].

4.2.4. Sensitivity Bandwidth

In this section sensitivity of the aperture arrays have been discussed. Antenna arrays which have constant aperture size with respect to the frequency variation [Ahmed El-makadema, 2014], their sensitivity depends significantly on the directivity of the pattern over that frequency range. Minimum side lobes over broad frequency range results in high sensitivity over that bandwidth. Equally spaced array offers high values of sensitivity but for limited bandwidth due the presence of increased side lobe level. Random arrays offer high sensitivity values at low frequency of 90 MHz and maintain this upto a frequency of 140 MHz. At higher frequencies increment in side lobes does not allow the design to main high sensitivity. Tapered arrays offer low sensitivity at lower side of the spectrum although tapered arrays provide improved peak side lobe level [Ahmed El-makadema, 2014].

In order to achieve high sensitivity values over a large bandwidth, it is important to have high directivity and low mean side lobe level over that frequency range of operation. The proposed design has been investigated for antenna noise and sensitivity over the lower side of SKA spectrum. The proposed design lies at the boundary of dense and sparse aperture arrays as the spacing between the elements has been kept constant to $\lambda/2$ and the aperture size varies with frequency. At lower frequencies, higher values of effective aperture areas leads to the high sensitivity values given that the array should produce highly directive main beam.

4.3. SKA Antenna Design Solutions

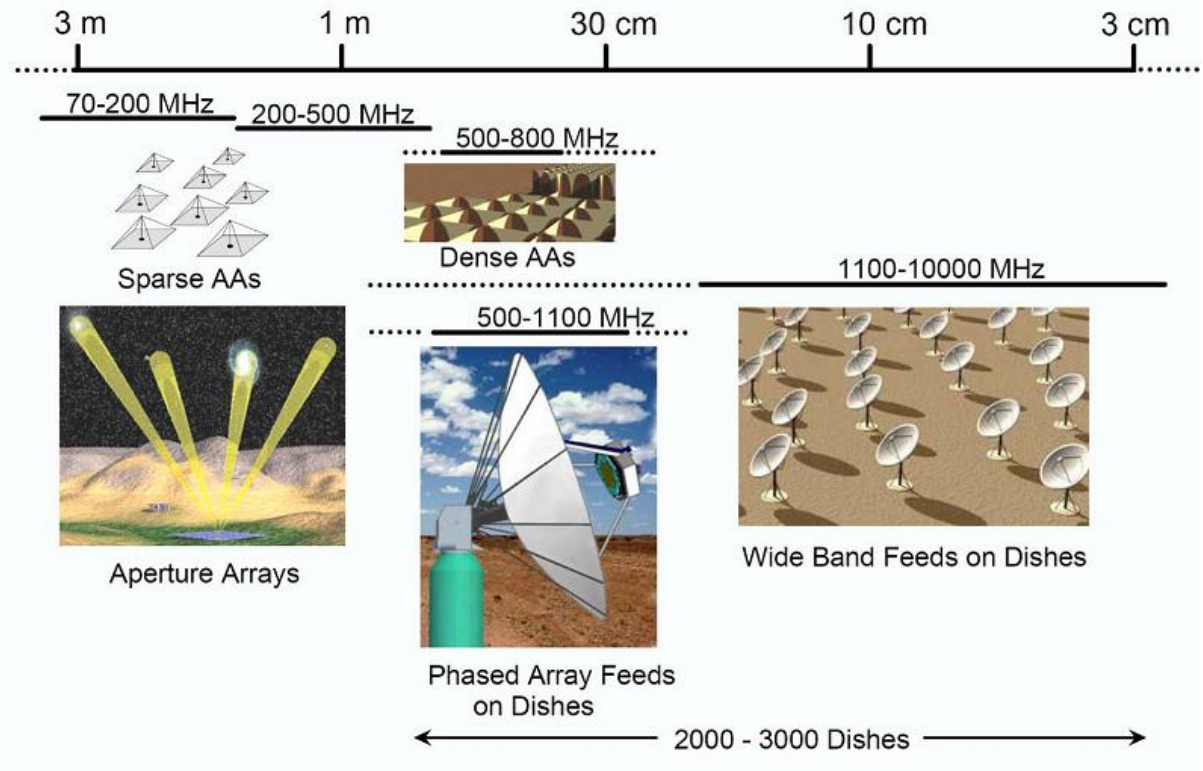

Figure 4. 2 Different antenna technologies over SKA frequency range of operation. Dotted lines are depicting the multiple choices of technology available at those frequency ranges. Lower left side of the figure is showing a picture of multiple beams formed by an aperture array [Peter E. Dewdney, 2009].

After looking at all the technical requirements, this section presents the antenna design solutions with keeping all the technical constraint in background for SKA application. One of the key solutions for SKA application is given by the use of array of small antennas with different configurations. Figure 4.2 shows the SKA spectrum with different antenna technology requirement. The SKA design custom allows us to use different antenna technology at different frequencies. Large (electrically large) parabolic reflectors with single pixel feed [P. J. Napier, 1983] are used at frequencies above 1.5 GHz. These antennas are not bounded by the need of high survey speed and are prevailing at these frequencies. For frequencies below 1.5 GHz, field of view is a deciding parameter and since large dimension antennas have small instantaneous field of view, small antennas (electrically small) with large instantaneous field of view are used for this frequency range. This derives the need of array of small size antennas to form an electrically large antenna known as phased array [SKA Memo 19, 2002.][Will P. M. N. Keizer, 2014] or aperture array [Ahmed El-makadema, 2014]. The maximum sensitivity is achieved in the direction of main beam and the size of this

main beam is approximately equal to that formed by a parabolic reflector. Phased arrays allow the formation of multiple beams enhancing the antenna field of view significantly [R. T. Schilizzi, 2007].

These aperture arrays are classified on the bases of inter-element spacing of the array elements at a given wavelength. When the inter element spacing remains less than or equal to half a wavelength then the array is called dense aperture array. The maximum separation between elements occurs at the lowest frequency of the spectrum. On the other hand, if the elements have the separation greater than or equal to half a wavelength than the array is called sparse aperture array [Ahmed El-makadema, 2014].These arrays have minimum separation of $\lambda/2$ at lowest frequency of operation. These phased arrays are also used to increase the field of view of single pixel filed (SPF) parabolic reflectors. These aperture arrays are used at the foci of parabolic reflector feeding the reflector with bunch of off axis beams. This type of feed in parabolic reflectors is known as phased array feed (PAF) [B. Veidt, 2006]. Clusters of standard feeds can also be used in place of PAF to increase the field of view. PAF can make the antenna design wavelength independent as radius of field of view depends upon the radius of SPF where radius of field of view is determined by the wavelength for a given size of parabolic reflector [Peter E. Dewdney, 2009].

For SKA frequencies below 300 MHz, the antennas which are used are called sparse aperture arrays as the antenna elements are placed a wider distances and the minimum separation between elements at highest frequency is $\lambda/2$. These arrays are designed to have large effective area because at lower frequencies antenna noise temperature becomes significant due to addition of considerable amount of noise from the sky. Here, one has the scope of improvement in the antenna noise temperature to enhance the sensitivity. A smaller array of such elements can provide higher sensitivity than a dense array of much more number of elements.

Hence the conclusion of the discussion is that the SKA application requirements are fulfilled by the aperture arrays even with the large parabolic reflectors as feeding elements. Both the classes of arrays have their own implementation zone but still the factor which remains common area of concern to both the types of array is cost. Sparse aperture arrays utilizes the higher effective area for increment in sensitivity whereas, dense arrays are highly directive and require more number of elements in comparison to the sparse arrays hence increased cost. In case, sparse aperture arrays with decrement in frequency the noise

increases and this generates the requirement of more number of antenna elements and results in higher cost. Moreover, sparse aperture array implementation is more costly because it requires deployment of antennas over a large area. The state of the art requirement is to design arrays which can provide high sensitivity value with less number of elements, smaller array size, wide band of sensitivity, and high sensitivity at lower side of the SKA spectrum. These arrays should be highly directive and do not rely only on the large values of effective area in order to cut the implementation cost.

In view of the previous discussion on the SKA design requirements, challenges and solution, it can be clearly observed that the AAs can provide potential solution for radio telescopes to achieve high spectral and spatial resolution, high sensitivity, large field of view, and high survey speed. As the noise at lower spectral side of SKA operation range is enhanced significantly due to the addition of the noise from sky. This noise addition becomes more significant when the radiation pattern of the antenna is not close to the desired one and hence a well behaved pattern is required. There is a direct relation between antenna system noise and the antenna temperature (see Eq. 4.24) which increases with increment in the unwanted radiation of antenna (see Eq.4.23). Sensitivity of antenna array at these higher wavelengths varies by a considerable amount with variation in the sky brightness temperature which is a function of atmospheric profile (temperature, pressure, water vapour density). The proposed work investigate the proposed planar antenna array (chapter2 and 3) for its sensitivity values and also a detailed analysis has been presented to see the performance of the planar array with variation in the atmospheric conditions. Minimum sensitivity variation while maintaining the sufficiently high sensitivity value is the desirable quality of an array and the proposed array has been tested for this quality.

Since, in the proposed work, the array element spacing has been taken half a wavelength, it corresponds to the dense aperture array. The proposed array with its highest wavelength of operation lies on the boundary of dense aperture array in design space depicted in figure 4.2. From above discussion it can be concluded that the proposed design offers a potential solution in the frequency range of aperture array, particularly dense aperture array, i.e., from 300 MHz to 1.5 GHz (20 cm to 1 m).

Next section presents the detailed sequential calculation of sky brightness temperatureT_b. Different atmospheric conditions have been considered along with different latitudinal positions. Absorption of radiation by different gaseous components present in the

atmosphere has been calculated. Layer by layer approach [ITU-R P.676-10, 2013] has been adopted for calculation of specific absorption coefficient.

4.4. Absorption by Gases

In earth space communication systems the major source of noise is the emission from the gaseous atmosphere in the frequency range from 1 GHz to 340 GHz. This source of noise needs to be addressed in order to have low noise receiving systems [R. K. Crane, 1981]. At radio frequencies attenuation by the scattering is not significant and it is mainly due to the gaseous absorption. Absorption at these frequencies is dominated by the water vapour and oxygen content in the atmosphere [Ernest K. Smith, 1982]. Water vapour for the above mentioned frequency range has absorption lines at 22.235 GHz, 183.31012, 323, 325.1538 GHz [F.T. Ulaby et al., 1981],[G. C Medellin, 2004]. From figure 4.4, the absorption lines of oxygen molecule spanning from 50 to 70 GHz collectively make a continuous absorption band centred around 60 GHz and it also has a single distinct absorption line at 118.75 GHz [rosenkranz][G. C Medellin, 2004]. These rotation absorption lines for water vapour are produced by the interaction of electric dipole with the incident filed, whereas oxygen molecule with its permanent magnetic moment causes the attenuation by the magnetic interaction with the incident field. Frequencies other than these absorption lines generally called valleys between the peaks are useful for the RF communication. Although, these absorption lines find their application in remote sensing, where emitted radio noise in a certain region is utilized to sense the temperature or water vapour content of that region [Robert K crane].

Various models such as atmospheric transmission (AT) [E. Grossman, 1989], atmospheric transmission at microwave (ATM) [J. R. Pardo et al., 2001] are there for the calculation of atmospheric absorption, and number of codes using Libe's microwave propagation model for attenuation calculation. Radiative transfer codes have also been used for the calculation of gaseous attenuation [L.S. Rothman et al., 1992],[H.M. Pickett et al.,1998]. In this paper, the calculation of gaseous attenuation has been carried out using [G. C Medellin, 2004],which utilizes the models given in [Ernest K. Smith, 1982] and [Rosenkranz, 1975] for the calculation of absorption by water vapors and by molecular oxygen, respectively. Absorption coefficients of these species have a dependency on various factors such as density of molecules, temperature, pressure, and the frequency which defines the atmospheric profile. Atmospheric profile changes with the height and consequently

changes the values of absorption coefficients of the gaseous molecules. At different latitudes the losses associated with the attenuation by atmosphere varies widely due to this dependency. In order to accurately calculate the specific absorption by the gaseous molecules it is required to define the atmospheric profiles as a function of height from the earth surface [G. C Medellin, 2004]. In this paper, layer by layer calculation of attenuation proposed in ref [ITU-R P.676-10] has been implemented. This approach provides an accurate estimation of the absorption of the incident field for a frequency range of 1 to 1000 GHz, as it calculates the absorption in each layer with the propagation distance in the corresponding layer. As the profile changes gradually with the height, it causes the ray banding from one layer to another layer. The whole atmosphere has been assumed to be divided in number of discrete horizontal layers and ray travels from one layer to another with an angle of arrival and departure. In each layer the travelling distance varies and hence its absorption by the gaseous molecules in each layer is different. In the end the absorption by each individual layer for a given resonance line is added to obtain the resultant absorption by the atmosphere. The calculation of absorption coefficients for water vapour molecules and oxygen molecules has been carried out using [G. C Medellin, 2004]. The atmospheric profiles as a function of height has been taken from the reference standard atmosphere defined in ref [P.ITU 835-5].

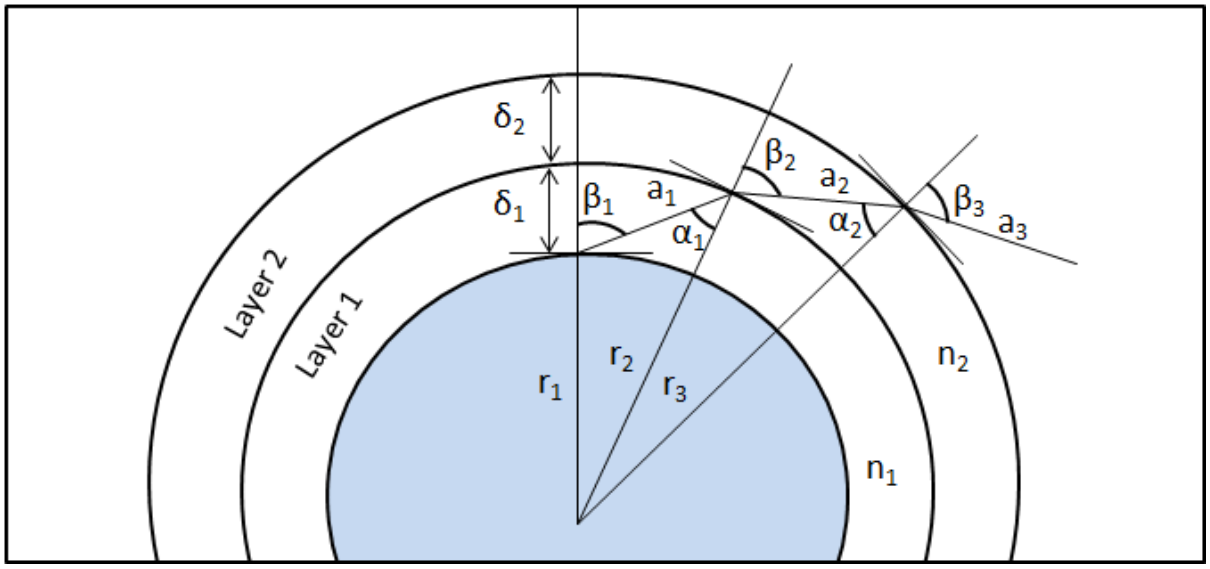

Figure 4. 3 Ray tracing in the atmosphere with atmosphere divided into number of layers with different atmospheric profiles (first two layers) [P.ITU 835-5].

4.5. Line by Line Calculation of Specific Attenuation

Specific attenuation of the signal by the molecules of water vapour and oxygen at each individual layer is required to be estimated with the atmospheric profile functions defined in [P.ITU 835-5]. In line by line calculation model, the atmosphere is divided into number of horizontal layers from the ground level to a level of 100km from the ground. In this model, the layer thickness varies exponentially in order to have an accurate estimation of the path attenuation [ITU-R P.676-10]. Starting from the lowest thickness of 10 cm at ground goes up to a maximum thickness of 1 km at a height of 100km from the ground level. At each individual layer the atmospheric absorption coefficients are calculated using the expressions referred in [G. C Medellin, 2004] corresponding to their height from the ground level. The absorption coefficient in dB/km for oxygen molecule is given by [G. C Medellin, 2004],[Rosenkranz, 1975]

$$k_{o_2}(\nu) = 1.61 \times 10^{-2} \nu^2 \left(\frac{P}{1013}\right)\left(\frac{300}{T}\right)^2 F_{o_2}(\nu, \nu_{if}) \tag{4.1}$$

Where ν is the frequency in GHz, P is the atmospheric pressure in mbars and T is the temperature in K. The oxygen line shape function has two components: one is the non resonant part and second one is the resonant part and it is defined as [G. C Medellin, 2004]

$$F_{o_2}(\nu, \nu_{if}) = \frac{0.7\gamma_b}{\nu^2 + {\gamma_b}^2} + \sum_{j=1, j\ odd}^{J_{max}} \phi_j \left[g_{j^+}(\upsilon) + g_{j^+}(-\upsilon) + g_{j^-}(\upsilon) + g_{j^-}(-\upsilon)\right] \tag{4.2}$$

$$\phi_j = 4.6 \times 10^{-3} \frac{300}{T}(2j+1) e^{-6.89\times10^{-3}\left(\frac{300}{T}\right)j(j+1)} \tag{4.3}$$

$$g_{j^\pm}(\upsilon) = \frac{\gamma_j {d_{j^\pm}}^2 + P(\upsilon - \upsilon_{j^\pm}) Y_{j^\pm}}{\left(\upsilon - \upsilon_{j^\pm}\right)^2 + {\gamma_j}^2} \tag{4.4}$$

$$\gamma_j = 1.18\left(\frac{P}{1013}\right)\left(\frac{300}{T}\right)^{0.85} \tag{4.5}$$

$$\gamma_b = 0.49\left(\frac{P}{1013}\right)\left(\frac{300}{T}\right)^{0.89} \tag{4.6}$$

$$d_{j^+} = \left[\frac{j(2j+3)}{(j+1)(2j+1)}\right]^{1/2} \tag{4.7}$$

$$d_{j^-} = \left[\frac{(j+1)(2j-1)}{j(2j+1)}\right]^{1/2} \tag{4.8}$$

Where ϕ_j is the fractional population of initial state of the j[th] line, γ_j and γ_b are the resonant and non resonant line width parameters, and $d_{j\pm}$ is the amplitude of lines $\upsilon_{j\pm}$. In the calculation of specific absorption by oxygen molecule first twenty absorption lines have been considered. The resonant frequencies and their corresponding interference coefficients are summarized in Table 4.1.

Table 4.1 first 20 resonant linea and corresponding interference coefficients for oxygen molecules [G. C Medellin, 2004] [Rosenkranz, 1975].

Resonant Frequencies (GHz)		Interference Coefficients (mbar^{-1})	
υ_{j+}	υ_{j-}	Y_{j+}	Y_{j-}
56.2648	118.7503	4.51×10^{-4}	-0.214×10^{-4}
58.4466	62.4863	4.94×10^{-4}	-3.78×10^{-4}
59.5920	60.3061	3.52×10^{-4}	-3.92×10^{-4}
60.4348	59.1642	1.86×10^{-4}	-2.68×10^{-4}
61.1506	58.3239	0.33×10^{-4}	-1.13×10^{-4}
61.8002	57.6125	-1.03×10^{-4}	0.344×10^{-4}
62.4112	56.9682	-2.23×10^{-4}	1.65×10^{-4}
62.9980	56.3634	-3.32×10^{-4}	2.84×10^{-4}
63.5685	55.7838	-4.32×10^{-4}	3.91×10^{-4}
64.1278	55.2214	-5.26×10^{-4}	4.93×10^{-4}
64.6789	54.6711	-6.13×10^{-4}	5.84×10^{-4}
65.2241	54.1300	-6.99×10^{-4}	6.76×10^{-4}
65.7647	53.5957	-7.74×10^{-4}	7.55×10^{-4}
66.3020	53.0668	-8.61×10^{-4}	8.47×10^{-4}
66.8367	52.5422	-9.11×10^{-4}	9.01×10^{-4}
67.3694	52.0212	-10.3×10^{-4}	10.3×10^{-4}
67.9007	51.5030	-9.87×10^{-4}	9.86×10^{-4}
68.4308	50.9873	-13.2×10^{-4}	13.3×10^{-4}
68.9601	50.4736	-7.07×10^{-4}	7.01×10^{-4}
69.4887	49.9618	-25.8×10^{-4}	26.4×10^{-4}

Another significant source of RF absorption is the water vapour present in atmosphere and absorption coefficient for water vapour molecule in dB/km is given by the following expression [F.T. Ulaby et al., 1981], [G. C Medellin, 2004]

$$k_{H_{2O}}(\nu) = 2\nu^2\rho_\nu\left(\frac{300}{T}\right)^{\frac{5}{2}}\sum_{i=1}^{i_{max}} A_i e^{-\frac{\varepsilon_i'}{T}} F_{H_{2O}}(\nu,\nu_i) + \Delta k(\nu) \tag{4.9}$$

The line shape function for water vapour molecule is given by [G. C Medellin, 2004]

$$F_{H_{2O}}(\nu,\nu_i) = \frac{\gamma_i}{({\upsilon_i}^2 - \upsilon^2)^2 + 4\nu^2{\gamma_i}^2} \tag{4.10}$$

$$\gamma_i = \gamma_{i0}\left(\frac{P}{1013}\right)\left(\frac{300}{T}\right)^{x_i}\left[1 + 10^{-2}a_i\frac{\rho_\nu T}{P}\right] \tag{4.11}$$

$$\Delta k(\nu) = 4.69\times10^{-6}\nu^2\rho_\nu\left(\frac{P}{1013}\right)\left(\frac{300}{T}\right)^{2.1} \tag{4.12}$$

Where, ρ_ν is the water vapour density in the atmosphere in g/m^3, P is the atmospheric pressure in mbars, T is the atmospheric temperature in K, and ν is the frequency in GHz. The term Δk is the empirically derived correction term of water vapour absorption coefficient [G. C Medellin, 2004]. Values for the first 10 water vapour absorption lines and associated transition parameters are summarized in Table 4.2 [G. C Medellin, 2004].

Table 4.2 First 10 line absorption transition parameters of water vapour molecules.

i	ν_i (GHz)	ε_i'	A_i	γ_{i0}	a_i	x_i
1.	22.23515	644	1.0	2.85	1.75	0.626
2.	183.31012	196	41.9	2.68	2.03	0.649
3.	323	1850	334.4	2.30	1.95	0.420
4.	325.1538	454	115.7	3.03	1.85	0.619
5.	380.1968	306	651.8	3.19	1.82	0.630
6.	390	2199	127.0	2.11	2.03	0.330
7.	436	1507	191.4	1.50	1.97	0.290
8.	438	1070	697.6	1.94	2.01	0.360
9.	442	1507	590.2	1.51	2.02	0.332
10.	448.0008	412	973.1	2.47	2.19	0.510

As discussed earlier, the tropospheric water vapour and oxygen molecules are the prime sources of attenuation of centimetre and millimetre wave signals and in order to calculate the total absorption by the atmosphere, following is the expression for the atmospheric absorption coefficient [G. C Medellin, 2004]

$$k_a(\nu, z) = k_{H_2O}(\nu, z) + k_{o_2}(\nu, z) \tag{4.13}$$

Here, the atmospheric absorption coefficient has a dependency on frequency and height from the ground level in terms of the atmospheric profile functions defined in terms of height in [P.ITU 835-5]. Eq. 4.13 gives the atmospheric absorption coefficient at each point in the atmosphere for a given frequency but it is not sufficient in order to calculate the total attenuation for a satellite communication link. As the wave travels through the earth's atmosphere, the phenomenon of ray banding occurs and this causes the path length to differ in each layer of atmosphere. Now, from [ITU-R P.676-10], let us assume that the ray travels through a path length of a_n in n^{th} layer of atmosphere. Thickness of the layer is δ_n and ray enters into the layer with an angle of α_n and departs with an angle of β_n. Figure 4.3 depicts the layer by layer propagation of ray through the atmosphere [ITU-R P.676-10], here r_n is the radial distance of the layer from earth centre.

$$a_n = -r_n \cos\beta_n + \frac{1}{2}\sqrt{4r_n^2 \cos^2\beta_n + 8r_n\delta_n + 4\delta_n^2} \tag{4.14}$$

The ray arrival angle α_n is given by [ITU-R P.676-10]

$$\alpha_n = \pi - \cos^{-1}\left[\frac{(-a_n^2 - 2r_n\delta_n - \delta_n^2)}{(2a_n r_n + 2a_n\delta_n)}\right] \tag{4.15}$$

At the ground observation, the ray incident with an angle of β_1 and this angle is same as the elevation angle in Figure 2.3 (Coordinate plot). The successive angles of incidence can be calculated using the Snell's low given by the following expression

$$\beta_{n+1} = \sin^{-1}\left(\frac{n_n}{n_{n+1}}\sin\alpha_n\right) \tag{4.16}$$

Where, n_n and n_{n+1} are the refractive index profiles of nth and $n+1^{th}$ layers respectively. These index profiles have been calculated from the radio refractive index functions defined in [ITU-R P.453]. Eqs. from 4.14 to 4.16 depicting the ray propagation are valid for the standard atmospheric conditions described in [P.ITU 835-5] and accurately model the ray tracing for all incidence angles considered here. The above set of equations does not hold true in case the ray incident parallel to the earth surface due to the presence of layers of radio refractive index gradient smaller than -157 N/km [ITU-R P.676-10].

Thickness of the layer varies exponentially and it is given by the following expression [ITU-R P.676-10]

$$\delta_l = 0.0001 \exp\left[\frac{l-1}{100}\right] \tag{4.17}$$

Where l=1 to 922, i.e., the atmosphere is divided into 922 layers starting from the ground level and up to a height of 100 kms.

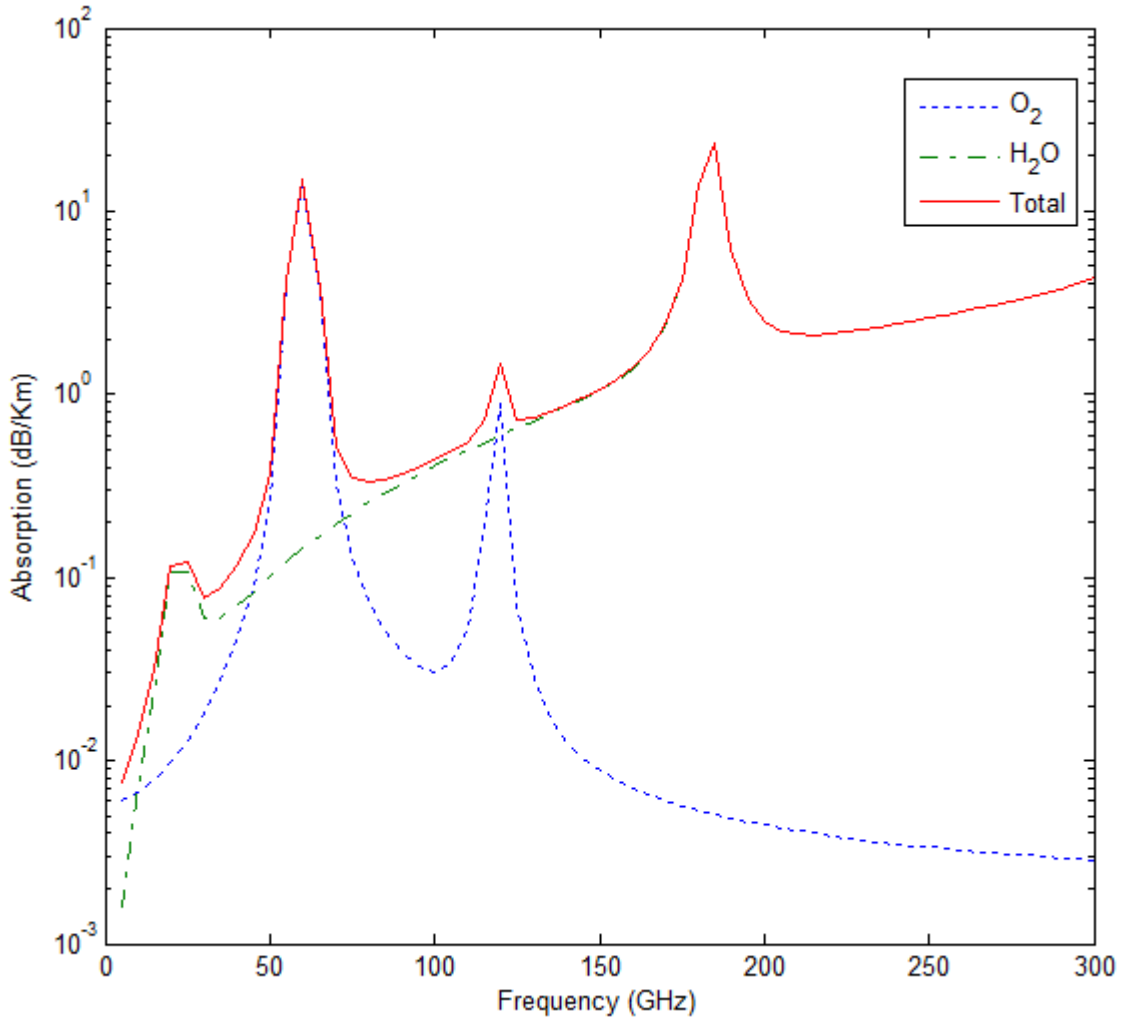

Figure 4. 4 Specific absorption by the oxygen and water vapour over microwave frequency range. Atmospheric conditions are given by $p = 1013\ mbar, T = 293\ K$, and water vapour density $7.5\ gm^{-3}$[G. C Medellin, 2004].

Now from Eq. 4.13, the atmospheric absorption coefficient of nth layer of atmosphere can be written as

$$k_a(\nu, z_n) = k_{H_2O}(\nu, z_n) + k_{o_2}(\nu, z_n) \tag{4.18}$$

Where z_n is denoting the height of the nth layer corresponding to which different height dependent atmospheric profile functions are evaluated to have the value of specific absorption coefficient at the given layer. Now the total attenuation due to atmospheric absorption can be derived as

$$k_{at}(\nu, z) = \sum_{n=1}^{l_{max}} k_a(\nu, z_n) \tag{4.19}$$

The power absorbed by these molecules is re-emitted as thermal radiation and it is one of the major contributors to the sky brightness temperature. Other sources of brightness temperature involve the background cosmic emission, and radiation and scattering from the ground.

4.6. Brightness Temperature and Antenna Temperature

Radiative transfer theory describes the intensity of radiation in a given medium, in the present case it is the atmosphere which absorb, emit and scatter radiation. At a specific frequency, the power flowing per unit area, per unit frequency interval, per unit solid angle is the specific intensity which describes the radiation field. The power attenuated through atmospheric absorption is re-emitted by the molecules as thermal radiation. The amount of power attenuation depends upon the distance over which the radiation travels the atmosphere. The specific intensity from a given direction is expressed as [G. C Medellin, 2004]

$$I_\nu = I_\nu(z_0) \exp[-\tau_\nu(0, z_0)] + \int_0^{z_0} k_a(\nu, z) B_\nu(T) \exp[-\tau_\nu(0, z)]\, dz \tag{4.20}$$

Where $I_\nu(z_0)$ the background intensity at a distance Z_0, $B_\nu(T)$ is the radiation source within the medium and it is given by Plank's function when the medium is isothermal. τ_ν is the opacity of the medium and k_a is the atmospheric absorption.

At microwave frequencies the Plank's function has a linear dependency on physical temperature and in this frequency range with Rayleigh-Jeans approximation the brightness temperature is defined as [G. C Medellin, 2004]

$$T_b(\nu) = T_{bo}(\nu) \exp[-\tau_\nu(0, z_0)] + \int_0^{z_0} k_a(\nu, z) T(z) \exp[-\tau_\nu(0, z)]\, dz \tag{4.21}$$

Where T_{bo} is the background cosmic emission term. More detailed discussion on the derivation of Eq.4.21 can be found in [G. C Medellin, 2004].

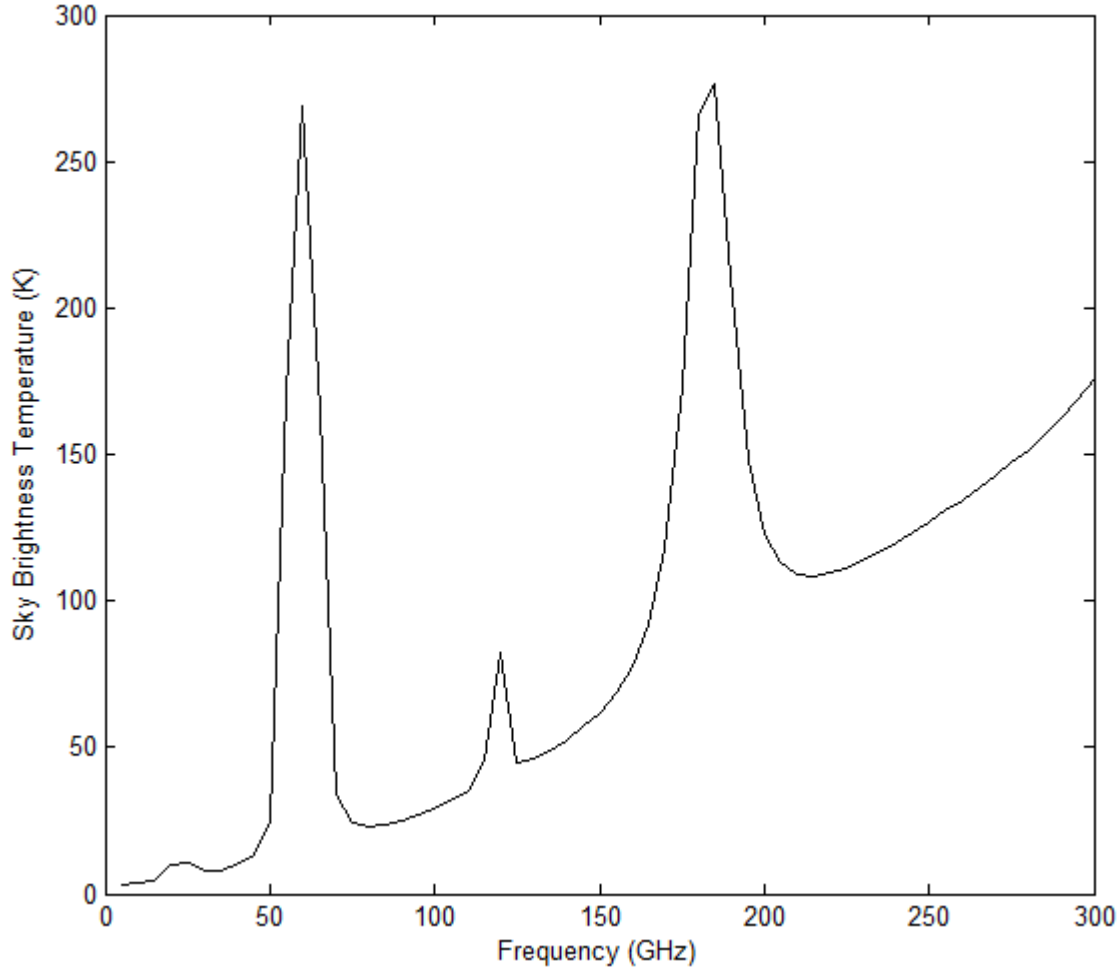

Figure 4. 5 Zenith attenuation through the atmosphere at surface conditions $P = 1013\ mbar, T = 293\ K$, water vapour density $7.5\ g/m^{-3}$[G. C Medellin, 2004].

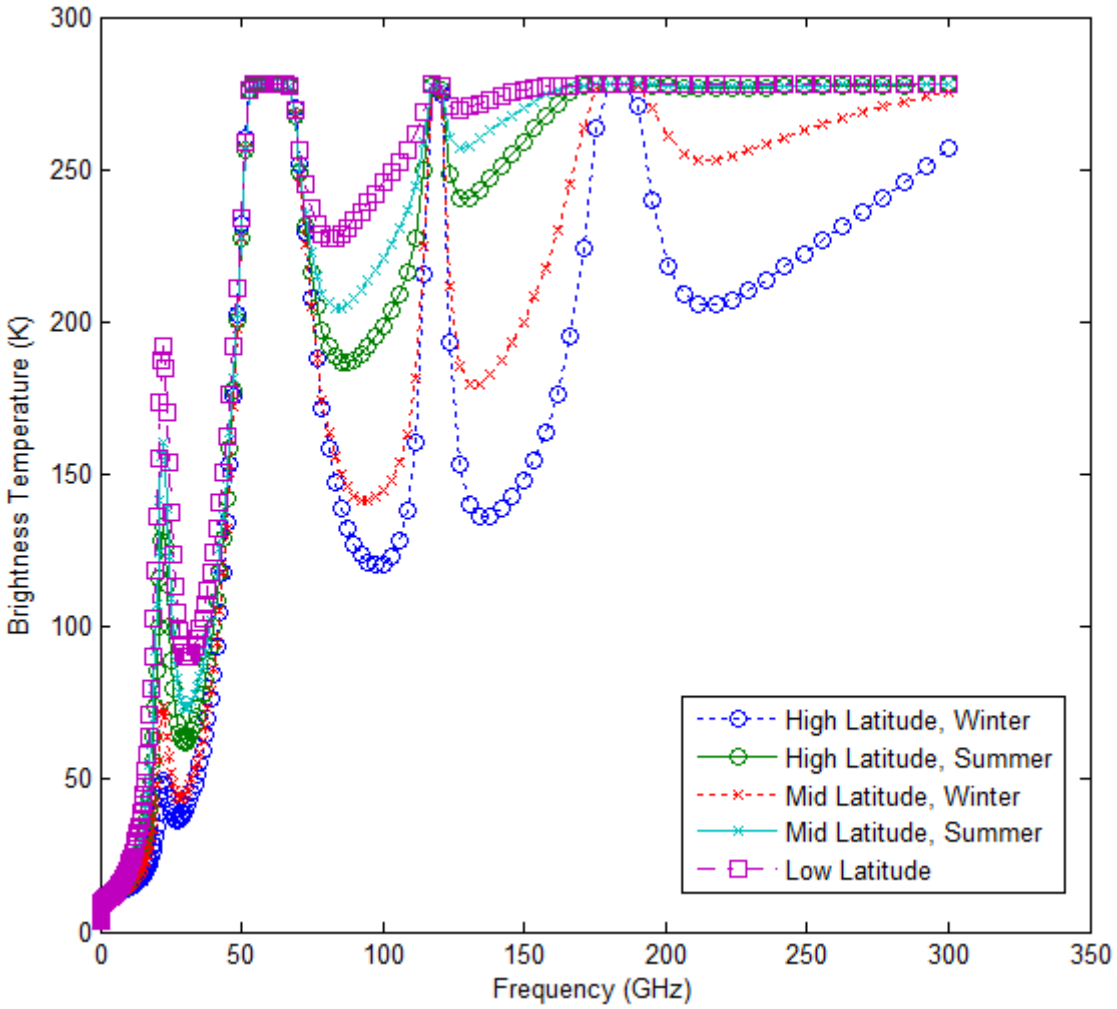

Figure 4. 6 Brightness temperature comparison at zenith for different atmospheric conditions.

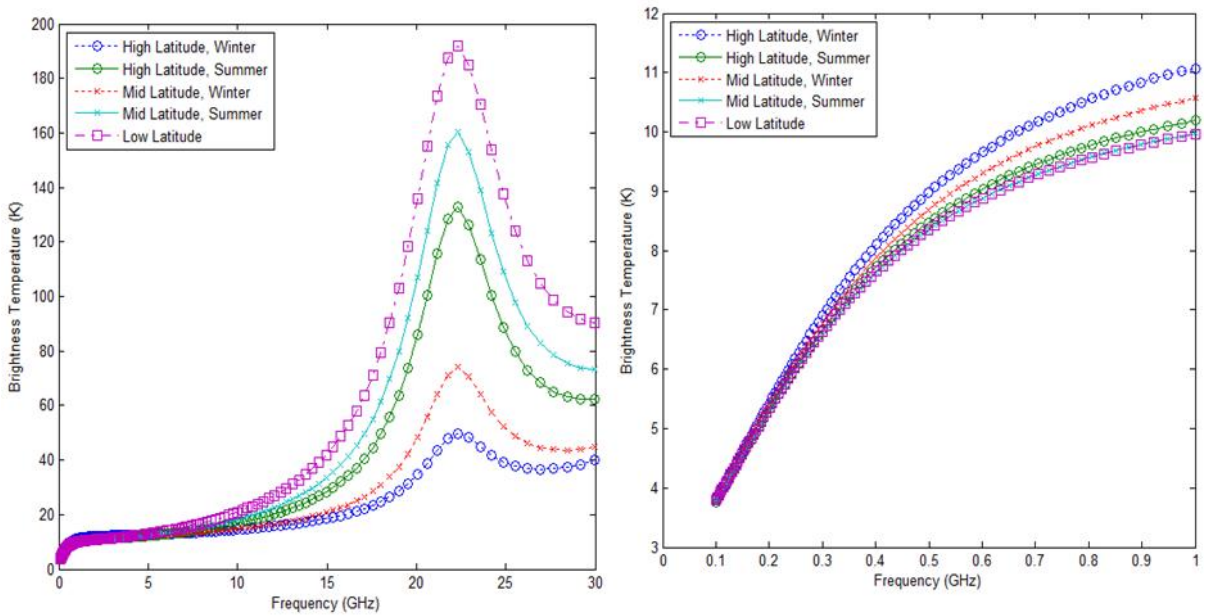

Figure 4. 7 Brightness temperature (a) over complete SKA frequency range of operation, (b) over low and mid SKA frequency range.

Sky brightness temperature is one of the major sources of noise in earth space communication as it contributes as antenna noise temperature and consequently to the antenna system noise temperature. A small improvement in noise performance can be very significant in order to have high sensitivity as far as radio telescopic applications such as SKA (square kilometre array) are concern. SKA covers a frequency range of 70 MHz to 30 GHz. It is a very wide range and cannot be served with a single antenna technology [SKA]. In this particular frequency range a good estimation of the brightness temperature can be done with the expression given by [ITU R P.372-7]

$$T_b(v) = T_{eff}\left[1 - \exp\left(-k_{at}(v,z)\right)\right] + T_{bo}(v) \tag{4.22}$$

Where the effective temperature T_{eff} is taken to be 275 K, k_{at} is the total absorption obtained from layer by layer calculation of specific absorption, and T_{bo} is the temperature due to background cosmic emission.

Figure 4.5 is showing the sky brightness temperature computed from Eq. 4.22 at zenith with surface atmospheric conditions $P = 1013\ mbar, T = 293\ K$, and water vapour density 7.5 g/cm^{-3}. It is reflecting the absorption lines shown by the water vapour near 22 GHz and 180 GHz and oxygen molecules between 50 GHz to 70 GHz and single line at 118.75 GHz. Figures 4.6 and 4.7 are showing the brightness temperature for the different latitudes [ITU-R P.835-5] over the whole microwave frequency range and over SKA frequency range of operation, respectively. SKA encounters noise mainly near 22 GHz due to the water vapour density present in the atmosphere. Sky brightness temperature also has a dependency on the elevation angle as with increment in the elevation angle brightness temperature encounters a decrement. As from the layer by layer calculation, it can be observed that the ray travel more oblique as the angle of elevation decreases and this causes more absorption by the atmospheric gases leading to the increment in brightness temperature. Figure 4.8 is showing the change in brightness temperature for an increment in elevation angle from $0°$ to $90°$. The maximum brightness temperature is observed at $0°$ whereas; it is lowest at $90°$ as expected.

Brightness temperature when convolved with the antenna radiation pattern gives the antenna noise temperature T_a (Eq. 4.23). This gives an idea that antenna noise temperature can be reduced by reducing the radiation in unwanted directions and hence can improve the system noise temperature and further the sensitivity. Here, it is to be noted that the parameters have been discussed in context of an antenna array as the proposed work has been

carried out for a planar antenna array. From Eq. 4.23, it is clear that the antenna radiation pattern with reduced side lobe levels and high directivity are required in order to have minimum antenna noise temperature.

$$T_a = \frac{\iint |F(\theta,\phi)|^2 T_{sky}(\theta,\phi) \sin\theta \, d\theta d\phi}{\iint |F(\theta,\phi)|^2 \sin\theta \, d\theta d\phi} \tag{4.23}$$

A typical antenna receiver system consists of a LNA (low noise amplifier), a transmission line, a circulator, and an antenna [E. Brookner, 2013]. Assuming the LNA noise temperature within limits, no antenna resistive losses and no mismatch losses between the antenna and the receiver, the driving factor of the system temperature is antenna noise temperature.

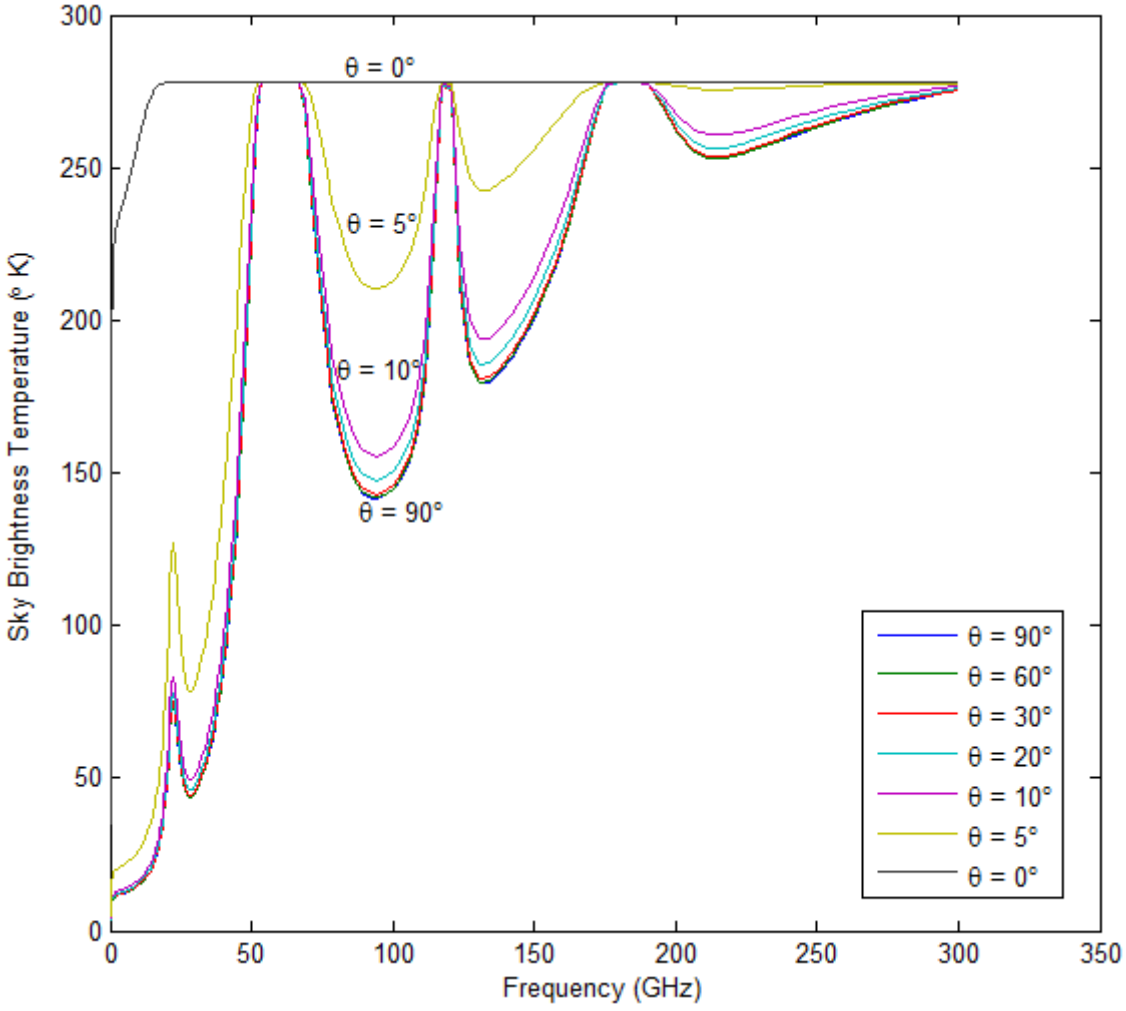

Figure 4. 8 Sky brightness temperature at mid latitude (winter) with variation in elevation angle θ.

One important figure of merit of antenna is antenna sensitivity and it has a direct dependency on antenna system noise temperature. Antenna sensitivity will be discussed in detail in the next section. As in our proposed work, all the parameters have been discussed in context of

the antenna array so for an antenna array with total array efficiency η_T, array antenna noise temperature T_a, the system noise temperature is given by [Ahmed El-makadema, 2014]

$$T_{Sys} = \eta_T T_a + (1 - \eta_T) T_{sur} + T_{LNA} \tag{4.24}$$

In some literature the system noise temperature is defined in terms of radiation efficiency of the antenna Karl F. Warnick and Brian D. Jeffs, 2008],[K. F. Warnick et al., 2010]. Total efficiency or antenna efficiency with the assumption of perfect matching condition is the product of aperture efficiency and radiation efficiency. A detailed discussion on the definition and derivation of antenna efficiencies has been provided in [Karl F. Warnick and Brian D. Jeffs, 2008],[K. F. Warnick et al., 2010].

$$\eta_T = \eta_{ap} \eta_{rad} \tag{4.25}$$

One more parameter which is important for antenna performance is effective area A_{eff} of the antenna. It describes the power capturing capability of the antenna and is defined as the ratio of the power available at the antenna terminals to the power flux density of a polarization matched plane wave incident on the antenna from that particular direction [Balanis, "Antenna Theory: Analysis and Design", 1997]. Higher effective area corresponds to the higher sensitivity of the antenna. An array effective area is given by [Ahmed El-makadema, 2014]

$$A_{eff} = \frac{\lambda^2}{4\pi} \eta_T D \tag{4.26}$$

Now the sensitivity of the antenna array can be defined as [K. F. Warnick and B. D. Jeffs, 2008]

$$S = \frac{A_{eff}}{T_{sys}} \tag{4.27}$$

On the basis of above figures of merit, the proposed design has been tested for antenna temperature and sensitivity values. The emphasis has been given to the SKA application requirement and hence the analysis has been carried out for low SKA range (70 MHz to 350 MHz) and mid SKA range (350 MHz to 1 GHz). High sensitivity and minimum sensitivity variation with atmospheric conditions are the most paramount requirement of the application as the arrays are deployed at different locations of the globe. In the next section, performance analysis of the proposed planar array with both the proposed methods, array thinning approach and GA modified discretizing technique of Taylor synthesis, has been presented in order to test the design for application over above mentioned frequency range of SKA

operation. In this chapter, sensitivity and antenna noise temperature has been checked. Other performance parameters for the application have been tested in the previous chapters of the thesis.

4.7. Performance Analysis

Figures 4.9 to 4.12 are showing the antenna temperature corresponding to different atmospheric conditions [ITU-R P P.835-5] for the radiation pattern obtained with the proposed geometry of hexagonal planar antenna array optimized with GA. The obtained thinned configuration had minimum side lobe peak and high directivity consequently minimising the amount of area of spurious radiation convolved with the sky brightness temperature (see Eq. 4.22). The antenna elements have been assumed to be isotropic in figures 4.9 and 4.10. Initially for low SKA the antenna temperature is approximately same for all the latitudes conditions and after 350 GHz (mid SKA) it starts diverging. For low SKA range the antenna temperature values are quite low and increment can be seen with the increment in frequency. High latitude in winter offers highest antenna temperature amongst all and low latitude conditions support minimum antenna temperature values. From figure 4.10, with steering of the main beam antenna temperature values increases slightly as the main beam steering causes the side lobes to increase. Still the increment in the antenna temperature is not significant and the pattern of antenna temperature with latitude variation remains the same as in case of end fire radiation pattern. For $\cos\theta$ element pattern the antenna temperature is shown in figures 4.11 and 4.12. Evidently the improvement is expected as the side lobe with $\cos\theta$ element pattern reduces (see figure 2.10) and with steered main beam as the increment in side lobe has been observed, it is reflected in the antenna temperature. A detailed analysis of antenna temperature is provided in [N. Razavi-Ghods, 2012], where different array geometries and element placing have been tested for antenna temperature. For element spacing of 0.5λ, antenna temperature at 100 MHz for different array element positions and arrangement (triangular, regular, sparse, thinned array, concentric ring array) was found to be above 500 K. Figure 4.13 compares the performance for different antenna element patterns. Antenna with $\cos\theta$ element pattern over all offers less antenna temperature than the isotropic pattern as expected from the radiation pattern. Main beam steering causes the rise in side lobe level and that is the reason for increment in antenna temperature.

Now sensitivity calculation involves both the system noise temperature and he effective area of the antenna aperture (Eq. 4.27). Increment in the size of the array increases

the sensitivity; particularly at lower frequency range noise from the sky brightness temperature is quite significant and increases the system noise. Size of the aperture can be increased to a point where side lobes start migrating into the visible region also depending upon the scan range of the antenna.

Equally spaced arrays offer improved sensitivity but for limited bandwidth of one octave. This is because of the increment in the side lobe level. Further, random arrays with large value of inter element separation achieves high sensitivity values (90 MHz) but sensitivity decreases with increment in frequency after 140 MHz. This trend in sensitivity can be explained with the increased antenna effective area. Although, tapered arrays have improved side lobe peak and improved mean side lobe level but as the sensitivity is dominated by the effective area at lower frequencies, these arrays offer comparatively low sensitivity values at low frequencies [Ahmed E. Makadema, 2014].

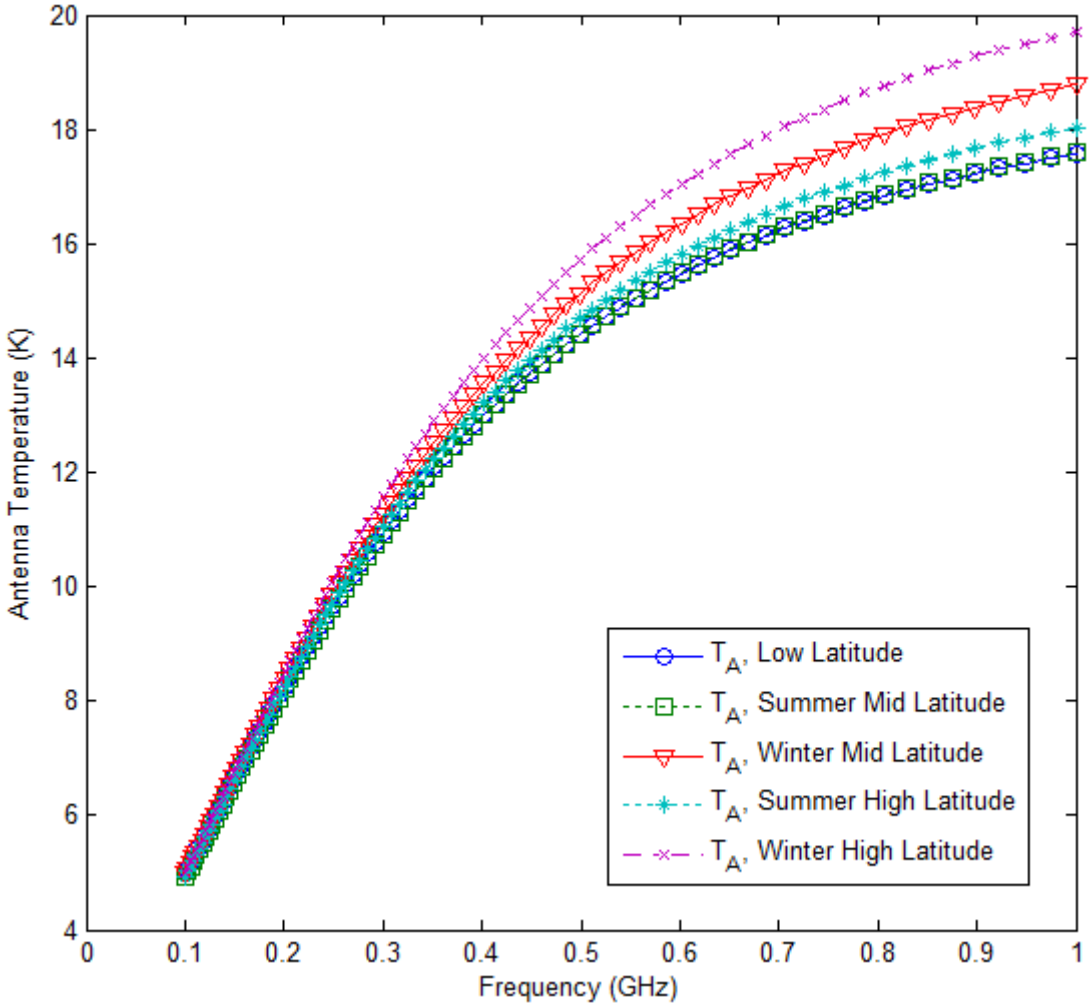

Figure 4. 9 Antenna Temperature for the proposed design optimized with array thinning approach at different latitudes (corresponding atmospheric conditions taken from Reference standard atmosphere ITU-R P.835-5). The antenna array is radiating in end fire direction with isotropic elements.

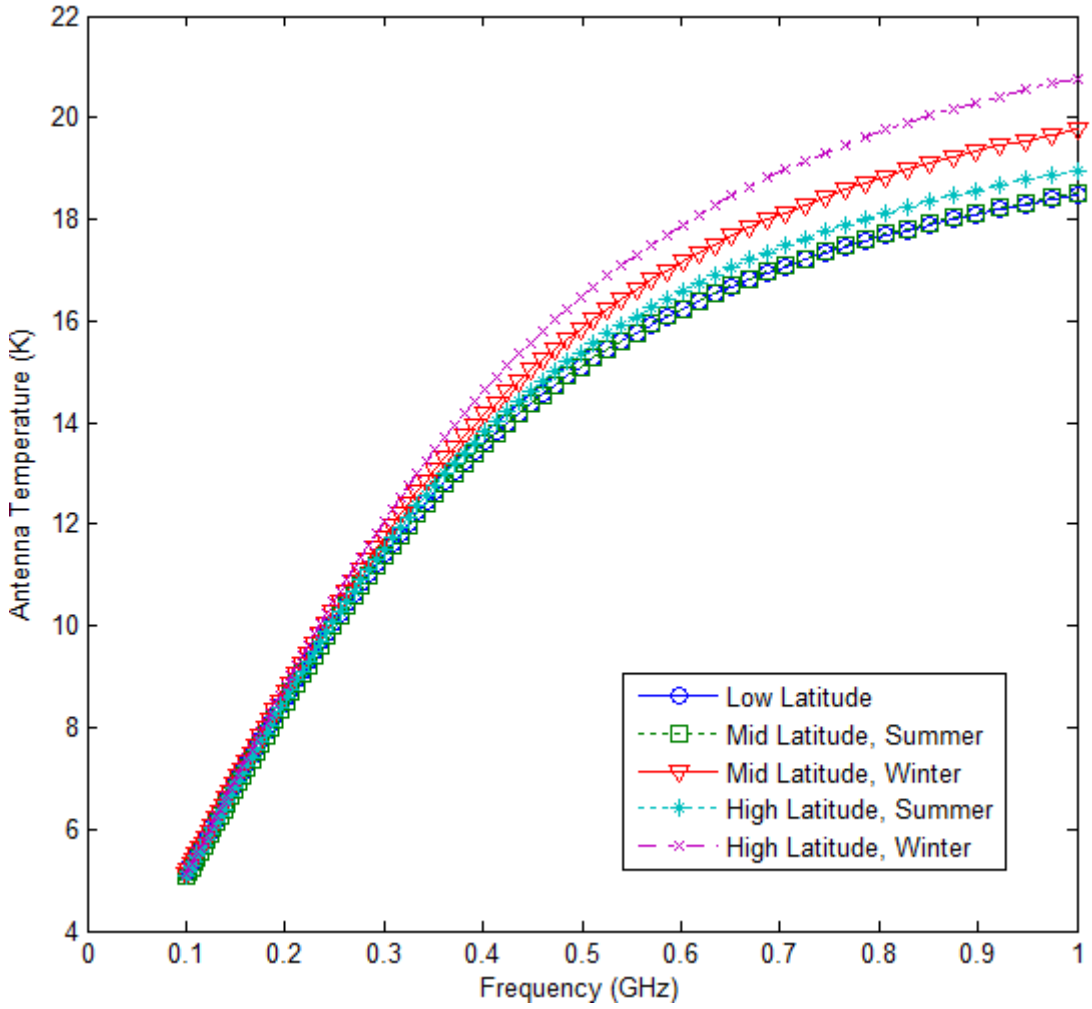

Figure 4. 10 Antenna Temperature for the proposed design optimized with array thinning approach at different latitudes (corresponding atmospheric conditions taken from Reference standard atmosphere ITU-R P.835-5). The main beam is pointing at $\theta = \frac{\pi}{4}, \phi = \frac{\pi}{4}$ with isotropic elements.

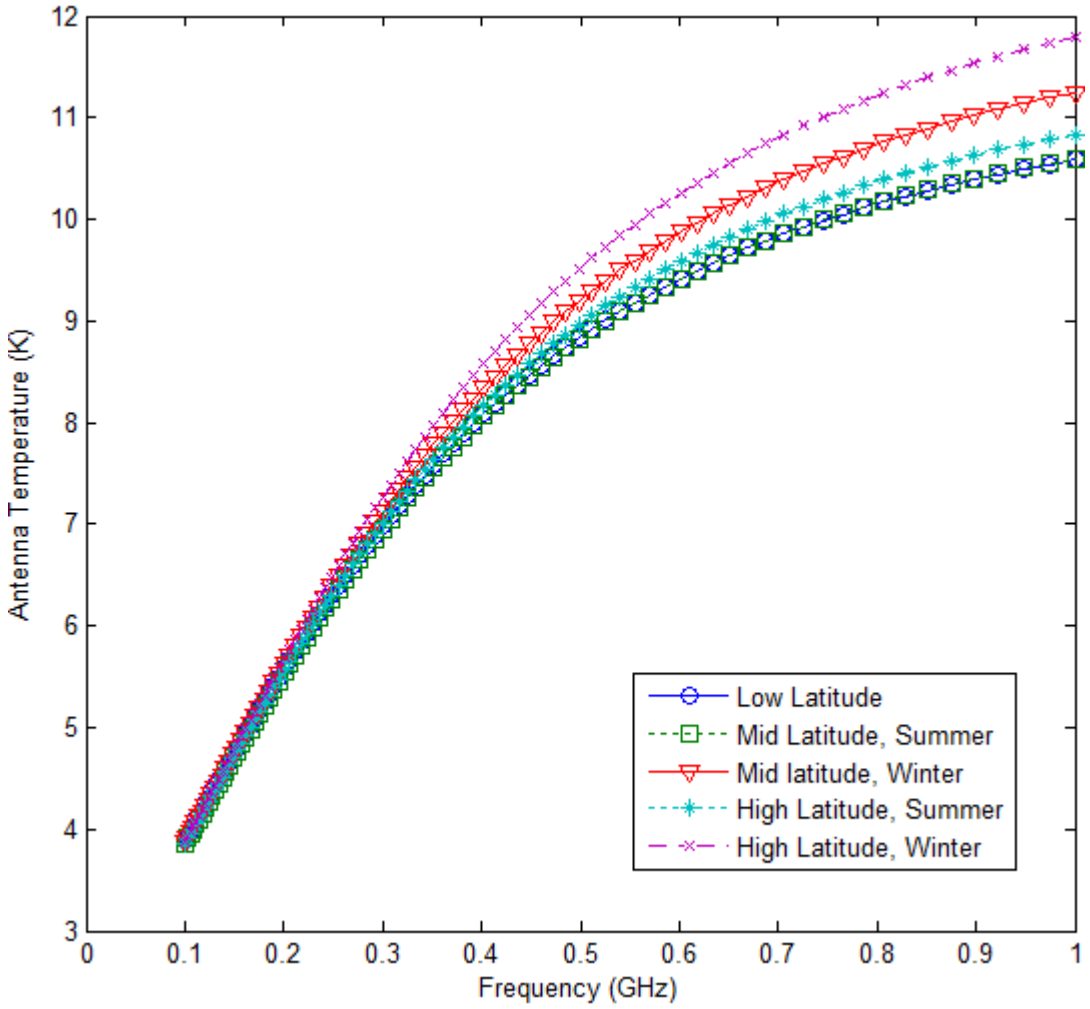

Figure 4. 11 Antenna Temperature for the proposed design optimized with array thinning approach at different latitudes (corresponding atmospheric conditions taken from Reference standard atmosphere ITU-R P.835-5). The main beam is pointing at $\theta = 0°, \phi = 0°$ with $\cos\theta$ element pattern.

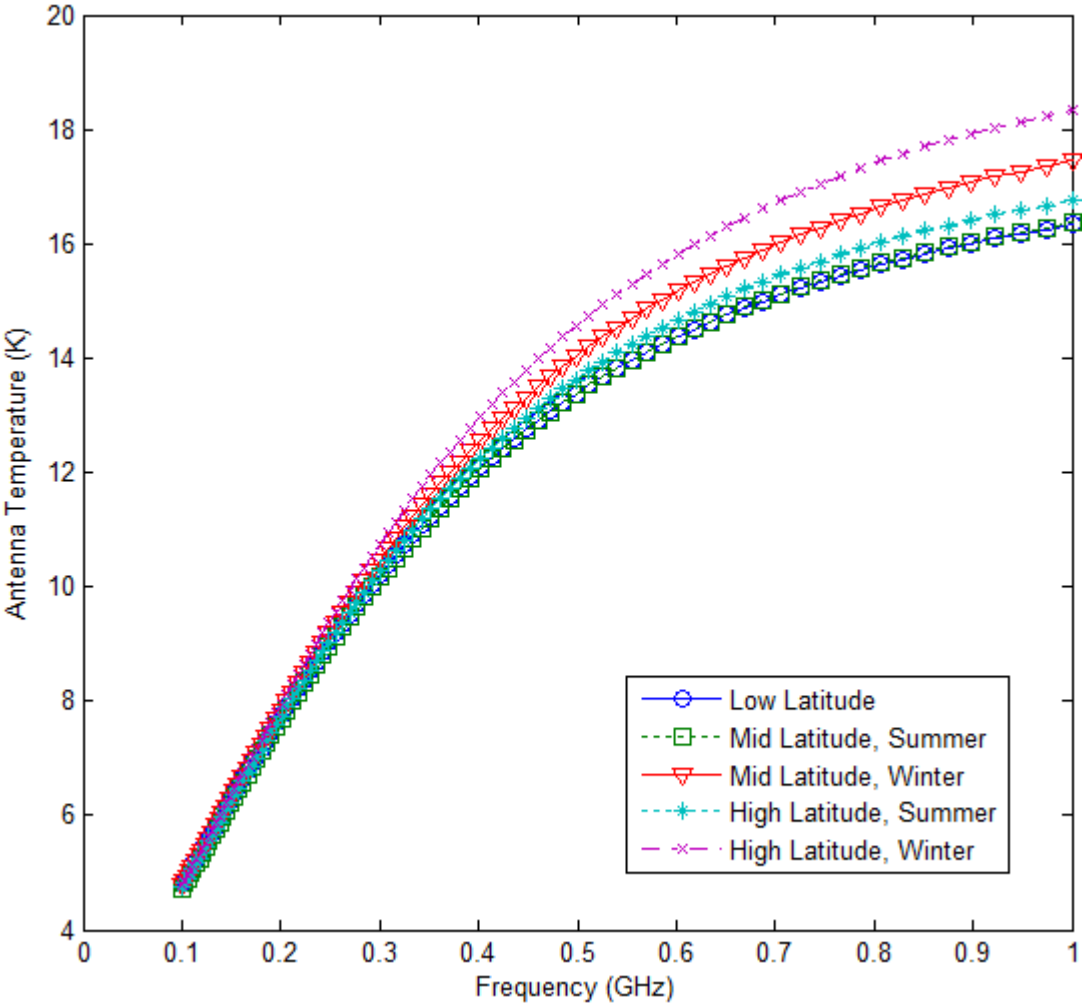

Figure 4. 12 Antenna Temperature for the proposed design optimized with array thinning approach at different latitudes (corresponding atmospheric conditions taken from Reference standard atmosphere ITU-R P.835-5). The main beam is pointing at $\theta = \frac{\pi}{4}, \phi = \frac{\pi}{4}$ with $\cos\theta$ element pattern.

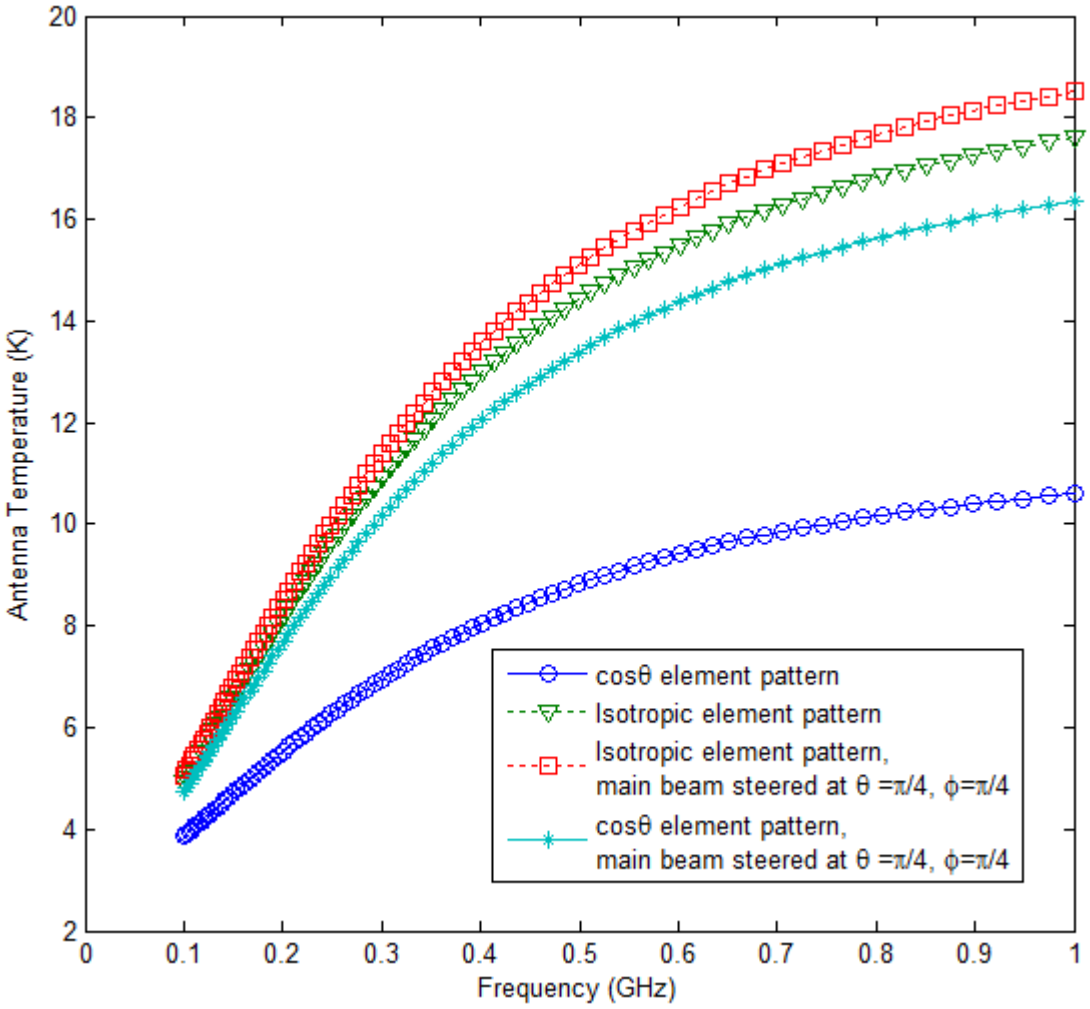

Figure 4. 13 Antenna temperature comparison at mid latitude (summer) for the proposed hexagonal planar antenna array design optimized with array thinning approach. The comparison is carried out for different element pattern and different main beam pointing directions.

4.7.1. Sensitivity Analysis of Proposed Design Optimized with Array Thinning Approach

In this section the results of antenna temperature for the design with array thinning approach have been analysed for sensitivity over the low SKA range of operation. Sensitivity of the antenna has been investigated for different latitudes as explained earlier that for SKA application the requirement of the variation of atmospheric conditions is very important. Observation of the performance parameter with variation in atmospheric condition proves the practical application eligibility of the design. Hence the design not only should perform well but it should also be consistent with that performance over the whole range of atmospheric parameter variation. To obtain the system noise temperature (Eq. 4.24), the assumptions made are: temperature of low noise amplifier (T_{LNA}) is 35 K, antenna total efficiency (η_T) is

90% and the surrounding temperature (T_{sur}) is 290 K. From figure 4.15 to 4.17 are showing the sensitivity variation with wavelength for different latitudes. Quite improved values of sensitivity have been obtained for low SKA range of operation. A sensitivity value of 10.29 m^2/k at 100 MHz has been obtained for the design with isotropic element and main beam pointing at $\theta = 0°$ and $\phi = 0°$ (end fire). This value remains approximately constant with the variation in latitudes and hence achieving both the desired characteristics as an antenna desired in SKA application. At 350 MHz sensitivity drops to a level of 0.8 m^2/k as the effective area of the aperture reduces with increment in wavelength due to the dependency of inter element spacing on wavelength. From figure 4.15, the sensitivity value for elements with $\cos\theta$ element pattern at100 MHz is 10.65 which is slightly increased in comparison to the isotropic elements. Steered main beam pattern have increased side lobe level causing the antenna noise to increase, and reduced directivity which reduces the effective area of the aperture. Both the factors results in decrement in sensitivity of the antenna and hence comparatively reduced values have been obtained. Although, proposed design still offer higher sensitivity values than the planar array designs investigated in [Ahmed El-makadema, 2014]. From figure 4.16 and 4.17, the sensitivity values obtained for the main beam pointing in $\theta = \frac{\pi}{4}, \phi = \frac{\pi}{4}$ with isotropic and $\cos\theta$ radiation pattern are 5.55 m^2/k and 5.6 m^2/k respectively. Table 4.3 contains the sensitivity values of the proposed design synthesized with array thinning approach and with the proposed GA modified discretizing technique. A comparison with some other recently reported approaches of array synthesis for SKA application has also been presented. It can be seen clearly that the design offer approximately double values of sensitivity offered by the tapered random and tapered GRS design reported in [Ahmed El-makadema, 2014].

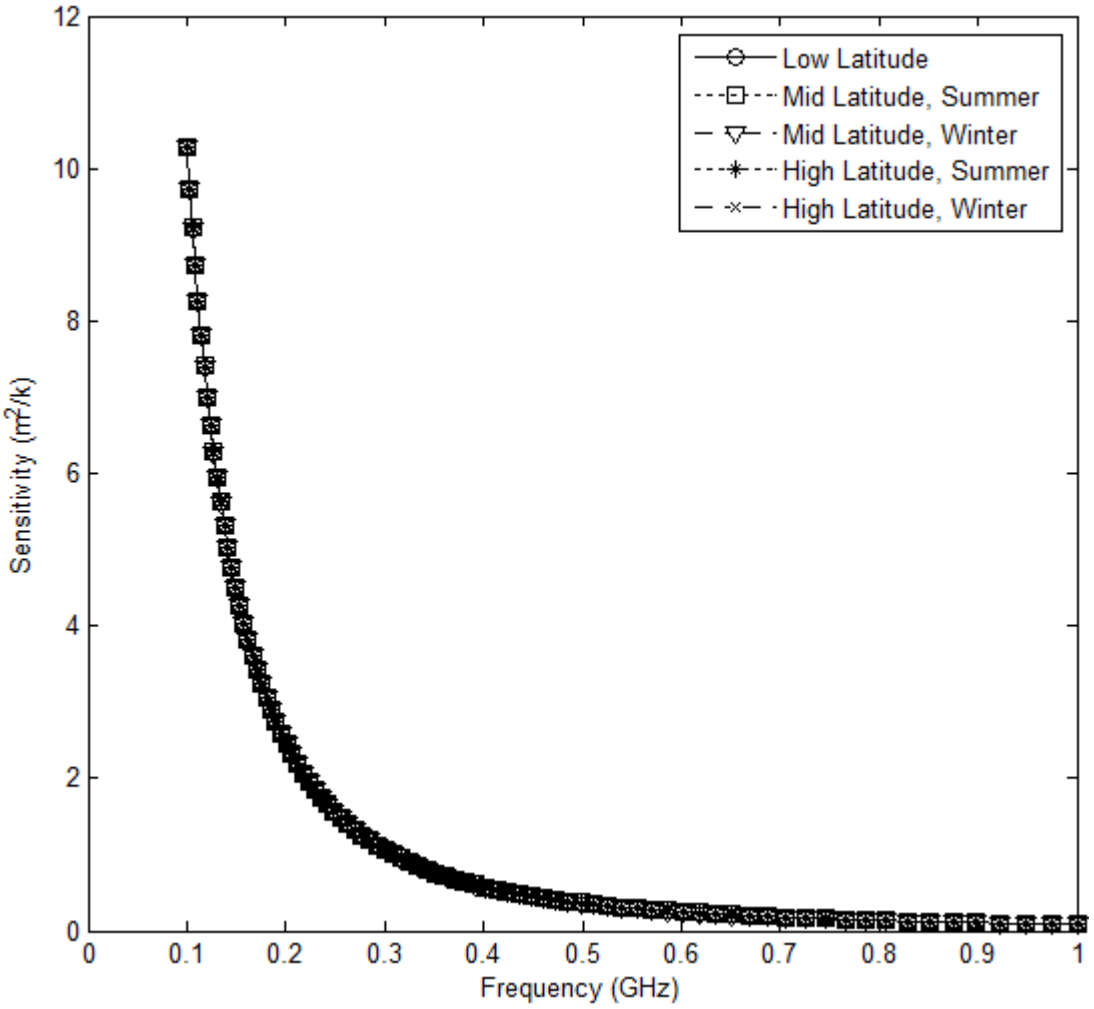

Figure 4. 14 Sensitivity for the proposed design optimized with array thinning approach at different latitudes (corresponding atmospheric conditions taken from Reference standard atmosphere ITU-R P.835-5). The main beam is pointing at $\theta = 0°, \phi = 0°$ with isotropic element.

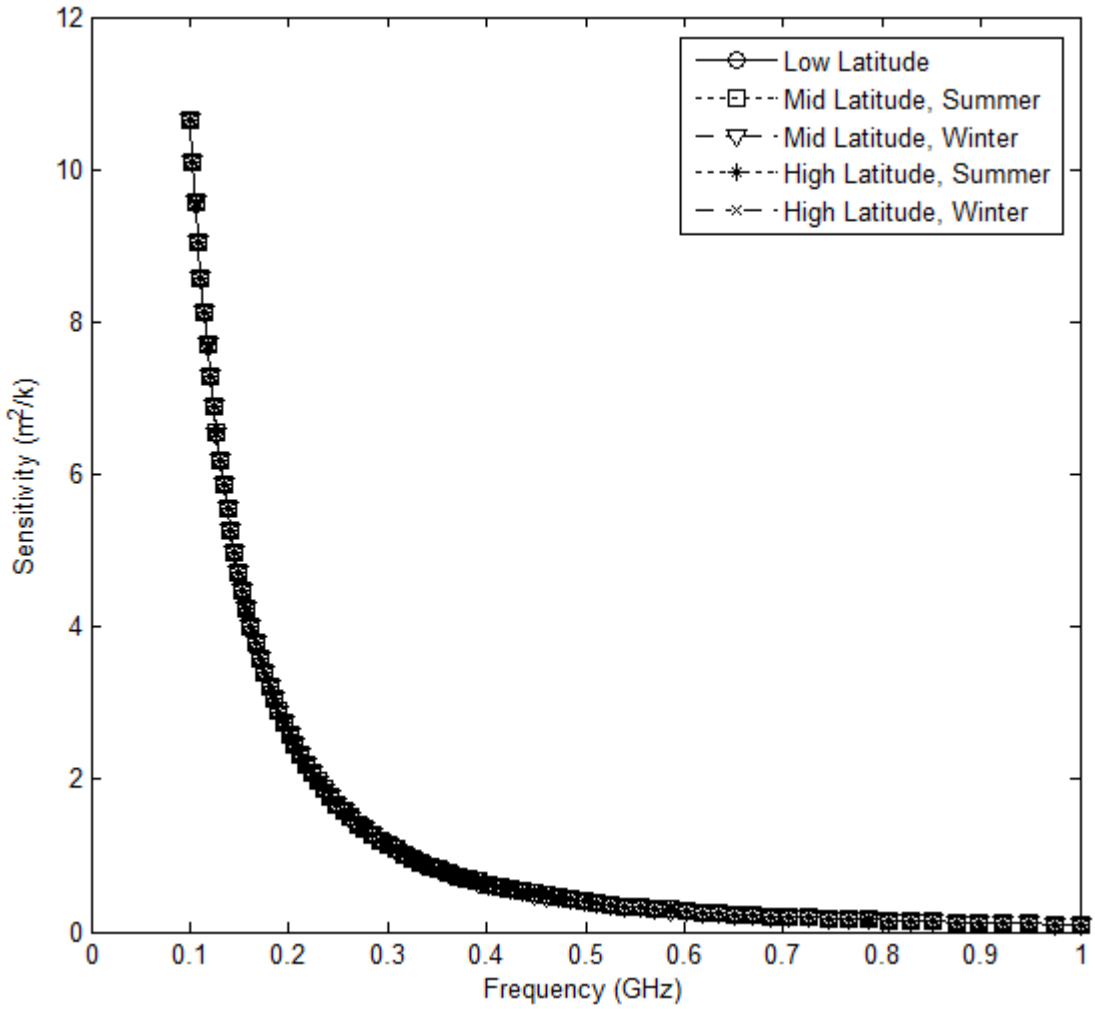

Figure 4. 15 Sensitivity for the proposed design optimized with array thinning approach at different latitudes (corresponding atmospheric conditions taken from Reference standard atmosphere ITU-R P.835-5). The main beam is pointing at $\theta = 0°, \phi = 0°$ (end fire) with $\cos\theta$ element pattern.

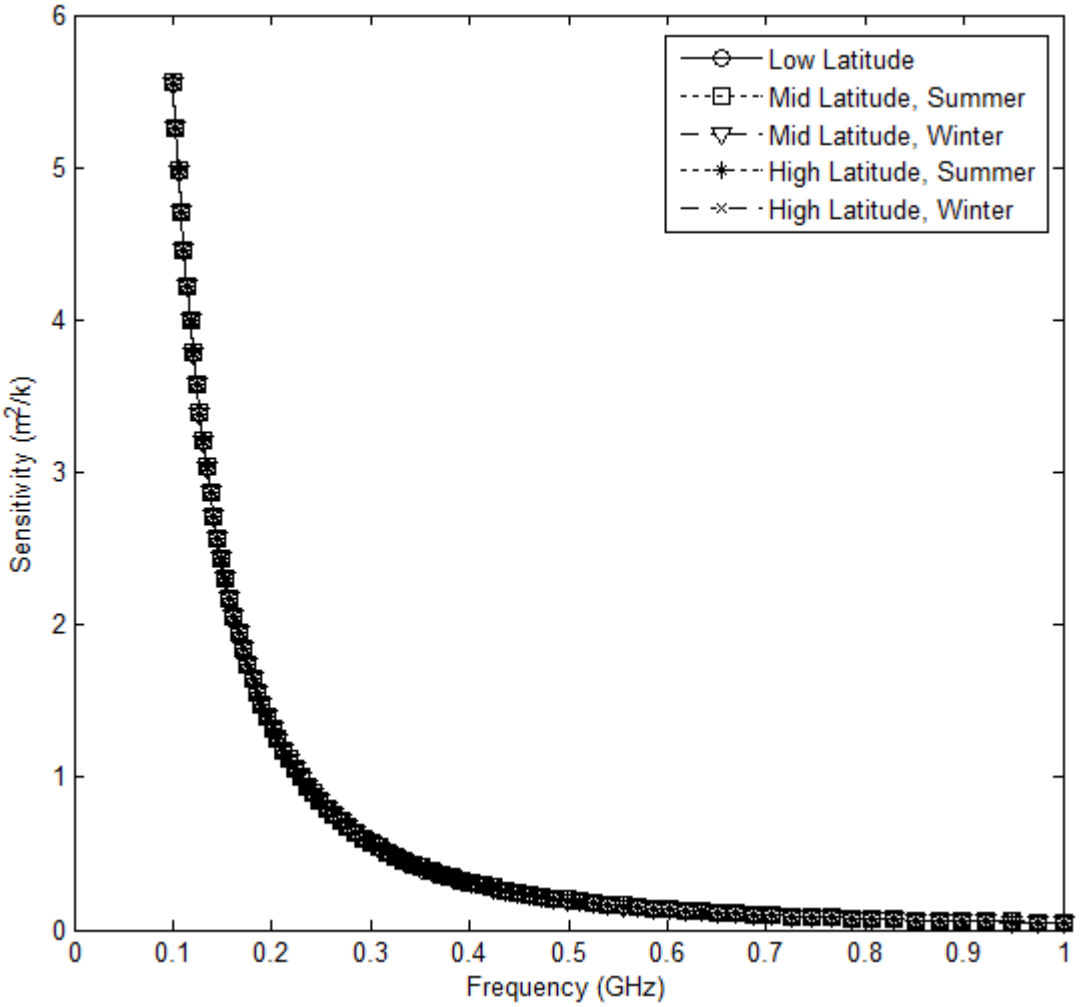

Figure 4. 16 Sensitivity for the proposed design optimized with array thinning approach at different latitudes (corresponding atmospheric conditions taken from Reference standard atmosphere ITU-R P.835-5). The main beam is pointing at $\theta = \frac{\pi}{4}, \phi = \frac{\pi}{4}$ (end fire) with isotropic element.

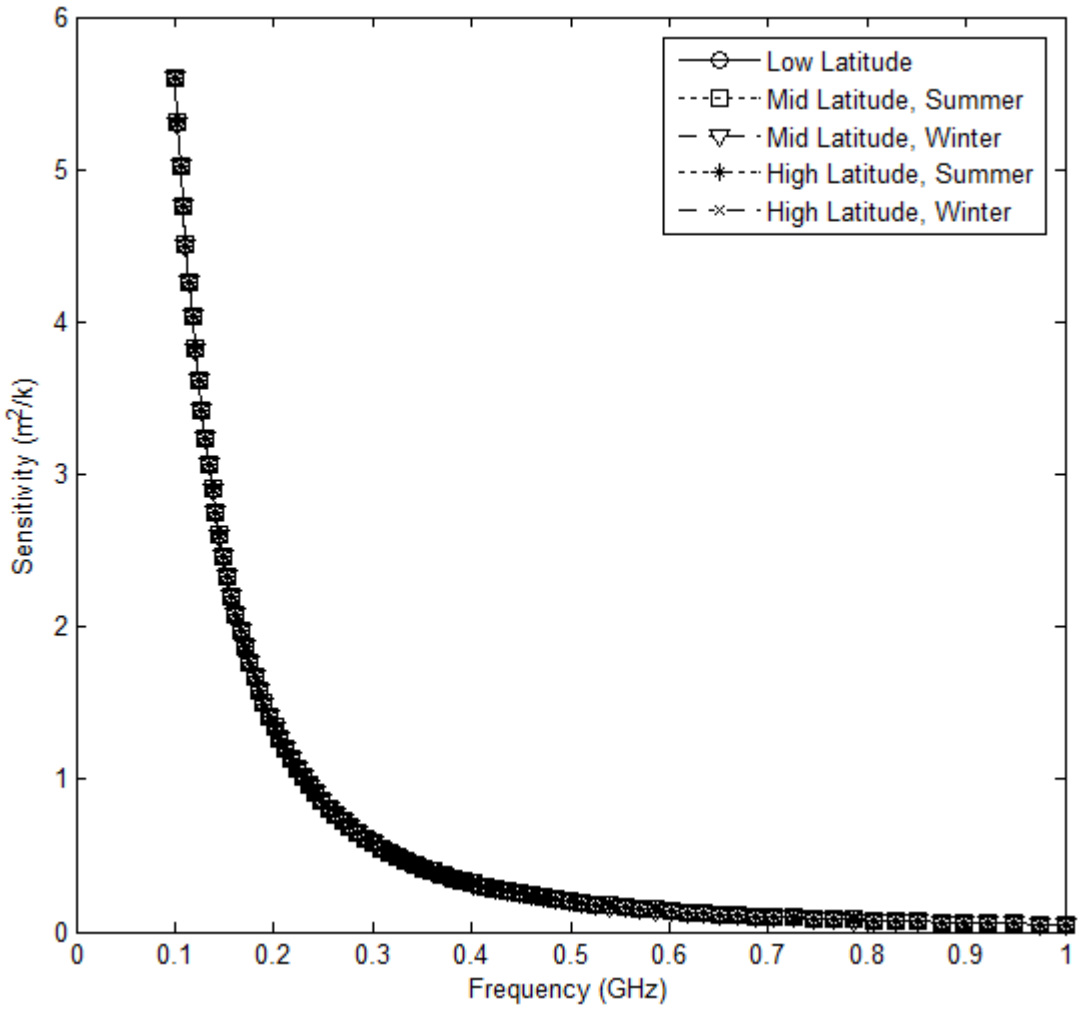

Figure 4. 17 Sensitivity for the proposed design optimized with array thinning approach at different latitudes (corresponding atmospheric conditions taken from Reference standard atmosphere ITU-R P.835-5). The main beam is pointing at $\theta = \frac{\pi}{4}, \phi = \frac{\pi}{4}$ (end fire) with $\cos\theta$ element pattern.

Figures 4.18 to 4.21 are showing the variation in sensitivity with change in weather conditions at mid and high latitudes. This is an important investigation for SKA application as the SKA sights may span a range of 1000s of kilometre and under such conditions the antennas deployed must operate with same sensitivity. High latitude offers comparatively high antenna temperature variations in comparison to the mid latitude and hence the sensitivity variation is expected to be higher for high latitude conditions. From Figure 4.18, design with isotropic element with end fire radiation offer maximum sensitivity change in comparison to the other pattern (see Figure. 4.19 to 4.21). Although, the variations are quite low and these are of the order of 10^{-3}. It should be noted that these variations are maximum at lower frequencies because at these frequencies the sensitivity is maximum and with increment in frequency sensitivity value reduces causing the reduction in this variation. Here we are concern with the variation over the range for which the sensitivity values are

acceptable. The maximum sensitivity variation of 0.00828 has been observed at 100 MHz for end fire radiation with isotropic element and high latitude conditions. The minimum sensitivity variation with a value of 0.0025 at 100 MHz has been observed for end fire radiation with $\cos\theta$ element pattern and mid latitude conditions.

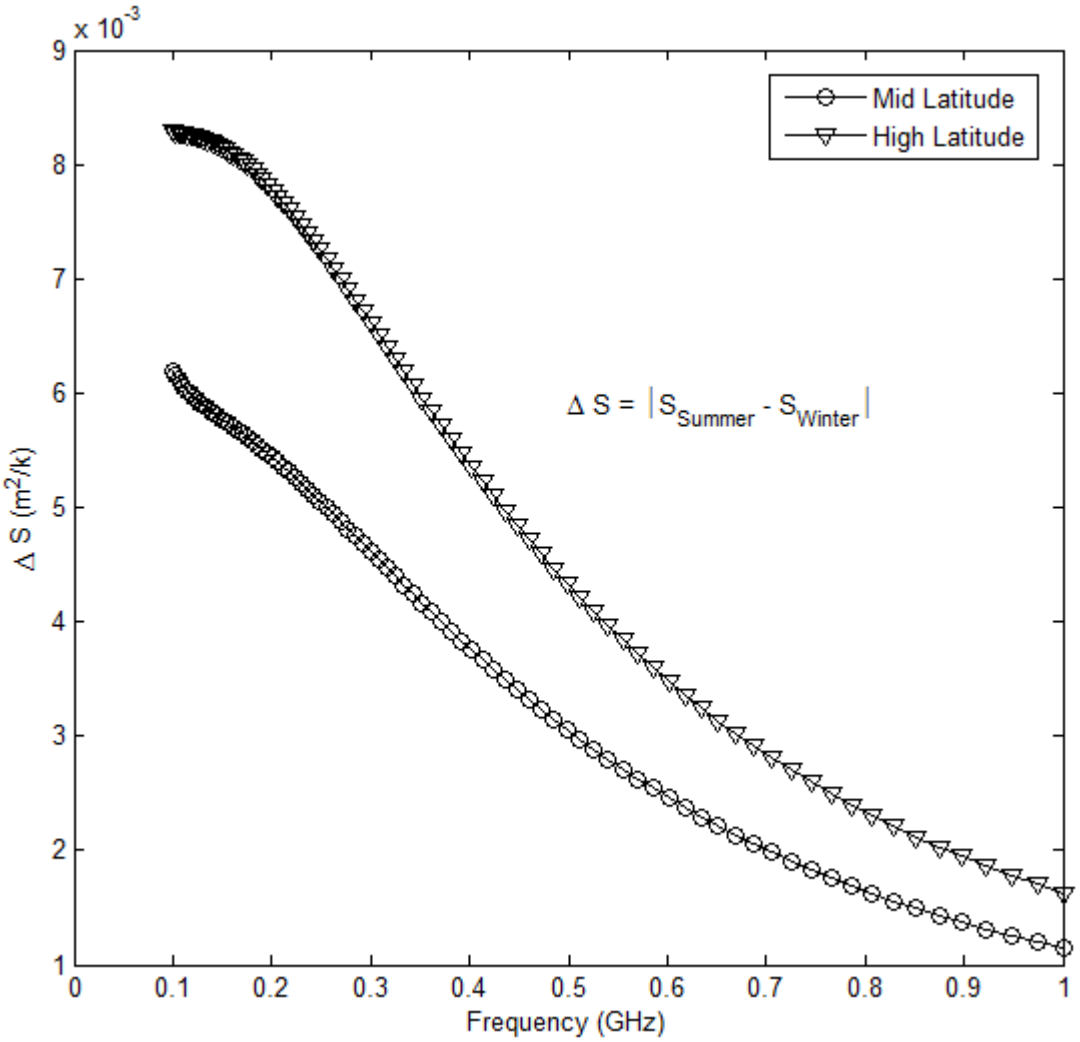

Figure 4. 18 Sensitivity variation with change in atmospheric conditions for the proposed planar array. Sensitivity change has been observed for different weather conditions at same latitude. The main beam is pointing in end fire direction with isotropic element. Sensitivity calculations for different environment conditions have been carried out using ITU reference standard [ITU-R P.835-5].

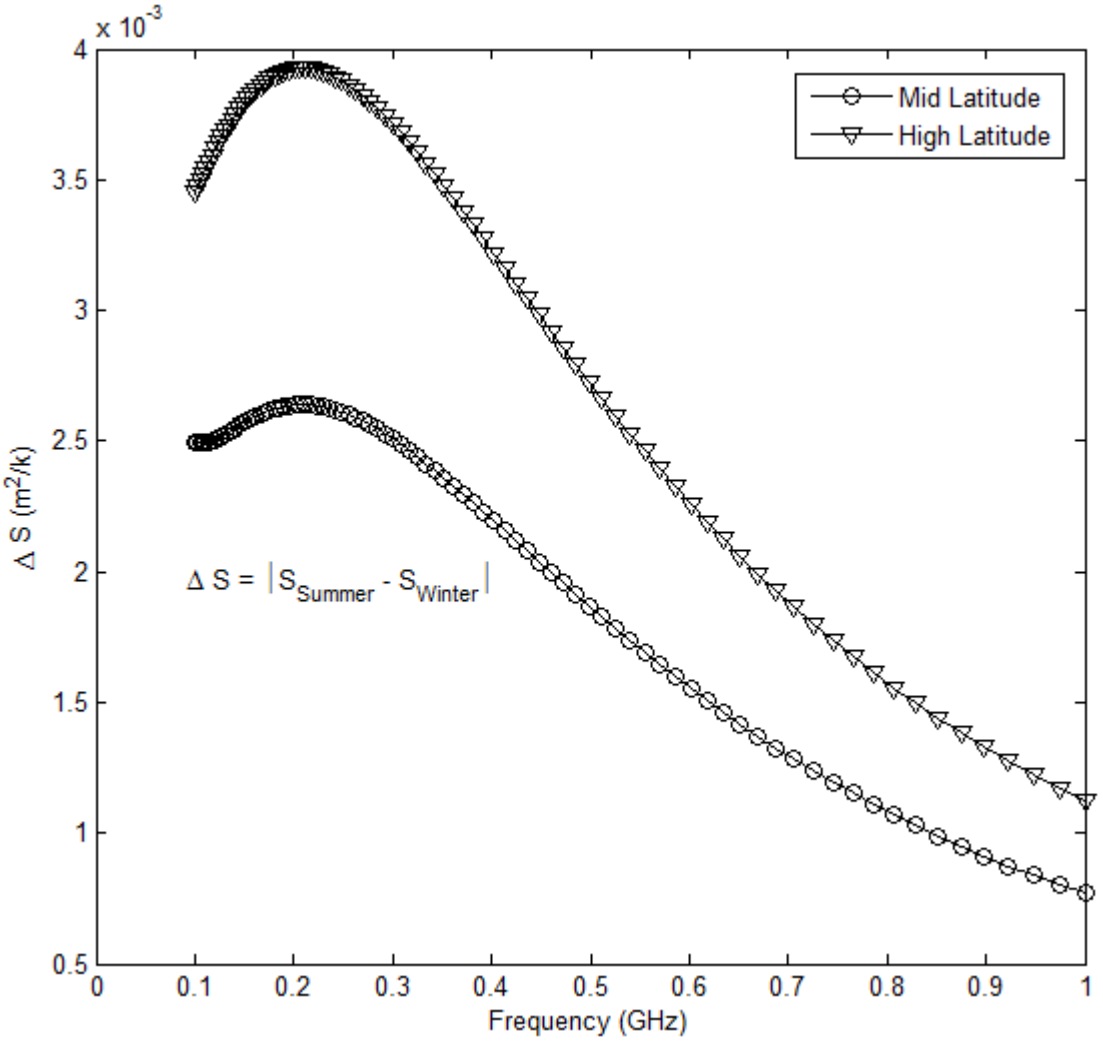

Figure 4. 19 Sensitivity variation with change in atmospheric conditions for the proposed planar array. Sensitivity change has been observed for different weather conditions at same latitude. The main beam is pointing in end fire direction with $\cos\theta$ element pattern. Sensitivity calculations for different environment conditions have been carried out using ITU reference standard [ITU-R P.835-5].

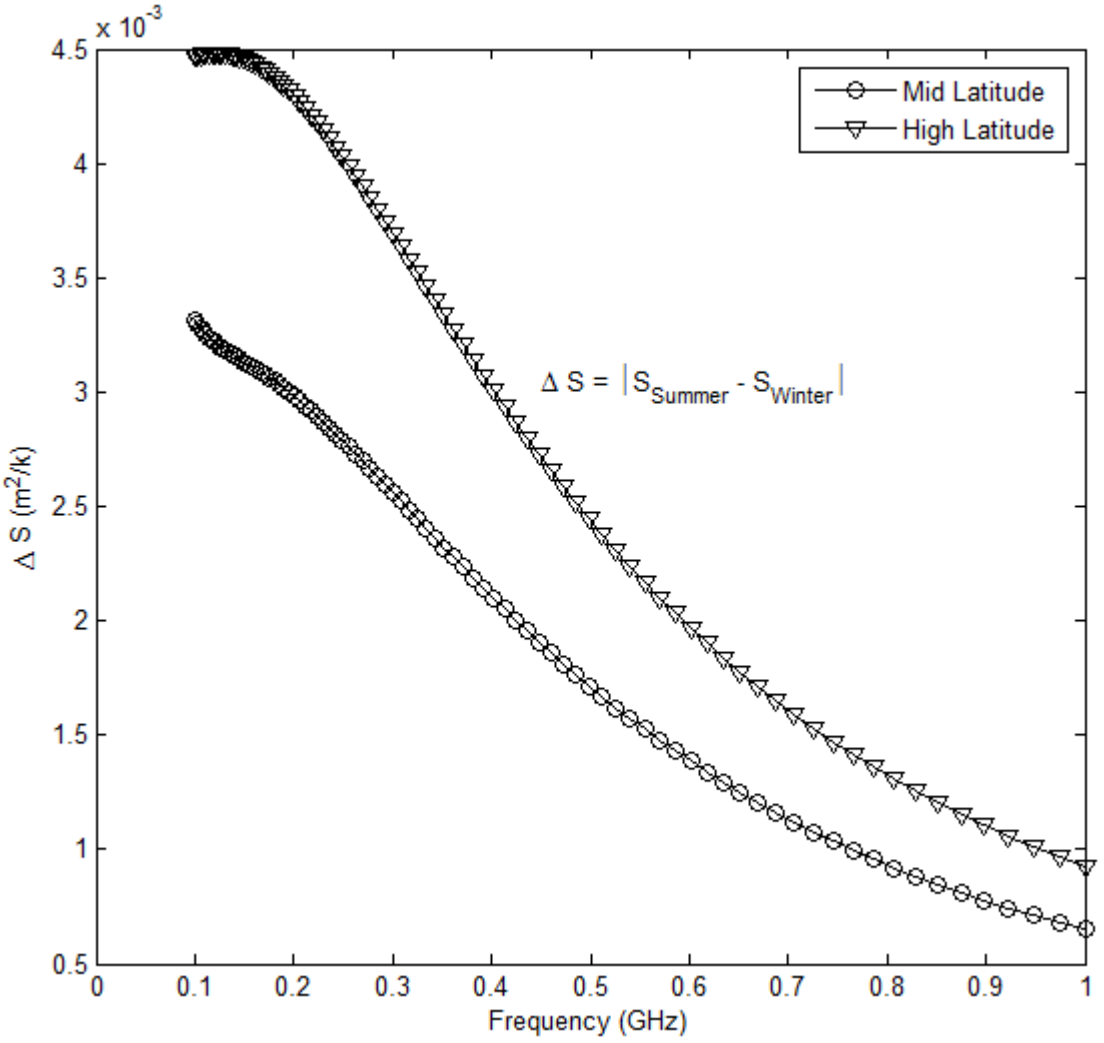

Figure 4. 20 Sensitivity variation with change in atmospheric conditions for the proposed planar array. Sensitivity change has been observed for different weather conditions at same latitude. The main beam is pointing at $\theta = \frac{\pi}{4}, \phi = \frac{\pi}{4}$ with isotropic elements. Sensitivity calculations for different environment conditions have been carried out using ITU reference standard [ITU-R P.835-5].

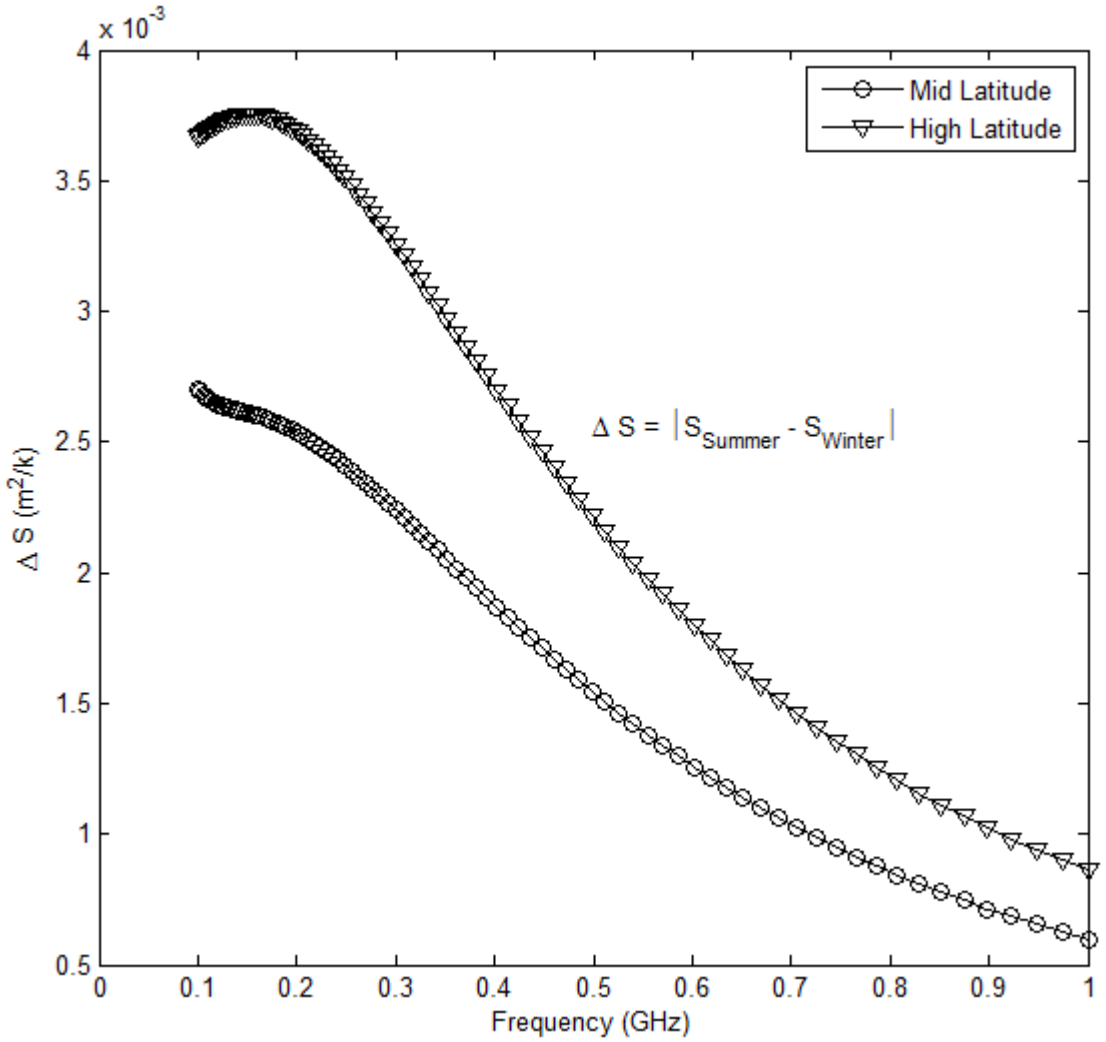

Figure 4. 21 Sensitivity variation with change in atmospheric conditions for the proposed planar array. Sensitivity change has been observed for different weather conditions at same latitude. The main beam is pointing at $\theta = \frac{\pi}{4}, \phi = \frac{\pi}{4}$ with $\cos\theta$ element pattern. Sensitivity calculations for different environment conditions have been carried out using ITU reference standard [ITU-R P.835-5].

4.7.2. Sensitivity Analysis of Proposed GA Modified Discretizing Technique for Sampled Taylor Distribution

In the previous section a detailed analysis of the proposed design with the GA optimized thinning approach has been investigated for antenna temperature, sensitivity, sensitivity variation over the low SKA and mid SKA frequency range. In this section same investigation has been carried out for the proposed GA modified discretizing technique. Recalling the proposed synthesis in which the continuous Taylor distribution is sampled to obtain the current excitation values for discrete array as given by the Taylor synthesis for discrete array in [Robert S. Elliot, "Antenna theory and design", 2003]. This sampled distribution is further improved in order to improve the pattern obtained by minimizing the difference between

desired pattern and obtained pattern. The approach of current perturbation method of Taylor synthesis is not feasible for larger arrays as required in SKA application. Hence the combination of heuristic search and Taylor synthesis has been adopted and a technique called GA modified discretizing technique has been proposed. This approach performed quite well for side lobe level, directivity, power requirement, aperture efficiency, and main beam shape along with maintaining the quasi constant height of side lobes near to the main beam. Performing well on these parameters shows the potential of the design to be utilized as SKA. A well behaved radiation pattern with high directivity is required for high sensitivity. Similar to the analysis carried out in previous section, the sensitivity has been examined for different main beam pointing directions. All the elements of the antenna array have been assumed isotropic in this analysis. Effect of certain element pattern had been investigated in the previous analysis and hence here it has been omitted. All the atmospheric parameters have been referred from ITU-R P. 835-5.

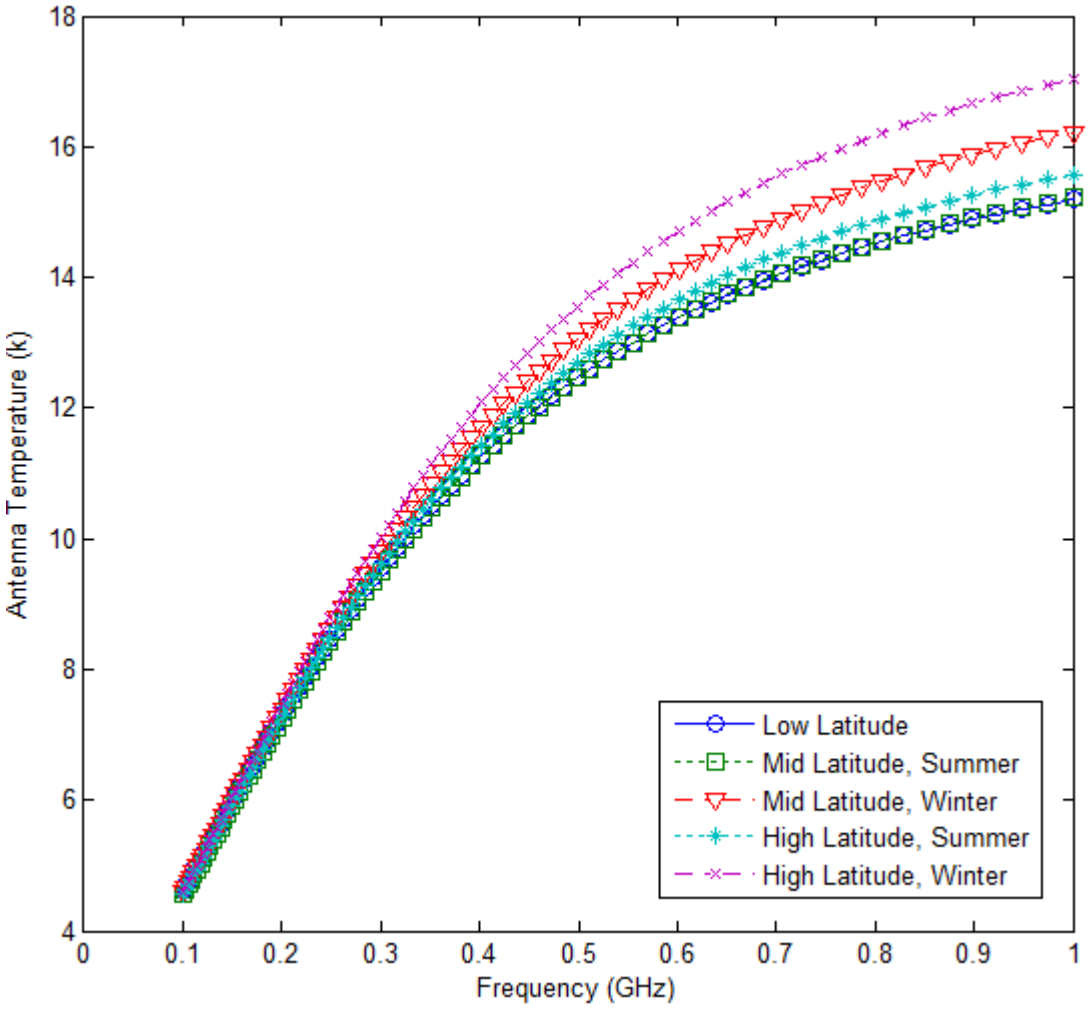

Figure 4. 22 Antenna Temperature for the proposed design optimized with the proposed GA modified discretizing technique at different latitudes (corresponding atmospheric conditions taken from Reference standard atmosphere ITU-R P.835-5). The main beam is pointing at $\theta = \frac{\pi}{4}, \phi = \frac{\pi}{4}$ with isotropic elements.

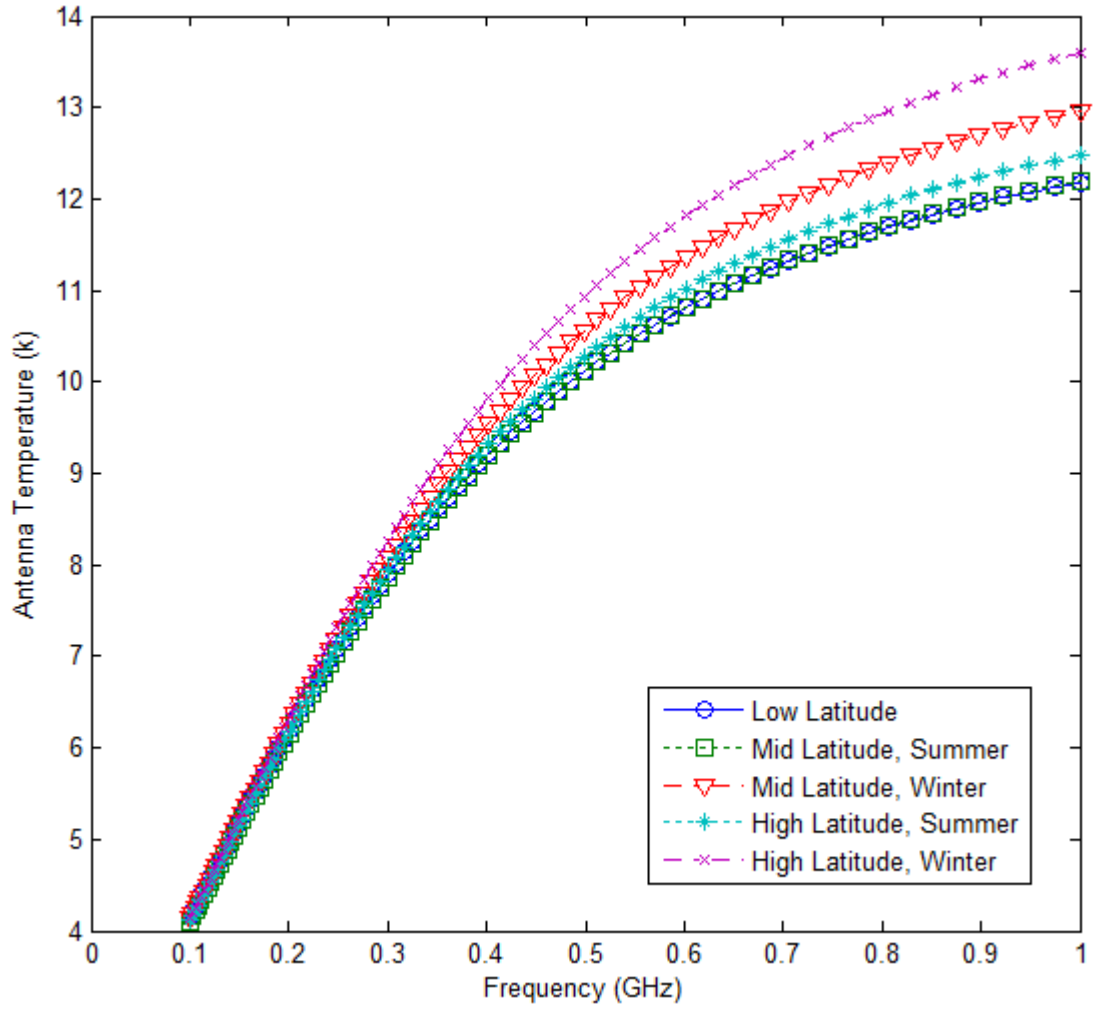

Figure 4. 23 Antenna Temperature for the proposed design optimized with the proposed GA modified discretizing technique at different latitudes (corresponding atmospheric conditions taken from Reference standard atmosphere ITU-R P.835-5). The antenna array is radiating in end fire direction with isotropic elements.

Figures 4.22 and 4.23 are showing the antenna temperature obtained for a frequency range of 100 MHz to 1 GHz for main beam pointing at $\theta = \frac{\pi}{4}, \phi = \frac{\pi}{4}$ and $\theta = 0°$ and $\phi = 0°$ respectively. It should be noted that for steered main beam pattern, unlike radiation pattern obtained with thinning approach, here the side lobe peak remains at the same height as it is in case of end fire radiation. With the proposed synthesis the pattern for steered main beam is quite improved and it also improves the antenna temperature values. The latitude wise behaviour of the antenna temperature remains the same as it was in the previous analysis. Antenna temperature at 100 MHz is approximately 4.1 K and 4.6 K for all the latitude conditions in case of main beam pointing at $\theta = 0°$ and $\phi = 0°$ and $\theta = \frac{\pi}{4}, \phi = \frac{\pi}{4}$ respectively. Quite improved values of antenna temperature for the whole considered frequency range of SKA have been achieved and these values have been compared with the

values obtained with array thinning. From figure 4.24, it is clear that proposed GA modified discretizing technique offer improved results for antenna temperature for all the latitudes and with different weather conditions. For mid latitude, at 100 MHz the difference is 1 K whereas, at 350 MHz it increases to value of 4 K. This difference of antenna temperature at both the frequencies is consistent with the change in latitudes. Figures 4.25 and 4.26 are showing the antenna temperature difference between both the synthesis approaches proposed in this work at low latitude and high latitude respectively.

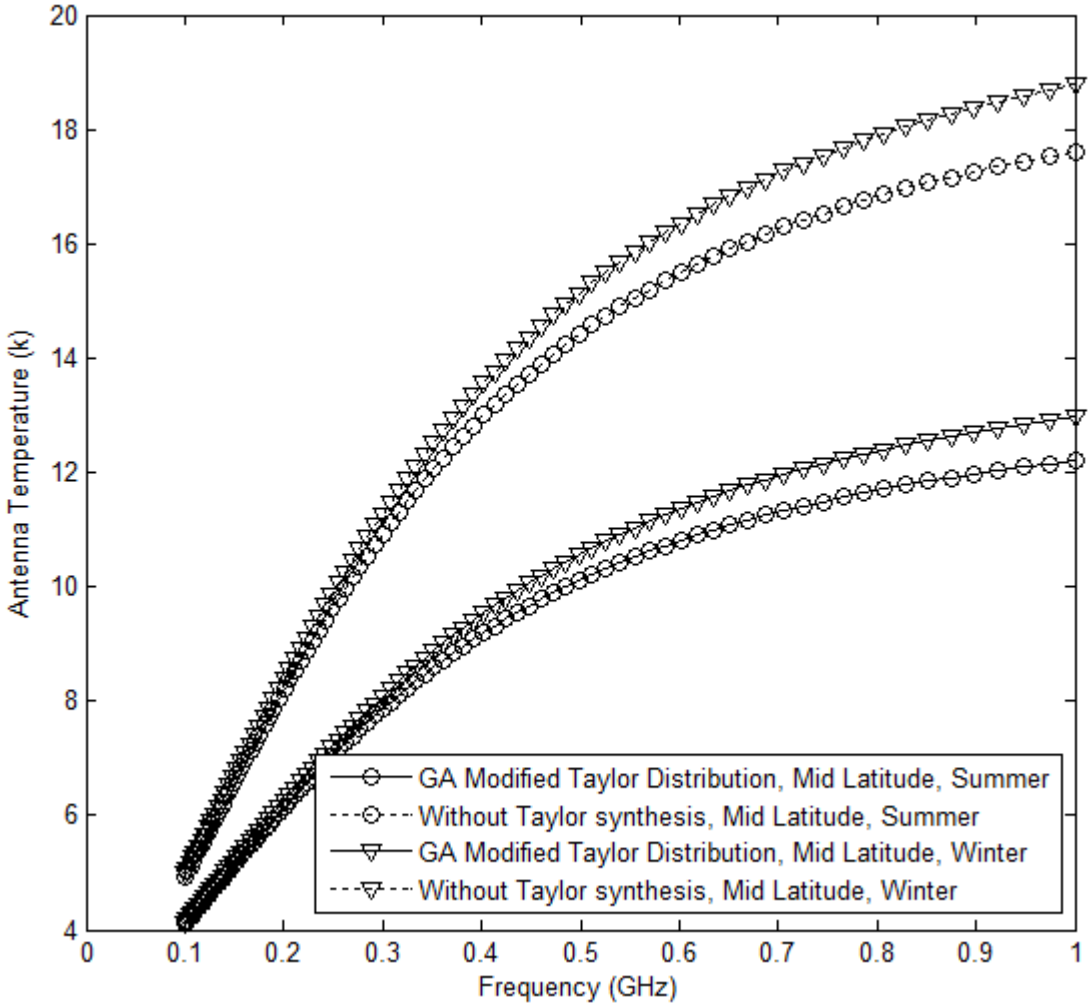

Figure 4. 24 A Comparison of antenna temperature values offered by the proposed planar array synthesized with the array thinning approach proposed in chapter 2 and Taylor synthesis with GA modified discretizing technique proposed in chapter 3. Comparison has been carried out at mid latitude with different weather conditions (reference standard atmosphere ITU-R P.835-5). Main beam is pointing at $\theta = 0°, \phi = 0°$ and elements are isotropic.

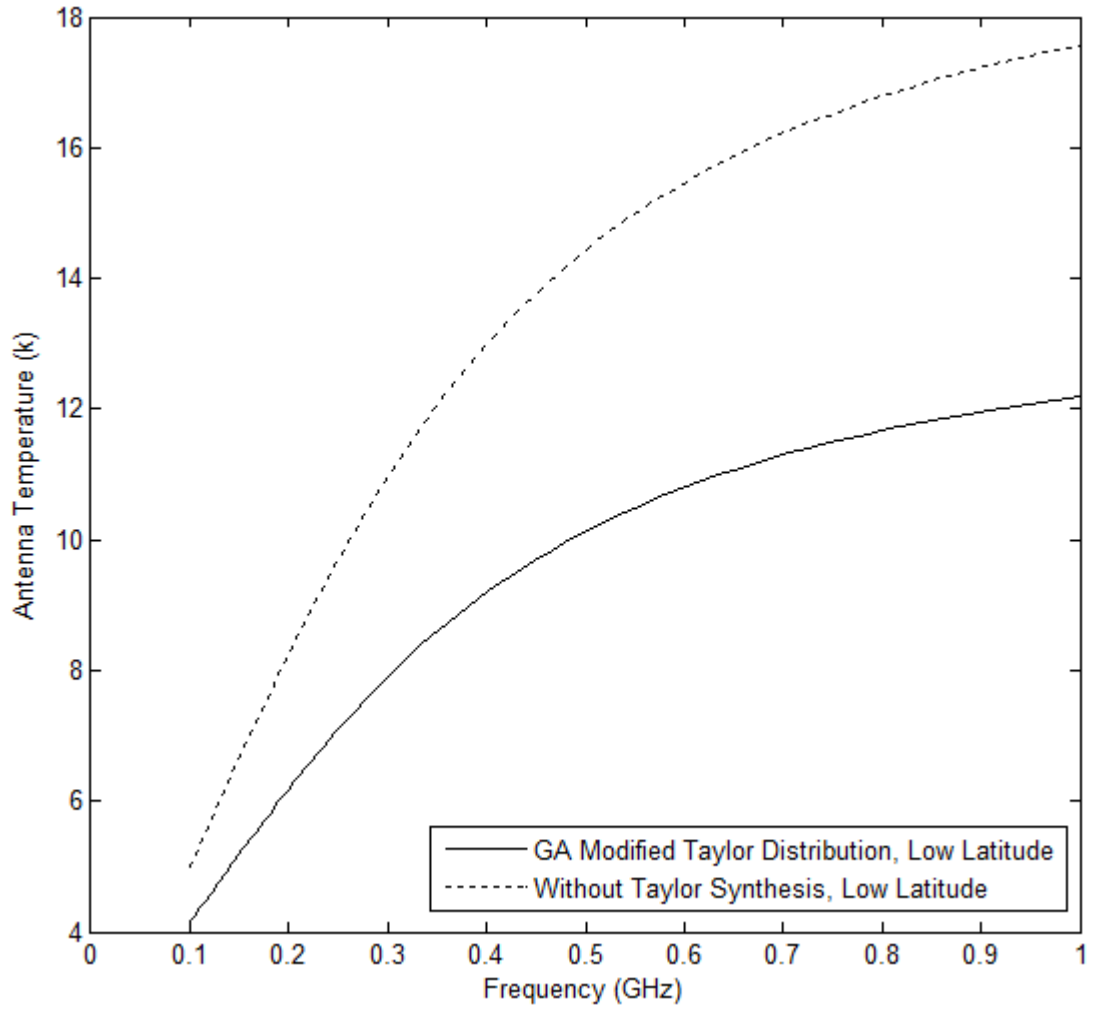

Figure 4. 25 A Comparison of antenna temperature values offered by the proposed planar array synthesized with the proposed array thinning approach and the proposed Taylor synthesis with GA modified discretizing technique at low latitude. Atmospheric conditions have been taken from reference standard atmosphere ITU-R P.835-5. Main beam is pointing at $\theta = 0°, \phi = 0°$ and elements are isotropic.

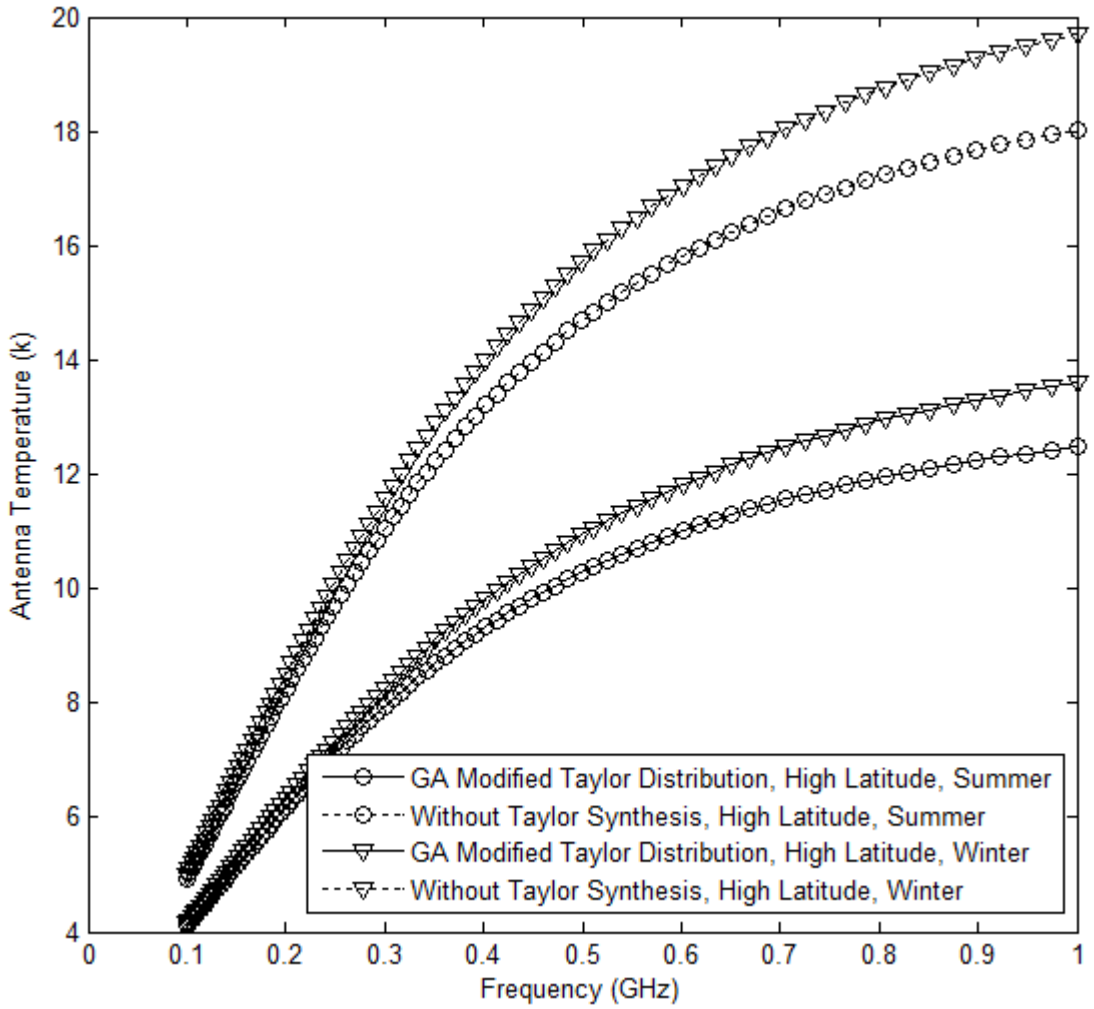

Figure 4. 26 Antenna temperature comparison between proposed planar array synthesized with the array thinning approach and with the proposed Taylor synthesis with GA modified discretizing technique. Comparison has been carried out at high latitude with different weather conditions (reference standard atmosphere ITU-R P.835-5). Main beam is pointing at $\theta = 0°, \phi = 0°$ and elements are isotropic.

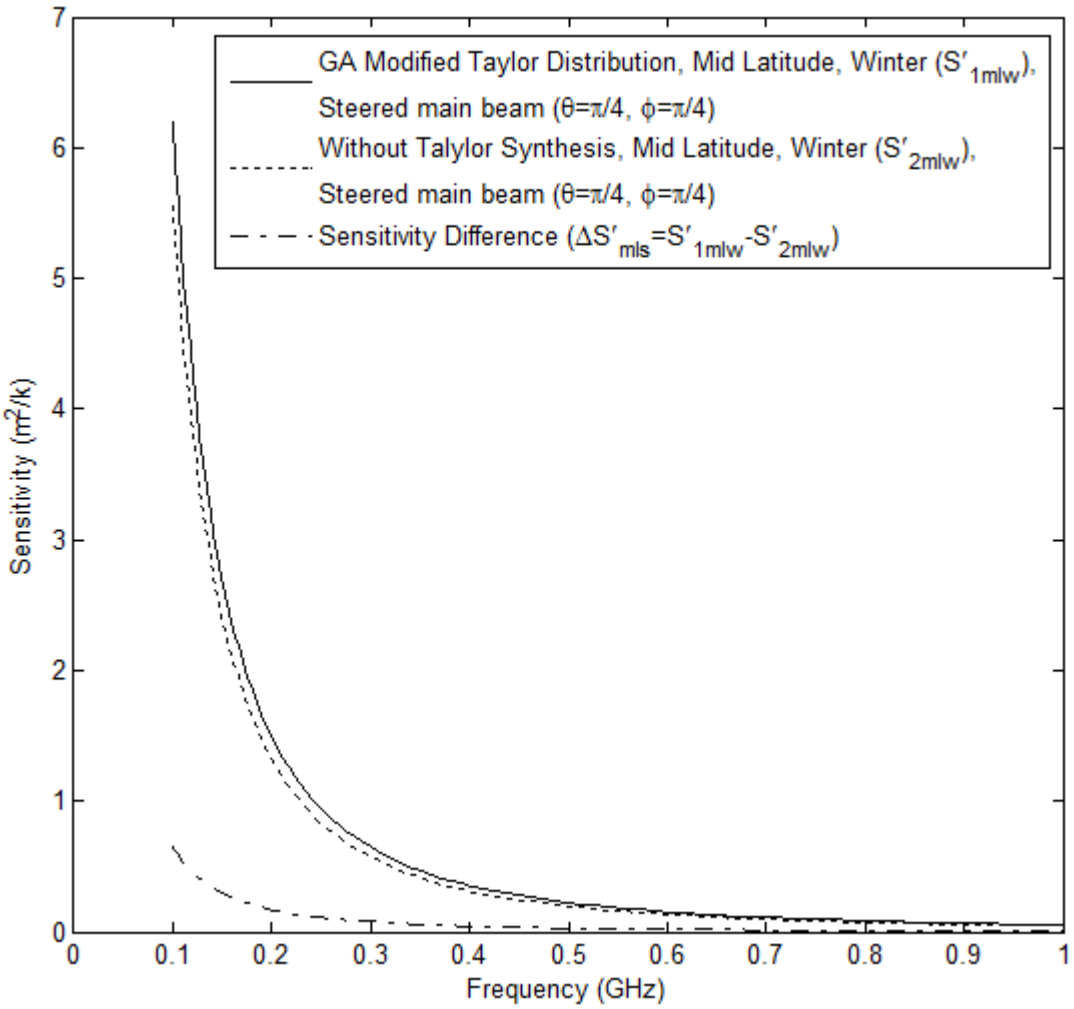
GA Modified Taylor Distribution, Mid Latitude, Winter (S′1mlw),
Steered main beam (θ=π/4, ϕ=π/4)
Without Talylor Synthesis, Mid Latitude, Winter (S′2mlw),
Steered main beam (θ=π/4, ϕ=π/4)
Sensitivity Difference (ΔS′mls=S′1mlw-S′2mlw)
Sensitivity (m²/k)
Frequency (GHz)
0
1
2
3
4
5
6
7
0.1
0.2
0.3
0.4
0.5
0.6
0.7
0.8
0.9

Figure 4. 27 (a)

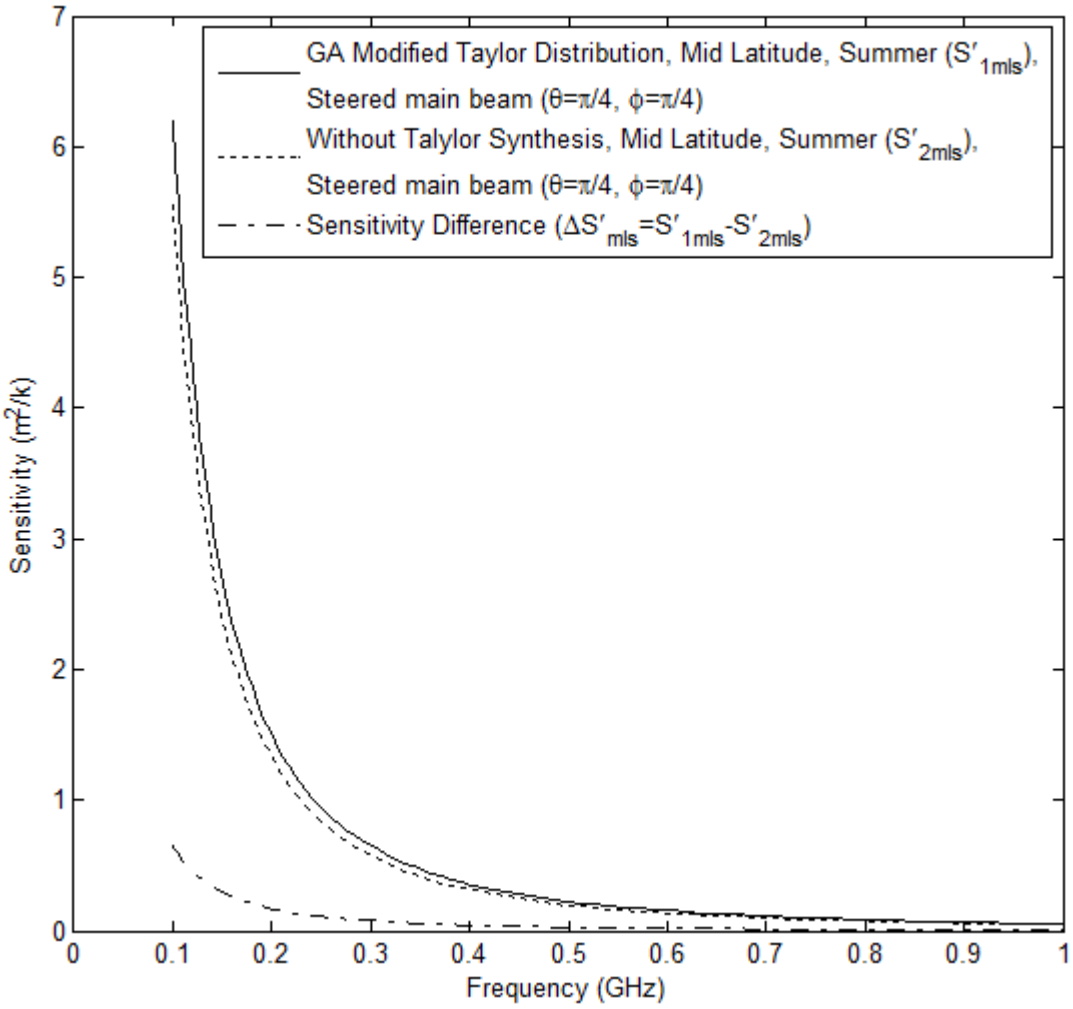
GA Modified Taylor Distribution, Mid Latitude, Summer (S′1mls), Steered main beam (θ=π/4, ϕ=π/4)
Without Talylor Synthesis, Mid Latitude, Summer (S′2mls), Steered main beam (θ=π/4, ϕ=π/4)
Sensitivity Difference (ΔS′mls=S′1mls-S′2mls)
Sensitivity (m²/k)
Frequency (GHz)
0
1
2
3
4
5
6
7
0.1
0.2
0.3
0.4
0.5
0.6
0.7
0.8
0.9

Figure 4. 28 (b)

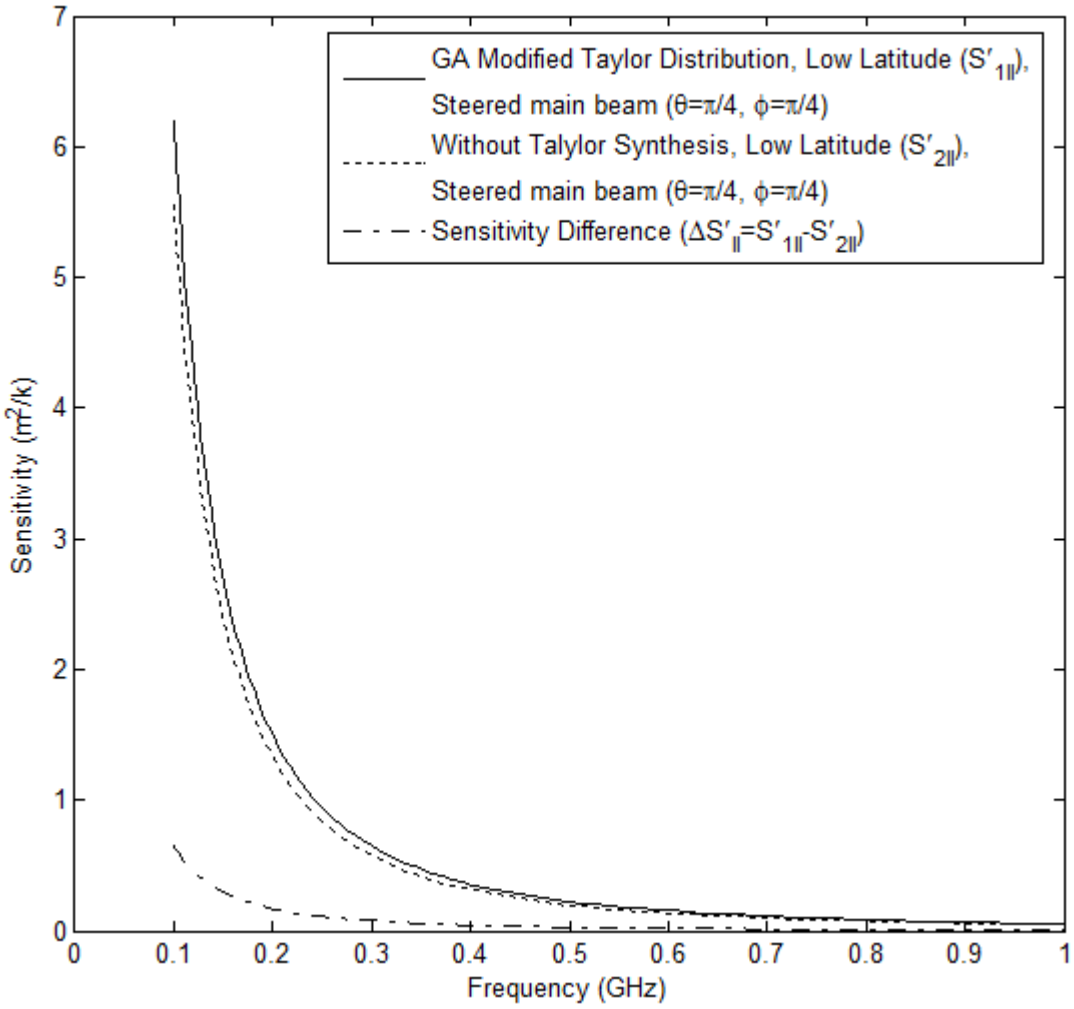
GA Modified Taylor Distribution, Low Latitude (S′1ll),
Steered main beam (θ=π/4, ϕ=π/4)
Without Talylor Synthesis, Low Latitude (S′2ll),
Steered main beam (θ=π/4, ϕ=π/4)
Sensitivity Difference (ΔS′ll=S′1ll-S′2ll)
Sensitivity (m²/k)
Frequency (GHz)
0
1
2
3
4
5
6
7
0.1
0.2
0.3
0.4
0.5
0.6
0.7
0.8
0.9

Figure 4. 29 (c)

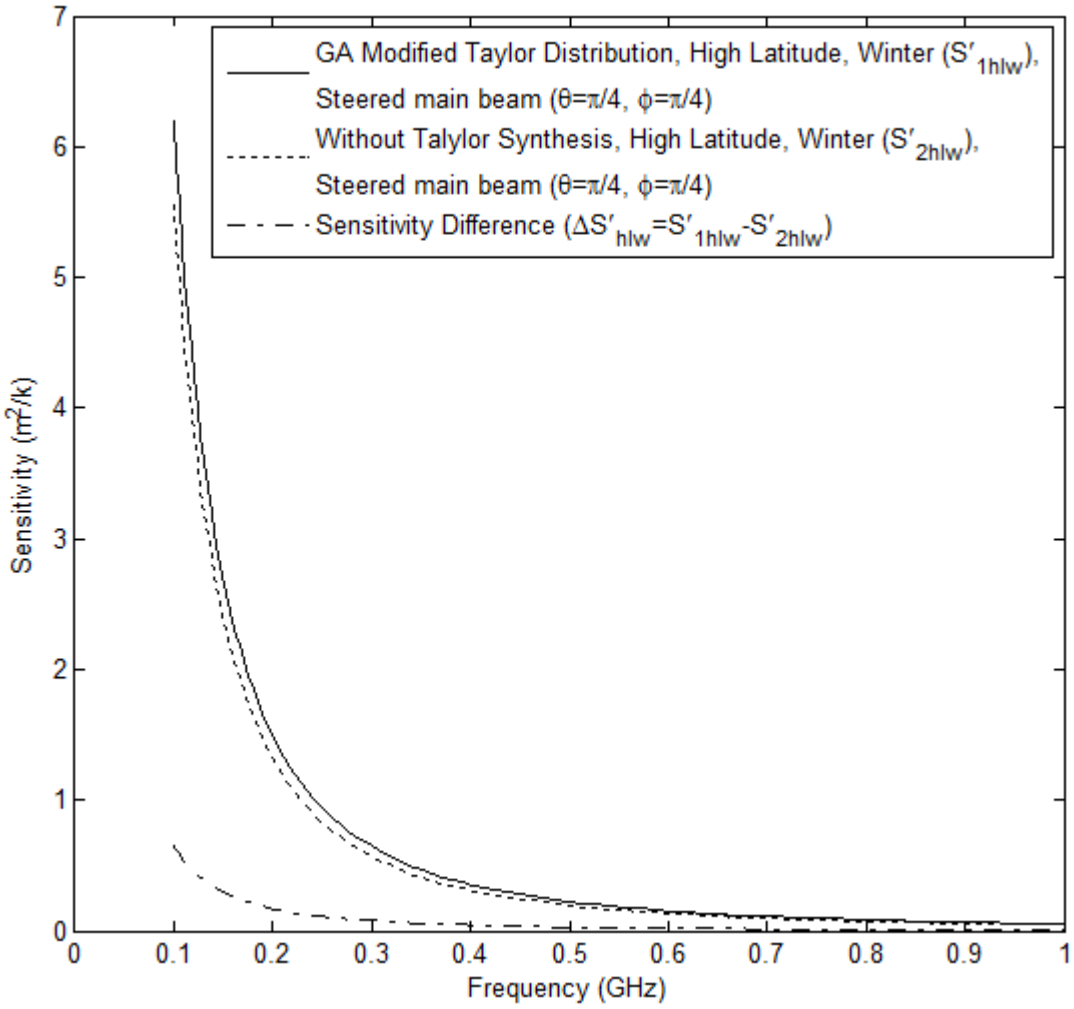
GA Modified Taylor Distribution, High Latitude, Winter (S′1hlw), Steered main beam (θ=π/4, ϕ=π/4)
Without Talylor Synthesis, High Latitude, Winter (S′2hlw), Steered main beam (θ=π/4, ϕ=π/4)
Sensitivity Difference (ΔS′hlw=S′1hlw-S′2hlw)
Sensitivity (m²/k)
Frequency (GHz)
0
1
2
3
4
5
6
7
0.1
0.2
0.3
0.4
0.5
0.6
0.7
0.8
0.9

Figure 4. 30 (d)

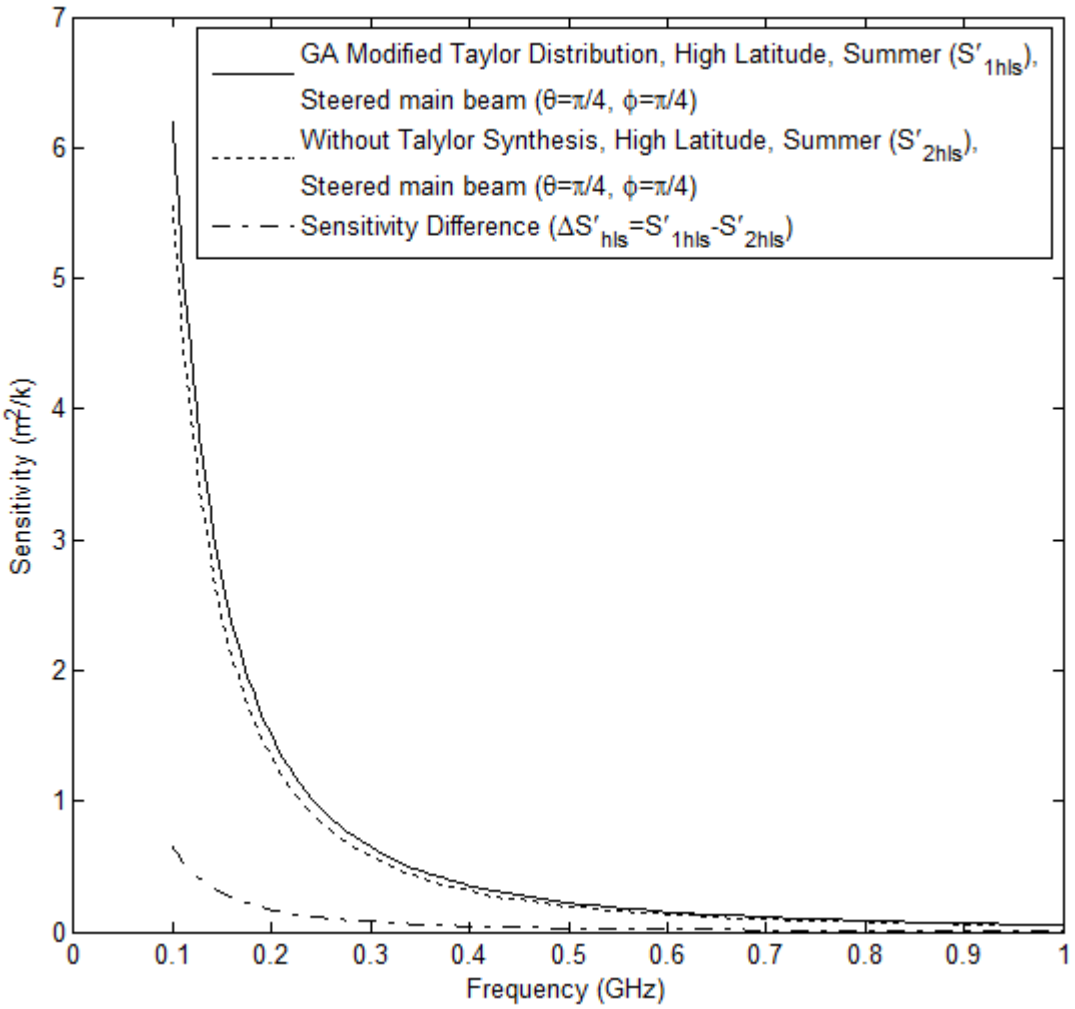

Figure 4. 31 (e)

Figure 4. 32 Sensitivity comparison between proposed planar array synthesized with the array thinning approach and with the proposed Taylor synthesis with GA modified discretizing technique. Comparison has been carried out at (a) mid latitude winter, (b) mid latitude summer, (c) low latitude, (d) high latitude winter, (e) high latitude summer(reference standard atmosphere ITU-R P.835-5). Main beam is pointing at $\boldsymbol{\theta = \frac{\pi}{4}}$ $\boldsymbol{\phi = \frac{\pi}{4}}$ and elements are isotropic. Difference between the sensitivity of for both the synthesis approaches has also been plotted.

Sensitivity performance of the proposed synthesis approaches has been plotted and compared over the whole frequency range of low and mid SKA with different latitude atmospheric conditions. Figures 4.27 (a) and (b) are showing the comparison for mid latitude conditions. Sensitivity offered by the proposed GA modified discretizing technique is slightly higher than that of array thinning approach. Steering of the main beam causes the side lobe level to increase and this increment in side lobe level has been controlled in the proposed technique. Figure 4.27 (c) is showing the comparison for low latitude and figures 4.27 (d) and (e) are of that high latitude. It should be noted that the difference between the sensitivity values for all

the latitude conditions are not too significant and the maximum difference of 1.2 $\boldsymbol{m^2/k}$ is obtained at 100 MHz.

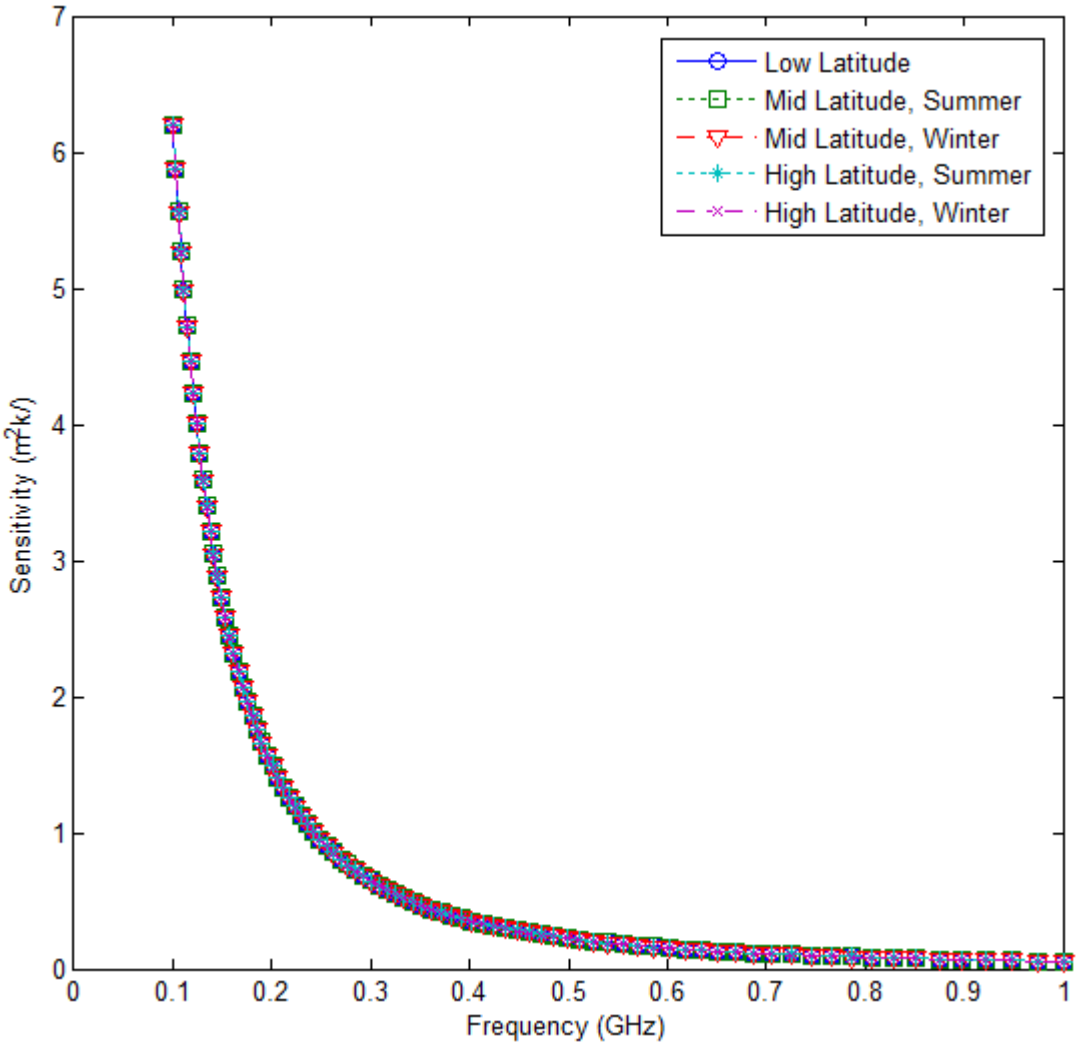

Figure 4. 33 Sensitivity performance of GA modified Taylor synthesis at different latitudes. Main beam is pointing at $\boldsymbol{\theta = \frac{\pi}{4}, \phi = \pi/4}$ and elements are isotropic.

Complete sensitivity analysis of the design for proposed technique with steered main beam at $\theta = \frac{\pi}{4}, \phi = \pi/4$ has been plotted in figure 4.28. It can be seen that the sensitivity values remain approximately constant with variation in latitude and satisfy the SKA application criteria. The highest value of sensitivity is 6.2 m^2/k obtained at 100 MHz and at 350 MHz this becomes $0.5m^2/k$. It is very important to maintain the high sensitivity value at smaller wavelength as the noise effects are quite significant at these frequencies. High sensitivity values correspond to the large effective area and the high directivity values offered by the designs (Eqs. 4.24-4.27). Proposed design offer improved values of directivity, high aperture efficiency (see Table 3.3) and minimum side lobe peaks resulting in highly sensitive antenna

design. Once again from figure 4.29, the sensitivity of proposed GA modified discretizing technique is slightly lesser than the array thinning approach. Though, the difference is not significant but still the array synthesized with thinning approach manages to achieve high sensitivity values. Here, the deciding factor is effective area of the array and for thinned configuration the effective area greater than that of obtained for GA modified discretizing technique. Effective area depends upon the directivity value (Eq. 4.26) and for the proposed array thinning approach (Chapter 2), design offer slightly higher directivity than that of GA modified discretizing technique.

There is a trade off between the directivity and side lobe level of an antenna. As the 3 dB beam width decreases, directivity increases and it also causes the side lobe peak to increase. For SKA application both directivity and minimum side lobe peak are equally important and need to be handled in an optimum way. Proposed design with GA modified discretizing technique offers reduction in side lobe peak but still it maintains a good directivity value and it can also be observed from figure 4.29. The shift in sensitivity due to the reduced directivity is not too significant and a maximum of 1.2 m^2/k sensitivity differences (approximately for all latitude conditions) at 100 MHz has been observed. For steered patterns, even though the directivity obtained with the array thinning approach was higher but the increased side lobe peaks affects the sensitivity considerably in terms of increased antenna temperature (see figure 4.27). Figure 4.30 is showing the sensitivity for all the latitudes with main beam pointing at $\theta = 0°, \phi = 0°$, and consistent with the behaviour observed earlier for the design. Not much variation is seen with change in latitude conditions and maintaining high sensitivity value of 9 m^2/k at 100 MHz which reduces to a value of 0.73 m^2/k at 350 MHz. Sensitivity values offered by the design under different atmospheric conditions have been compared with the values obtained with some recent array synthesis approaches reported (see Table 4.3). Values obtained with the proposed work clearly outperforms the values corresponding to the random arrays, tapered random arrays, equally spaced arrays, and tapered square arrays [Ahmed El-makadema, 2014].

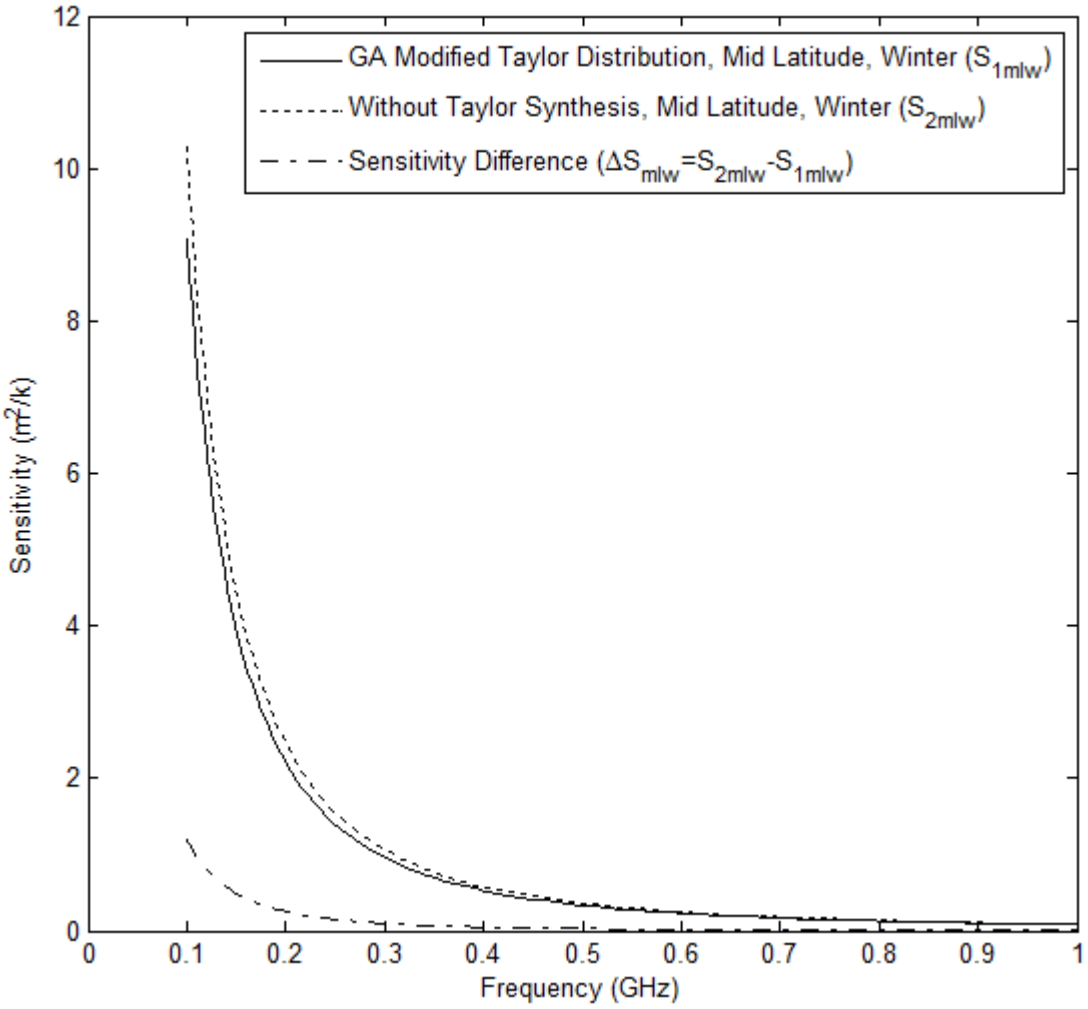
GA Modified Taylor Distribution, Mid Latitude, Winter (S_{1mlw})
Without Taylor Synthesis, Mid Latitude, Winter (S_{2mlw})
Sensitivity Difference ($\Delta S_{mlw}=S_{2mlw}-S_{1mlw}$)
Sensitivity (m^2/k)
Frequency (GHz)
0
2
4
6
8
10
12
0
0.1
0.2
0.3
0.4
0.5
0.6
0.7
0.8
0.9
1

Figure 4. 34 (a)

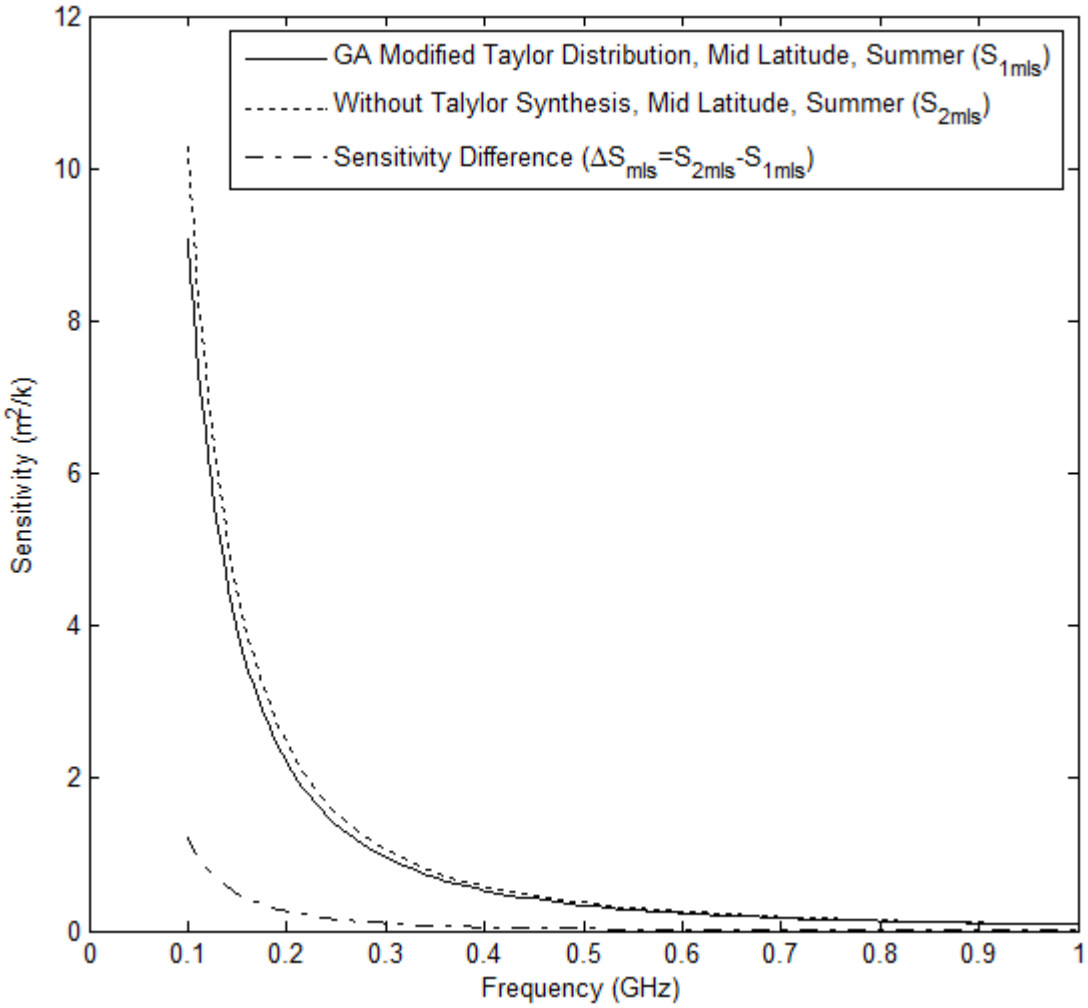
GA Modified Taylor Distribution, Mid Latitude, Summer (S_{1mls})
Without Talylor Synthesis, Mid Latitude, Summer (S_{2mls})
Sensitivity Difference ($\Delta S_{mls}=S_{2mls}-S_{1mls}$)
Sensitivity (m^2/k)
Frequency (GHz)
0
2
4
6
8
10
12
0
0.1
0.2
0.3
0.4
0.5
0.6
0.7
0.8
0.9
1

Figure 4. 35 (b)

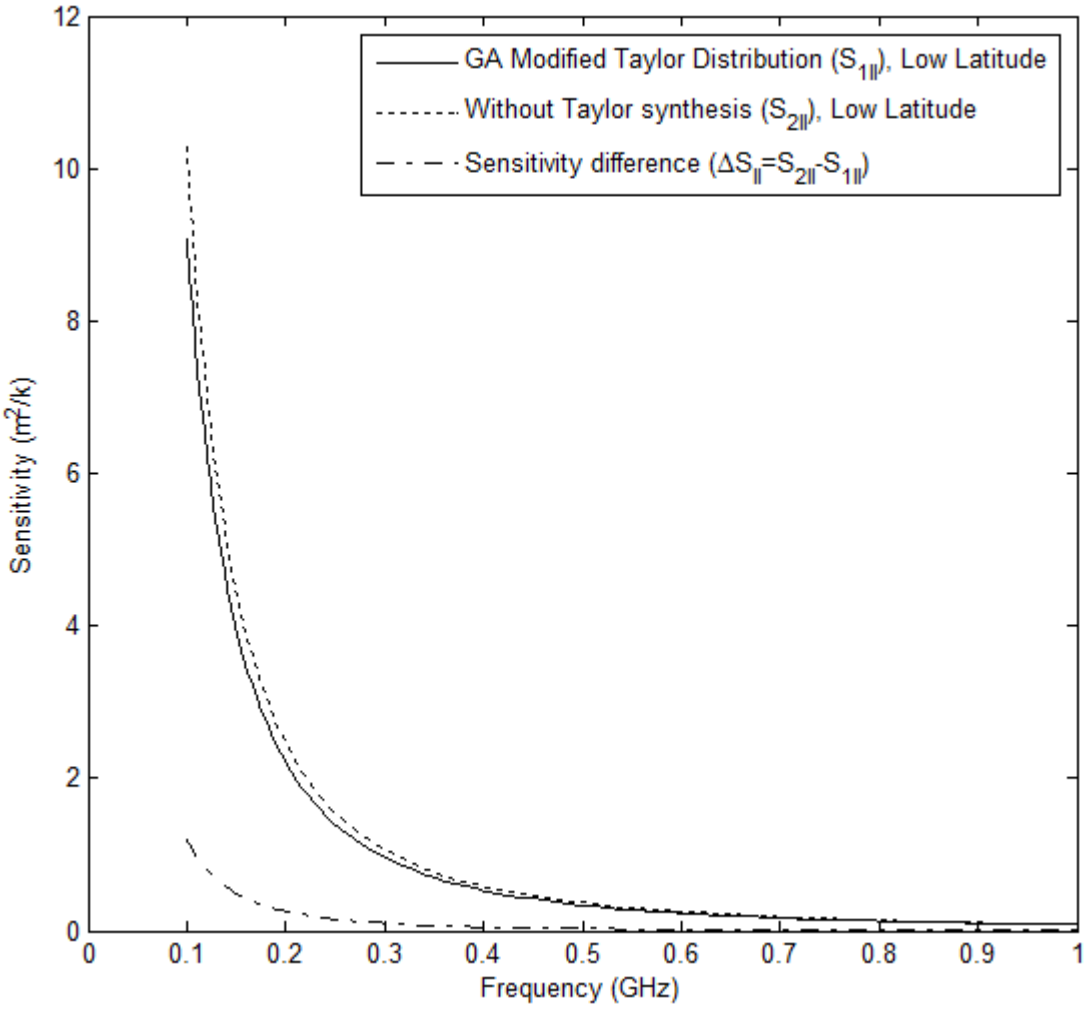
GA Modified Taylor Distribution (S_{1ll}), Low Latitude
Without Taylor synthesis (S_{2ll}), Low Latitude
Sensitivity difference ($\Delta S_{ll}=S_{2ll}-S_{1ll}$)
Sensitivity (m^2/k)
Frequency (GHz)
0
2
4
6
8
10
12
0
0.1
0.2
0.3
0.4
0.5
0.6
0.7
0.8
0.9
1

Figure 4. 36 (c)

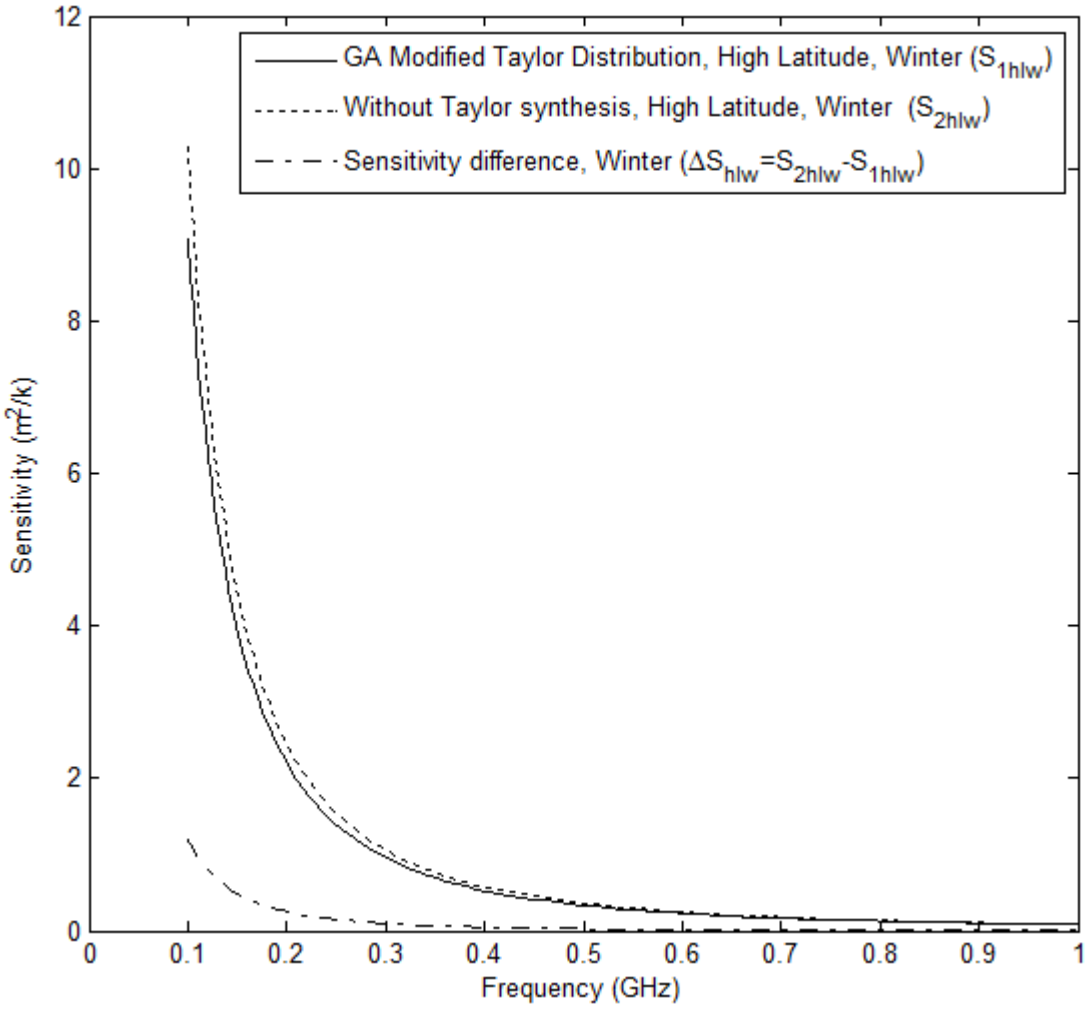
GA Modified Taylor Distribution, High Latitude, Winter (S_{1hlw})
Without Taylor synthesis, High Latitude, Winter (S_{2hlw})
Sensitivity difference, Winter ($\Delta S_{hlw}=S_{2hlw}-S_{1hlw}$)
Sensitivity (m^2/k)
Frequency (GHz)
0
2
4
6
8
10
12
0
0.1
0.2
0.3
0.4
0.5
0.6
0.7
0.8
0.9
1

Figure 4. 37 (d)

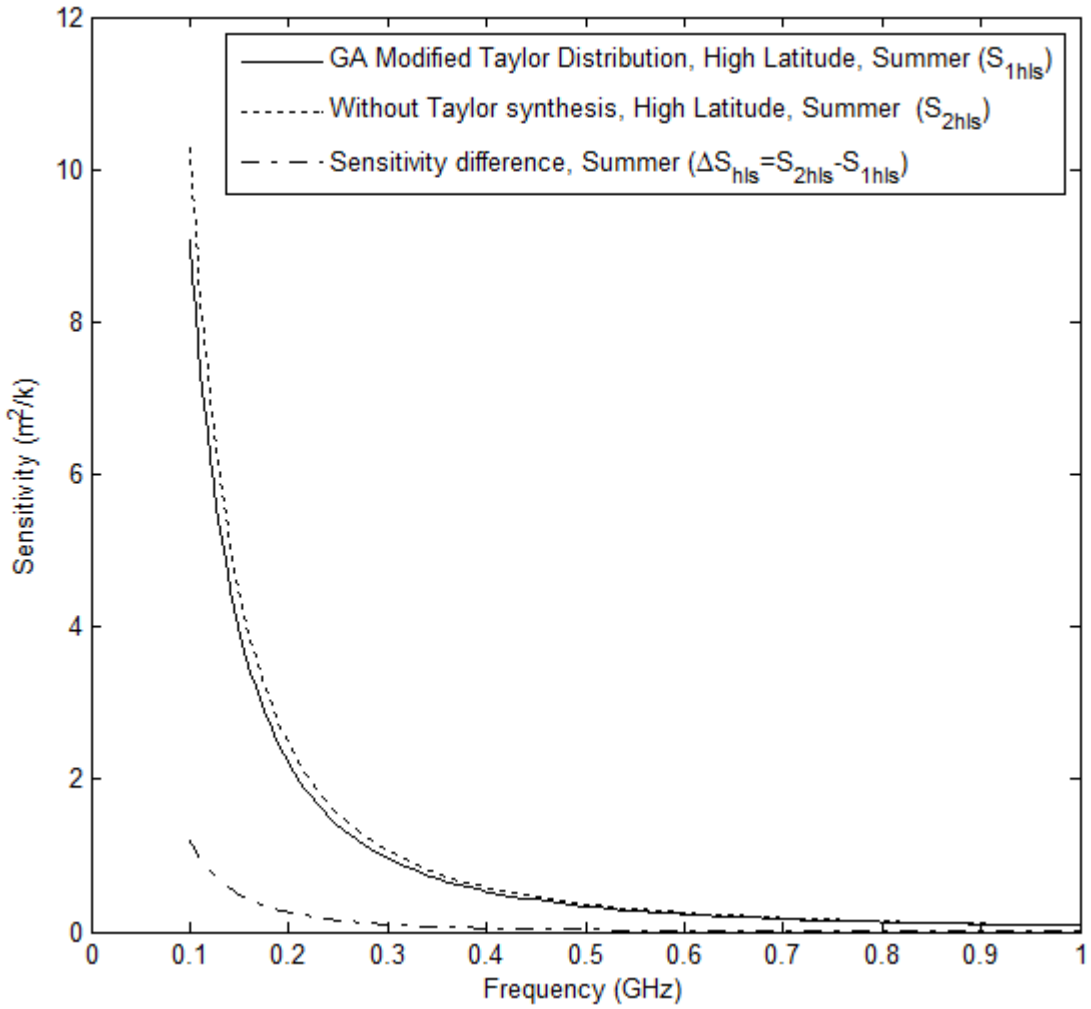

Figure 4. 38 (e)

Figure 4. 39 Sensitivity comparison between proposed planar array synthesized with the array thinning approach and with the proposed Taylor synthesis with GA modified discretizing technique. Comparison has been carried out at (a) mid latitude winter, (b) mid latitude summer, (c) low latitude, (d) high latitude winter, (e) high latitude summer(reference standard atmosphere ITU-R P.835-5). Main beam is pointing at $\theta = 0° \phi = 0°$and elements are isotropic. Difference between the sensitivity of for both the synthesis approaches has also been plotted.

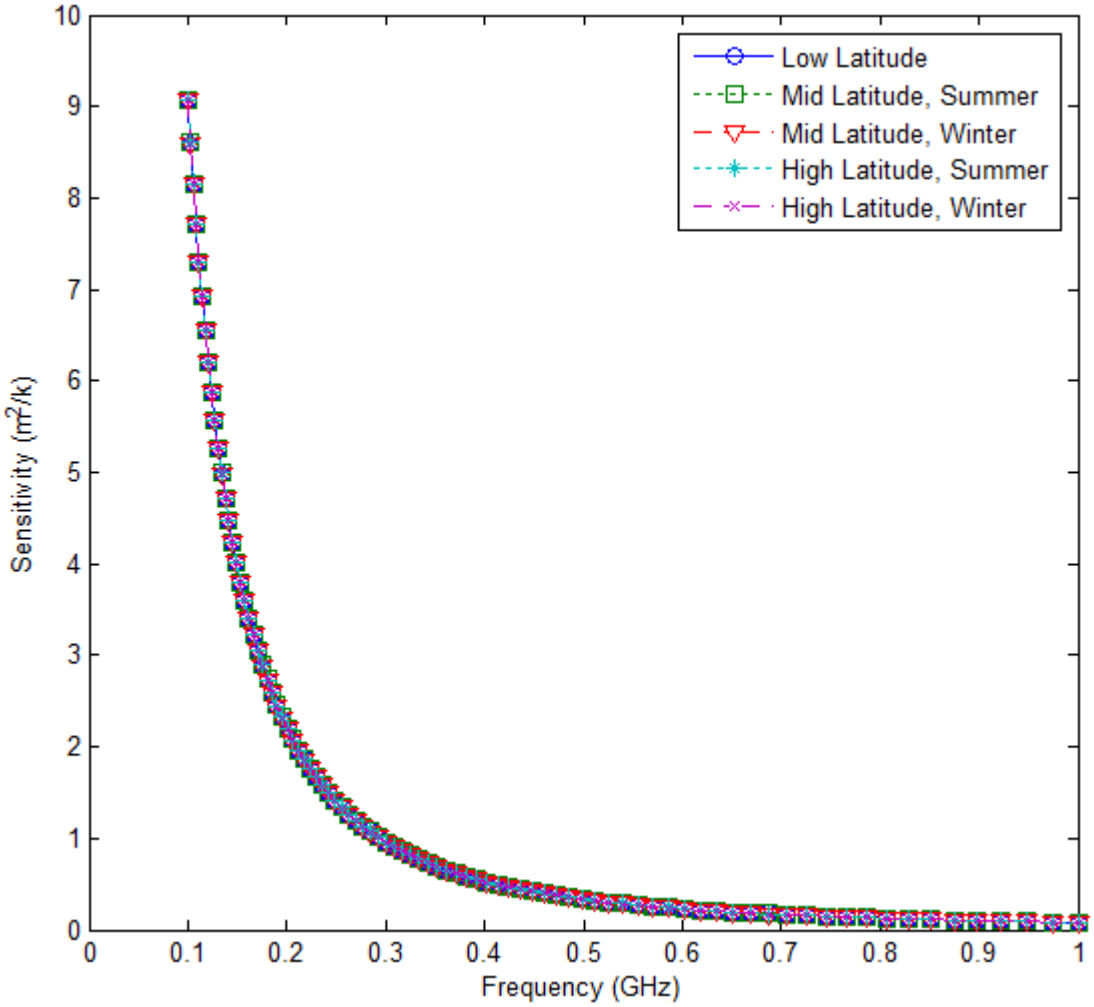

Figure 4. 40 Sensitivity performance of GA modified Taylor synthesis at different latitudes. Main beam is pointing at $\theta = 0°, \phi = 0°$ and elements are isotropic.

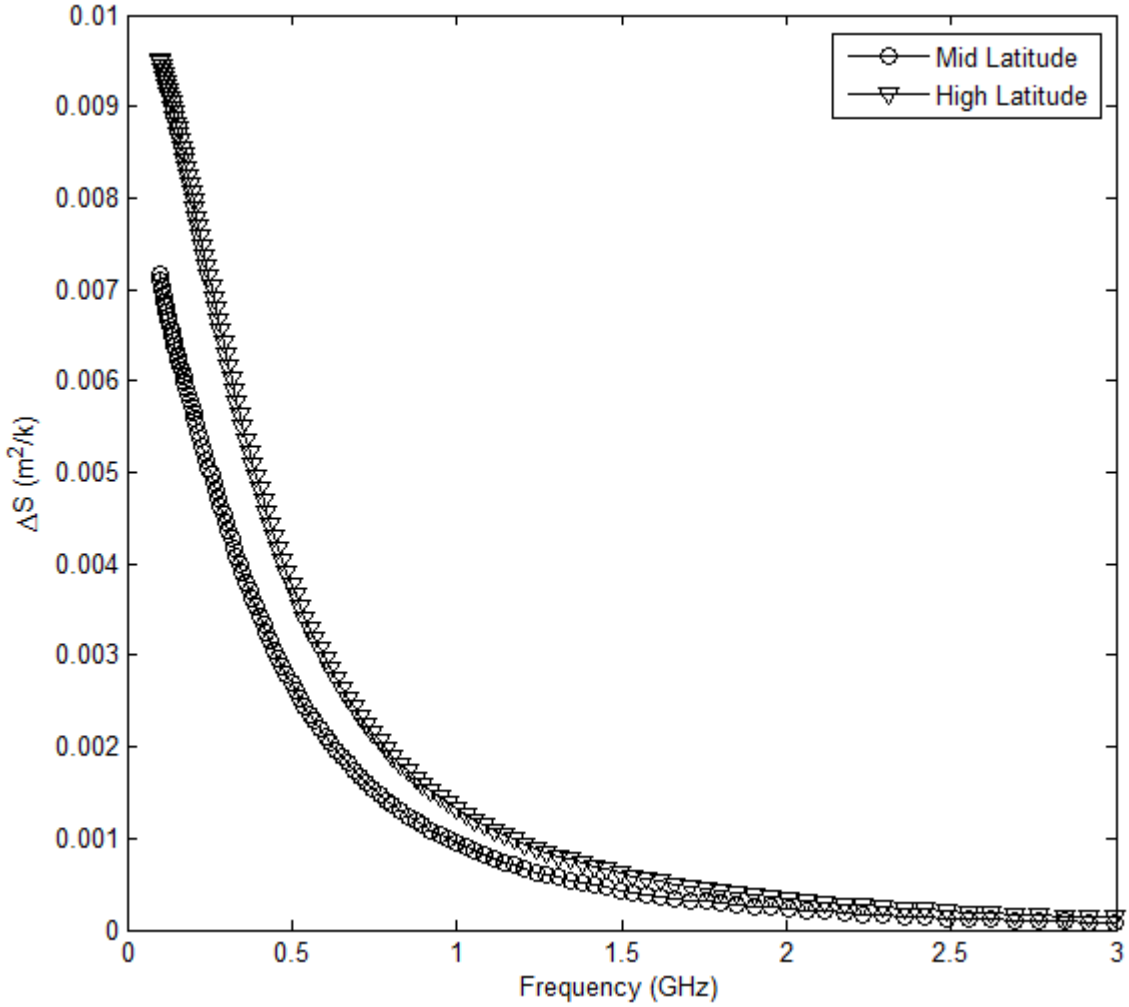

Figure 4. 41 Sensitivity variation at different latitudes in summer and winter weather conditions (reference standard atmosphere ITU-R P.835-5) for the proposed GA modified Taylor synthesis. The main beam is pointing at $\theta = \frac{\pi}{4}, \phi = \pi/4$ and elements are isotropic.

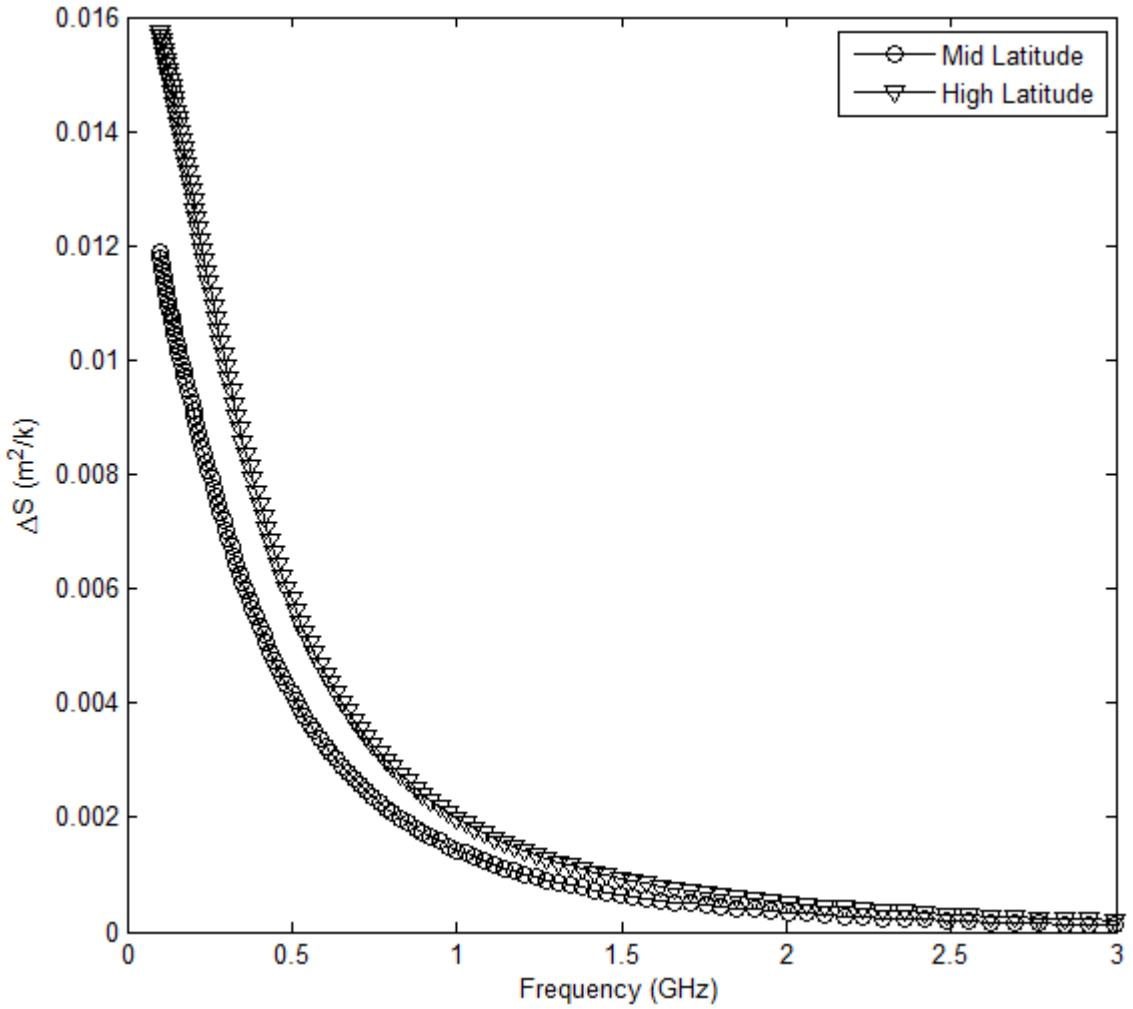

Figure 4. 42 Sensitivity variation at different latitudes in summer and winter weather conditions (reference standard atmosphere ITU-R P.835-5) for the proposed GA modified Taylor synthesis. The main beam is pointing at $\boldsymbol{\theta = 0°, \phi = 0°}$ and elements are isotropic.

Figures 4.31 and 4.32 are showing the sensitivity variation at different latitudes with respect to the change in weather conditions. As expected, at high latitude antenna encounters more sensitivity variation in comparison to the low latitude. Variations for end fire radiation are higher in comparison to the steered main beam as the sensitivity values for end fire radiation pattern are higher and since it is more environment sensitive, encounter more variations. All the variations in sensitivity observed are on the order of 10^{-2} ($\theta = 0°, \phi = 0°$) to 10^{-3} ($\theta = \frac{\pi}{4}, \phi = \frac{\pi}{4}$) which are considerably small and can be accepted for SKA application.

Table 4.3 contains the sensitivity comparison of the proposed antenna design synthesis approaches with some recently proposed antenna array synthesis approaches in different latitude conditions. At lower frequencies, proposed design synthesis approaches outperform the other synthesis approaches in comparison. Proposed synthesis approaches offer sensitivity

more than twice the values reported previously. Sensitivity values degrade with increment in frequency due to reduction in the effective area of antenna aperture and become less than the values achieved in the other synthesis approaches. Although the values are quite low at higher side of the spectrum but still for a wide range (up to 150 MHz) of frequencies proposed synthesis techniques offer values higher than the maximum value reported amongst the other synthesis approaches considered in comparison.

Table 4.3 sensitivity comparison of the proposed synthesis approaches.

Synthesis	**Sensitivity (m^2/k) , Latitude (Degree), Weather**	**Frequency range**
Proposed synthesis with GA	10.29 to 0.8, $22° < L < 45°$, summer 10.28 to 0.8, $22° < L < 45°$, winter	100 MHz to 500 MHz
	10.29 to 0.8, $L < 45°$	
	10.29 to 0.8, $L > 45°$, summer 10.28 to 0.8, $L > 45°$, winter	
Sampled Taylor distribution with GA Modified discrediting technique	9.08 to 0.4, $22° < L < 45°$, summer 9.08 to 0.4, $22° < L < 45°$, winter	100 MHz to 500 MHz
	9.08 to 0.4, $L < 45°$	
	9.08 to 0.4, $L > 45°$, summer 9.08 to 0.4, $L > 45°$, winter	
Equally spaced square array [Ahmed El-makadema, 2014]	3.9-1.9 , Sea level	70 MHz to 450 MHz
Tapered Square [Ahmed El-makadema, 2014]	2.8-1.9 , Sea level	70 MHz to 450 MHz
Tapered random [Ahmed El-makadema, 2014]	4.5-1.9 , Sea level	70 MHz to 450 MHz

Tapered GRS [Ahmed El-makadema, 2014]	3.9-1.9 , Sea level	70 MHz to 450 MHz

4.8. Conclusion

In this chapter, the state of the art radio telescope application of antenna array as SKA has been introduced and the proposed planar array geometries synthesized with array thinning approach and with the proposed GA modified discretizing technique have been investigated for the application. These radio telescopes can unveil some hidden phenomena of universe such as the theory related to its generation, the matter which is present in the universe and its characteristics. As the universe is expanding with time and hence the radio signal pertaining to the information regarding its generation becomes very weak and this form the base of requirement of high sensitivity and high spatial resolution of radio telescopes.

Some of the important figures of merit for an antenna in SKA application involve low brightness temperature at lower frequencies of the SKA operating frequency range and high sensitivity with minimum sensitivity variation over the different atmospheric condition for a given operating frequency. Layer by layer model for calculation of specific absorption by the water vapour and oxygen molecules has been adopted. At the microwave frequency range from 70 MHz to 340 GHz, the atmospheric absorption is dominated by these molecules. In layer by layer model the whole atmosphere is divided into a large number of spherical layers and then absorption is calculated for each layer. In the end, the whole absorption values from layers are added to have final specific absorption value. Calculation of sky brightness temperature has been carried out after the calculation of specific absorption. Brightness temperature determines the amount of noise added by the sky for given atmospheric condition. Antenna temperature is the convolution result of brightness temperature and the spurious radiation by the antenna. Hence the desired quality of an antenna is to have minimum side lobe peaks with reduced mean side lobe level. Finally the sensitivity is given by the ratio of effective aperture area of antenna to antenna system noise temperature. Higher values of effective area and less system noise temperature results in higher directivity. At lower frequency range of SKA it is difficult to achieve minimum system noise temperature and hence antennas are designed with larger effective area. This ultimately increases the cost of implementation. Hence it is desired to have high sensitivity with minimum antenna noise

temperature and minimum possible effective area in order to have low cost and high performance.

First the radiation pattern of the proposed design with array thinning approach has been tested for antenna temperature and sensitivity values. Considering different latitude conditions, design offer quite reduced values of antenna temperature below 25 K for all the environment conditions and for different element pattern and different main beam pointing directions. Radiation pattern of elements with certain element pattern offer lesser values of antenna temperature than isotropic elements. When main beam is steered with certain angle, it causes increment in the level of side lobe peaks and hence increased antenna temperature. Sensitivity values as high as 10.65 (isotropic element, end fire radiation) and 5.55 (isotropic element, steered main beam) have been obtained at 100 MHz. Sensitivity variations with the change in atmospheric conditions on the order of 10^{-3} have been obtained. For deployment of antenna arrays over an area of 1000s of kilometers require minimum sensitivity variation with change in environment and hence with such negligible amount of sensitivity variation design achieves the SKA requirement of minimum sensitivity variation. At higher latitudes the sensitivity variations are higher in comparison to the mid latitudes. Further, antenna temperature and sensitivity values have been computed for the pattern obtained with GA modified discretizing technique of sampled Taylor distribution. As the side lobe peaks in this case for both end fire radiation and steered main beam are same, the antenna temperature for steered beam pattern are improved from that obtained with array thinning approach. Since here improvement in the side lobe level has been achieved, the cost is paid in terms of directivity due to the inverse dependency of directivity and 3 dB beam width. Though, the design offers considerably good values of antenna temperature. At 100 MHz, the achieved antenna temperature values for end fire radiation and steered main beam are 4.1 K and 4.6 K respectively. These results are significantly improved from that obtained for regular, triangular, thinned, sparse, concentric ring, and random planar array geometries investigated in [N. Razavi-Ghods,2012]. A comparison for antenna temperature values has been carried out between array thinning approach and GA modified discretizing technique. The GA modified discretizing technique offers an antenna temperature improvement of 1 K to 4 K for a low SKA frequency range from 100 MHz to 350 MHz. The difference in antenna temperature values is consistent with the change in latitude conditions. Sensitivity for the proposed GA modified technique has been evaluated and negligible variation with the latitude was found. Sensitivity variations on the order of 10^{-3} have been achieved making

the sensitivity approximately constant with change in environment conditions. The sensitivity values on the order of 6.2 m^2/k at 100 MHz and 0.5 m^2/k at 350 MHz have been achieved. In comparison to the array thinning approach high sensitivity has been achieved with steered main beam due to reduced side lobe peak. Though the peak sensitivity difference, at 100 GHz, between the two approaches has been found to be on the order of 1.2 m^2/k. Slightly reduced values of sensitivity for end fire radiation pattern have been obtained due the effect of smaller directivity values. Here the higher values of directivity dominate the sensitivity and sensitivity values of 9 m^2/k at 100 MHz and 0.73 m^2/k at 350 MHz have been achieved. These values are not much lesser than the values obtained with array thinning approach and a maximum of 1.2 m^2/k sensitivity differences (approximately for all latitude conditions) at 100 MHz has been observed. Sensitivity variation due to change in weather conditions has been obtained on the order of 10^{-2} ($\theta = 0°, \phi = 0°$) to 10^{-3} ($\theta = \frac{\pi}{4}, \phi = \frac{\pi}{4}$). Such small variation in sensitivity can be accepted for SKA application where antenna arrays are deployed over hundreds of kilometres of area span. In the end, a comparison of sensitivity with different atmospheric conditions has been carried out to analyse the performances of the proposed designs.

References

- P. E. Dewdney, P. J. Hall, R. T. Schilizzi and T. J. L. W. Lazio, "The Square Kilometre Array," in Proceedings of the IEEE, vol. 97, no. 8, pp. 1482-1496, Aug. 2009.
- C. A. Balanis, Antenna Theory. Boca Raton, FL: CRC Press, 2002.
- C. Carilli and S. Rawlings, Eds., BScience with the square kilometre array, New Astron. Rev.,vol. 48, Dec. 2004.
- A. El-makadema, L. Rashid and A. K. Brown, "Geometry Design Optimization of Large-Scale Broadband Antenna Array Systems," in IEEE Transactions on Antennas and Propagation, vol. 62, no. 4, pp. 1673-1680, April 2014.
- G. C Medellin, "Antenna Noise Temperature Calculation." US-SKA TechMemoSeries,Sep.,2004,Memo95
- A. R. Thompson, J. M. Moran, and G. W. Swenson, Interferometry and Aperture Synthesis in Radio Astronomy, 2nd ed. New York: Wiley, 1986.

- R. T. Schilizzi, P. Alexander, J. M. Cordes, P. E. Dewdney, R. D. Ekers, A. J. Faulkner, B. M. Gaensler, P. J. Hall, J. L. Jonas, and K. I. Kellermann, BPreliminary specifications for the Square Kilometre Array, SKA Memo 100, Dec. 2007.
- P. J. Napier, A. R. Thompson, and R. D. Ekers, BThe very large array: Design and performance of a modern synthesis Dewdney et al. : The Square Kilometre Array Vol. 97, No. 8, August 2009 Proceedings of the IEEE 1495radio telescope, Proc. IEEE, vol. 71, pp. 1295–1320, 1983.
- European SKA Consortium, BEuropean concept for the SKA: Aperture array tiles, SKA Memo 19, Jul. 2002.
- B. Veidt, BFocal plane array architectures: Horn clusters versus phased array techniques,[SKA Memo 71, Feb. 2006.
- P. J. Hall, R. T. Schilizzi, P. E. F. Dewdney, and T. J. W. Lazio, BThe Square Kilometre Array (SKA) radio telescopeVProgress and technical directions, Radio Sci. Bull., no. 326, pp. 4–19, Sep. 2008.
- N. Razavi-Ghods, E. de Lera Acedo A. El-MakademaP. AlexanderA. Brown, "Analysis of sky contributions to system temperature for low frequency SKA aperture array geometries", Exp Astron (2012) 33: 141.
- K. F. Warnick and B. D. Jeffs, "Efficiencies and System Temperature for a Beamforming Array," in IEEE Antennas and Wireless Propagation Letters, vol. 7, no. , pp. 565-568, 2008.
- K. F. Warnick, M. V. Ivashina, R. Maaskant and B. Woestenburg, "Unified Definitions of Efficiencies and System Noise Temperature for Receiving Antenna Arrays," in IEEE Transactions on Antennas and Propagation, vol. 58, no. 6, pp. 2121-2125, June 2010.
- E. Brookner, "Active electronically scanned array (AESA) system noise temperature," 2013 IEEE International Symposium on Phased Array Systems and Technology, Waltham, MA, 2013, pp. 760-767.
- P.W. rosenkranz, "Shape of the 5 mm oxygen band in the atmosphere"IEEE Trans. Antenna and Propagation vol AP-23, pp. 498-506, 1975
- Ernest K. Smith, "Centimeter and millimeter wave attenuation and brightness temperature due to atmospheric oxygen and water vapor", Radio Science, Volume 17, Number 6, pages 1455-1464, November-December 1982

- E. Grossman, AT atmospheric transmission software, Airhead software, Boulder, CO (1989).
- J. R. Pardo, J. Cernicharo and E. Serabyn, "Atmospheric transmission at microwaves (ATM): an improved model for millimeter/submillimeter applications," in IEEE Transactions on Antennas and Propagation, vol. 49, no. 12, pp. 1683-1694, Dec 2001.
- F.T. Ulaby, R.K. Moore and A.K. Fung, Microwave Remote Sensing, vol 1 Addison-Wesley Publishing company, ch. 4-5, 1981
- L.S. Rothman, R.R. Gamache, R.H. Tipping, C.P. Rinsland, M.A.H. Smith, D.B. Chris, V.D. Malathy, J. M. Flaud, C. Camy-Peyret, A. Perrin, A. Goldman, S.T. Massie, L.R. Brown, and R.A. Toth, "HITRAN database:1991 and 1992 editions"Journal of Quantitative Spectroscopy Radiative Transfervol 48, pp. 469-507, 1992
- H.M.Pickett, R.L.Poynter, E.A. cohen, M.L. Delitsky, J.C. Pearson and H.S.P. Muller, "Sub-millimeter, Millimeter and Microwave Spectral Line Catalog" Journal of Quantitative Spectroscopy Radiative Transfervol 60, No. 5 pp. 469-507, 1998
- R. K. Crane, "Fundamental limitations caused by RF propagation," in Proceedings of the IEEE, vol. 69, no. 2, pp. 196-209, Feb. 1981.
- Recommendation ITU-R P.676-10, 2013
- Recommendation ITU-R P.835-5, 2012
- Recommendation ITU-R P.372-7 ,2001

Chapter 5

Analysis of Metal Nano Particles for Optical Antenna and Filter Design

This chapter describes the properties of metal nano particles particularly noble metals exhibiting some unique properties in the visible and infrared part of the spectrum. Behaviour of these nano particles towards the change in size, shape and environment enclosing them will be seen. These properties will be explored for some new applications of these nano particles such as optical filters.

5.1. Introduction

In optics, the light in terms of electromagnetic waves is radiated as wave fronts with the help of lenses, mirrors, and diffractive elements. This manipulation depends upon the wave nature of electromagnetic field and controlling fields on sub-wavelength scale is not possible. In contrast to this, radio waves and microwaves can be controlled efficiently using antennas at sub-wavelength wavelength scale [P. Bharadwaj et al., 2009]. In communication, light detection has been a part of the semiconductor technology, and these detectors have got improvement in their detection capability as the technology grew up providing better long-haul communication and larger bandwidth. In case of radio waves and microwaves, the detection is done with the help of antennas, which receive signals and convert them by using a specific electronic circuitry into a usable form. "Optical antenna" is a combination of both: photo detectors and radio electric antennas [M. A. van Dijk, 1979]. Optical antennas are said to be non-existing today because not much of the work has been done in this area. However, in recent past researchers have shown interest in the field of nano-optics and plasmonics and number of studies are being done to map the radio wave and microwave technology to the field of optics. The main reason behind the lack of application oriented research in the field is the size of the antenna. Antennas are made according the application area such as radio wave antennas have dimensions of the order of some meters, but in case of optical frequencies these dimension can go up to a few nano meters (about 10 nm). Fabrication accuracies at that scale are quite crucial. With the help of the new discoveries in nano technologies such as focused ion beam milling and electron-beam lithography, it has become easy to realize these antennas and there is a huge scope for further improvement in the field of fabrication technology of optical antennas, providing new research opportunities [P. Bharadwaj et al., 2009]. The light metal interaction has been explained by the Drude model and Lorentz model,

defining the dielectric function of the metal varying as a function of wavelength. These nano particles can enhance the electromagnetic field by several orders to produce a huge intensity of light in the vicinity of the particle, called a hot spot near the particle.

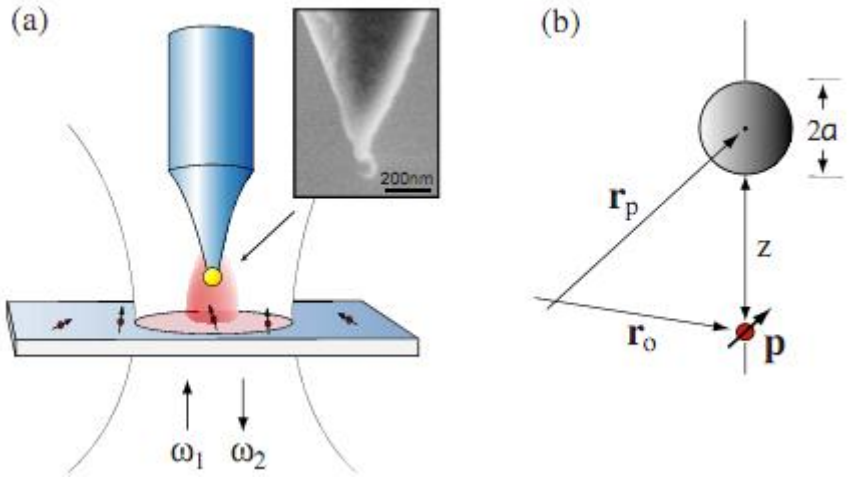

Figure 5. 1 (a) An optical antenna in the form of a gold or silver nanoparticle attached to the end of a pointed glass tip is interacting with a single molecule. The inset shows an scanning electron microscope image of a 80 nm gold particle attached to a glass tip. (b) Theoretical model [P. Bharadwaj et al., 2009].

This opens up an opportunity for the nano particles to be applied as an antenna in visible frequency range [B. B. Yousif and A. S. Samra, 2012]. In applications such as tip-enhanced Raman spectroscopy or surface-enhanced Raman spectroscopy, these particles with their hot spot building capability work as radiative emitters with sensitivity down to single molecule [B. B. Yousif and A. S. Samra, 2012]. In recent years, a number of schemes taking advantage of localized near fields generated by metallic nano particles have been proposed to use them as optical nano antennas [B. B. Yousif and A. S. Samra, 2012; D. P. Fromm et al., 2004; P. Mhlschlegel, 2005]. Using these nano particles the light can be confined to a very small spot, far beyond the diffraction limit and hence provide an improvement in size mismatch between the diffraction limited spot of the excitation light and fluorescent molecules that are much smaller than the excitation wavelength [B. B. Yousif and A. S. Samra, 2012; P. J. Schuck et al., 2005].

5.2. History

Near field analysis in optical domain has given rise to the invention of optical antennas. As the information in the near field vanishes with the distance of few nano meters, researches in the field when identified the unique properties of small particles (nanometer scale), propagation of the near filed to the detector was looking possible. In 1928, Edward Synge

managed to break the diffraction limit by identifying the properties of colloidal gold particle in order to radiate the localized field [D. W. Pohl, 2000] [L. Novotny, 2007]. In 1995, John Wessel concluded that the gold nano particle can work as an optical antenna [J. Wessel, 1985]. This was for the first time a nano particle was seen as a device to transfer information at such nano scale level. In 1995, the concept given by the John Wessel was experimentally proved by the two scientists Dieter Pohl and Ulrich Fischer in their work using a gold coated polystyrene particle [U. C. Fischer, &, D. W. Pohl, 1989]. After this researches were focusing of the detector application of these nano particles and optical antennas were being used in near-field microscopy and spectroscopy as a sharp metal tip probing element [L. Novotny, S. J. Stranick, 2006]. Today itself these are used in 'tip-enhanced near-field optical microscopy'. Apart from visible detection, optical antennas are used for infrared signal since 1966 as whisker diodes and now have evolved with growing research in the field [J. Alda, *et al.*, 2005][F. Gonzalez & G. Boreman, 2004]. In 1997, Bow-tie antennas were came into picture and was first used as probing element in microwave frequency range [R. D. Grober *et al.*, 1997]. Later optical antennas became well established as a detecting element and were used in various applications such as on the tip of atomic force microscopes [J. N., Farahani *et al.*, 2005] aperture based near field detectors [T. H. Taminiau, *et al*., 2007][H. G. Frey *et al.*, 2004]. Various geometries of optical antennas were proposed and investigated as different types of probing element at particular frequency or frequency ranges. Generation of surface plasmons at a particular frequency is the attribute of optical antenna which makes it a potential solution for various applications such as optical detection, biological sensing, optical sources, data storage, etc [Schuller, J. A. *et al.*, 2010][C. Hoeppener, L. Novotny, 2008][T. S. van Zanten *et al.*, 2010].

5.3. Analogy between RF Antenna and Optical Antenna

Nano technology has now evolved tremendously and fabrication of nano antenna is a part of this extremely growing field. Nano particles are being looked as nano detectors in optical and infrared domain due to their unique properties of scattering and emission of light at a particular wavelength. Objectives of optical antenna design include a proper transmission of optical information from its generation at the nano scale of light matter interaction to far field radiation. Due to the generation of high intensity light at nano scale these can also act as coherent sources of light for illumination of sub wavelength materials. In order to establish an analogy between RF antenna and optical antenna here both the devices have been discussed corresponding to their technology platform and the attributes which can be derived from RF

antenna design to optical counterpart. Functionality of both the antennas is same but still there is a complete difference between the operating principles of two antennas in terms of excitation, reception and transmission of the signal.

Optical antennas have been studied and experimentally tested on the base of various geometries (Dipole, Yagi-uda, Bow-tie) already being used in RF domain to analyze the effect of different geometries on antenna parameters such as operating frequency, radiation pattern and amplitude [P.Muhlschlegel et al., 2005; J. N. Farahani et al., 2005; K.B.Crozier et al., 2003; P.Bharadwaj et al., 2009]. Moving from the geometry resemblance, it has been proved that optical antennas transmits the near filed information generated by a quantum dot or florescence emitter to the far filed, similar to their RF counter parts. Researchers from various fields including chemistry, biology and electrical engineering are working together to apply this phenomena generated by light matter interaction for technical development in their respective fields. In order to establish a theoretical background for the optical antenna operations, the extensive research carried out in RF domain can be utilized. This includes the modelling of far filed radiation pattern, side lobes, antenna excitation, directivity, relation between wavelength and optical antenna structures. Although both light and RF signals are classically defined on the same platform and are governed by the Maxwell equations but the direct mapping of the technology from RF to optical domain is not possible. The interaction of light with nano particles is explained by the quantum theory of physics where the wavelength of input signal becomes comparable to the antenna structures. In this area various theoretical approaches have been proposed [H.Mertens et al., 2007; A. F.Koenderink, 2010; J. J. Greffet et al., 2010]**.** Metal nano particles have been studied for application as antennas but at the same time due to their power extinction property, these nano particles offer a potential to be utilized as nano optical filters. In the proposed work, combined application of nano particle working as an antenna and filter have been discussed. These nano particles when arranged with some specific configuration may lead to a design performing both the operations simultaneously.

Fundamental difference between the working of optical antenna and RF antenna lies behind the physics involve in it. Metal behaves differently as the frequency of operation changes from optical domain to RF domain. In RF domain antennas are highly conductive, negligible skin depth and sub wavelength in dimension. In optical domain, antennas are dominated by polarization and displacement effect and this changes the physics behind the antenna operation from that of in RF domain. When EM signal in optical domain interacts

with metal nano particles, the displacement current along the metal have shorter wavelength and causes the penetration of signal whereas, in RF domain the frequency of conduction current is equal to that of EM signal in free space leading to negligible penetration. This explains how the size of antennas of sub wavelength dimensions in RF domain become too small in optical domain for resonant conditions [A. Alù and N. Engheta, 2007; L. Novotny, 2007; A. Alù and N. Engheta, 2008; Andrea Alù and Nader Engheta, 2013]. Due to this optical antennas encounter more absorption losses in comparison to the RF antennas. Moreover, the unique phenomenon of surface plasmons, supported by the metal nano particles at optical frequencies is responsible for the intensity enhancement at the sharp edges of the antenna structures unlike their RF counterparts [Andrea Alù and Nader Engheta, 2013]. These two characteristics shown by the nano particles construct the base of their combined operation capability as antenna and filter, investigated in the thesis.

5.4. Metal Nano Particles and Interaction with Light

Metal nano particles are in the midst of molecules and extended solids, and these particles can have their diameters from 1nm to 100nm. These particles have reduced size and quantum confinement of electrons and phonons with a complex many electron system, providing some unique properties which can be controlled by the particle size and shape. There are two factors which can justify the increasing attention of researchers in metal nano particles: one is that it can leads to a new branch of fundamental science and another one is its potential technological applications. These nano particles can find their potential applications in the devices utilized in nonlinear optics, for optical data storage, for surface-enhanced spectroscopy [K. Kneipp et al., 2002] and catalysis, for biological labelling and sensing [J. Yguerabide and E. E. Yguerabide, 1998], [P. K. Jain et al., 2007], and even for cancer therapy [G. Raschke et al., 2003].

5.4.1. Surface Plasmons

Plasmons are collective oscillations of the free electron density with respect to the fixed positive ion in metal. Plasmon is a quantum of plasma oscillation and can be considered as a quasi particle just like phonon. Plasma oscillation take place under the influence of external electromagnetic field applied on the metal, when electrons shifts from their equilibrium position and a restoring force of the nucleus pulls electrons back to their original position, resultantly causing the electrons to oscillate at plasma frequency. Surface plasmons (SPs) as

their name indicates are the electron density oscillations at the interface between the two materials of dielectric functions with opposite sign, for example a metal dielectric interface.

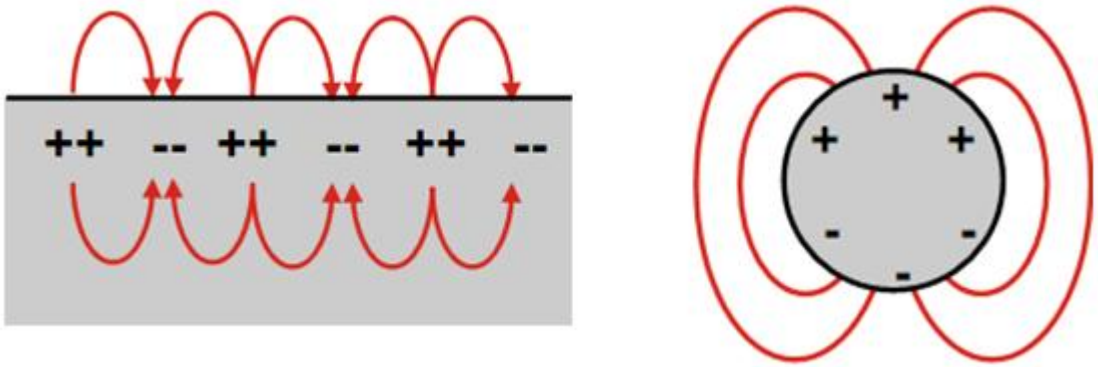

(a) **(b)**

Figure 5. 2 Geneartion of surface Plasmon polaritons (a); and localized surface plasmons (b)

Generation of the surface plasmons on the surface of metal nano particles can be classified on the basis of the size of the nano particle. One is propagating surface plasmons that generates on the structures larger in size with planar geometry where light trapped at the interface travels along the surface as surface Plasmon polaritons (SPPs). Second class corresponds to the generation of surface plasmons at the interface of curved surfaces and these are non propagating in nature and hence termed as Localized surface plasmons (LSPs). In this thesis, spherical nano particles have been analysed for their antenna and filter application. These fall under the category of localized surface plasmons and hence properties of LSP will be discussed. Figure 5.2 is depicting the schematic representation of SPPs and LSPs. In SPPs the charge density oscillations are along the surface whereas, in LSPs oscillations are localized.

5.4.2. Localized Surface Plasmon Resonance

In contrast to surface Plasmon-polaritons, which are the electromagnetic waves, a combined effect of surface electrons and photons, propagating along the metal-dielectric interface, localized surface plasmons (LSPs) are charge density oscillations confined to matellic nano particles and matellic nano structures [N. Dmitruk, et al., 2010]. This is trapping of light at the surface of nano particles of size smaller than the wavelength of light (see figure 5.2). Excitation of LSPs at the surface of nano particle occurs at a particular wavelength and that frequency or wavelength is called resonance wavelength or localized surface Plasmon resonance (LSPR). At resonance, light gets strongly scattered resulting in intense surface

plasmons absorption bands, and enhancement of the local electromagnetic field. Resonance frequency and the intensity of the surface Plasmon absorption bands depend upon some factors and these factors are: type of material (Gold, Silver, etc.), size and size distribution, shape of the nano structure, and the environment which is surrounding the particle [E. Hutter and J. Fendler, 2004]. These properties have a key role in bringing the intense research interest towards LSPs and development of the devices based on generation of LSPs. Mainly gold and silver nano particles are used for antenna application as the transition of electrons occur between the energy bands corresponding to the release of energy in visible spectrum. Although, silver nano particles have higher optical efficiency (ration of scattered power to the total extincted power) over a large frequency band but gold nano particles are chemically inert in nature and fulfil the desirable criteria for bio applications. A detailed analysis of small nano particles of different shapes generating localized surface plasmons and its applications in bio-sensing have been discussed in [Eleonora Petryayeva and Ulrich J. Krull, 2011].

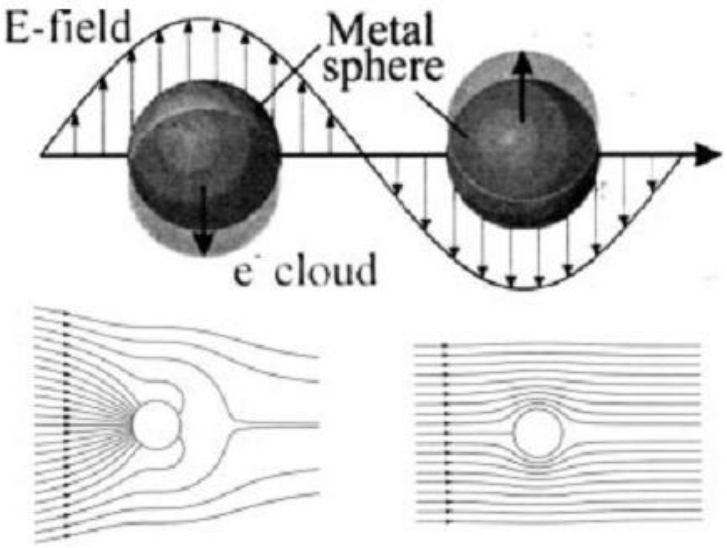

Figure 5. 3 Top: Plasmon oscillation for a sphere, showing the displacement of the conduction electron charge cloud relative to the nuclei; Bottom: field lines of pointing vector around a small aluminium sphere illuminated by light of energy 8.8 ev where resonance occur (left) and 5 ev where there is no resonance (right) [E. Hutter and J. Fendler, 2004].

5.5. Electromagnetics of Metals

Interaction of metals and electromagnetic wave can be understood on the basis on the Maxwell Eq. in classical physics without incorporating the assumptions of quantum theory of physics as the energy level density is much higher than thermal excitation bands. The behaviour of metal can be classified with the different ranges of frequencies. At low frequencies (up to visible) metals are reflective, non-absorbing and are used in waveguides at

microwave frequencies. As moving towards high frequencies metals are more absorbing in nature leading to the change in behavioural modelling of the metals. At higher frequencies (ultraviolet) metals behave like a dielectric material. Noble metals such as Gold and Silver show inter band transitions at optical frequencies causing the power absorption in this frequency range. The dielectric function of metal nano particle is given by the Drude dispersion model and Lorentz dispersion model.

In order to calculate the dielectric constant of metal as a function of frequency, first it is required to calculate the wave equation for the light propagating along the surface of a metal. Starting from the macroscopic Maxwell's equation [Stefan A. Maier, "Plasmonics: Fundamentals and Applications", 2007]

$$\nabla . D = \rho_{ext} \tag{5.1}$$

$$\nabla . B = 0 \tag{5.2}$$

$$\nabla \times E = \frac{-\delta B}{\delta t} \tag{5.3}$$

$$\nabla \times H = J_{ext} + \frac{\delta D}{\delta t} \tag{5.4}$$

These four equations link the four macroscopic fields D (dielectric displacement), B (Magnetic flux density), E (electric filed), and H (magnetic field).

Once again rewriting these four fields in terms of polarization P and magnetization M we have

$$D = \epsilon_0 E + P \tag{5.5}$$

$$\mathrm{H} = \frac{B}{\mu_0} - M \tag{5.6}$$

Here ϵ_0 electric permittivity and μ_0 magnetic permeability in vacuum. Now the electric dipole moment P per unit volume inside the material is related to the current density as

$$\mathrm{J} = \frac{\delta P}{\delta t} \tag{5.7}$$

Now from Eq.5.1

$$\nabla . E = \frac{\rho_{tot}}{\varepsilon_0} \tag{5.8}$$

For a linear, isotropic and non magnetic media the relation between the four macroscopic fields are given by

$$D = \varepsilon_0 \varepsilon E \tag{5.9}$$

$$B = \mu_0 \mu H \tag{5.10}$$

Here ε is the dielectric constant of the material and for a non magnetic mediam the relative magnetic permeability$\mu = 1$. Further, the dielectric susceptibility χ gives the linear relation between the dipole moment and electric field as

$$P = \varepsilon_0 \chi E \tag{5.11}$$

In order to complete the basic relationship between the fields derived from the Maxwell's equations, it is required to mention the linear relation between current density and electric field as

$$J = \sigma E \tag{5.12}$$

To describe the electromagnetic phenomena of metal in optical domain, it is required to derive the relationship between dielectric constant ε and conductivity σ. At higher frequencies, behaviour of metals depends upon the frequency. Simplified relation of linear Eqs. 5.9 and 5.12 in terms of wave vector K and angular frequency ω in Fourier domain is

$$D(K, \omega) = \varepsilon_0 \varepsilon(K, \omega) E(K, \omega) \tag{5.13}$$

$$J(K, \omega) = \sigma(K, \omega) E(K, \omega) \tag{5.14}$$

Finally, the dielectric function as a function of frequency and conductivity is given by

$$\varepsilon(K, \omega) = 1 + \frac{i\sigma(K, \omega)}{\varepsilon_0 \omega} \tag{5.15}$$

At low frequencies the response of bound electrons to the incident field is explained by ε, whereas, response of conduction electrons is measured through conductivity σ. In case of optical frequency range if the response of bound electrons is described through a static dielectric constant $\delta\varepsilon$ and that of free conduction elecrones by σ' then after rewriting the Eq. 5.15 we have

$$\varepsilon(\omega) = \delta\varepsilon + \frac{i\sigma'(\omega)}{\varepsilon_0 \omega} \tag{5.16}$$

Dielectric constant and conductivity can be assumed to have real and imaginary parts, given by

$$\varepsilon(\omega) = \varepsilon_1(\omega) + i\varepsilon_2(\omega) \tag{5.17}$$

$$\sigma(\omega) = \sigma_1(\omega) + i\sigma_2(\omega) \tag{5.18}$$

$$n'(\omega) = n(\omega) + ik(\omega) \tag{5.19}$$

$$n' = \sqrt{\varepsilon} \tag{5.20}$$

$$\varepsilon_1 = n^2 - k^2 \tag{5.21}$$

$$\varepsilon_2 = 2nk \tag{5.22}$$

Where n' is a complex valued refractive index function and k is the absorption coefficient. For a electromagnetic wave propagating through the medium with $S(x) = Se^{-\alpha x}$, the absorption coefficient of Beer's low α in terms of k is given by

$$\alpha(\omega) = 2k(\omega)\frac{\omega}{c} \tag{5.23}$$

Hence it can be concluded from Eq. 5.17 that imaginary part of dielectric function determines the amount of absorption of electromagnetic signal inside the medium and for $|\varepsilon_1| >> |\varepsilon_2|$, the real part of complex refractive index n' is determined by the ε_1. Form Eq. 5.16 the real part of σ determines the amount of absorption and imaginary part determines the amount of polarization.

Once again from the Maxwell's Eq. 5.1 to 5.4 the wave Eq. are given by

$$\nabla \times \nabla \times E = -\mu_0 \frac{\delta^2 D}{\delta t^2} \tag{5.24}$$

$$K(K.E) - K^2 E = -\varepsilon(K,\omega)\left(\frac{\omega}{c}\right)^2 E \tag{5.25}$$

Eq. 5.24 representing the wave equation in time domain and Eq. 5.25 represnting the equation in Fourier doamin. Here $c = 1/\sqrt{\varepsilon_0 \mu_0}$ is the velocit of light.

Now for transeveerse propagation, $K.E = 0$, the dispersion relation is given by

$$K^2 = \varepsilon(K, \omega) \left(\frac{\omega}{c}\right)^2 \tag{5.26}$$

Once again for longitudinal propagation, from Eq. 5.25, the dispersion relation is given by

$$\varepsilon(K, \omega) = 0 \tag{5.27}$$

Hence longitudinal propagation of electromagenetic wave in a medium can only occur at frequencies for which the value of dilectric constant become zero.

5.5.1. Dielectric Function of Metals in Optical Domain

Dielectric function of metals in optical domain is given by the free electron gas model or popularly known as Drude model. This model explains the behaviour of metal dielectric function over a wide range of frequencies in optical domain. At high frequencies the metals are quite sensitive to frequency changes and generation of surface Plasmon depend upon the frequency of incident light. The model explains the behaviour of alkali metals up to ultraviolet range whereas, for noble metals application of the model is limited up to a part of optical spectrum due to the occurrence of interband transitions. In this model, interactions between electrons and lattice potential are not taken into account. The model assumes that the oscillations of electrons around their equilibrium position occur in response to the applied electric field and these oscillations are damped by the collisions occurring with a collision frequency $\upsilon = 1/\tau$. Here τ is called the relaxation time of the free electron gas. At room temperature τ has a value on the order of 10^{-14}, which corresponds to a collision frequency of 100 THz.

Now after solving the equation of motion for an electron of plasma sea under the influence of external electric field, the expression for dielectric function for metal is given by [Stefan A. Maier, "Plasmonics: Fundamentals and Applications", 2007]

$$\varepsilon(\omega) = 1 - \frac{\omega_p^2}{\omega^2 + i\upsilon\omega} \tag{5.28}$$

Where ω_p is known as plasma frequency. Eq. 5.28 holds true for $\omega < \omega_p$ and as the frequency increases, the product $\upsilon\omega$ also increases. For the frequencies close to the plasma frequency, $\upsilon\omega \gg 1$, due to negligible damping the dielectric function is given by

$$\varepsilon(\omega) = 1 - \frac{\omega_p^2}{\omega^2} \tag{5.29}$$

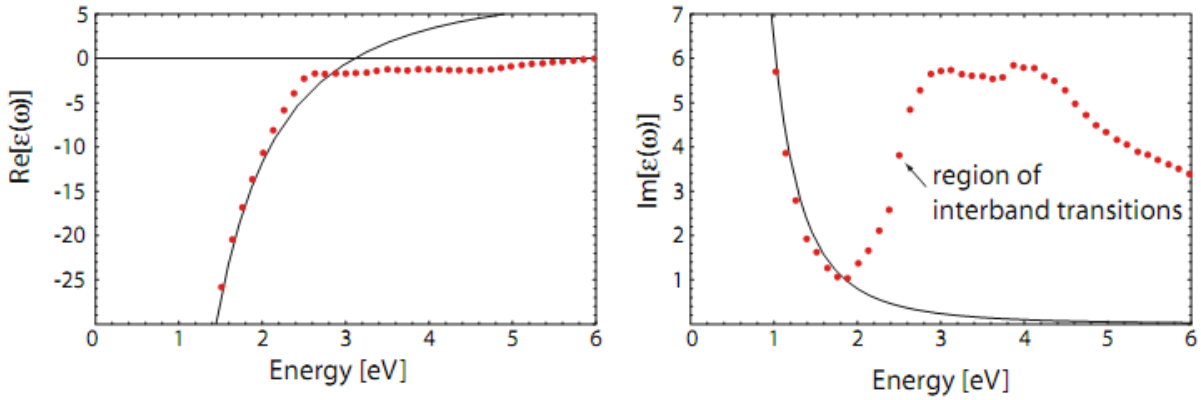

Figure 5. 4 Drude model fit of the dielectric function of gold. At higher frequencies the model deviates from the actual pattern as can be seen from real and imaginary part of gold. Actual pattern is depicted by the dotted lines [Stefan A. Maier, "Plasmonics: Fundamentals and Applications", 2007].

For frequency range $\omega > \omega_p$, the free electron gas model start deviating from the actual response of the metal as it does not take in account the effect of polarization due to filled d band near Fermi level (figure. 5.4 is showing the validity of free electron gas model for the case of gold). It is required to redefine the dielectric function given by the ideal free electron gas model for noble metals in the frequency regime $\omega > \omega_p$. The effect of polarization is described by a dielectric constant ε_∞ which takes the value in the range$1 < \varepsilon_\infty < 10$.

Rewriting the Eq. 5.28 as

$$\varepsilon(\omega) = \varepsilon_\infty - \frac{\omega_p^2}{\omega^2 + i\upsilon\omega} \tag{5.30}$$

Drude model explains the behaviour of metal in the optical frequency range till the interband transitions in metal occurs. As the frequency reaches above a threshold level the dielectric function, described by the model, starts deviating from the actual response. It can be understood as the absorption of the photons occurs due to the excitation of electrons from the

filled band below the Fermi level to the higher energy bands. These interband transitions affect the generation of surface plasmons by absorbing a part of incident energy and by increasing the damping effect. For Gold, these transition starts occurring at the boundary of near infrared and visible spectrum. To model these interband transitions, the expression of dielectric function given by the Drude model was modified by adding a Lorentz-oscillator term $\frac{A_i\omega_i^2}{\omega_i^2-\omega^2-i\upsilon\omega}$ and the dielectric function is now given by

$$\varepsilon(\omega) = \varepsilon_\infty - \frac{\omega_p^2}{\omega^2 + i\upsilon\omega} + \sum \frac{A_i\omega_i^2}{\omega_i^2 - \omega^2 - i\upsilon\omega} \tag{5.31}$$

5.5.2. Approximations Based on Particle Size

Excitation of metal nano particle from a light source causes the electrons to oscillate and this oscillation results in scattering from the particle consequently particle said to be radiating. A fraction of energy is consumed in the radiation, whereas some amount of incident energy gets converted into another energy source, such as heat and light is said to be get absorbed [M. A. van Dijk, 1979]. The total extinction of the light is the sum of scattering and absorption. In 1908 Gustav Mie proposed the theory of scattering from nano particles, providing the relation between the scattering cross section, and the direction and polarization of the incident light. With the help of Mie theory, the incident power can be related to the scattered power and absorbed power with the help of a geometrical quantity called scattering cross section. From mie theory the scattering and absorption cross section are given by [M. A. van Dijk, 1979; N. Dmitruk et al., 2010]

$$\sigma_{ext} = \frac{2\pi}{k^2} Re(a_n + b_n) \tag{5.32}$$

$$\sigma_{sca} = \frac{2\pi}{k^2} \sum_{n=1}^{\infty} (2n+1)\,(|a_n|^2 + |b_n|^2) \tag{5.33}$$

$$\sigma_{sca} = \frac{2\pi}{k^2} \sum_{n=1}^{\infty} (2n+1)\,(|a_n|^2 + |b_n|^2) \tag{5.34}$$

$$\sigma_{abs} = \sigma_{ext} - \sigma_{sca} \tag{5.35}$$

The coefficients a_n and b_n are defined as [M. A. van Dijk, 1979]

$$a_n = \frac{m\psi_n(mx)\psi'_n(x) - \psi_n(x)\psi_n'(mx)}{m\psi_n(mx)\xi'_n(x) - \xi_n(x)\psi_n'(mx)} \tag{5.36}$$

$$b_n = \frac{\psi_n(mx)\psi'_n(x) - m\psi_n(x)\psi_n'(mx)}{\psi_n(mx)\xi'_n(x) - m\xi_n(x)\psi_n'(mx)} \tag{5.37}$$

Where ψ and ξ are Ricatti-Bessel functions of order n, $x = kR$ is size parameter (R is radius of metal particle) and $m = \sqrt{\frac{\varepsilon_p}{\varepsilon_m}}$ is the square root of the ratio of dielectric functions of particle and of the medium. Figure 5.5 is showing the variation in the scattering cross section with the particle size, keeping the environment refractive index same. Particles of diameter 10nm and 30nm have been considered and we can see that resonance is red shifted for larger particles and scattering peaks lie further red than absorption peaks [M. A. van Dijk, 1979].

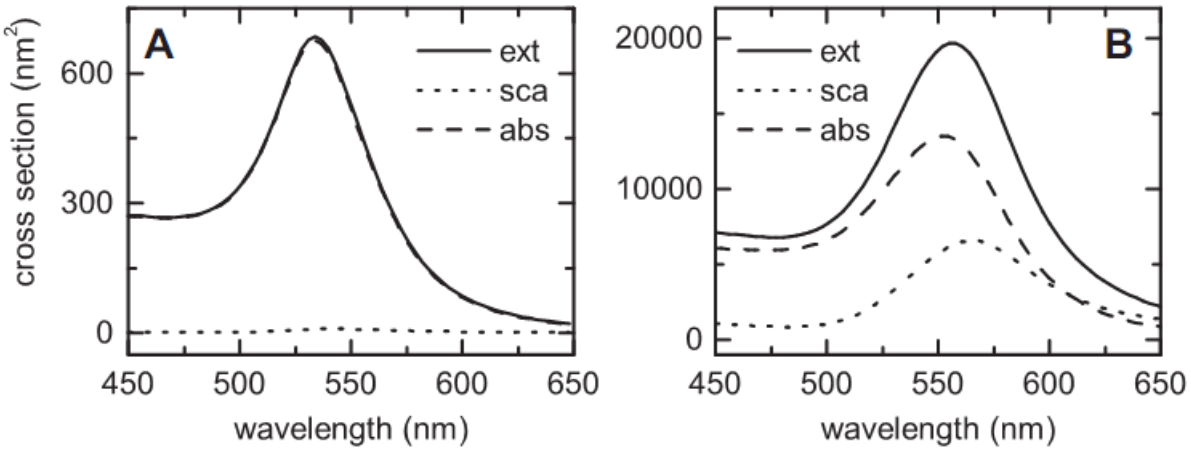

Figure 5. 5 Extinction, scattering and absorption spectra of a particle with a radius of 10 nm (A) and a radius of 30 nm (B). In both cases, the refractive index of the environment is 1.5. Note that for the 10-nm particle, the scattering cross section nearly vanishes, and as a result of that, the absorption and extinction cross sections are approximately equal [M. A. van Dijk, 1979].

In the limit of very small particles, the electromagnetic interaction between different parts of the metal is almost instantaneous (i.e., the speed of light can be taken as infinite) [V. Myroshnychenko et al., 2008]. Although with Mie theory we get exact solution but to simplify things, some approximations for very small particles (smaller than the wavelength of the light) can be used to have simple expressions for the scattering and absorption cross sections. Since these approximation can only be applied to the particles up to a certain size, in this limit the condition that must be satisfied is $mx << 1$, where $x = kR$, and this limit is called Rayleigh limit [M. A. van Dijk, 1979]. The simplified expressions for the cross sections are [M. A. van Dijk, 1979; V. Myroshnychenko et al., 2008]

$$\sigma_{abs} \approx \sigma_{ext} = k\, Im(\alpha) = 4\pi k R^3 Im(\frac{\varepsilon_p - \varepsilon_m}{\varepsilon_p + 2\varepsilon_m}) \tag{5.38}$$

$$\sigma_{abs} \approx \sigma_{ext} = k\, Im(\alpha) = 4\pi k R^3 Im(\frac{\varepsilon_p - \varepsilon_m}{\varepsilon_p + 2\varepsilon_m}) \tag{5.39}$$

$$\sigma_{sca} = \frac{k^4}{6\pi} |\alpha|^2 Im(\alpha) = 8\pi k^4 R^6 \left|\frac{\varepsilon_p - \varepsilon_m}{\varepsilon_p + 2\varepsilon_m}\right|^2 \tag{5.40}$$

Where α is the polarizability of the particle which is defined as [M. A. van Dijk, 1979; V. Myroshnychenko et al., 2008]

$$\alpha = 4\pi R^3 \frac{\varepsilon_p - \varepsilon_m}{\varepsilon_p + 2\varepsilon_m} \tag{5.41}$$

ε_p and ε_m are the dielectric constants of the particle and the medium, respectively.

The Eqs. 5.39 and 5.40 of absorption and scattering by the nano particle also holds true for dielectric nano particles [Stefan A. Maier, "Plasmonics: Fundamentals and Applications", 2007]. At resonance the scattering and absorption cross sections become greater than the physical cross-section of the particle and this condition is given by the Frohlich criteria

$$Re[\varepsilon(\omega)] = -2\varepsilon_m \tag{5.42}$$

Eq. 5.39 and Eq. 5.40 also give information on the size dependence of the absorption and scattering cross sections. Whereas scattering increases with the sixth power of the size of the particle, absorption scales with the third power. As a result of this, for small particles, the absorption cross section is larger than the scattering cross section, and an absorption-based detection technique is therefore much more sensitive to detect small particles than a method based on scattering. From Eq. 5.42 it is clear that as the refractive index of the environment changes the frequency of generation of surface plasmons also changes.

These phenomena can be utilized to have an array of nano particles radiating in closely spaced frequency spectrum or for designing a narrow band filter for applications such wavelength division multiplexing (WDM) and dense wavelength division multiplexing (DWDM).

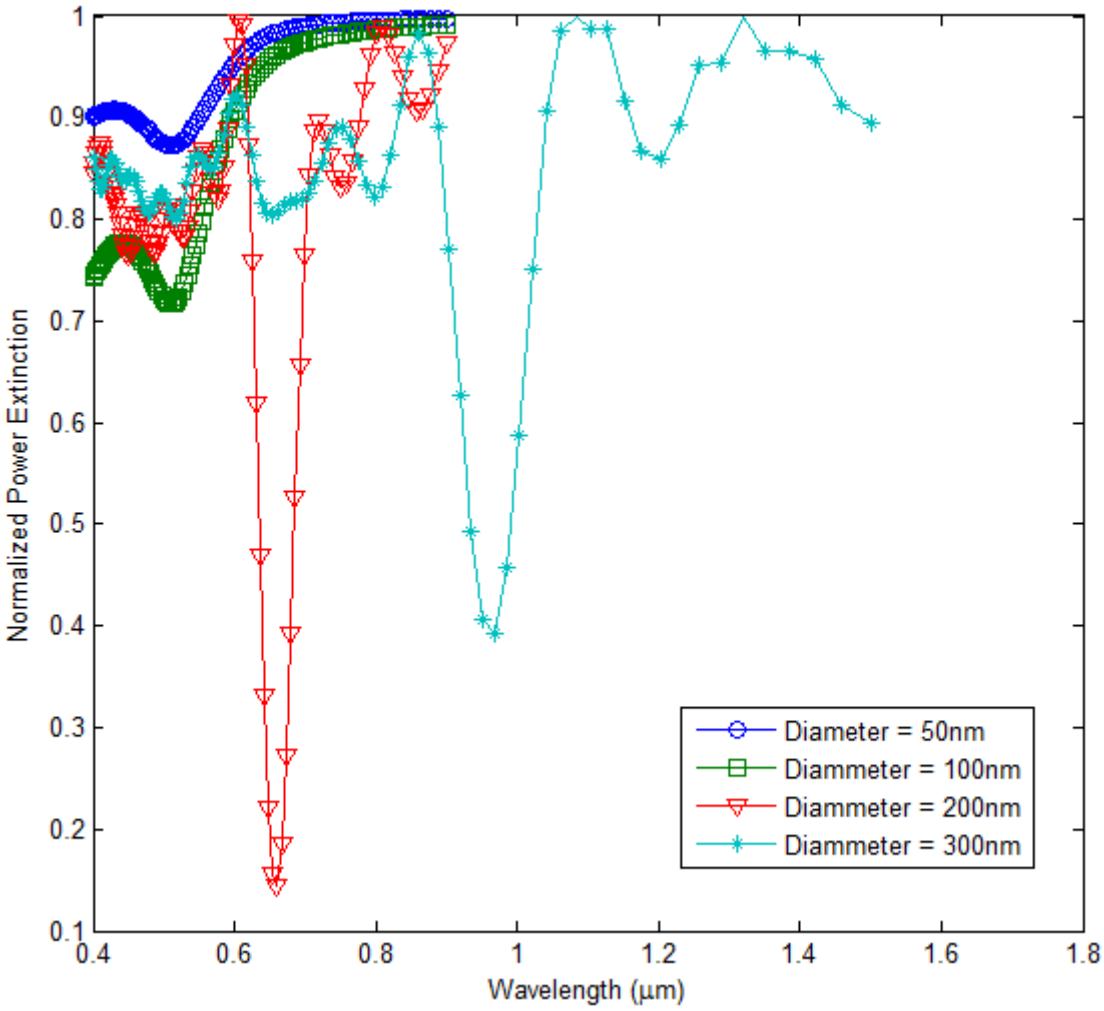

Figure 5. 6 Extinction spectra of different diameter gold nano particles

5.6. Analysis of Gold Nano Particle in Optical Domain

In this section, all the theoretical concepts of gold nano particles have been tested through simulations and the behavioural change of gold nano particle with change in particle size, shape, surrounding environment have been studied. All the simulations have been carried out FDTD tool of Optiwave. A gold nano sphere has been considered to carry out the whole simulations. Spherical nano particle do not require any specific condition matching to excite the surface plsmons as in the case of planar particle for generations of surface Plasmon polariton [Stefan A. Maier, "Plasmonics: Fundamentals and Applications", 2007]. Nano sphere can be excited from a direct light and are amongst the mostly used geometries of nano particles in sensing application. Their geometry also makes them easy to fabricate and hence comparatively less chances of errors unlike complex geometries resulting in less design cost.

Moreover, complex nano structures are very difficult to analyse and require complex mathematical modelling.

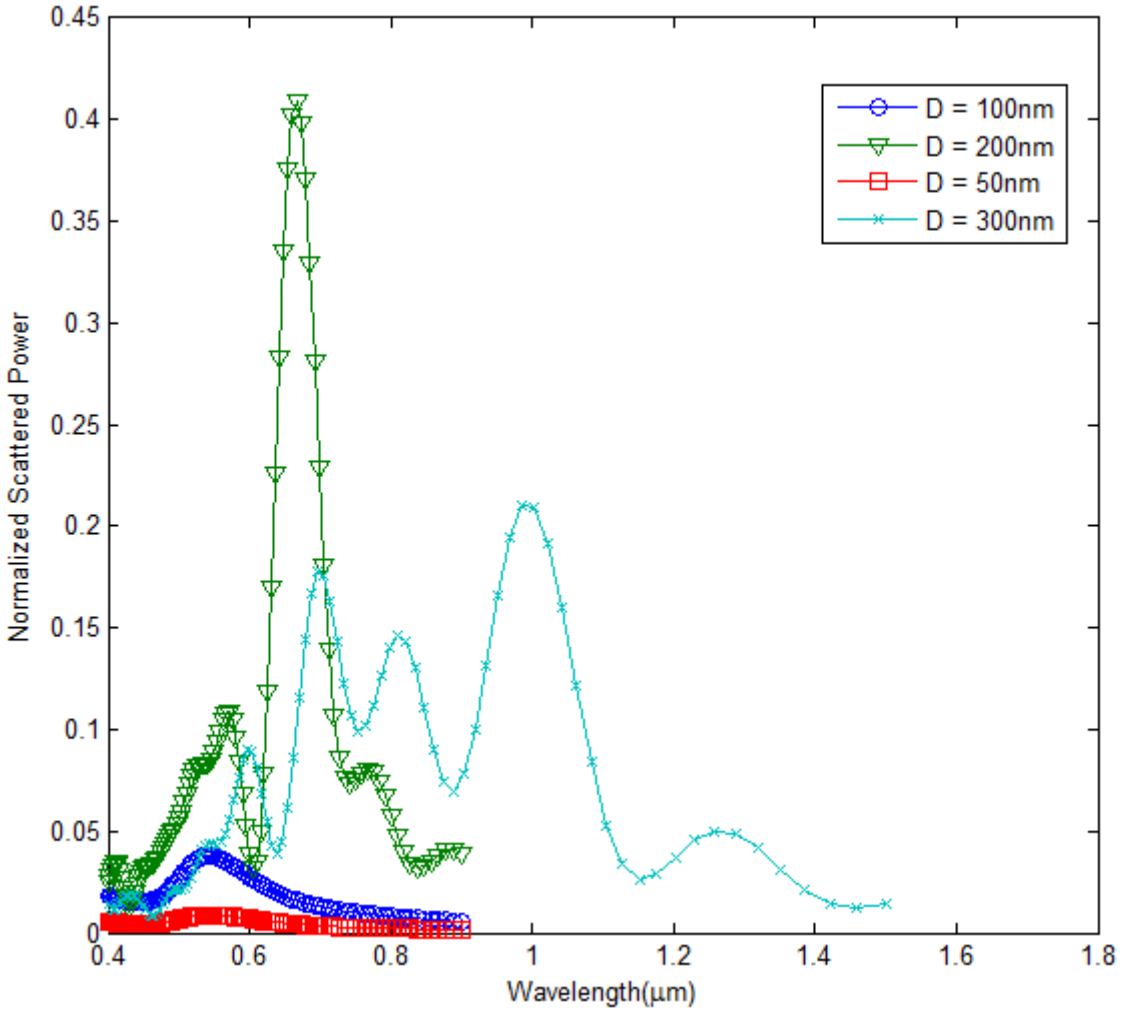

Figure5.7 Scattered power by the different diameter gold nano particles. Higher order modes can be observed with size increment.

Initially the particle behaviour with change in its size and as aspect ratio has been studied. Scattering and absorption spectrum of the nano particle has been plotted to see the frequency shift due change in physical parameters of the nano particle. Effect of change in environment outside the particle has also been observed with different dielectric materials. Amount of variation in the scattering wavelength from that of extinction wavelength for different aspect ratio of nano particle is studied in order to have an idea about the other losses associated with the power extinction by the nano particle. Moreover, this shift also indicates that the extinction and scattering resonance conditions occur at different wavelength. In order to utilize the property of change in surrounding refractive index on metal scattering and absorption a design of nano particle array with different refractive index for each particle has

been proposed. These nano particles have been embedded in the shells of different dielectric materials. The selection of the size of these dielectric shells have been made on the basis of analysis carried out to observe the minimum variation in particle behaviour from that observed without shell. The changes in extinction and absorption wavelength due to the change in the outside index of dielectric nano shell have also been studied. This variation result is very important in antenna and filter design using the nano particle arrays embedded in dielectric nano shells which are further placed in a dielectric medium. Finally nano particle arrays formed using the dielectric nano shells have been simulated for antenna and filter applications.

5.6.1. Effect of Size Variation

As the size of nano particle increases, the scattering and absorption cross-section increases with the Eq. 5.39 and 5.40 further increments in particle size causes a red shift in resonance wavelength. This red shift can be explained by the retardation effect [Stefan A. Maier, "Plasmonics: Fundamentals and Applications", 2007]. This effect becomes significant with particle size increased to a value comparable to the resonant wavelength. As the particle have charge densities at their opposite ends and with increment in the particle size, the phase delay in the reaction at one end of particle towards the changes at opposite end increases and to meet that phase delay the period of one mode oscillation increases [Stefan A. Maier, "Plasmonics: Fundamentals and Applications", 2007],[Viktor Myroshnychenko et al., 2008]. Higher order modes at the particle surface generates with further increment in the particle size. Figure 5.6 is showing the variation in the diameter of nano particle from 50 nm to 300 nm and it can be seen clearly that how the red shift in the resonance wavelength take place with size increment. Moreover, as the particle size increases the higher order mode start dominating the spectral response of nano particles. Particle behaves as dipole up to approximately a diameter size of 150 nm and after that multipoles are generated [Stefan A. Maier, "Plasmonics: Fundamentals and Applications", 2007]. From figure 5.6, we can see the higher order modes generated for 200 nm and 300 nm diameters along with significant red shift. Figure 5.7 is showing the corresponding radiated power spectrum by the nano particles with varying size. It should be noted that with size increment the radiated power wavelength further red shift from that of extinction wavelength.

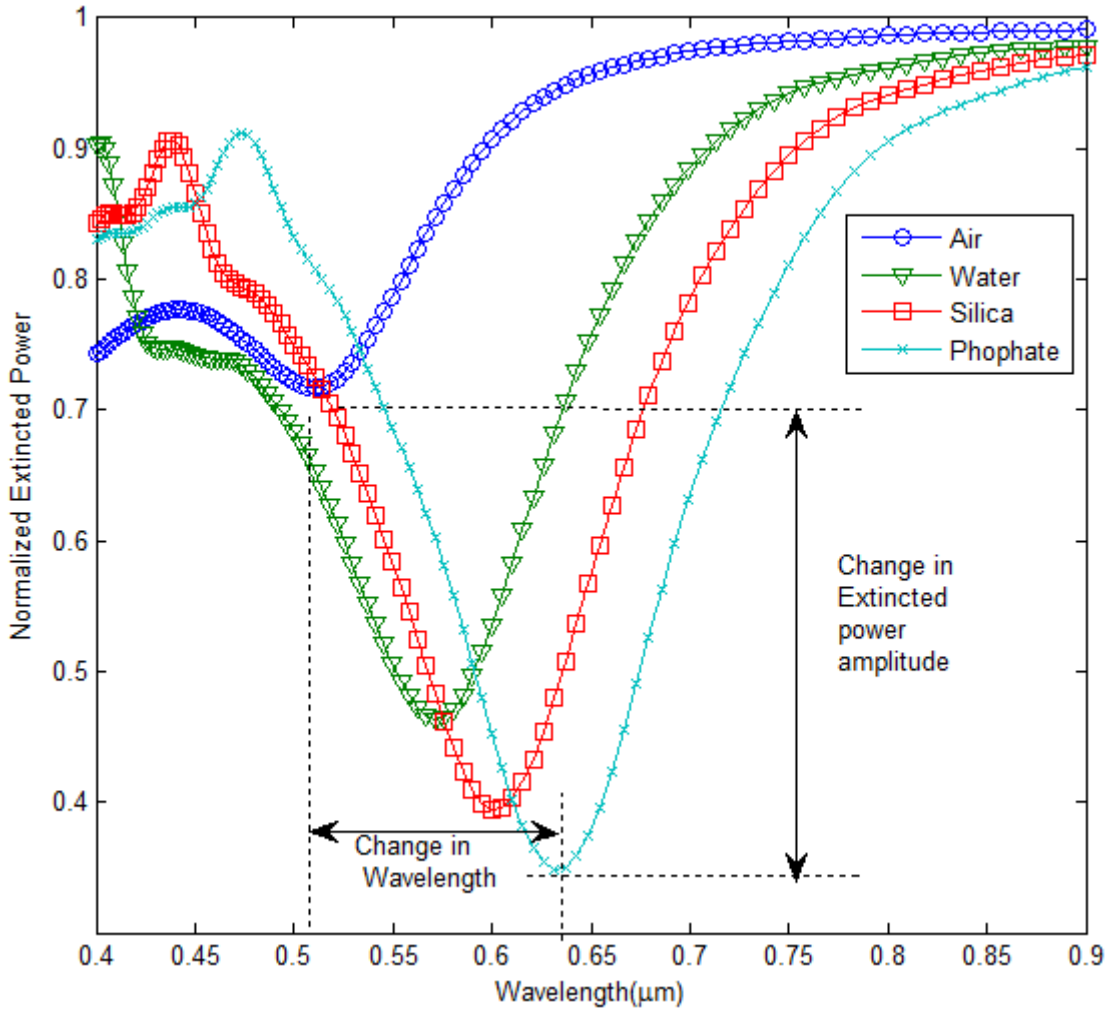

Figure5.8 Effect of change in surrounding index of metal nano particle on extinction resonance wavelength

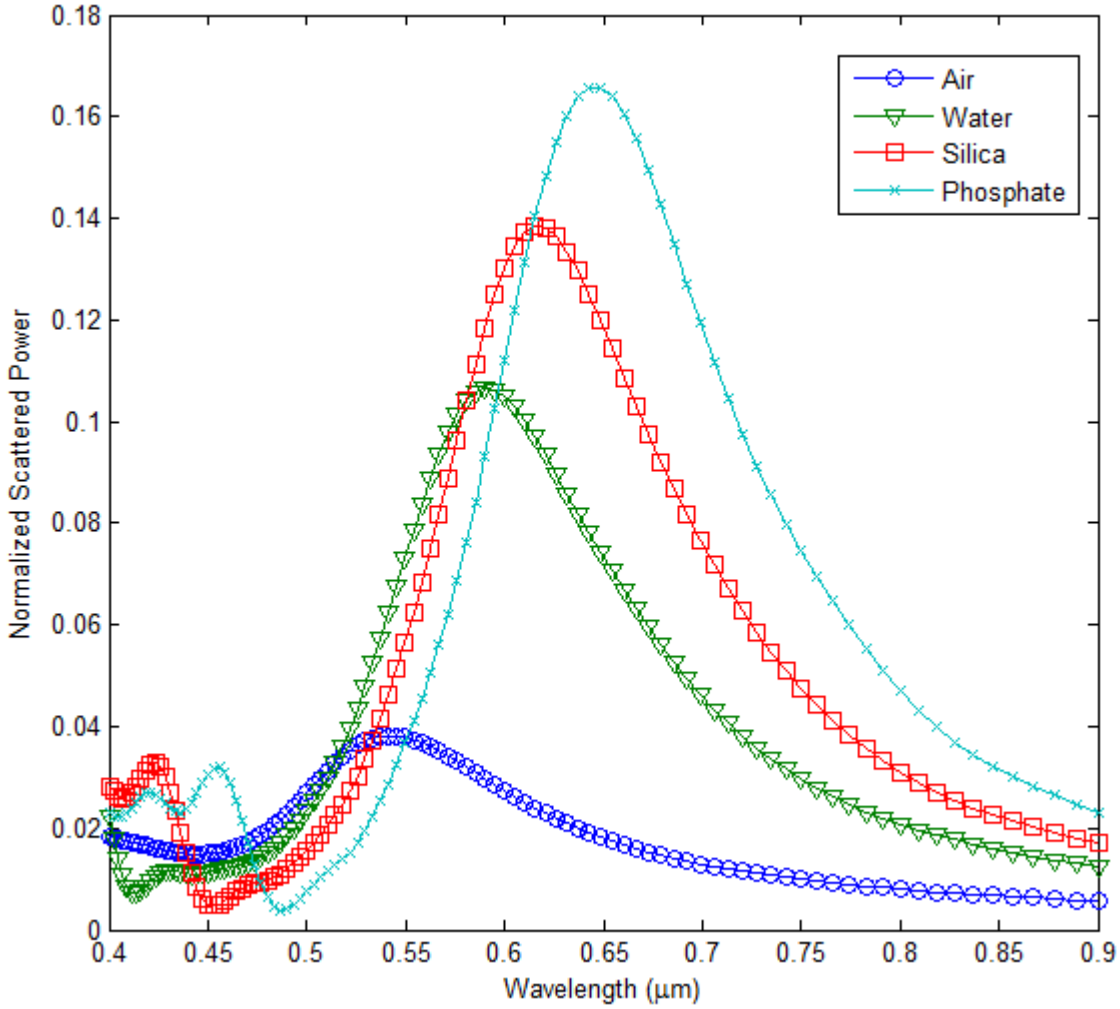

Figure 5. 9 Effect of change of refracyive index of the medium on the scattered power by the nano particle.

5.6.2. Effect of Surrounding Index Variation

Frohlich condition gives a relation between the dielectric function of the host material and the resonance frequency of surface plasmons generation. With increment of ε of the material the resonance wavelength moves towards higher wavelength side. This red shifting allows the dielectric function to become more negative in order to match the amplitude of the surrounding dielectric environment. Figure 5.8 is showing the effect of change in dielectric material, in which the 100 nm diameter gold nano particle is embedded, on extinction spectra of the particle. It should be noted here that the power extinction amplitude increases with increment in the surrounding index and this effect can be explained through the increased scattering at higher index surrounding. Figure 5.9 is showing the radiated power by the particle embedded in different index environment.

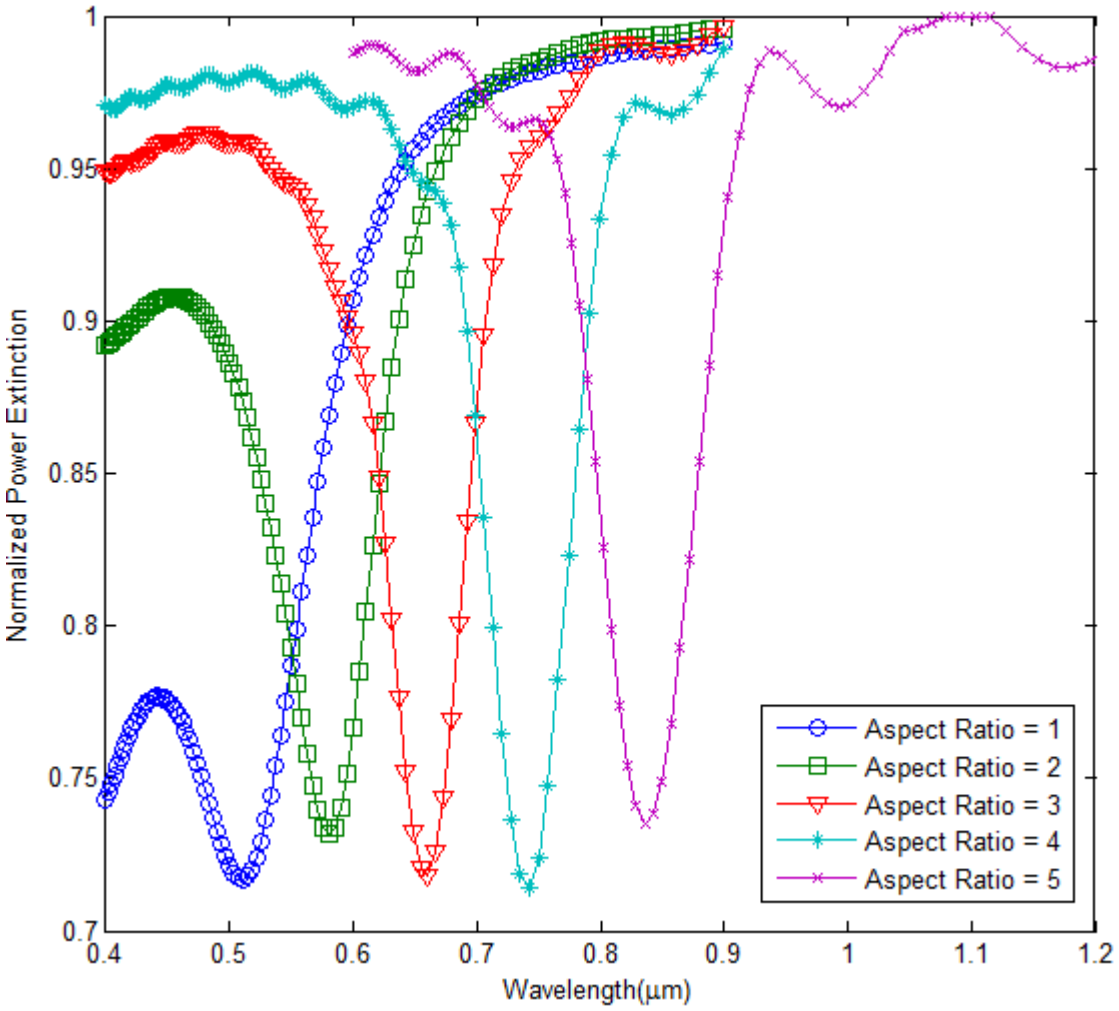

Figure 5. 10 Effect of variation in the aspect ratio on extinction spectra of the gold nano particle.

5.6.3. Change in Particle Shape

Ellipsoids are among the important geometries in optical applications. There are two types of geometries possible with change in aspect ratio one is prolate where two minor axis are equal and second is oblate where two major axis are equal. In the proposed analysis prolate sphere has been used. Change in aspect ratio causes the change in the expression of polarizability and along the principle axis it is given by [Stefan A. Maier, "Plasmonics: Fundamentals and Applications", 2007]

$$\alpha_i = 4\pi a_1 a_2 a_3 \frac{\varepsilon(\omega) - \varepsilon_m}{3\varepsilon_m + 3L_i(\varepsilon(\omega) - \varepsilon_m)} \tag{5.43}$$

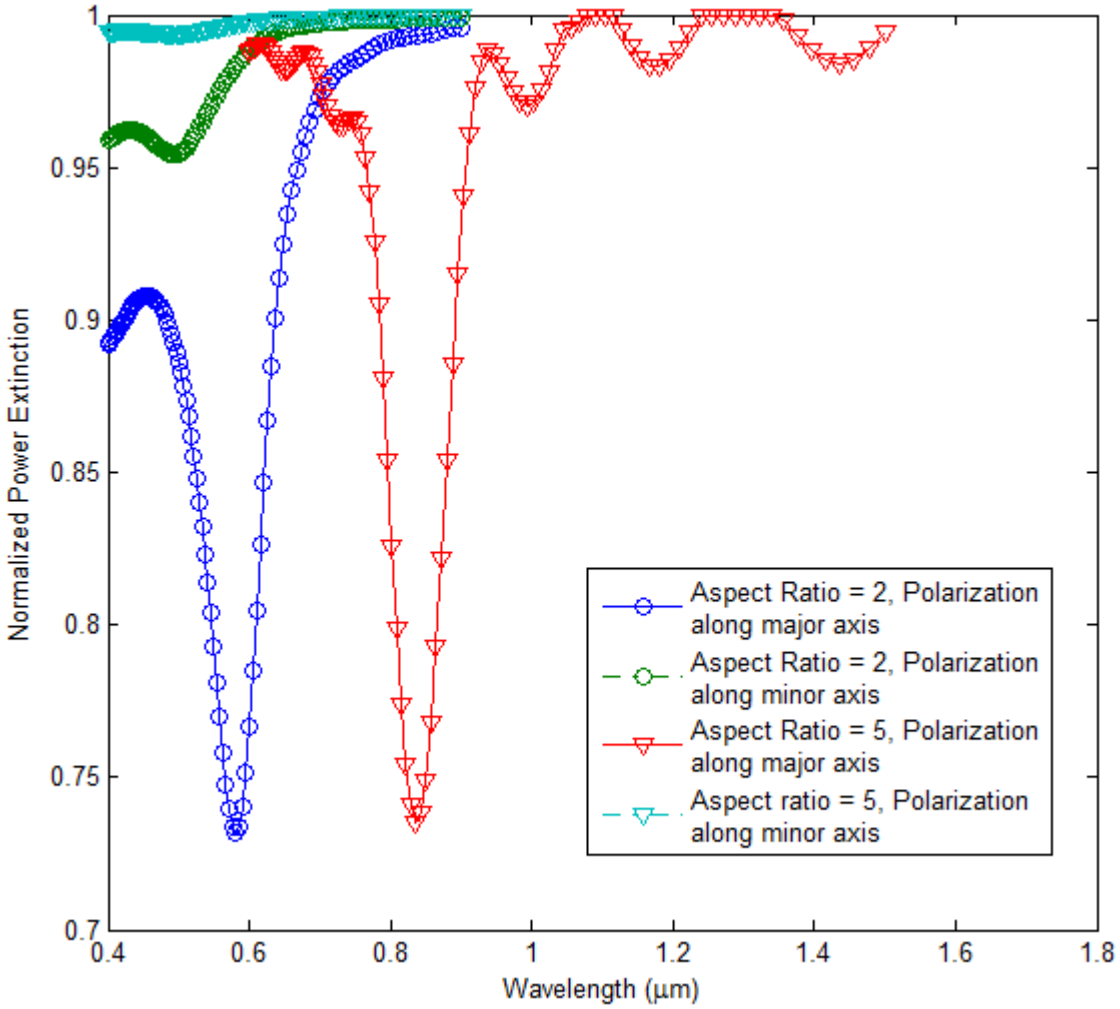

Figure 5. 11 Power extinction along the major and minor axis of a prolate nano particle of gold.

Where L_i is known as geometrical factor or depolarization factor, and $a_1,\ a_2,\ a_3$ are semi-axes of ellipsoid [Stefan A. Maier, "Plasmonics: Fundamentals and Applications", 2007].

Changing the dimension of the particle also changes the position of resonance wavelength. Increment in the aspect ratio (ratio of major axis length to minor axis length) causes the resonance wavelength to increase due to the shape dependent depolarization [Stefan A. Maier, "Plasmonics: Fundamentals and Applications", 2007],[Viktor Myroshnychenko et al., 2008]. When the particle aspect ratio changes the oscillation of electron density along its major and minor axis changes the resonance wavelength. Along the major axis, the resonance wavelength is red shifted due to increment in the phase shift is managed by increased oscillation period. Increased aspect ratio can be applied in application where resonance wavelength is required to be red shifted from that of a spherical nano particle of same volume. It should be noted here that without changing the external environment, it is possible to shift the extinction spectra of the particle and it can be a

potential solution for designing wide band optical filters. An evident red shift in extinction spectra of gold nano particle can be observed from figure 5.10. From figure 5.11, resonance along the major axis is red shifted due to the shape dependent depolarization effect given by Eq. 5.43

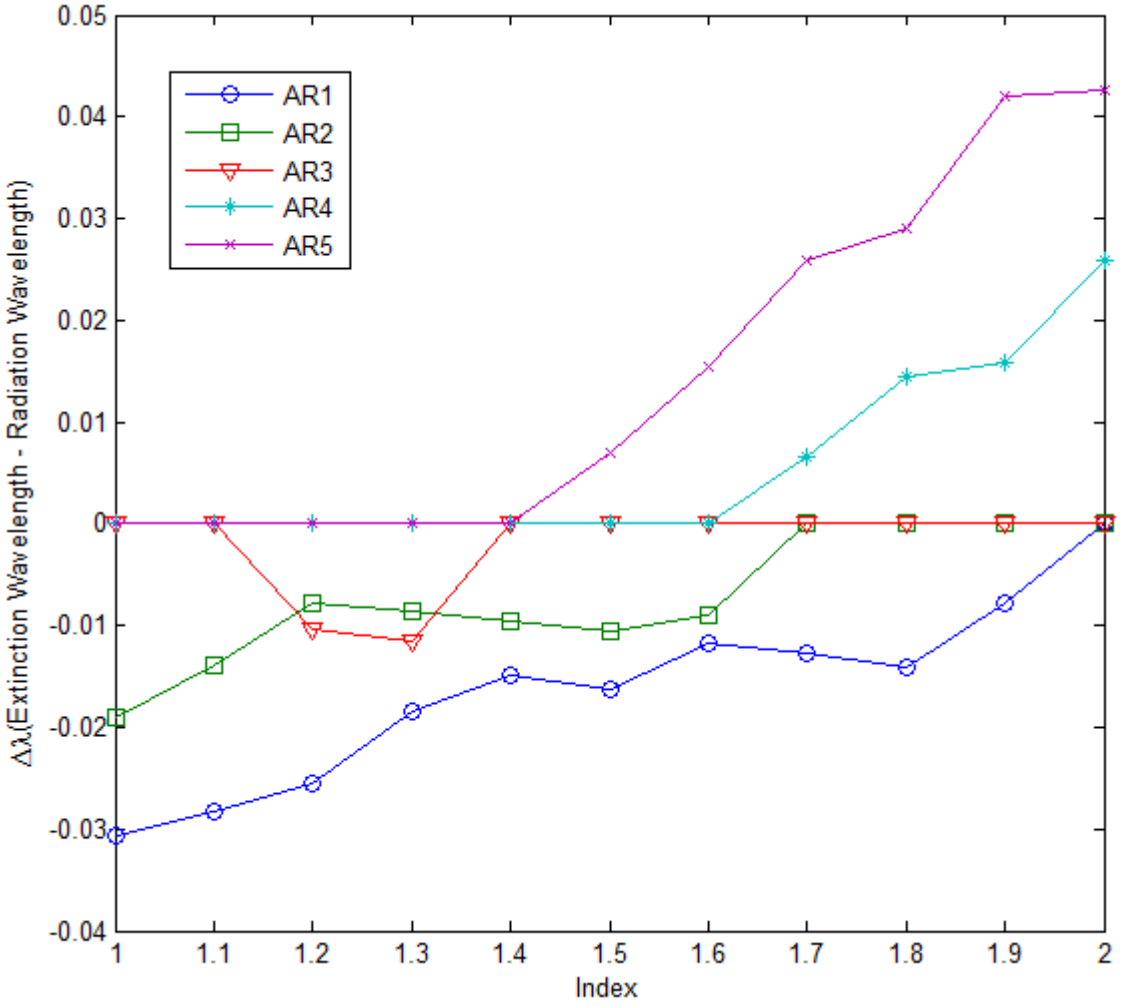

Figure 5. 12 Shift between extinction and radiation wavelength of a gold nano particle with change in refractive index for given aspect ratio. Aspect ratio = 3 shows the minimum variation among all the designs.

The scattering and extinction resonance wavelengths of a nano particle vary due to the fact that the extinction wavelength of nano particle is combination of all the losses that a nano particle encounters. In this thesis, a detailed analysis of nano particle in context of the variation in extinction wavelength and radiation wavelength has been done. Figure 5.12 is showing the difference in extinction wavelength and radiation wavelength variation with surrounding index of a nano particle for given aspect ratio. There is a dependency that has

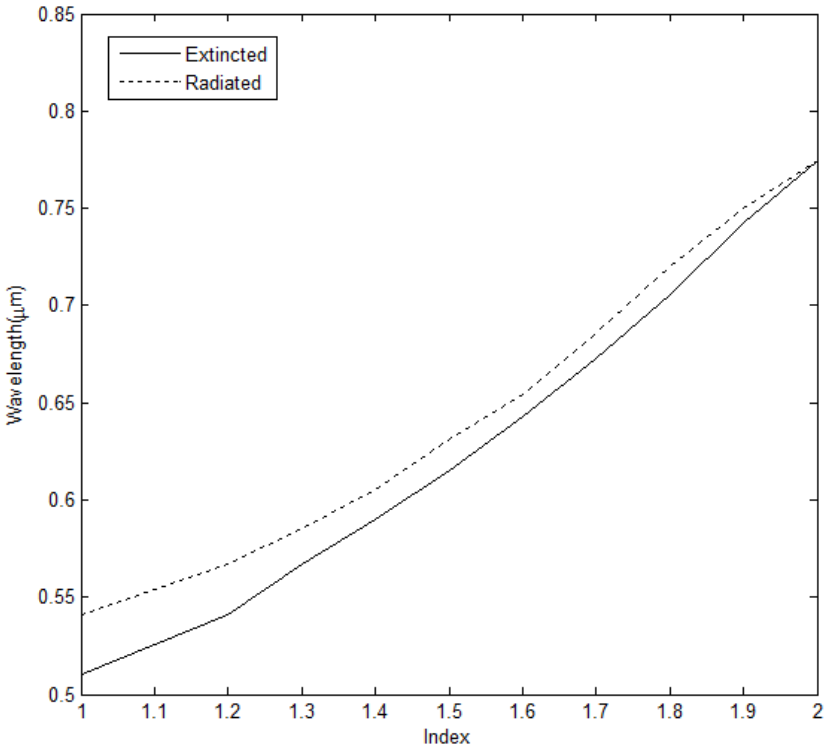

Figure 5. 13 (a)

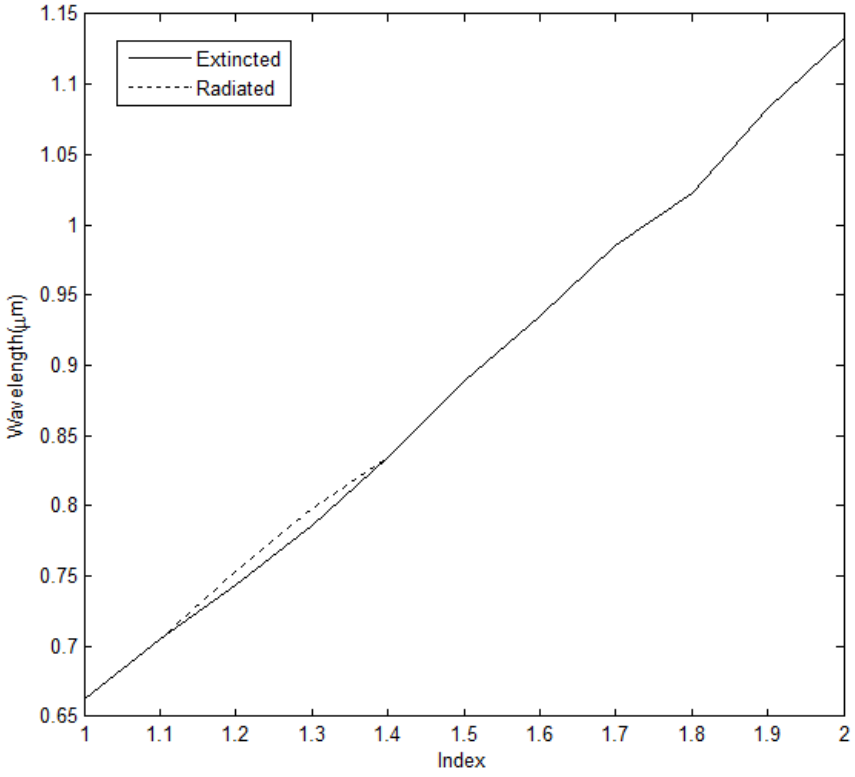

Figure 5. 14 (b)

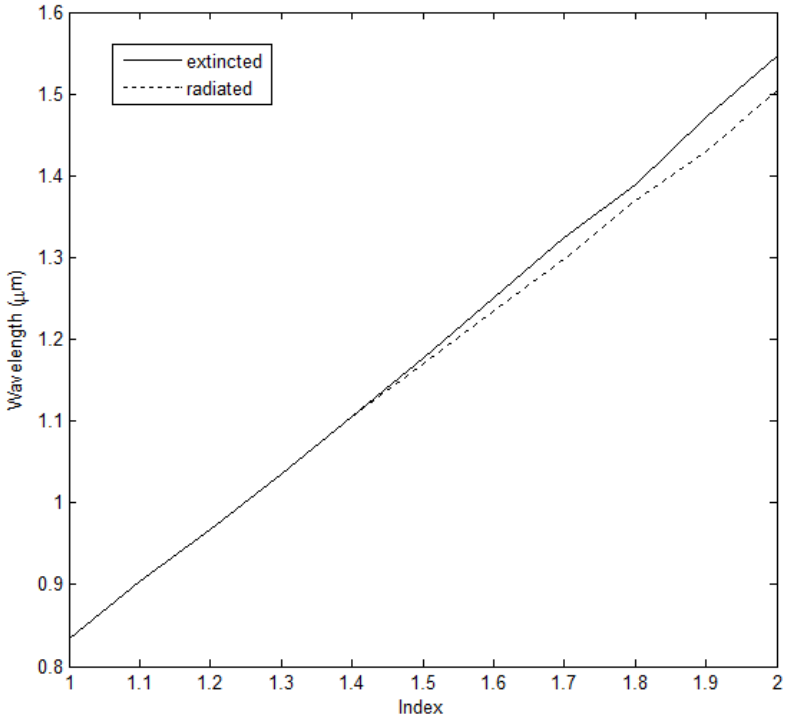

Figure 5. 15 (c)

Figure 5. 16 Shift between extinction and radiation wavelength is evident from the three figures corresponding to a aspect ratio of (a) one, (b) three, and (c) five.

been observed in the difference between wavelengths and aspect ratio with change in index of the host material embedding the nano particle. For spherical particle the difference is more significant at lower indices whereas, it shifts towards higher indices values with increment in aspect ratio. A boundary between this difference pattern shifts has been observed at aspect ratio 3 where the variation between the corresponding wavelengths is minimum and maximum time curve stick to a level of zero. Hence, a nano particle (within the diameter limit of retardation effect) with aspect ratio 3 shows a coherency in all the losses due to which power get extincted. Moreover, it should be noted that for lower refractive indices the radiation wavelength is red-shifted in comparison to extinction wavelength whereas, as refractive index increases this condition reverses and extinction wavelength is more red-shifted than radiation wavelength of the particle (in figure 5.13. the dotted line is showing the radiation wavelength and continuous line is extinction wavelength).

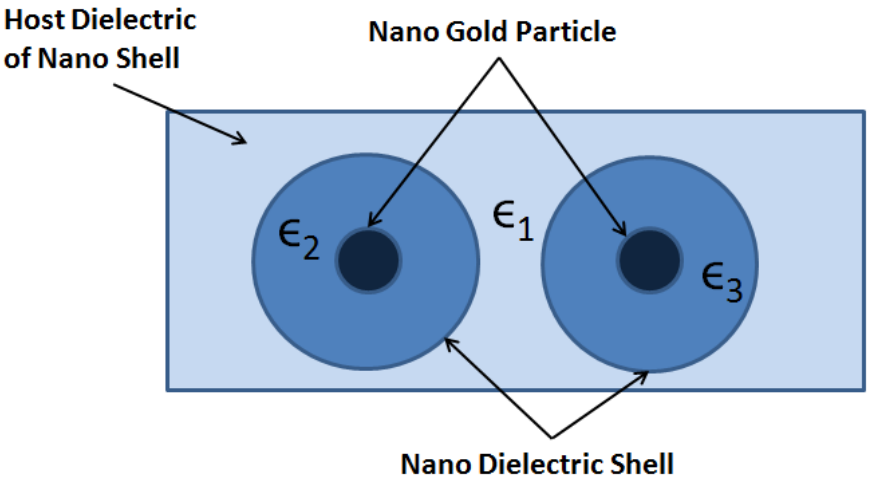

Figure 5. 17 (a)

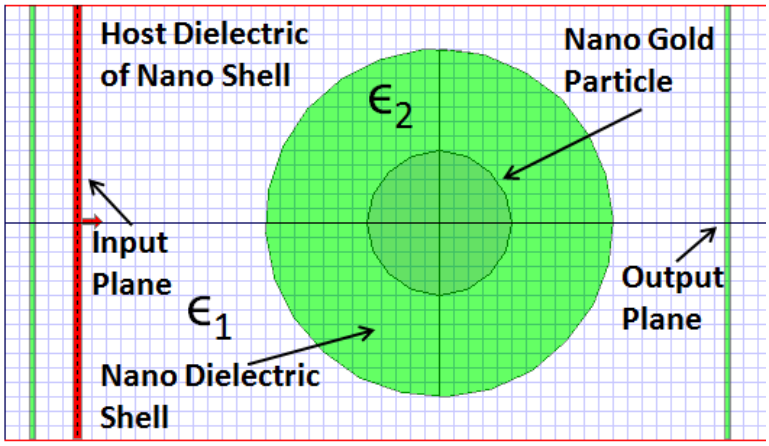

Figure 5. 18 (b)

Figure 5. 19 Arrangement of metal nano particle array embedded in dielectric shells of different dielectric constant ε_2 and ε_3 with surrounding dielectric constant ε_1 (a); Side view of an array of dielectric shell containing the gold nano particle (b)

5.6.4. Particle Embedded in Spherical Dielectric Shell

In order to utilize the unique properties of particles for antenna and filter design, a design for particle array placement has been proposed. This design utilizes the dielectric shell of larger diameters to embed the gold nano particle in it. Figures 5.14 (a) and (b) are showing the schematic of the proposed particle array arrangement with dielectric shell. Where ε_1 and ε_2 are the dielectric constant of the shell environment and of dielectric shell. Since the interaction between the particle scales with d^{-3}, in case of particle array design, shells are placed three times the shell radius apart from each other which is sufficient to recover the behaviour of isolated particle [Stefan A. Maier, "Plasmonics: Fundamentals and Applications", 2007]. More on nano particle array element spacing in detail has been

discussed in [Stefan A. Maier, "Plasmonics: Fundamentals and Applications", 2007]. There is no direct coupling between the nano particles and hence they individually extinct the incident power. Power losses due to dielectric shell have also been investigated in order to observe the existence of any interference with the surface Plasmon resonance wavelength.

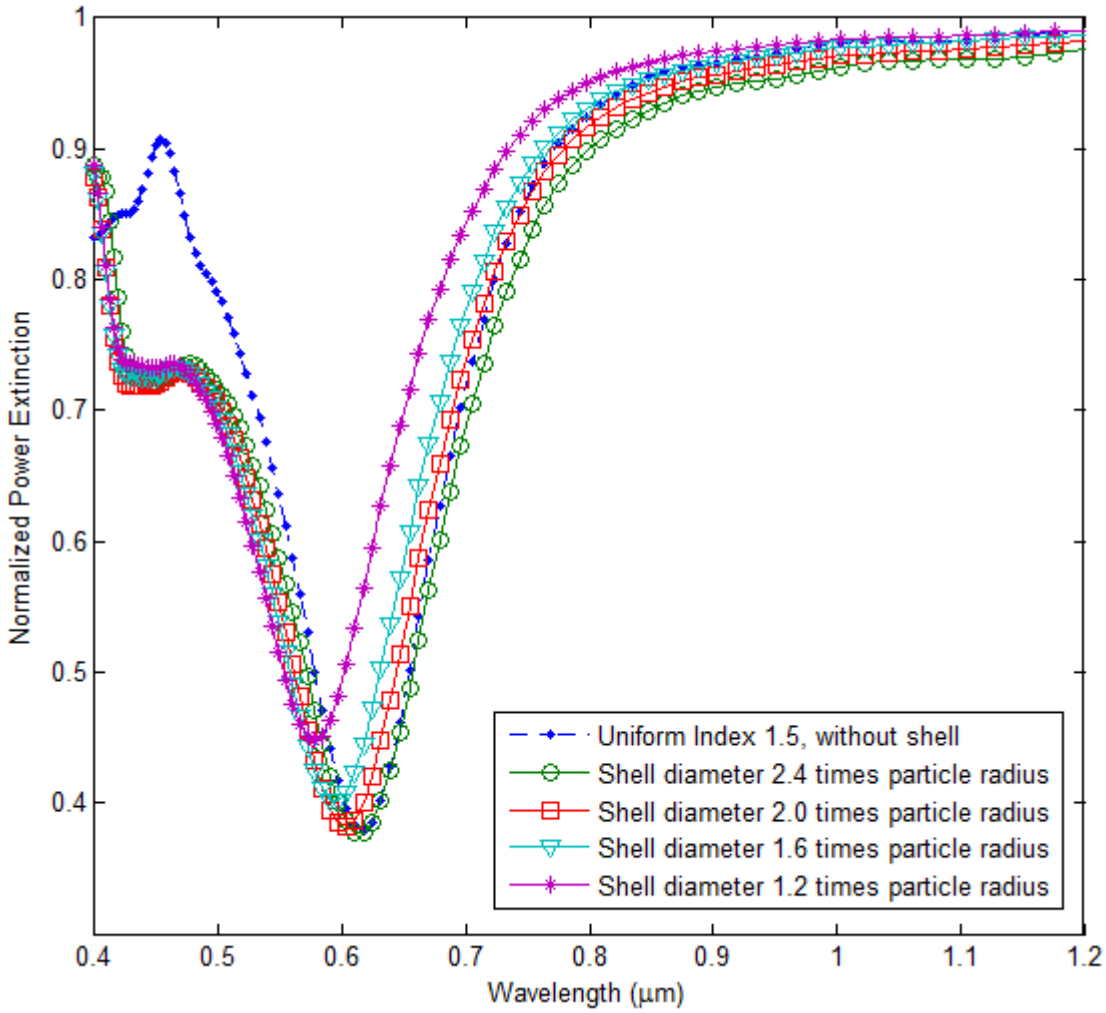

Figure 5. 20 (a)

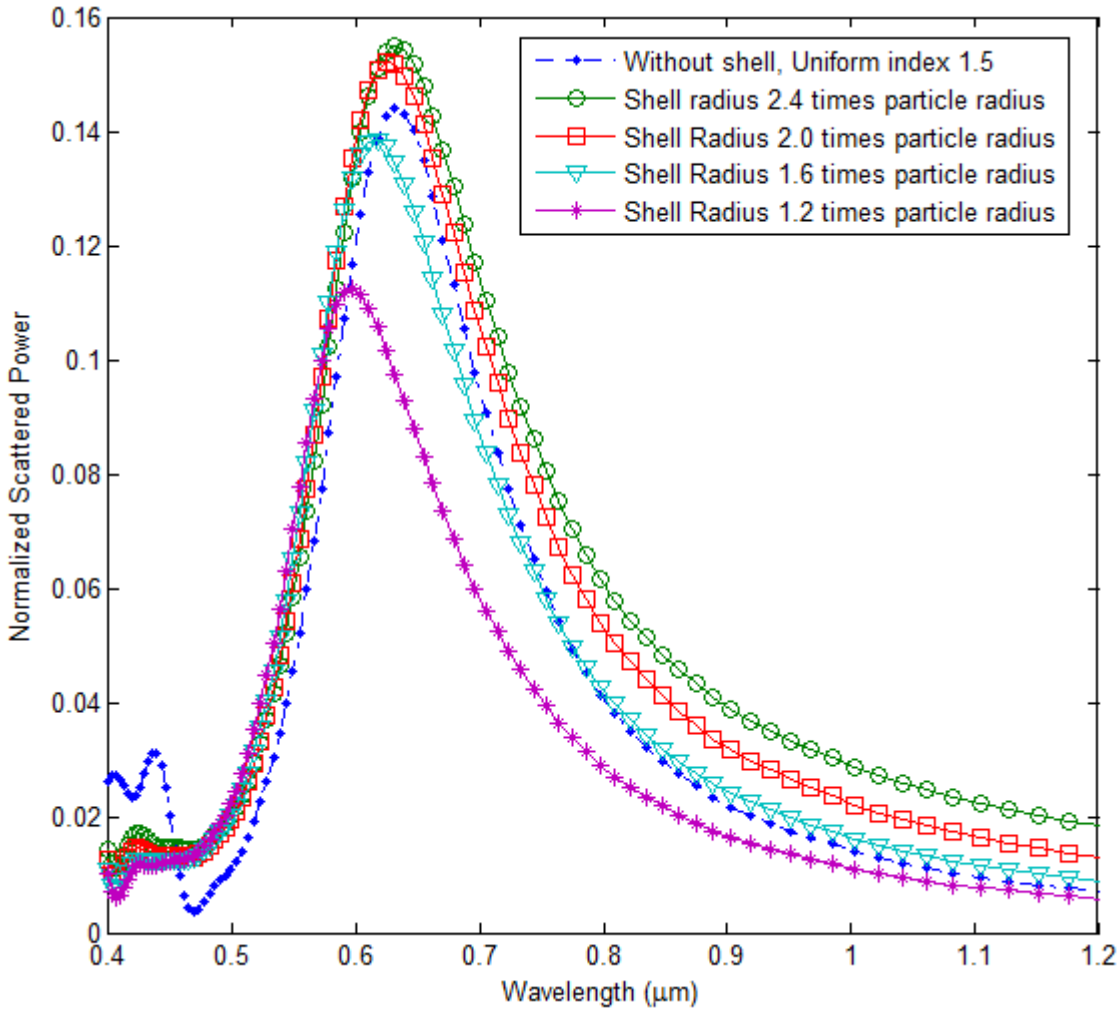

Figure 5. 21 (b)

Figure 5. 22 The extincted and scatted power by the nano particle placed in a dielectric shell with variation in the shell radius. (a) Power extinction; (b) power absorption

Figures 5.15 (a) and (b) are showing the selection of the size of dielectric shell carried out in order to have the characteristic behaviour of nano particle unchanged with the introduction of dielectric shell. Here the refractive index of shell is 1.5 and a gold nano particle of radius 50 nm is placed in the shell. With small size of shell the power scattering wavelength encounter a blue shift with respect to the design with no shell present (particle embed in same dielectric). Wavelength corresponding to the design with no shell present will be referred as original scattering or original extinction wavelength in the subsequent content of thesis. With increment in shell size, the resonance shift towards the higher wavelength and it is at minimum difference when shell radius is 2.4 times the particle radius for the maximum index contrast. Index contrast is defined as the ratio of the refractive index of shell to the refractive

index of the shell environment. Power extinction with shell size variation is shown in figure 5.15 (a) and this result is also in agreement with the radiation result as the minimum separation with original extinction wavelength curve. Blue-shift with shell size decrement is observed, similar to the scattered response. Amplitude of the scattered power increases with increment in the shell size as the scattered component of dielectric shell at the wavelengths near to the particle scattering wavelength gets added up and increase the amplitude of scattered power.

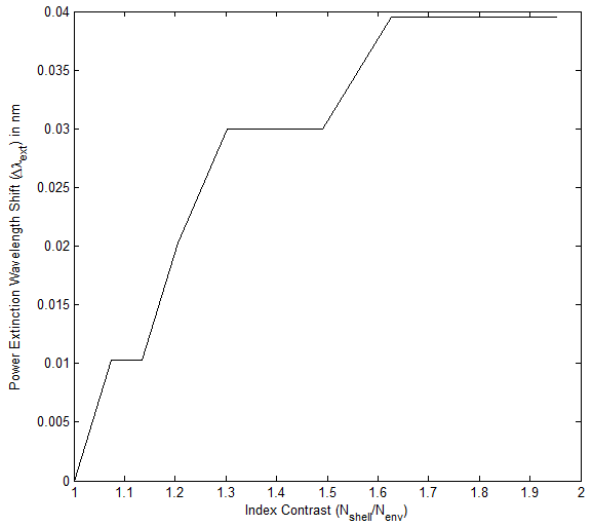

Figure 5. 23 (a)

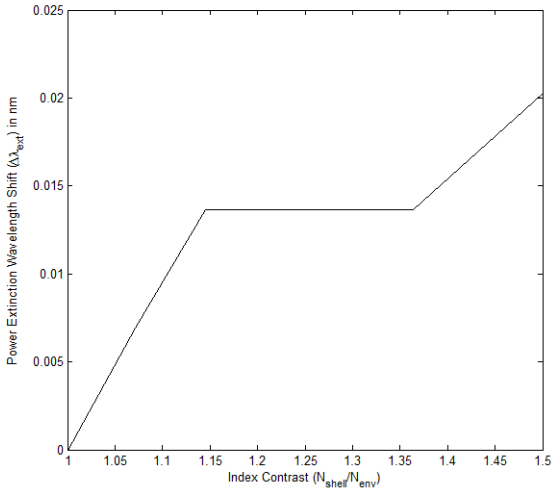

Figure 5. 24 (d)

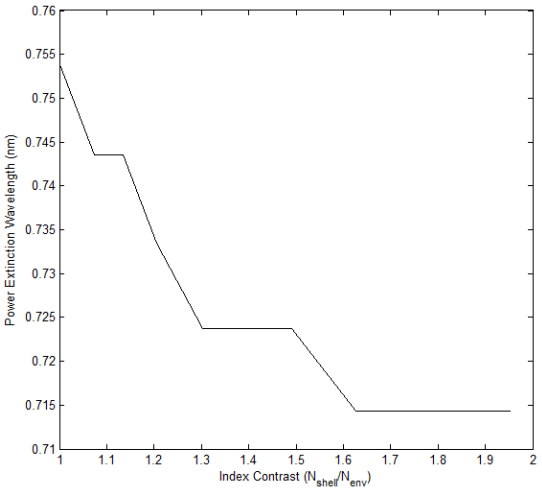

Figure 5. 25 (b)

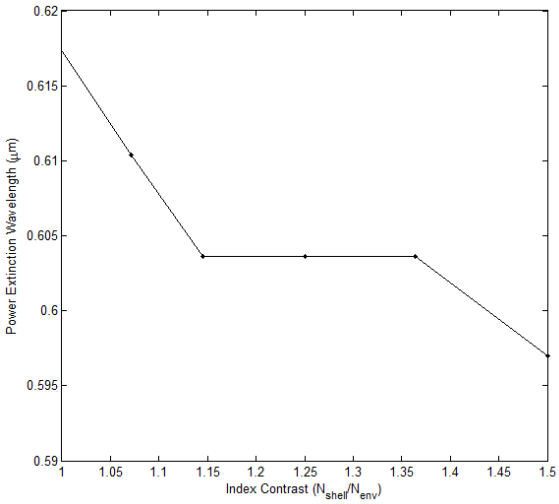

Figure 5. 26 (e)

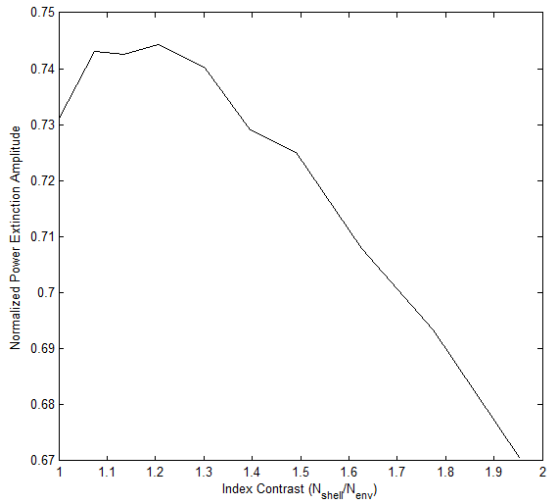

Figure 5. 27 (c)

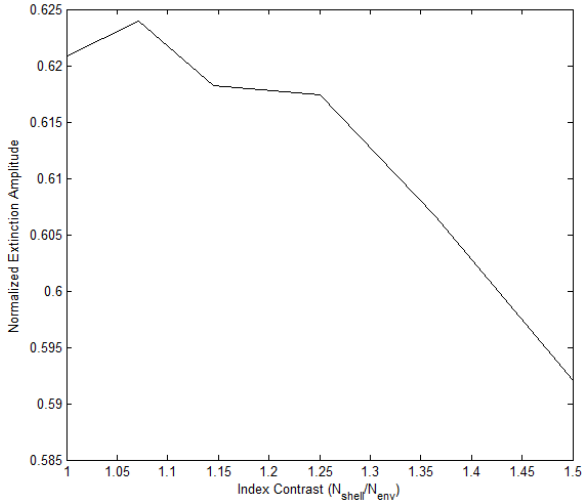

Figure 5. 28 (f)

Figure 5. 29 Amount of shift in power extinction wavelength (difference from the original wavelength) (a); shift in extinction wavelength (b); change in extincted power (c) with index contrast change for shell index =2. Same in order for shell index 1.5 are depicted by (d), (e), and (f).

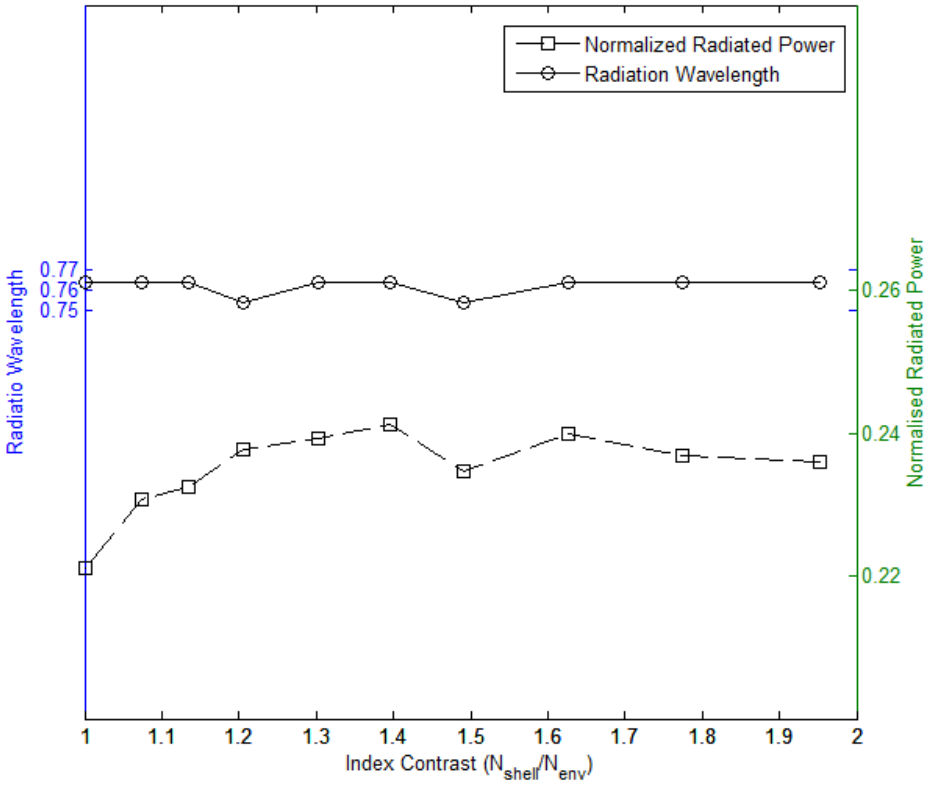

Figure 5. 30 (a)

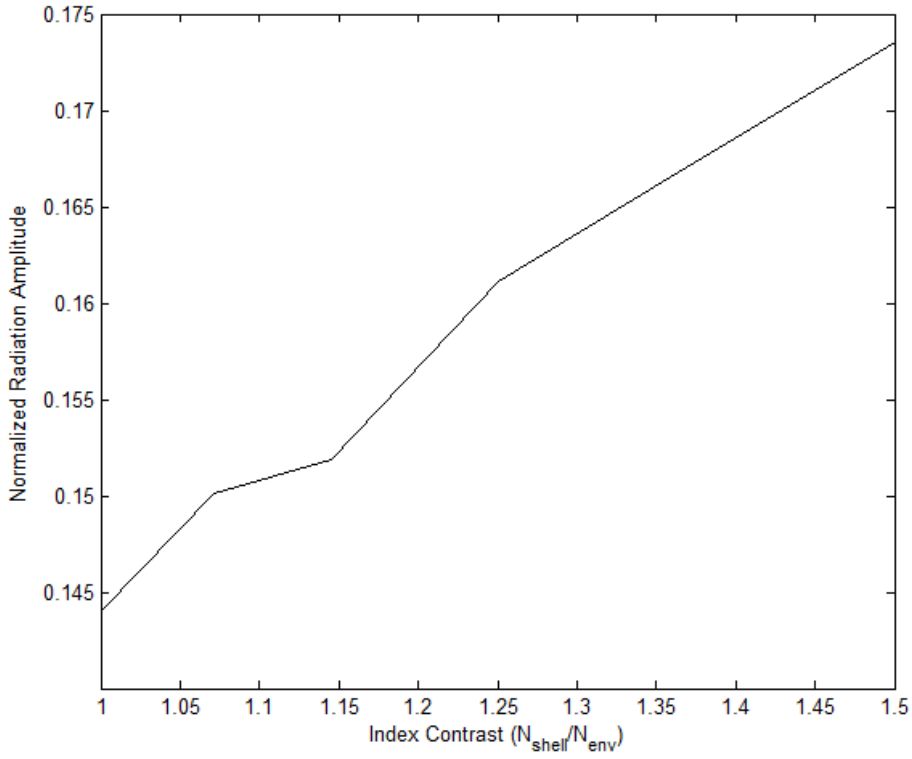

Figure 5. 31 (b)

Figure 5. 32Shell index contrast variation effect on: (a) Variation in radiation amplitude and wavelength with index contrast for shell index =2 ; (b)) Variation in radiation amplitude with index contrast for shell index =1.5

Index contrast variation for the selected shell size (discussed above) causes the original wavelength of extinction to shift due to the presence of dielectric shell. From figure 5.16 (a), for a dielectric shell of index 2, and radius 2.4 times the particle radius, a maximum shift of 40 nm has been observed with maximum index contrast. As the index contrast increases, it leads to more shifted resonance peak from the original resonance wavelength. This phenomenon can be utilized to realize the narrow band optical filters by placing the nano particles in dielectric shells with different dielectric contrast together forming a dielectric shell array. Figure 5.16 is depicting the shift in wavelength range corresponding to the original wavelength. The variation in wavelength and extinction amplitude (see figure 5.16 (b), (c)) is due to the variation of shell index contrast and hence these variations are dependent on the higher order wavelength components which get added up with the nano particle wavelength response. As the index of outer medium decreases, causing the index contrast to increase, the extinction amplitude shifts towards lower wavelengths as was observed for nano particle case (see figure 5.8). Same happens to the amplitude curve and it follows the conventional wavelength shift depicted in figure (5.16 (c), (f)) for nano particle extinction amplitude.

Figure 5.17 (a) is showing the radiation wavelength and amplitude shift corresponding to the change in dielectric shell environment. Here power scattered by the nano particle has a very negligible amplitude variation and the scattered wavelength also remains approximately constant. With this observation it can be concluded that the dielectric shell does not interfere with scattering of the particle and it has all its impact on extincted power due to other losses (such as absorption and heat) contributed by the shell. Observations for nano shell of refractive index 1.5 have also been investigated in order to establish the phenomena more firmly (see figure 5.17 (b)). Here the shift in extinction wavelength remains approximately 20 nm for maximum index contrast variation. Since the index contrast variation range decreases with reduction in shell index, it affects the overall variation range of extinction wavelength and amplitude and remains consistent with the phenomena observed in case of shell index 2.

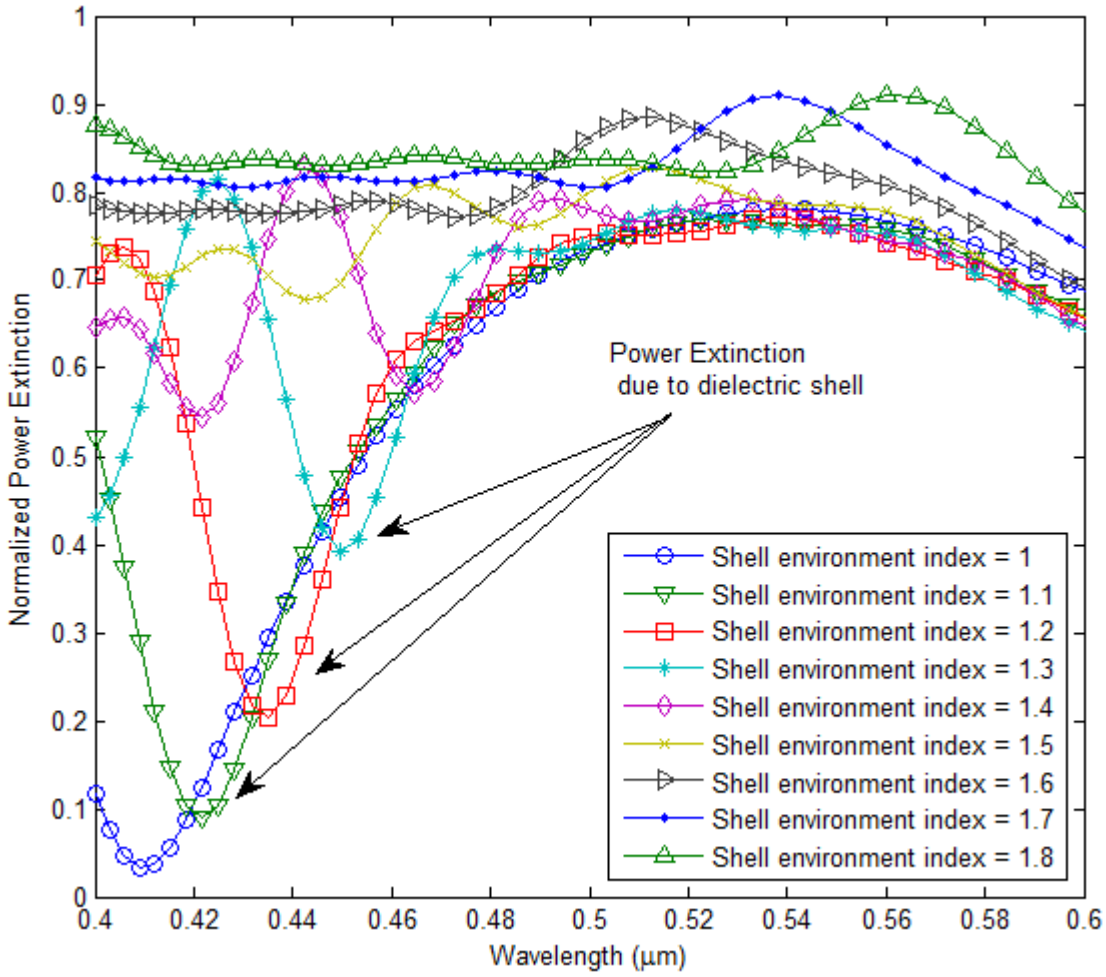
Normalized Power Extinction
Wavelength (μm)
Power Extinction
due to dielectric shell
Shell environment index = 1
Shell environment index = 1.1
Shell environment index = 1.2
Shell environment index = 1.3
Shell environment index = 1.4
Shell environment index = 1.5
Shell environment index = 1.6
Shell environment index = 1.7
Shell environment index = 1.8

Figure 5. 33 (a)

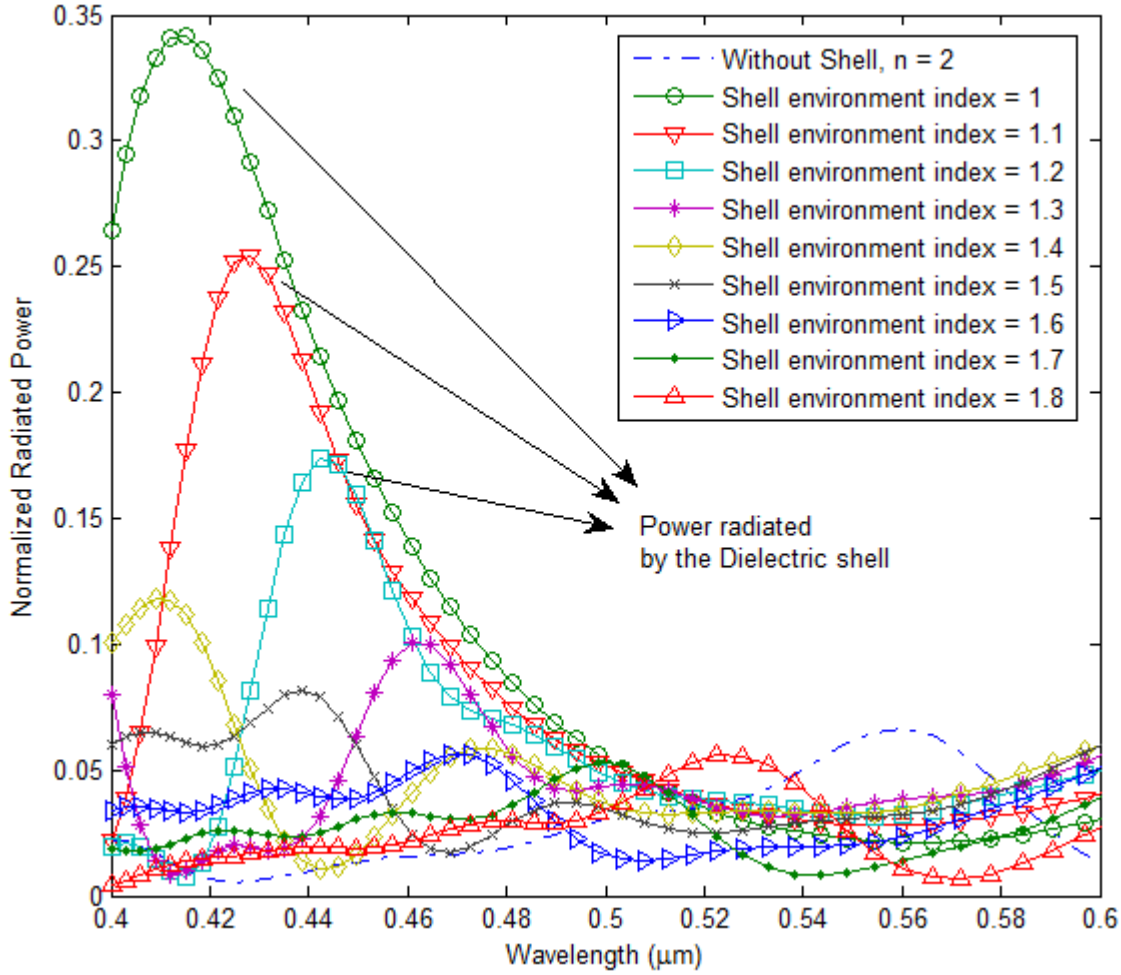

Figure 5. 34 (b)

Figure 5. 35 Losses due to scattering and absorption by the dielectric shell. (a) Power extinction by the dielectric shell for different shell indices; (b) Power scattered by the dielectric shell with different shell indices. The losses are encountered at shorter wavelengths.

5.6.5. Power Losses Associated With Dielectric Shell

In the extinction curve losses are seen due to the dielectric shells containing the nano particles (see figure 5.20-5.22). These loses are due to the reflections, refraction and absorption by the material and theses loses occurs at the starting edge of the visible spectrum, limiting the bandwidth of the filter design. These loses can be computed with respect to the index contrast change and shell size changes to observe the variation in the available bandwidth for filter and antenna application. Figure 5.18 is showing the power loss due to dielectric shell occurring at the lower side of the spectrum. These power losses increase with increment in the index contrast as expected. These losses get suppressed as the index of medium surrounding the shell increases. With increment in index contrast the wavelength peak at which the loss occur shifts towards shorter wavelength. Similar effect can be seen for

power scattered by the nano dielectric shell. The bandwidths over which these losses occur do not interfere with the surface Plasmon resonance wavelength of gold nano particle. Figure 5.19 is showing the wavelength over which these losses occur and it can be seen that losses are minimum with minimum index contrast whereas, maximum value of loss occur at maximum index contrast. The wavelengths corresponding to the minimum and maximum loss are 0.52 μm and 0.41 μm respectively. Coordinates in the figure 5.19 are showing the wavelengths (x axis) and power extinction amplitude (y axis) corresponding to the losses.

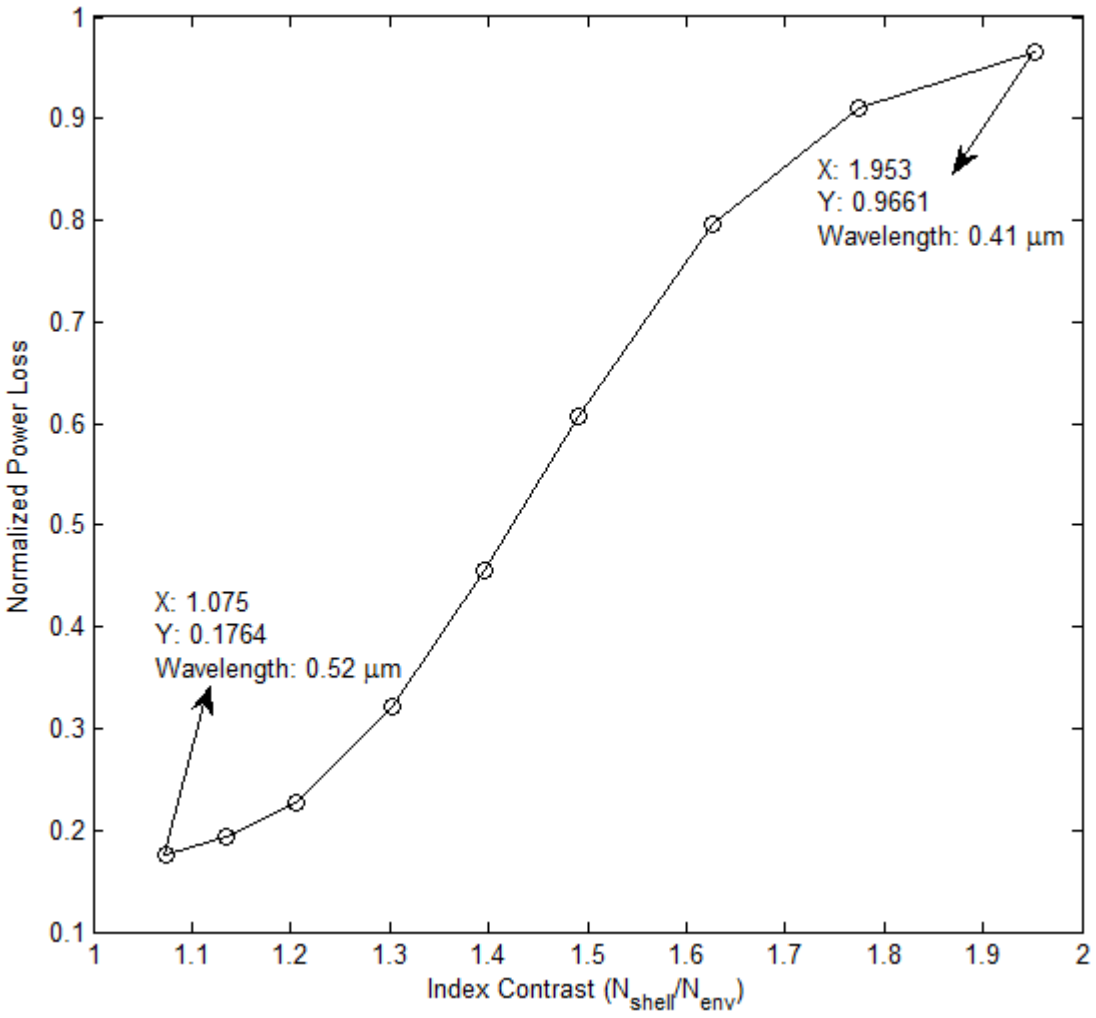

Figure 5. 36 Power loss spectrum of the dielectric nano shell with shell index contrast variation. Highest loss occur at 0.41 μm, starting of the visible spectrum and quickly end at 0.52 μm. Losses for maximum index contrast variation occurs over a bandwidth of 0.1 μm.

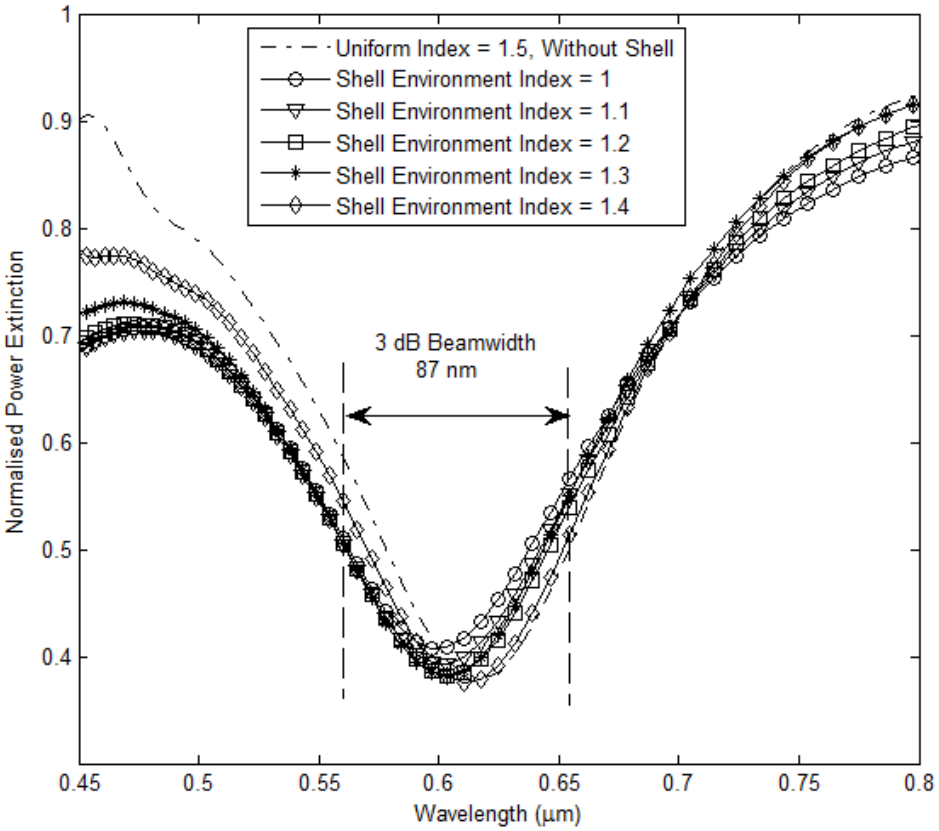

Figure 5. 37 (a)

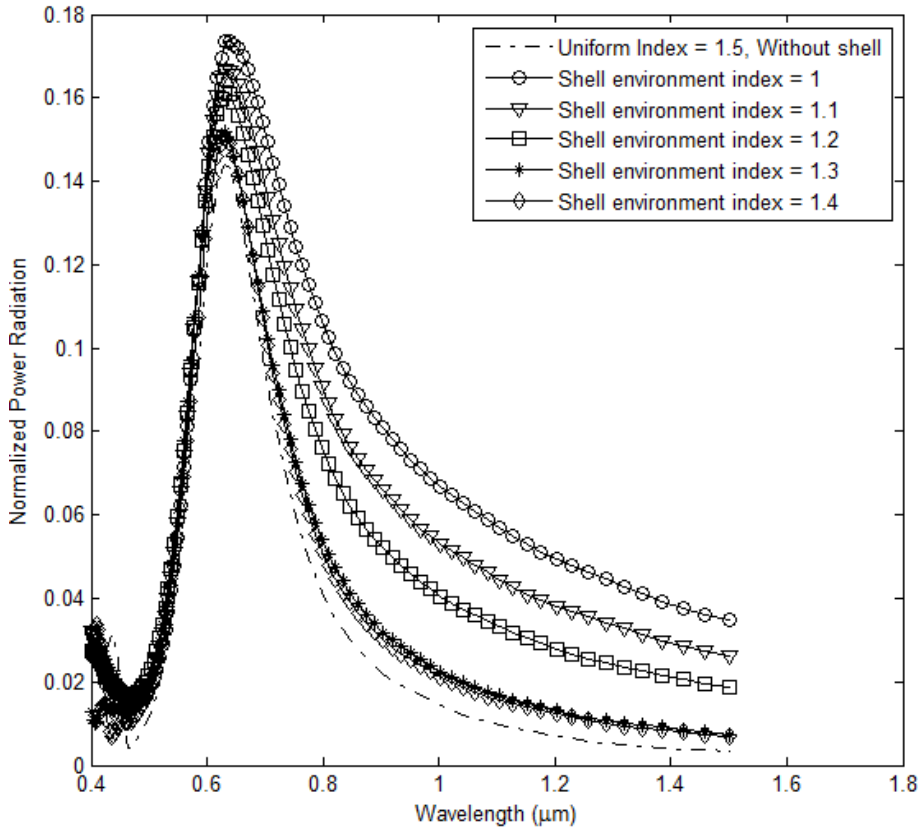

Figure 5. 38 (b)

Figure 5. 39 Power Extinction (a) and radiation (b) curve for change in index contrast of a dielectric shell of index 1.5.

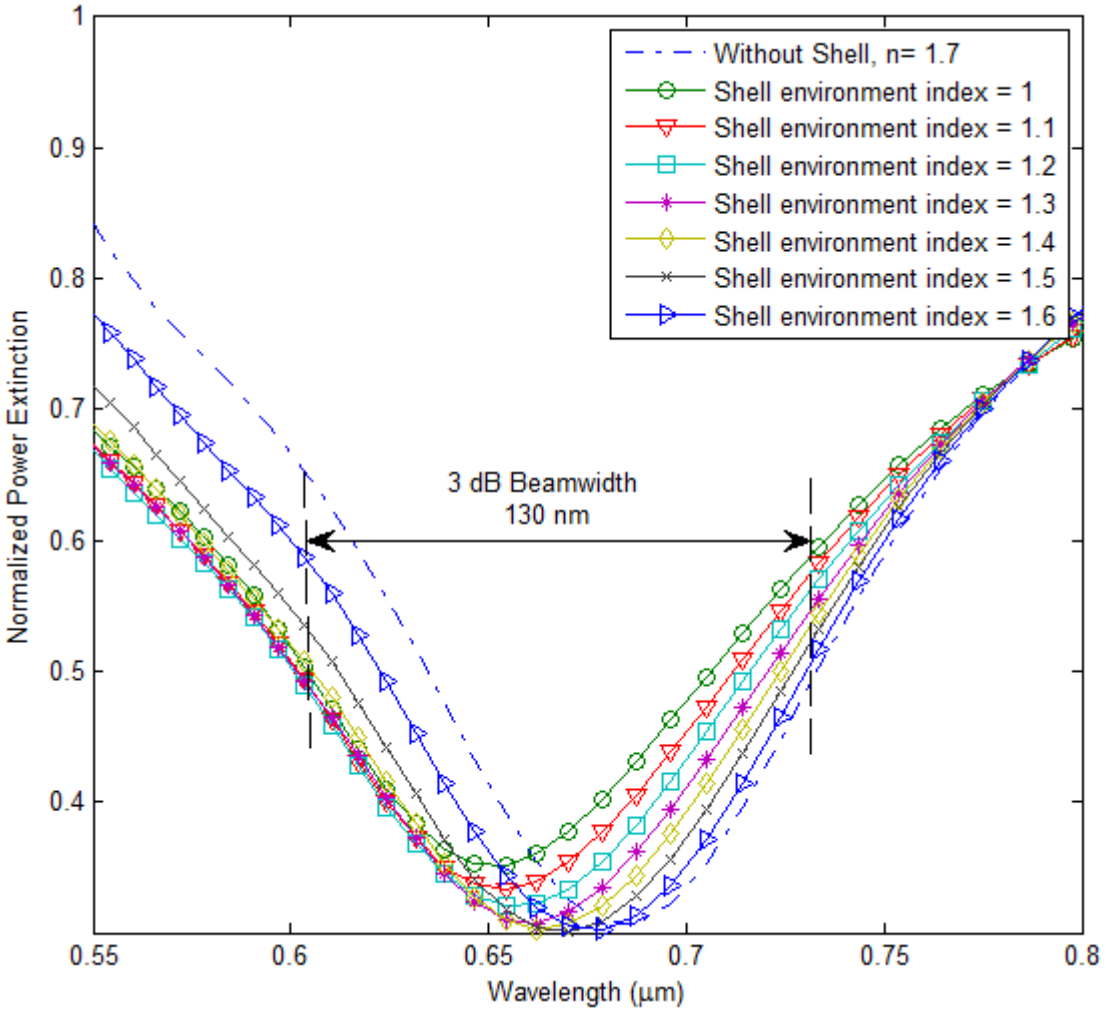

Figure 5. 40 Power extinction by metal nano particle in a dielectric shell of index 1.7.

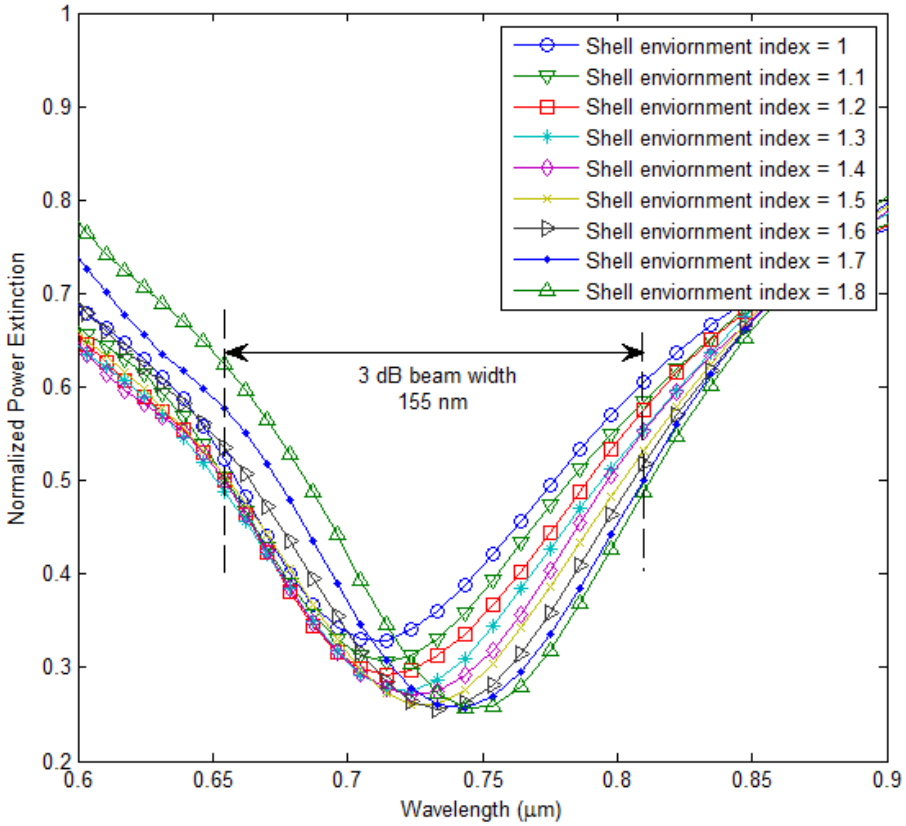

Figure 5. 41 (a)

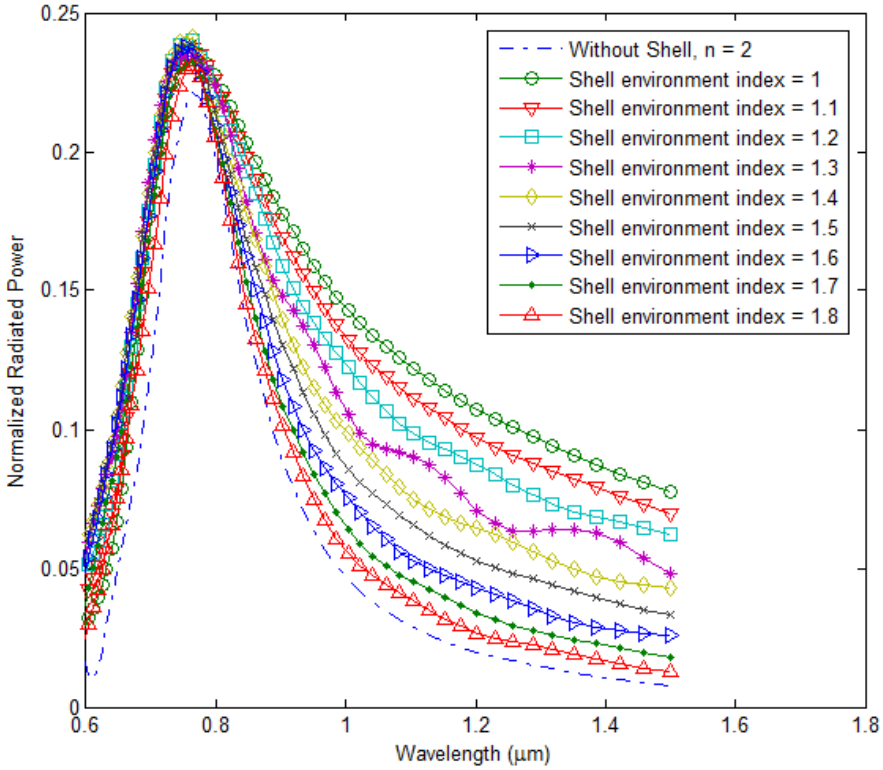

Figure 5. 42 (b)

Figure 5. 43 Power extinction (a) and radiation (b) of by the metal nano particle in a shell of index =2.

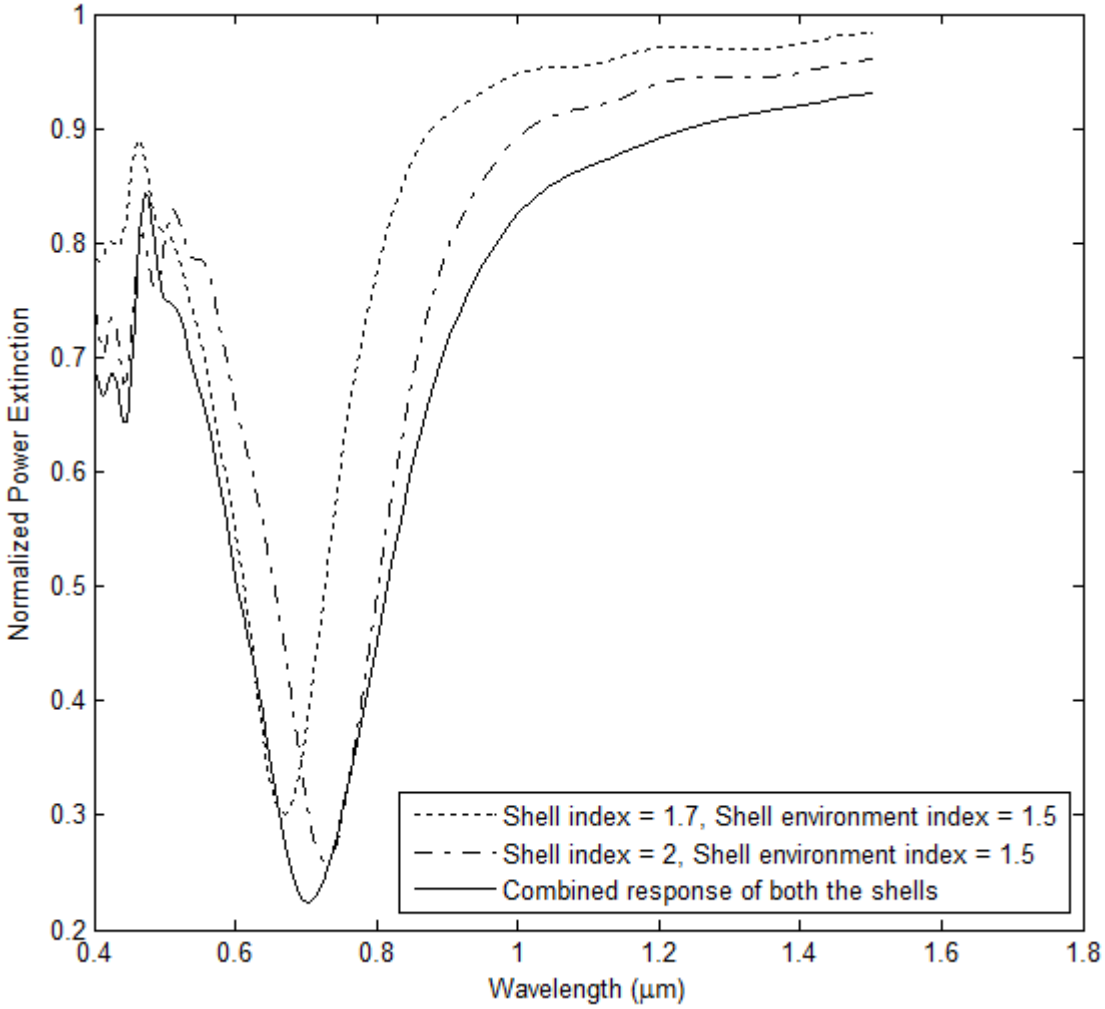

Figure 5. 44 Power extinction by an array of two nano particles embed in shells of dielectric index 1.7 and 2. The metal particle is identical in both the shells.

5.7. Filter and Antenna Application of the Proposed Nano Particle Array

In the proposed work, a comprehensive analysis of the nano particle has been presented in order to identify the characteristics of nano particle in optical domain useful in antenna and filter design. A nano particle array with nano particles placed in dielectric shell has been proposed (see figure 5.14). These nano particles take advantage of the variation in the surrounding index through which filtering operation at different wavelength can be achieved. There are two possibilities of index contrast variation. One is to change the index contrast of the environment of dielectric shell and make an array with keeping the index inside the shell constant. This results in a narrow band filter and the filtering bandwidth depends upon the shell index. From figures 5.20 (a), 5.21, 5.22(a) , with increment in index contrast values the extinction wavelength encounters a blue shift and this gradual change in wavelength

extinction spectra forms a narrow 3 dB beam width of the filter. The bandwidth of the filter can be controlled by changing the refractive index inside the shell. It should be noted here that in all the cases discussed here, the nano particle radius is 50 nm. Once again from figures 5.20 (a), 5.21, 5.22(a), a 3 dB beam width of 87 nm has been achieved with shell index of 1.5, it increases to 130 nm for shell index 1.7 and finally the widest beam width of 155 nm has been achieved for shell index of 2. This establishes a relationship between the shell index and filter bandwidth. Simultaneously, the radiated or scattered power by the particle array remains approximately at the same wavelength for all the index contrast change and for all the shell index cases (see figure 5.20 (b), 5.22 (b)). This gives an idea that the dielectric nano particle array containing metal nano particle with same shell index and different index contrasts can simultaneous work as filter whose bandwidth depends on the shell index and a radiator which is radiating on a single wavelength.

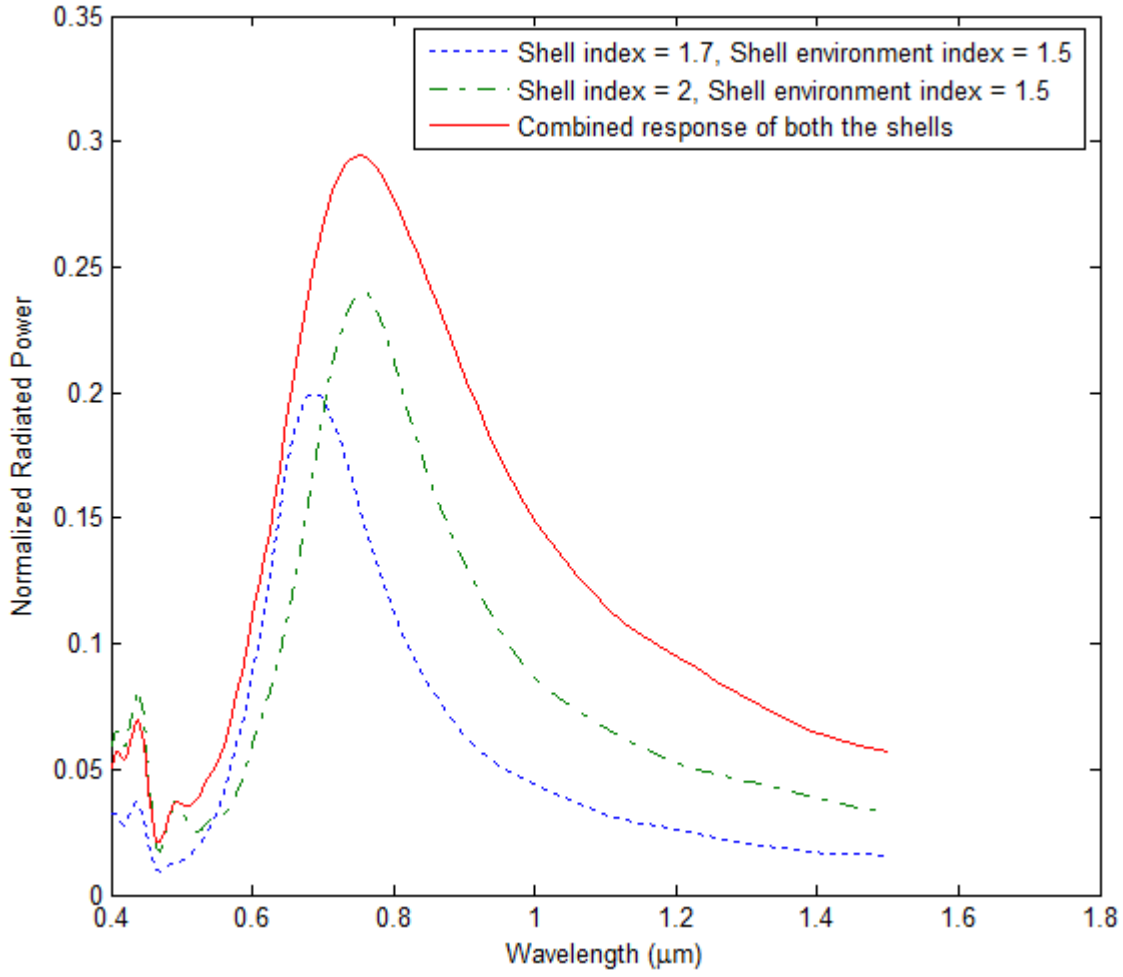

Figure 5. 45 Radiation spectra of the particle array in figure 5.23.

Second approach of filter design involves variation in shell index in place of shell surrounding index. Here all the nano particles are identical and placed in different dielectric shells. Figure 5.14 (b) is showing the side view of a two element array of dielectric nano shells containing the metal nano particle. This array has been simulated for two dielectric shells of index 1.7 and 2, placed in a dielectric constant of 1.5. Each shell encounter different index contrast and hence their resonance wavelength is different. These shells individually extinct the incident power at different wavelengths but when placed collectively offers the filtering operation over the bandwidth of both the designs. Moreover, array offer a collective radiation pattern of both the design containing the radiation spectrum of both the individual elements of the array. Figures 5.23 and 5.24 are showing the extinction and radiation spectra of the dielectric shell array of different dielectric constant. The array of nano dielectric shells have a 3 dB beam width containing the 3 dB beam width offered by both the shells and hence perform filtering operation over a combined bandwidth.

5.8. Conclusion

In this chapter, noble metal (gold) in optical domain has been investigated for its unique properties. The whole work is focussed on the localized surface plasmons and a spherical gold nano particle has been considered for the analysis in context of antenna and filter application. Metal nano particle array design has been proposed in order to realize the optical antenna and filter applications. Extinction and radiation properties with change in metal size, shape and surrounding environment index have been studied. Shift in the corresponding extinction wavelength and radiation wavelength have been studied in order to have an idea about the radiation and extinction resonant wavelengths for antenna and filter design respectively. A design for nano particle array has been proposed in which metal nano particles are placed in a dielectric shell of radius three times the radius of nano particle. The selection of the nano shell radius is based upon the minimum separation of resonance wavelength from the original resonance wavelength in extinction spectra for maximum index contrast variation. Wavelength shift corresponding to the variation in the index surrounding the dielectric shell have been computed in order to realize the filter and antenna using dielectric nano shell array containing the metal nano particle. Shells of refractive index 2 and 1.5 have been considered for the analysis of change in resonance wavelength and the corresponding amplitude for power extinction and radiation by the metal dielectric geometry. A maximum of 40 nm shift in extinction resonance wavelength was found in the case of shell with index 2 and maximum refractive index contrast. This shift was lesser in case of a shell

with index 1.5 as the shell had a lower range of refractive index contrast. Resonance wavelength of radiation by the dielectric metal arrangement was found to be insensitive toward the index contrast variation and all the peaks were observed approximately at the same wavelength. 3 dB beam width of power extinction for shell indices 2, 1.7, and 1.5 with same identical metal nano particle embed in it, have been evaluated. A filtering beam width of 87 nm, 130 nm, and 155 nm have been achieved for shell index = 1.5, 1.7, and 2 respectively. Due to the negligible variation in radiation spectra of different index contrast arrangement, the array radiate collectively on approximately at single wavelength and can work as a radiator or antenna at that wavelength. Second approach of filter and antenna design has been proposed with the variation in the shell index of an array containing different shells while keeping the index of surrounding medium of the shell constant. The design has been simulated successfully performing both filter and antenna operations.

References

- P. Bharadwaj, B. Deutsch, and L. Novotny, "Optical antennas," Adv. Opt. Photon., vol. 1, no. 3, pp. 438–483, Nov 2009.
- M. A. van Dijk, "Nonlinear-optical studies of single gold nanoparticles," Ph.D. dissertation, 1979.
- B. B. Yousif and A. S. Samra, "Modeling of optical nanoantennas," Physics Research International, vol. 2012, pp. 1–10, 2012.
- D. P. Fromm, A. Sundaramurthy, P. J. Schuck, G. Kino, and W. E.Moerner, "Gap-dependent optical coupling of single bowtie nanoantennas resonant in the visible," Nano Letters, vol. 4, no. 5, pp. 957–961, 2004.
- P. Mhlschlegel, H.-J. Eisler, O. J. F. Martin, B. Hecht, and D. W. Pohl,"Resonant optical antennas," Science, vol. 308, no. 5728, pp. 1607–1609,2005.
- P. J. Schuck, D. P. Fromm, A. Sundaramurthy, G. S. Kino, and W. E. Moerner, "Improving the mismatch between light and nanoscale objects with gold bowtie nanoantennas," Phys. Rev. Lett., vol. 94, p. 017402, Jan 2005.
- N. Dmitruk, S. Malynych, I. Moroz, and V. Kurlyak, "Optical efficiency of ag and au nanoparticles," pp. 369–373, 2010.
- E. Hutter and J. Fendler, "Exploitation of localized surface plasmon resonance," Advanced Materials, vol. 16, no. 19, pp. 1685–1706, 2004.
- V. Myroshnychenko, J. Rodriguez-Fernandez, I. Pastoriza-Santos, A. M.Funston, C. Novo, P. Mulvaney, L. M. Liz-Marzan, and F. J. Garcia de Abajo, "Modelling the optical response of gold nanoparticles," Chem. Soc. Rev., vol. 37, pp. 1792–1805, 2008.
- P.Muhlschlegel,H.J.Eisler,O.J.F.Martin,B.Hecht,andD.W.Pohl,"Resonant optical antennas," Science, vol. 308, pp. 1607–1609, 2005.

- J. N. Farahani, D.W. Pohl, H.-J. Eisler, and B. Hecht, "Single quantum dot coupled to a scanning optical antenna: A tunable superemitter,"Phys. Rev. Lett., vol. 95, no. 1, p. 017402, 2005.
- K.B.Crozier,A.Sundaramurthy,G.S.Kino,andC.F.Quate,"Optical antennas: Resonators for local field enhancement," J. Appl. Phys., vol.94, no. 7, pp. 4632–4642, 2003.
- P.Bharadwaj,B.Deutsch,andL.Novotny,"Opticalantennas," Adv. Opt. Photon., vol. 1, pp. 438–483, 2009.
- L. Novotny and N. F. van Hulst, "Antennas for light," Nat. Photon.,vol. 5, no. 2, pp. 83–90, 2011.
- H.Mertens, A. F. Koenderink, and A. Polman, "Plasmon-enhanced luminescence near noble-metal nanospheres: Comparison of exact theory and an improved Gersten and Nitzan model," Phys.Rev.B, vol. 76, p.115123, 2007.
- A. F.Koenderink, "On the use of Purcell factors for plasmon antennas," Opt. Lett., vol. 35, pp. 4208–4210, 2010.
- J. J. Greffet, M. Laroche, and F. Marquier, "Impedance of a nano antenna and a single quantum emitter," Phys. Rev. Lett., vol. 105, no. 11,p. 117701, 2010.
- Alù and N. Engheta, "Input impedance, nano-circuit loading, and radiation tuning of optical nano antennas," Phys.Rev.Lett., vol. 101, pp. 043901, Jul. 21, 2008.
- A. Alù and N. Engheta, "Anomalies of sub-diffractive guided-wave propagation along meta-material nano-components," Radio Sci., vol. 42, no. 6, p. RS6S17, Nov. 7, 2007.
- L. Novotny, "Effective wavelength scaling for optical antennas," Phys. Rev. Lett., vol. 98, p. 266802, 2007.
- K. Kneipp, H. Kneipp, I. Itzkan, R. R. Dasari, and M. S. Feld, "Surface-enhanced Raman scattering and biophysics," J. Phys.-Condes. Matter 14(18), R597–624, 2002.
- J. Yguerabide and E. E. Yguerabide, "Light-scattering sub-microscopic particles as highly fluorescent analogs and their use as tracer labels in clinical and biological applications- II. Experimental characterization," Anal. Biochem. 262(2), 157–176, 1998.
- P. K. Jain, I. H. El-Sayed, and M. A. El-Sayed, "Au nanoparticles target cancer," Nano Today 2(1), 18–29, 2007.
- G. Raschke, S. Kowarik, T. Franzl, C. S¨ onnichsen, T. A. Klar, J. Feldmann, A. Nichtl, and K. Kurzinger, "Biomolecular recognition based on single gold nanoparticle light scattering," Nano Lett. 3(7), 935–938 , 2003.
- Stefan A. Maier, "Plasmonics: Fundamentals and Applications" (2007).

Chapter 6

Conclusion

In this thesis, a comprehensive investigation of planar antenna array for square kilometre application has been presented. In addition, antenna and filter design in optical domain by using the unique property of noble metals have been proposed. First of all, a planar antenna array containing 484 elements has been proposed and the array thinning approach has been used to achieve the desired performance. Although, the thinning approaches have been used in various planar array geometry previously but in the present work a cascaded approach of optimization has been adopted. This approach overcomes the disadvantages of multi objective optimization approaches. As in case of multi objective heuristic approaches, a trade off between the parameters exists due to which it becomes difficult to achieve the best possible values of all the parameters, possible in case of single objective optimization. In multi-objective searches the obtained pareto front contains the solutions not as good as obtained through dominated search solutions. Proposed design contains a hexagonal grid of elements with elements omitted from the four corners to have a design with minimum non-contributing elements to the radiation pattern. After geometry selection the thinning configuration of the design has been achieved with the application of genetic algorithm modified in its operation. Geometry induced modification in the crossover operation has been done and double stage uniform crossover operation has been proposed. The design initially has been optimized in specific directions offering a side lobe level as low as -31 dB and directivity as high as 32 dB. A comprehensive optimization of the design, covering a scan range of ϕ and θ from 0 to π and $-\pi/2$ to $\pi/2$, respectively, has been presented. The obtained radiation pattern was containing an elliptical shaped main beam with well behaved radiation pattern. The side lobe peak as low as -21 dB and directivity as high as 30 dB was achieved. A 3 dB beam width of 0.088 has been achieved with the design, making it suitable for high spatial resolution requirement of SKA. The radiation patterns have been investigated for different element patterns and different main beam pointing directions. Further, to achieve side lobe level improvement in case of steered main beam while maintaining the desired shape of the main beam, low power consumption, high directivity with reduction in mean side lobe level, a new synthesis approach have been proposed. Taylor distribution for the circular aperture has been used for array excitation. Taylor distribution has the advantage of the applicability to any shape of antenna aperture and it can be sampled for discrete apertures. The proposed GA modified discretizing technique overcomes the disadvantages of

conventional discretizing technique of sampled Taylor distribution. A hybrid linear crossover operation has been proposed in the optimization of the design using GA. Proposed synthesis approach improves the mean side lobe level and peak side lobe level with improvement in the power requirement. The design offers a peak side lobe of -23.16 dB and directivity of 29.8 dB. High aperture efficiency of 85 % has been obtained in order to have increased effective area of antenna and reduced antenna noise. Improvement in the peak side lobe level in case of steered main beam has been achieved. Design offers characteristics for the application in SKA over the frequency range of 70 MHz to 1 GHz (low SKA range). A well behaved radiation pattern with reduced side lobe peaks results in lesser antenna noise temperature and consequently improved sensitivity. This is one of the important figures of merits required in SKA. Both the planar array synthesis approaches proposed in the work have been investigated for antenna noise temperature and sensitivity. For different latitude conditions, design offer quite improved antenna temperature values. It remains below a level of 25 K for all the environmental conditions and for different element pattern and different main beam pointing directions. For array thinning approach, sensitivity values as high as 10.65 (isotropic element, end fire radiation) and 5.55 (isotropic element, steered main beam) have been obtained at 100 MHz. Sensitivity variations with the change in atmospheric conditions on the order of 10^{-3} have been obtained. It was found that at higher latitudes the sensitivity variations are higher in comparison to the mid latitudes. For GA modified discetizing technique, the achieved antenna temperature values, at 100 MHz, for end fire radiation and steered main beam are 4.1 K and 4.6 K, respectively. GA modified discretizing technique offers an antenna temperature improvement of 1 K to 4 K for a low SKA frequency range from 100 MHz to 350 MHz in comparison to the array thinning approach. Sensitivity variations on the order of 10^{-3} have been achieved making the sensitivity approximately constant with change in environmental conditions. The sensitivity values on the order of 6.2 m^2/k at 100 MHz and 0.5 m^2/k at 350 MHz have been achieved.Sensitivity variation due to change in weather conditions has been obtained on the order of 10^{-2} $(\theta = 0°, \phi = 0°)$ to 10^{-3} $(\theta = \pi/4, \phi = \pi/4)$. Such small variation in sensitivity can be accepted for SKA application where antenna arrays are deployed over hundreds of kilometres of area span.

Second section of the thesis investigates the metal nano particle for optical antenna and filter design. Metal nano particles have been studied for their unique optical response and the variation in that response due to variation in particle size, shape, enclosing dielectric, inter-particle spacing. A detailed study of the power extinction spectra of nano particle has

been carried out with an investigation of wavelength shift between extinction and radiation resonance. A design with dielectric metal combination has been proposed to realize the optical filter and antenna. Dielectric shell containing the metal nano particle provides the facility to design an array with different surrounding index of the nano particle causing them to radiate at different wavelengths. Filtering band width of 83 nm, 130 nm and 155 nm have been achieved with an array of dielectric shells surrounded by different environment. It was found that the radiation wavelength of nano particle remains unaffected by the shell contrast variation and hence it can work as a radiator while working as a filter simultaneously. Simulations on FDTD have been carried out to design filter and antenna with nano particles embedded in dielectric shells. Lorentz-Drude dispersion model have been chosen for the calculation of power spectra. It has been shown with the simulation that an array of nano dielectric shells with different refractive index and containing metal nano particle can work as a filter whose 3 dB beam width covers the 3 dB beam width of extinction response of individual array element. Proposed work focuses on applications such as WDM and DWDM and optical antennas required to radiate the near field efficiently to the detectors [P. Bharadwaj, 2009].